Passive Motion Control for Industrial Robot Arm and Teleoperation System

BY

Achala Pallegedara

A dissertation submitted in partial fulfillment of
the requirements for the Doctor of Philosophy
degree in Electrical and Electronic Engineering,
Department of Science and Advanced Technology,
Graduate School of Science and Engineering,
Saga University

September, 2013

Supervisor: Professor Satoru Goto

Abstract

This thesis mainly addresses issues related to passive motion and its necessity for various applications of industrial robots. It is motivated by the increasing need to have more flexible and cost effective way of changing existing original versions of industrial servo controllers with minimal effort and cost. And further, by doing so, robots are improved with the flexibility, safety and robustness of factory automation systems in uncertain work environments.

The thesis mainly focuses on two issues: 1) Flexible motion against passive contact forces from an external environment acting on existing general purpose industrial type robot arms, and 2) Analyze the existing technologies against the force compliance passive motion control (alias of Force-free control-FFC) and its extensions, which are more emphasized based on applications oriented total behavior simulations under real robot parameters and conditions. Theoretical derivations and model development of the common industrial mechatronic servo systems including their application constrains are also provided with appropriate explanations. The dynamic and kinematic attributes of different versions of force compliance passive motion controllers are explained in details with required mathematical models and also provided the explicit proofs of derived equations.

A considerable weight is given to an application of teleoperation, based on existing industrial type robots. The proposed approach vigorously highlighted that needless of major hardware or costly original factory fitted control architecture changes. In addition to that fault tolerance aspects are considered. Moreover, loses and delays during communication of data through networks are also illustrated in places which they are underlying, and with faithful experiments.

The core of the entire research is focused based on the force compliance passive motion control (FCPMC or FFC) technique and its derivatives. However, the above technique is derived based on the dynamic compensations of gravity and friction forces combined with inverse characteristics of the industrial type servo controller and parameters. Therefore, research is again extended to establish the above controller based on twofold intelligent controller representations. Initially, a Gaussian neural network model representation is introduced to eliminate the errors incurred due to uncertainty of parameter estimations (eg: interference dynamic effect of multi-link industrial articulated platforms) in original model based analytical approach. Then, the Gaussian network is also further improved by means of initial state of the weights determination fortified the authenticity of Gaussian-neural network implementation, hence, an industry expertise heuristics being adapted during initial estimations of weights to govern the correct performance of the controller.

Besides, one of the early development models of force-free control by independent compensation was derived by confining the speed of the robot movements to "very low" thus, such assumption was questioned and argued. This thesis also provides the algebraic analytical solution to the subjective issue and for which Genetic Algorithm (GA) is used to evaluate optimal values for coefficients.

Throughout the research, experiments were carried out by using a Performer MK3s industrial type robot and for all simulations were also carried out based on same real robot parameters.

Approval

Graduate School of Science and Engineering
Saga University
1-Honjomachi, Saga 840-8502, Japan

CERTIFICATE OF APPROVAL

Ph.D. Dissertation

This is to certify that the Ph.D. Dissertation of

ACHALA PALLEGEDARA

B.Sc. Engineering in Chemical and Process Engineering,
University of Peradeniya, Sri Lanka, 2002
M.Eng. in Manufacturing Systems Engineering,
University of Moratuwa, Sri Lanka, 2006

has been approved by the Examining Committee
for the dissertation requirement for the Doctor of Philosophy
degree in Electrical and Electronic Engineering
at the September, 2013 graduation.

Dissertation committee:

Satoru Goto
Supervisor, PROF. SATORU GOTO
Dept. of Advanced Technology Fusion

Member, PROF. EIJI TAKAHASHI
Dept. of Advanced Technology Fusion

K. Muramatsu
Member, PROF. KAZUHIRO MURAMATSU
Dept. of Advanced Technology Fusion

Co-supervisor, ASSOC. PROF. TAKENAO SUGI
Dept. of Advanced Technology Fusion

Copyright©

Dedication

To my beloved farther Gunapala Pallegedara and late
mother Sheela Perera
For bringing and raising me up this far...
and my Teachers...

Acknowledgements

First, I hat off, for the useful lessons that the Japanese society taught me. I am profoundly indebted to Prof. Satoru Goto, my main supervisor, who guided me through my academic life and taught me professional standards. Except being my main advisor, he dared to be my guarantor in Japan. I appreciate his help that extended beyond teaching. I will never forget the valuable advices given by my co-supervisor Assoc. Prof. Takenao Sugi throughout the research work. I am grateful to Prof. Naruto Egashira, Kurume National College of Technology, for his generous assistance and valuable suggestions from the beginning of the entire research. I convey my humble gratitude to the committee members, Prof. Kazuhiro Muramatsu and Prof. Eiji Takahashi for their valuable comments and suggestions to improve the thesis. My deep, respectful gratitude goes to the ministry of education of the Japanese Government, for awarding me the Monbukagakusho full-bright scholarship.

My thanks go to Dr. Matsuda, for helping and guiding me in entire period of research work. I would like to express my gratitude to Mr. Nakafugi for helping me when I need without any hesitation. My sincere thanks go to Mr. Goto for being my friend and my tutor for helping me to fill documents which are needed to be filled in Japanese, and also to understand and adjust to the laboratory environment. Many thanks go to my past and present Japanese friends in the laboratory and my Sri Lankan friends in Saga, your support in many ways will never be forgotten. Many thanks go to the international students section of the Saga University and SPIRA for their vibrant service on behalf of the foreign students.

During my stay in Saga, Masuda sensei played a central role in backing me and my family up in many ways to make my studies and stay a success. she has truly been a mother in Japan to my family away from home. Through her, I came to know a very matured Japanese society and culture in Saga, and that contributed many valuable memories about Japan. Many thanks and we are indebted for making sure to fill delicious Japanese meals in at least two three times a month with us, I and my family will never forget her indispensable support and care in entire period of stay in Saga.

Unlimited thanks to my loving wife, Chilani, my daughter Amaya and my son Achintha the great support and love they gave me all along this way. Without their supreme care and support, I cannot imagine how I would have performed in my research work. I cant pen off without a word on the great love and constant care extended by my family in Sri Lanka. Nothing was like a call from home, my farther and then my brother, a call from father who always gave me reasons to fight. Last but not least my ever beloved late mother's blessings has constantly been keeping me being alive and always will be.

Contents

Page

Title i
Abstract ii
Approval iii
Dedication v
Acknowledgements vi
List of Figures xi
List of Tables xiv

Chapter

1 Introduction **1**
1.1 Historical background and overview 1
1.1.1 Mechatronics and robotics 1
1.1.2 Force, Compliance and impedance control of industrial robotics . 4
1.2 Motivation 5
1.3 Contributions of the Thesis 5
1.4 A Preview: Outline of the Thesis 6

2 Mechatronics and Robotic System Platform: An Overview **8**
2.1 Preliminaries and experimental setups 8
2.1.1 Common industrial servo system control configurations and parameters 8
2.1.2 First order kinematic model 10
2.1.3 Second order kinematic model 10
2.1.4 Fourth order kinematic model 10
2.2 Real time and semi-software based servo operation 11
2.2.1 RT-Linux for real time platform 11
2.2.2 RT semi-software based servo operation 13
2.2.3 Specifications of a typical industrial robot 14
2.2.4 Software implementation architecture of a revolute joint 16

3 Evaluation of Force-free Control Models and Strategies **19**
3.1 Introduction 20
3.1.1 Force-free control strategies based on Lagrangian dynamic models 21
3.1.2 Comparison of force-free control by a mass point concept model vs impedance control model 22
3.2 Force-free control and flexible motion realization 24
3.2.1 Development of FFC concept and background 25
3.2.2 FFC mathematical model using Lagrange dynamics 25
3.2.3 General FFC function and properties 28
3.3 Simulations of force-free control technique 29
3.3.1 Condition parameters for simulation 29
3.3.2 Simulation results of basic FFC for 1-link robot arm scenario . . 29
3.3.3 Simulation force-free control (FFC) for 2-link robot arm scenario 30
3.4 Dynamics and derivations of two different force-free control strategies . 33

3.4.1 Derivation of force-free control mathematical models 33
3.4.2 FFC-ET type structure and properties 36
3.4.3 FFC-TIC type structure and properties 37
3.5 Simulation of force-free control (FFC) strategies 37
3.5.1 Simulation setup for FFC-ET and FFC-TIC 37
3.5.2 Simulation results of FFC-ET and FFC-TIC 41
3.5.3 Important characteristics of simulation results 41
3.6 Analysis of force-free control and general type impedance control 44
3.6.1 Robot mechanical model 44
3.6.2 Dynamic model and equations 44
3.6.3 Kinematics 46
3.6.4 Controller model 46
3.6.5 Modeling of the wall environment 47
3.6.6 Modeling of contact force by Jacobian 48
3.6.7 Modeling of impedance controller 48
3.6.8 Modeling of force-free control (FFC) 49
3.6.9 Simulation of force-free control vs typical impedance control . . 52
3.7 Concluding Remarks 53

4 Teleoperation of Industrial Robot Arms Using a Visual Servo Technique 56
4.1 Teleoperation and visual servo control 56
4.1.1 Introduction 56
4.2 Teleoperation System by force-free control and template matching . . . 58
4.2.1 Concept and overview of the system 58
4.2.2 Configuration of the teleoperation system 62
4.3 Validation of the teleoperation system 65
4.3.1 Experimental condition 65
4.3.2 Experimental results by actual industrial robot arms 67
4.4 Discussion 72
4.4.1 Maneuverability 72
4.4.2 Accountability of network delays and data losses 72
4.4.3 Practical usability and advantages 73
4.5 Summary with concluding remarks 75

5 Evaluation of the Teleoperation System for Human Operator Perceptions 76
5.1 Introduction 76
5.2 Teleoperation by force-free conrol and visual servo control 78
5.2.1 Force-free control (FFC) 78
5.2.2 Visual servo control (VSC) 79
5.3 Human operator's perception 79
5.4 Experimental results 82
5.5 Discussion 84
5.6 Summary with concluding remarks 85

6 Analysis of Teleoperation System for Lighting Variations 86
6.1 Introduction 86
6.2 Overview of main system components 89
6.2.1 Force-free control 89
6.2.2 Visual servo control 90
6.2.3 Lighting level measurements 91
6.3 Experimental evaluation 91

6.3.1 Experimental setup . . . 91
6.3.2 Experimental results and discussion . . . 93
6.4 Concluding remarks . . . 94

7 Force Compliance Passive Motion Control Implemented Using AI Techniques 96
7.1 Introduction and background . . . 96
7.2 Particulars of industrial type robot arms: an overview . . . 98
7.2.1 System architecture . . . 98
7.2.2 Kinematics of a robot arm . . . 99
7.2.3 Dynamics properties of industrial robot arm . . . 100
7.2.4 Industrial robots servo controller properties . . . 100
7.3 Force compliance passive motion control (FCPMC) strategies . . . 102
7.3.1 External torque method . . . 102
7.3.2 Torque independent compensation method . . . 103
7.3.3 New algebraic solution to the contradictory zero dynamics assumption . . . 104
7.3.4 Optimized coefficient of torque method (OCT) . . . 105
7.3.5 Neural network based force compliance method . . . 106
7.4 Evaluation of proposed control methodology . . . 107
7.4.1 Simulation setup and conditions . . . 107
7.4.2 Simulation results . . . 107
7.4.3 Discussion . . . 108
7.5 Concluding remarks . . . 110

8 Discussion and Conclusions 111
8.1 General discussion and conclusions . . . 111
8.2 Future directions . . . 113

Appendices 114

A Digital Control Analysis 115
A.1 DC motor for robotic systems . . . 115
A.1.1 Equation of motion . . . 115
A.1.2 Feed back control . . . 116
A.1.3 Changing proportional gain K_p . . . 117
A.1.4 Changing sampling time ΔT . . . 117
A.1.5 Simulation for motor properties . . . 118
A.1.6 Digital representation of a motor controller model . . . 118

B Motor Anatomy and Digital Architecture 120
B.1 DC Motor Characteristics . . . 120
B.1.1 Analysis of the DC motor . . . 120
B.1.2 Angular acceleration and rotational force of the armature by electromagnetic force . . . 121
B.1.3 The counter-electromotive force by electromagnetic induction . . . 121
B.1.4 Electrical circuit of DC motor . . . 122
B.1.5 Equation of motion of the DC motor . . . 123
B.2 Rigid coupling with the two mass model . . . 124
B.2.1 Connection of the motor mechanism . . . 124
B.2.2 œRigid body combined model . . . 125
B.3 Measurement of the parameters of the DC motor . . . 126
B.3.1 Total armature resistance . . . 129

B.3.2 Measurement of the induced voltage constant torque and constant 129
B.3.3 œMeasurement of the moment of inertia (inertia) 130
B.3.4 Measurement of viscous friction coefficient 130
B.4 Control of the DC motor 130
B.4.1 Configuration of the current loop 130
B.4.2 Configuration of the velocity loop 131
B.4.3 Structure of the position loop 132
B.4.4 Connection to the PC controller 134

Publications **137**

References **139**

List of Figures

Figure		Page
2.1	Common Structure of an Industrial Mechatronic Servo System	9
2.2	First Order Representation of Mechatronic Servo System	9
2.3	Second Order Representation of Mechatronic Servo System	10
2.4	Fourth Order Representation of Mechatronic Servo System	11
2.5	Detailed Architecture of RT-Linux Kernel	12
2.6	Schematics of a Typical Robot Manipulator System	13
2.7	Three Degree of Freedom Joint Dynamic Model of an Industrial Robot Arm	14
2.8	The 2nd Order Model of Software Servo System Including Quantization	15
2.9	Software Servo Motor Mechatronic Control System	15
2.10	Software Architecture of a Single Decoupled Servo Joint Method: A	16
2.11	Software Architecture of a Single Decoupled Servo Joint Mothod: B	18
3.1	Schematic Diagram of Industrial Articulated Robot Arm with Force-free Controller.	25
3.2	Functional and Implementation Flow Diagram of a Torque Monitor Based Force-free Controller.	26
3.3	Diagram of Matlab/Simulink Model for Single Arm Robot with FFC.	28
3.4	Schematic Diagram of the Robot Arm for FFC.	28
3.5	Flexible Motion Due to FFC.	30
3.6	Reference Position and Joint Position.	31
3.7	Position Plot X and Y.	31
3.8	External Force ($\mathbf{F}$) and Generated Torque ($\boldsymbol{\tau}^f$).	32
3.9	Joint Angles ($\mathbf{q}, \mathbf{q^d}$) and Generated Torque ($\boldsymbol{\tau}^s$).	32
3.10	Time Trajectory and (x, y) Plot of the Tip Position.	33
3.11	Schematic Diagram of 2-link Articulated Type Robot Arm	34
3.12	Industrial Type Servo Controllers for n-link Robot Arm	35
3.13	Conceptual Illustration of Force-free Control Principle	36
3.14	Algorithm with Implementation Flow Diagram of FFC-TIC	38
3.15	Simulink High Level Model Diagram of FFC-ET and FFC-TIC	39
3.16	Simulation Results for FFC-TIC, External Force ($\mathbf{F} = [\mathbf{15}, \mathbf{70}]^{\mathbf{T}}$N)	40
3.17	Simulation Results for FFC-ET, External Force ($\mathbf{F} = [\mathbf{15}, \mathbf{70}]^{\mathbf{T}}$N)	41
3.18	Simulation Results for 2-link Robot of FFC-TIC for Varying External Torque	42
3.19	Simulation Results for 2-link Robot of FFC-ET for Varying External Torque	43
3.20	Manipulator in Contact with the Environment.	47
3.21	Block Diagram of Impedance Controller.	49
3.22	Schematic of Mass Point Orientation.	50
3.23	Block Diagram of Mass Point Type FFC.	50
3.24	Functional and Implementation Flow Diagram of a Mass-point Considered Force-free Controller.	51
3.25	Complete System Block Diagram for Simulation of IC and FFC in Matlab/Simulink.	53
3.26	Robot Orientation of Hitting Wall at (x,y).	54
3.27	Simulation Results of Tool-end Position After Hitting the Wall for FFC, IC and without Force Controller.	54

4.1 Schematic Overview Diagram of the Teleoperation System 59
4.2 Block Diagram of the Proposed Teleoperation Mechanism 60
4.3 Overall Flow Chart of the Teleoperation System 61
4.4 Concept Flow Chart of Switching of Remote Control to Visual Servo Control 65
4.5 Experimental Setup Diagram of the Proposed Teleoperation System 68
4.6 Reference Position Generation with Time by Force-free Control for Experiment Number 1 (Top) and 2 (Bottom) 69
4.7 Reference Position Generation with Time by Template Matching for Experiment Number 1 (Top) and 2 (Bottom) 69
4.8 Tip Position of the Robot Arm in the Working Side 70
4.9 Locus of the Tip Position of the Working Side 71
4.10 Reference Position Generation by FFC for Experiment No. 1 and No. 2 . . 73
4.11 Reference Position Generation by Template Matching for Experiment No. 1 and No. 2 74
5.1 Schematic Diagram of General Supervisory Controlled Semi-autonomous Teleoperation System. 77
5.2 Schematic Diagram of the Investigated Teleoperation System with Visual Feedback 79
5.3 Communication Network and Data Flow Directions 80
5.4 Monitor PC User View and Guide Map 80
6.1 Schematic Diagram of the Teleoperation System 87
6.2 Flow Chat of the Motion State Switching 90
6.3 Schematic Diagram of Template Matching Technique 92
6.4 Pictorial View of the Experimental Setup 92
7.1 (a): Performer MK3s Robot and Data Flow Directions (b): Wire Frame Diagram of Two Links of an Articulate Robot Arm (c): Mechatronic Servo Controller Block Diagram for Single Joint Motor 99
7.2 Block Representation of Common Industrial Servo Controller for Two Active Joints 101
7.3 (a): Block Diagram of FFC-ET and (b): Block diagram of FFC-TIC . . . 103
7.4 Gaussian Neural Network Model Representation for New FCPMC 107
7.5 Results of FCPMC-OCT Method for Passive Motion Against Defined Locus in y-direction with Restricted x 108
7.6 Results of FFC-TIC Vs FCPMC-GNN Method for Same Input External Force 109
A.1 Mobile Robot Model 115
A.2 Mobile Robot Controller 116
A.3 Simulation of Mobile Robot,($\Delta T = 0.1$ [s]) 117
A.4 Simulation of Mobile Robot, ($K_P = 10$) 118
A.5 Motor Model 118
A.6 2nd Order Model of a Mobile Robot 119
A.7 Digital Control Model 119
A.8 Overshoot Varying Characteristics of a Digital Control 119
B.1 Configuration of the DC motor 120
B.2 Cross-sectional view of the DC motor 121
B.3 Generation of induced electromotive force 122
B.4 Electrical circuit diagram of the motor 123
B.5 Block diagram of the DC motor 124
B.6 Block diagram of the case constant smaller electrical time 124
B.7 Connection of the motor mechanism 125
B.8 Block diagram of the two mass model 125
B.9 Block diagram of the rigid body binding model 126
B.10 Block diagram of the rigid coupling simple model 126
B.11 Circuit diagram for the measurement 127

B.12 Step response of the DC motor 129
B.13 Transfer function of the current loop 130
B.14 The current loop in the motor 131
B.15 The velocity loop in rigid upon binding 132
B.16 Approximate model of the speed loop 132
B.17 Simple approximate model of the speed loop 133
B.18 The position loop in rigid upon binding 133
B.19 2-order approximation model 134
B.20 First approximation model 134
B.21 System configuration diagram for building the current loop 134
B.22 Mobile Robot Model 135
B.23 (Part 1) system configuration diagram in the case of using a torque monitor 135
B.24 System configuration diagram of the case of not using the torque monitor . 136

List of Tables

Table		Page
2.1	Control System Parameters for Servo Control for Performer MK3s Robot Arm	16
3.1	High Level Comparison of FFC and IC According to Properties and Functions.	55
4.1	Parameters of Performer MK3s and SCARA Robot	66
4.2	Communication Data Format for Operational Side (os) to Working Side (ws)	68
4.3	Communication Data Format for Camera Side (cs) to Working Side (ws)	68
5.1	Experiment Data and Results for Teleoperation Using Different Users	81
5.2	Correlation Variations with Skill Level	84
5.3	Probability of Success Level Variation With Category	84
6.1	Recommended Standards Levels of Indoor Lighting for Industrial and Laboratory Work	88
6.2	Summary of Experimental Data and Results for SSD Type	94
6.3	Summary of Experimental Data and Results for NCC Type	95

Chapter 1

Introduction

This research work is respectively bounded on mechatronics aspects of industrial robot control strategies, especially passive motion and compliance against external forces are being extensively studied and discussed. Therefore, following section is given for more specific and sensible coverage of a historical background and some of the milestones of relative researches.

The Universal Automation, later shortened to Unimation was established by Engleberger known as first robot company, who was later known to be the father of robotics [1]. Meantime, with collaboration of George Devol, who worked with Engleberger, designed the first programmable robot called "Unimates" in 1954 and which was held the patent for the first industrial robot in history [2]. First ever computer controlled robot was developed by MIT scientist named Ernst in 1961, details of the design is described in [3]. The rapid increment and development in robotics hardware, research and theoretical innovations made robotics into an emerging industrial discipline at later stages. In 1980's robot manufacturing and programming industry entered a new era that growing rapidly as being a sunrise technology. Thereby, many companies were introduced and conducted programs and courses for robotics in industrial applications. Although, in late 70's and 80's most of the researches were devoted to find out the correct dynamic models and their optimal control systems of the industrial robot manipulators. Those aspects were not only emerging but also found to be the most critical task even today itself, for which, large number of high calibre researchers are interested in finding the optimal configurations. In last few decades a lot of contributions were seen upon such research topics and some of the crucial work have been identified, a few of the indirect but relatively useful scenarios are cited in following sections.

1.1 Historical background and overview

1.1.1 Mechatronics and robotics

Industrial robots by nature, provide fast, and even accurate performance in long run, and also maintaining high performances in repetitive tasks. They are mostly employed

in assembling, handling and manufacturing processes in industry. To survive in the industry, robot designs should be inline with low cost and reduced complexity on handling, and system features such as efficiency, precision etc., have mainly been compromised appropriately based on the industrial trade-offs. Mechatronic structure of the robot can generally be described as interconnection of links by different kinds of joints constitutes the mechanical structure of the robot and it is an open kinematic chain by its nature too. Links could be either rigid (rigid link robots) or flexible (flexible robots) while joints could be prismatic, revolute or twist type. Each joint is equipped with a prime mover; generally an electric motor and sensors are devised to detect position and velocity information of each joint to detect controlling attributes and functions. The separate controllers are coupled to motion control of each joint and PID category type controllers [4],[5] are generally popular in industrial robots due to their ease of implementation and some significant intrinsic robust characteristics such as robust to large disturbances, which would proliferate the industrial application benefits.

In the classical control approach of the robot manipulators, the end-effector motion is resolved into joint motions and actuate joints with rate and acceleration control [6, 7, 8] schemes. Generally, homogeneous transformations are used to transform arm motion to joint motions which are independently controlled [9, 10]. Although, the cost of computed torque control methods [10] is very high, manipulators dynamics based on Euler-Lagrange formulations can be adopted by using homogeneous transformations. In addition to that adaptive and robust control schemes were highlighted in [11], and by using approximate dynamics (unmodeled) method is also given for control manipulators with improved performance. On the other hand , intelligent computation methods were also proposed in [12, 13, 14] to learn the complex dynamics of the robot manipulator and declared higher grade control performance actions. Comprehensive study of industrial type robot manipulators was presented in [15] with more insight illustrations. In [16] and [17, 18] describe that most suitable control architecture for industrial manipulator is the decoupled PI mechatronic servo system, which is more consistently depicted in [19] and several examples were illustrated in [20, 21, 22].

Decoupled version of PI servo controller clearly separate the input data for trajectories from the servo controller as two independent compartments so that input data for working trajectories can be implemented as off-line process which is very convenient in user perspectives. Despite a fact of the off-line approach, trajectory generation for input data should be carried out by careful consideration of physical robot system constraints and parameters. Apart from the above, methods needed to accurately grasp the full dynamics of robot manipulators is also much importance in assuring the robustness of model-based control strategies such as computed torque controllers, which are however rarely used in the context in popular industrial applications due to higher complexity and the cost of computation. The problem however often encountered in the identification of dynamics of multi-link industrial manipulators is the lack of knowledge of necessary data such as input joint torques or the gains of the servo controllers. Studies done by [23] in 1986 and H. Kawasaki and K.

Nishimura [24] in 1998 investigate the problems of identifying the inertia parameters using the least-squares algorithm. Yet these methods need the input information of joint torque, which needs special hardware changes in an industrial manipulator, those are even non-motivating factors in business domain. Identification of dynamics using artificial neural networks (NN) has been studied in [25, 26, 27].

These methods suffer from several drawbacks: one is the tendency of back-propagation algorithms to converge to local minima. Another is that, in some of these methods a trained NN depends on the sampling time width of the training data. And also the other is that these methods do not make use of the inherent structure of the dynamics of manipulators. Therefore the ability of these methods to accurately grasp the dynamics of a manipulator with high degrees-of-freedom is still questionable. C. Y. Su *et al.* [28] have proposed a hybrid method to control manipulators driven by brush-less DC motors, which suffers from the problem of computation of the changing rate of the regression matrix, which is quite a challenging task. H. Searaji *et al.* [29] and P. Fiorini *et al.* [30] have studied motion control of 7-degree-of-freedom manipulators based on a configuration control approach by introducing user defined conditions into the Jacobian matrix to eliminate redundancy. Addressing the problem of inverse kinematic computation of redundant manipulators, a Lagrange neural network based approach to control 7-degree-of-freedom manipulators has been presented by J. Wang *et al.* [31]. Yet non-of these approaches are based on model based control. C. C. Cheah *et al.* [32] has presented an approach to control robot manipulators with kinematic and dynamic uncertainties. Some derivations of stability conditions are also given. G. Liu *et al.* [33] have investigated the problem of identifying the inertial parameters of a robot manipulator using a six-axis force/torque sensor at the base of the manipulator.

A discussion on fuzzy structure and parameter identification of dynamics of robot manipulators is given by M. R. Emami *et al.* [34]. J. Swevers *et al.* [35] have developed a method to experimentally identify the dynamics of a manipulator using an approach based on both internal and external models. The spatial operator approach is reviewed in its application to robot manipulator dynamics identification. Besides, current applications to modeling, simulation and control of space robot dynamics and large molecular structures are outlined by [36]. R. Featherstone and D. Orin [37] have given a good coverage of the algorithms used for derivation of the dynamics of robots. D. K. Pai *et al.* [38] have given a framework for derivation of several forward dynamics algorithms used in robots. An adaptive trajectory tracking control of a robot manipulator with unknown dynamics, using NNs is given in [39].

Artificial intelligence based controllers and trajectory generators are capable of compensating uncertain phenomena like friction and inertia which are varied with robot's configuration. They can be developed by means of principles of fuzzy logic, genetic algorithm or neural network [40, 41, 42] etc. Furthermore, impedance control is also quite often used as an effective way in improving the interaction between the manipulator and environment, and it widely and practically adopted in industrial practices successfully [43].

In addition to the generic explanation given for robot's basic constructional

details, a more specific and detailed description is provided; pertaining to a common typical articulated type industrial robot called Performer MK3, in [19] [44]. Performer MK3s, which is the type has been used in entire thesis for experimentations and also parameter values of the same have been used for most forms of simulations throughout the research .

In history of evolution of robots, Japanese Industrial Association (JIA) identified six categories, and those referring to robots defined by Japanese Industrial Association are: 1. Manual handling devise, 2. Fixed sequence robot, 3. Sequence robot, 4. Playback robot, 5. Numerical control robot, 6. Intelligent robot, respectively.

1.1.2 Force, Compliance and impedance control of industrial robotics

The manipulator control strategies for interaction tasks are grouped usually under two categories: indirect force control and direct force control. The first category is given for cases such as a movement with an implicit force which is exerted by the external environment or an operator feedback, which is generally applied for controlling robot movements against uncertain forces. The second category is used in cases where possibility of force to be controlled for desired value, through an explicit force feedback [45, 46].

The classic impedance control approach describes taking contact force indirectly by modeling the interaction as a mass-spring-damper system. The indirect relationship is a consequence of force sign influence on control law, the objective is to adapt the manipulator dynamic behavior in contact with the environment and not to fulfill a position and/or force trajectory. This way, an explicit force feedback doesn't exist in system, because, this signal just supplies the system impedance in contact with a surface. Therefore, the fundamental principle of impedance control, described in [47], is that the control system regulates the manipulator impedance, that is defined by relationship between the speed and applied force.

Industrial type robot systems represent a particular group of flexible automated manufacturing systems, in which the contact force generation belongs to the most complex and challenging tasks. The robotized technologies (machining, grinding, finishing, welding, pulling out work, painting, cleaning etc.), based on the direct contact between the robot tool and the product, have to deal with the problem of unwanted features of this interaction. At the end of the reaching phase, after positioning to a workplace, the number of degrees of freedom of the robot arm decreases and the plant in the robot control system undergoes the structure modification. Historically, a list of the force compliance control techniques begins with the conventional PID controllers [48, 49] and continues with more advanced adaptive control methods [50, 51] and robust algorithms [52, 53]. Most topical approaches are the methods of sliding mode control [54], as well as the fuzzy control [55, 56] and neural network approach [57, 58, 59]. The modern force control systems comprise the force-position or velocity-position hybrid control [60, 61, 62], and impedance or admittance type control [63, 64, 65] and their derived variations.

In addition to that the force control structures are mostly dependent on both the features of the task and the environment of the robot. However, implementing a

system that compliance the external forces or interaction forces between the environment and the robot, is generally a highly expensive and complex task if the original version does not support for functional requirements. Costs of modifications are really high in practice and need high skilled technical support even from the robot manufacturers so that most industrial managers reluctant to adopt those modifications. Therefore, externally pluggable module would be an alternative and an ideal solution of cause. Therefore, this thesis is basically discussed how an external modification to the original system, can offer the force compliance requirements against external interactions on a working robot without disturbing to the original working capacity as well as manufacture's factory fitted control setups.

1.2 Motivation

However, in some important industrial business requirement cases such as grinding or assembly operations rigidity of robot arms must be kept lower, because the flexible motion by external force is required [47, 66]. In general, industrial articulated robot arms are designed to have high rigidity for application requirements of accurate positioning and contouring. Therefore, those robot arms are not adaptable to flexible motion requirements such as grinding and assembling with pulling work out cases, if they are going to be used by their original form.

To realize flexible motion of robot arms in industries, a flexible device is attached to the tip of the robot arm, or a torque limit is induced to the joint actuator, which is named as "servo float method" [67, 68]. The other established force control methods such as impedance control and compliance control have been proposed to reduce the rigidity of robot arms are also described in [66, 69]. However, those methods are relatively complex and also required additional changes to the existing controllers of industrial robots. Stems form the above fact that it is really valuable and important to develop a external pluggable module that can be attached externally without changing the original hardware or software configurations of the industrial robots. Hence, such a module should be designed to be cost effective and light weight, rather than highly complex once. Subjected module should also be capable of at least compliance the external interactions rather than controlling the exact forces.

1.3 Contributions of the Thesis

The factors of this contribution represent the specific feature from the total model based simulations of the FCPM/FFC (Force Compliance Passive Motion Control/ Force-free control) approches, earlier FFC was not analyzed based on mathematical or structural or behavioral characteristics, but solely implement on a working robot. However, lot of hidden characteristics were remained since earlier FFC was introduced, as "unclarified". Therefore, comprehensive modeling and analysis required to be performed for basic type of FFC at first, since then vigourous attempts were repetitively undergone to solve the control model uncertain characteristics which were not fully understood for long. To analyze the actual behavior of FFC, single arm characteristics were identified after implementing integrated simulations which comprised

of an analysis of a modular and intrinsic characteristics. Moreover, simulation study has been expanded to behavior analysis of each of the FFC technique and its near derivatives. Thus chapter 3 gives the detailed implementation of the integrated simulation and analysis of FFC and comparisons of characteristics against with a general impedance control approach. Finally, the Matlab/Simulink based full-fledged integrated simulation verifies the implementation of the basic "Force Compliance Passive Motion Control (FCPMC)" (or "Force-free control (FFC)" in short form) structures and its modified extended versions.

Total simulations has drawn a satisfactory intention to apply the the FFC (or FCPMC) to realize a part of teleoperation of industrial robots. Thereby, trajectory generation for the remote side robot is carried out by means of FFC in the operating robot, which generates online data are being sent through a TCP/IP network to the remote robot. The problem of the performance deterioration due to stochastic environmental factors especially lighting inconsistencies. Therefore, an investigation has been executed under above teleoperation system for different template matching algorithms against different lighting levels, as an extension of a main research theme. The lighting investigation was carried out to address the varying performance due to lighting changes under different environmental conditions. In addition to that integrated research was undergone to observe and clarify how a human operator perception rectifying efficiency and performance of the above mentioned teleoperation system which is highly coupled with FFC. The consequence of the limited diversity and number of users deform the results regression analysis, yet total correlation analysis brought the clear understanding of objective relationships, particularly under the circumstances of system being operated by new users.

The provided approach of FFC and its derivative approaches always depend on the modeling accuracy of the mechatronic servo systems of a robot arm. For all cases, mainly, approximated dynamic model is used for synthesizing of inverse dynamics which is not totally eliminated the negative influence of the possible uncertainties incurred when modeling of any real system. Which is obvious while preserving both dynamics of the control process and desired limits on the real system variables. A one solution is presented in the form of a non-linear formulation of dynamics using a neural network where, a Gaussian objective function based method for compensating correct dynamics to achieve smooth FFC behavior. The other solution is suggested to address the optimization of FFC parameters which are driven the entire function of the FFC. For which, a genetic algorithm is used to find out the correct and optimal coefficients of the governing equation of FFC, by being directed the cost function towards global minimum.

1.4 A Preview: Outline of the Thesis

The main objective and focus of this thesis are the design, modeling and analysis of FCPMC control by means of integrated simulation and application realization by using teleoperation system which consists of two industrial robot arms. The behavior analysis investigations are also carried out for each of different FCPMC strategies. Based on the contact force interactions, an integrated simulation is proceeded by

comparing characteristics of FCPMC against impedance control which conventionally applied in industrial domain. Some of the unsolved issues concerning passive motion against external forces; such as robot move to a desired location by applying a small interactive force from human user, are also investigated through simulations. Moreover, desired motion generation attribute is used to be applied in cases where devising safety and fault tolerance against robot malfunctions caused by unexpected interaction forces.

Flow of the thesis representation is abstracted in following paragraph. Initially, it moves towards the modeling and analysis of the industrial mechatronics systems. Those modeling cases are illustrated with detailed of real valued simulations including comparison and understanding for different cases of force compliance passive motion studies. Moreover, simulations are also extended the behavior studies of different cases of controlling passive motion of industrial robots based on contact with external forces, which are exerted by an external environment. Force compliance passive motion control (FCPMC) are also referred by the phrase Force-free control (FFC) throughout the thesis and latter is more likely and frequently used at early stages of the thesis. **Chapter 2 3** are devoted for highlighting the above sections respectively.

In addition to that **Chapter 4, 5 and 6** are cascaded subsequently by illustrating a possible application of FFC/FCPMC for teleoperation. A considerable amount of research is performed to investigate the design of a teleoperation system by applying the FCPMC technique alongside with the visual servo control (VSC) which is based upon online image template matching. Thereafter, teleoperation research is also extended to carry out for evaluating the system performance when cases where an operator (or a user) changes, for which interactions between different set users were evaluated. Human interaction and the system performance of the teleoperation system are compared with correlation analysis. Next to that an extensive study is given to show how proposed teleoperation system efficiency and accuracy tend to change based on environmental conditions, especially, against the lighting variations.

Finally, more simulation attempts are executed to model the FCPMC by implementing a Gaussian neural network. And also by optimizing the hyper parameters using Genetic algorithms are carried out as modified new extensions to the original FFC techniques. Which is further extended as an investigation, which is subjected for replacing Gaussian neural network with a method of initial weight parameter determination of the Gaussian network. In which, heuristic knowledge of robot characteristics generally uses in the industry to find out the optimal and fine-tuned servo controller parameters, is tried to be embedded and which are reflected through initial values of weight parameters. Thus, convergence of Gaussian neural network becomes much faster and convenient than before.

At the end, **Chapter 8** summarizes the main results of this thesis and then, discussion is given and elaborates possible directions of future research. It is also devoted for concluding remarks and recommendations.

Chapter 2

Mechatronics and Robotic System Platform: An Overview

2.1 Preliminaries and experimental setups

2.1.1 Common industrial servo system control configurations and parameters

In general, manipulator characteristics could be represented either with a dynamic model or/and with a kinematic model. In dynamic models, joint torques and forces are taken into account and in kinematic models; non forces behavior but consider resulting positions, velocities and accelerations. Though the dynamic constraints are natural in existence, they can be transformed into equivalent kinematic constraints (constant or piecewise constant bounds), concerning the supremum (global limits of minimum and maximum) of accelerations and velocities despite hampering 100% efficiency and ideal capabilities of manipulators.

A detailed explanation of dynamic models is illustrated in [70]. However, this discussion is basically focused on regular and well-known industrial kinematic models used for robotic systems and also those basic structure is illustrated as Fig. 2.1. Depending on the operational speed of the servo system and the degree of influence of the simultaneous movements of other joints on a particular joint, the selection of kinematic model may vary according to the accuracy required for particular applications. It can be considered that the other joints have negligible effect, the joint dynamics can be decoupled and as a result planning of trajectories will be done as appropriately and easiest manner. Following diagrams are given to illustrate the anatomy of the dynamic and control models.

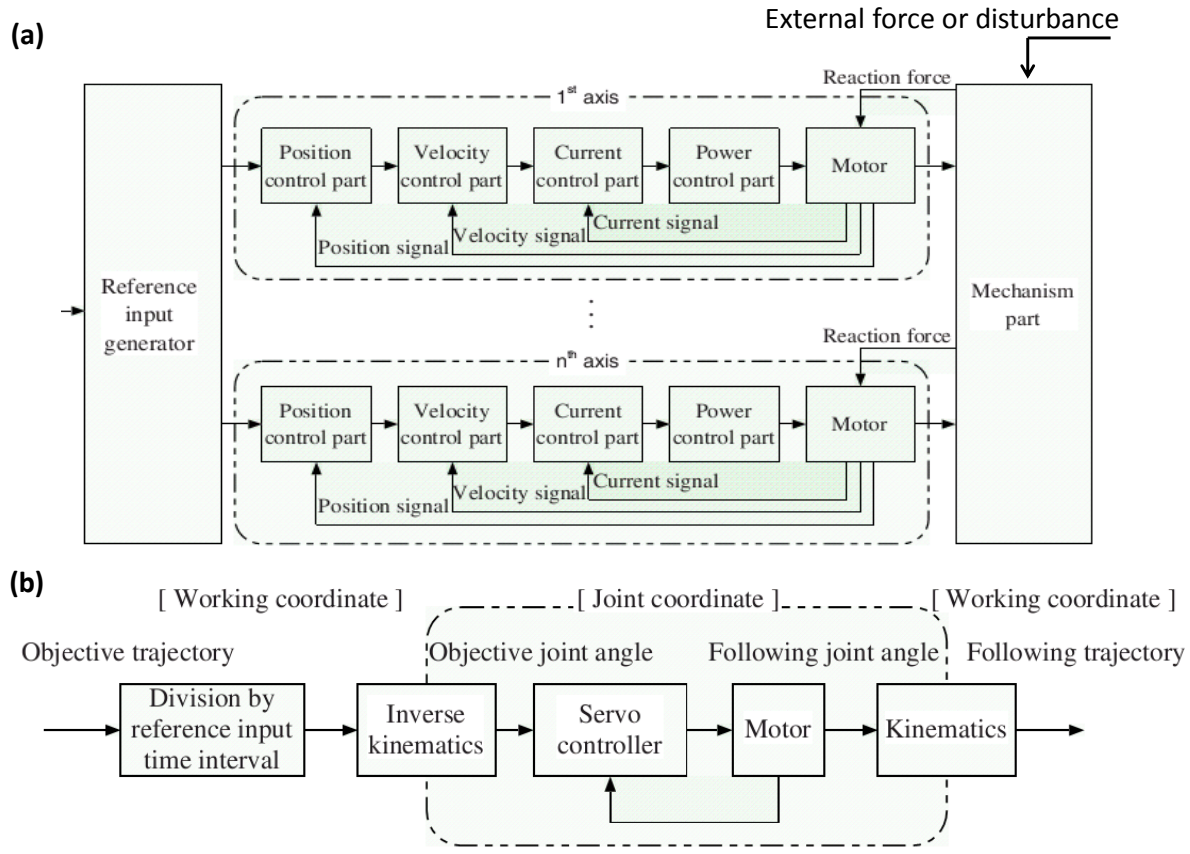

Figure 2.1: Common Structure of an Industrial Mechatronic Servo System

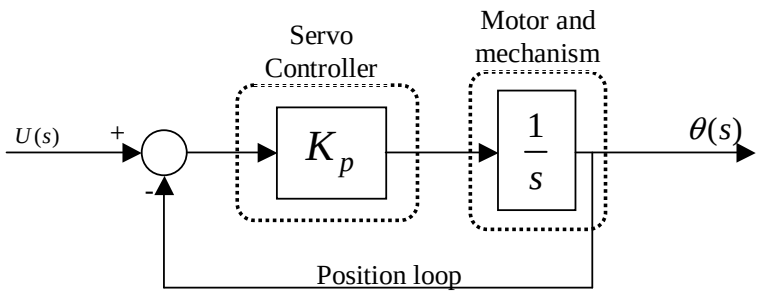

Figure 2.2: First Order Representation of Mechatronic Servo System

2.1.2 First order kinematic model

A decoupled joint of a mechatronic servo system can be mathematically represented with a first order linear kinematic model as follows:

$$G(s) = \frac{K_p}{s + K_p} \tag{2.1}$$

where K_p is the position loop gain of the servo controller and it is briefly illustrated in Fig. 2.2. The first order model can be used when the velocity of the servo motors as the actuators of the mechatronic servo system is about 1/100 times of the rated velocity of motors [20].

2.1.3 Second order kinematic model

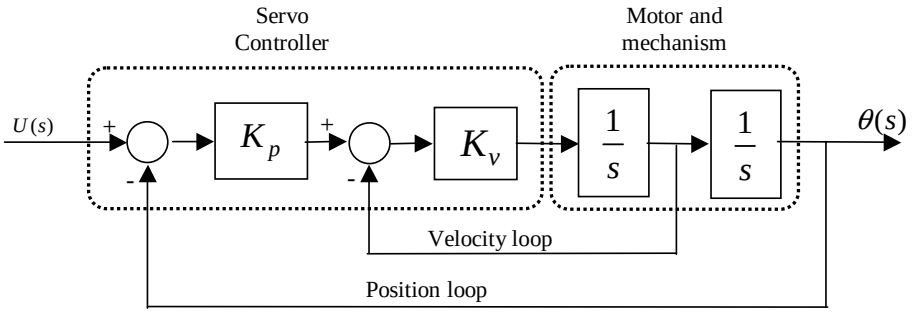

Figure 2.3: Second Order Representation of Mechatronic Servo System

When the velocity of the motors are much faster, about 1/20 to 1/100 times of the rated velocity, the kinematics of the mechatronic servo system must be treated as a second order model. The mechatronic servo system is described independently for each axis with the second order model given below.

$$G(s) = \frac{K_p K_v}{s^2 + K_v s + K_p K_v} \tag{2.2}$$

where K_v is the velocity loop gain as shown in Fig.2.3.

2.1.4 Fourth order kinematic model

For higher velocities greater than 1/20 times of the rated speed, in other words high-speed operation of servo control joints, second order model can not represent the kinematics of joint adequately, as the reaction force/torque is considerably high and the elastic deformation can not be further neglected. In such cases, fourth order representation of the decoupled servo joint can precisely illustrate the characteristics and it is briefly shown in Fig.2.4.

Fourth order model of independent servo joint can mathematically expressed in the following form:

$$G(s) = \frac{a_0}{a_4 s^4 + a_3 s^3 + a_2 s^2 + a_1 s + a_0} \tag{2.3}$$

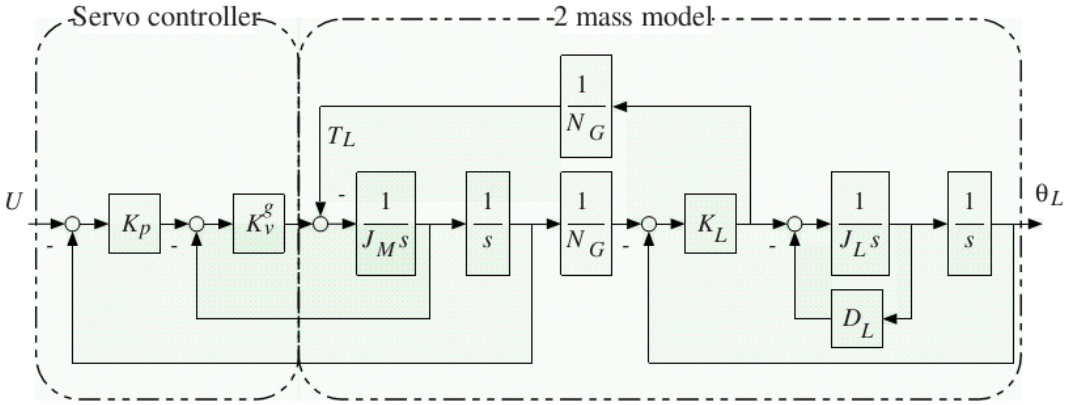

Figure 2.4: Fourth Order Representation of Mechatronic Servo System

where $a_0 = K_p K_L K_v^g$, $a_1 = K_L K_v^g + K_p D_L K_v^g$, $a_2 = K_L J_M + D_L K_v^g + K_p J_L K_v^g + K_L J_L$, $a_3 = D_L J_M + K_v^g J_L$ and $a_4 = J_L J_M$. In that case K_p, K_L, K_v^g, J_M and J_L denote position loop gain, elastic constant of the mechanism, servo amplifier gain, damping coefficient of the mechanism alone with load, motor inertia and load inertia respectively. As the load inertia is a function of the manipulator configuration, the payload and the shape of the payload, fourth order model is not a time invariant model.

When the joints move simultaneously, due to many functions including frictional, gravitational and inertial forces of the manipulator, one joint may be influenced by other joints. Therefore each joint can not be dissociated from the others and therefore, model should be developed concerning the complete dynamics of the manipulator; not a single joint. Since, interactive joint model is highly dependant on the number of joints, the complexity proportionately increases as the number of joints is increased. Due to unavailability of generic model, interactive joint model is beyond discussion here.
Please refer the *Appendix A* for servo parameters and their characteristics which are shown with illustrated simulations. In *Appendix B* a detailed illustration of servo motor modeling and control in robot systems is annotated.

2.2 Real time and semi-software based servo operation

2.2.1 RT-Linux for real time platform

In the case of accurate and real time path tracking, timely provision of appropriate reference joint position/velocity to servo controller must be ensured. Failure to feed reference input at correct time results in undesirable consequences jeopardizing the safe operation of the robot, and in extreme case it may possibly lead to catastrophic consequences. Correctness of real time system does not depends only on the logical result or correct reference input, but also the physical instances at which the reference inputs are produced. In other words, timeliness is a key characteristic in real time

servoing and hence the program in charge of tracking must produce time critical outputs.

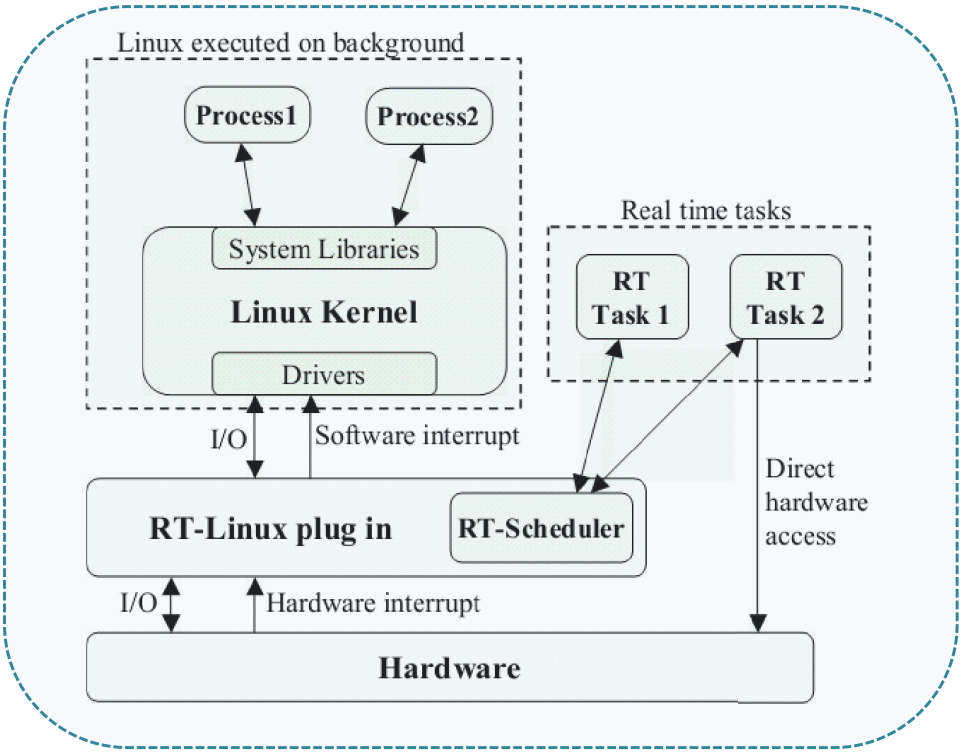

Figure 2.5: Detailed Architecture of RT-Linux Kernel

Control programs run on general-purpose operating systems may produce intolerable inaccuracies in time, particularly in fine-grained synchronization of program output with hardware operation (when using higher update rates of reference trajectory), since the timing of execution is not guaranteed due to inherent time-sharing execution. However by increasing the priority of the thread, at which the control program executes, can improve the current situation and can make the system a soft real time, but it is not a concrete solution to crack the fundamental issue of making the system hard real time to enable handling of interrupts in real time. A high priority thread cannot preempt a low priority thread during a system call and has to be delayed until either execution returns from system call to kernel decides that it is safe to reschedule (preemption point). Improving kernel preemptability is a viable option to manage this situation, still it may also associated with many pragmatic issues like difficulty in maintenance, non-guaranteed worse case response time, increase in response time due to new drivers. Therefore full-fledged real time operating system, RT-Linux has been selected as a platform for real time servoing, since minute errors are even intolerable.

RT-Linux is a patch to Linux which is basically developed to overcome the

conflicts of RT constraints of Linux. RT-Linux possesses efficient time management capability and the ability to direct access of hardware [42]. The basic architecture of the RT-Linux can be briefly given in Fig. 2.5.

RT-Linux creates a virtual machine interface (second kernel) located in between hardware and own operating system, and thereby Linux kernel becomes second kernel's idle thread. The second kernel, RT-Linux module, based on interrupt abstraction can process real time interrupts independent from what is happening under Linux. The FIFO is a communication mechanism based on FIFO of Linux but adapted-real on time. RT-Scheduler is a priority driven scheduler that uses Round Robin or FIFO algorithms. It also supports preemption and priority inheritance.

2.2.2 RT semi-software based servo operation

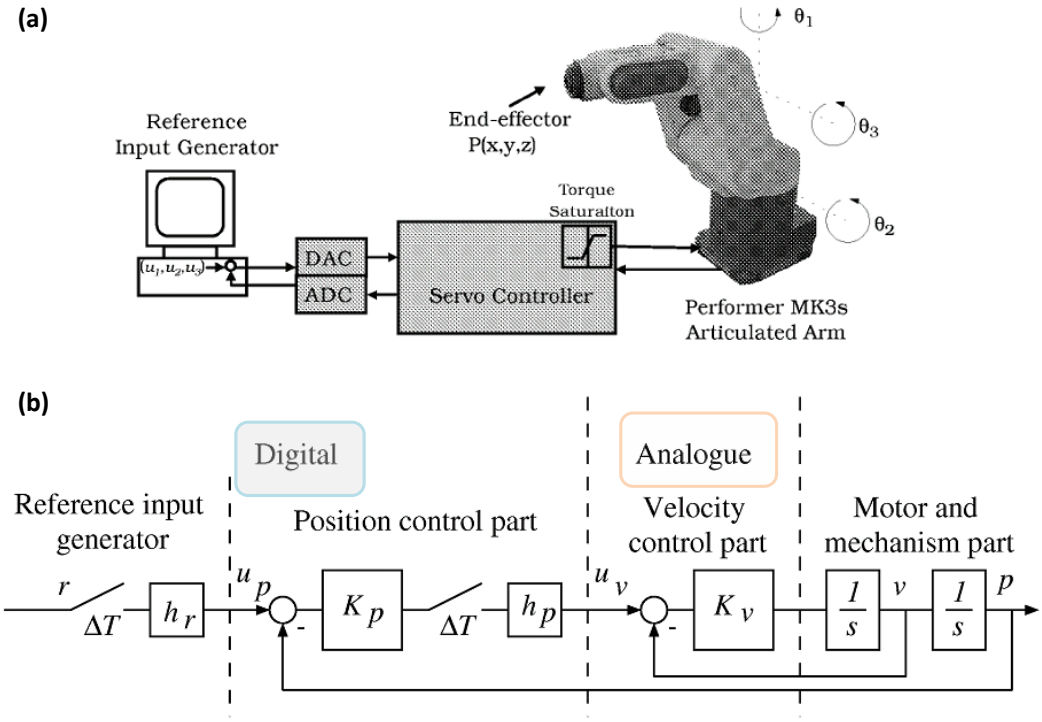

Figure 2.6: Schematics of a Typical Robot Manipulator System

Schematics of a typical industrial robot manipulator (Performer MK3) are depicted in Fig.2.6. Basically, an industrial robotic system is composed of reference input generator, data interface, servo controller, position and velocity sensors, mechanical structure of robot manipulator along with actuators [71], emergency switch and connecting wires. Reference input generator can be a stand-alone computer, or preferably a computer connected to a network. Data interface converts digital data generated by reference input generator into its analog format so that it could be used by servo controller as depicted in Fig. 2.7 and to acquire analog sensor data of the

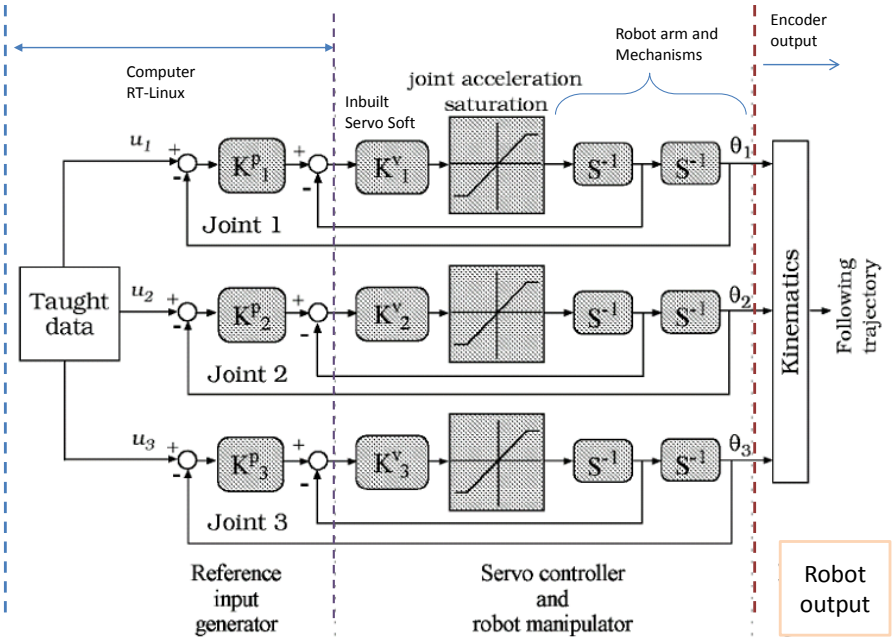

Figure 2.7: Three Degree of Freedom Joint Dynamic Model of an Industrial Robot Arm

robot manipulator through servo controller. Each joint of the robot manipulator is equipped with an actuator, usually AC or DC servo-motor, and sensors to measure position and velocity. Connecting wires establish the electrical connectivity while the emergency button is for safety and it overrides all the operating functionalities.

2.2.3 Specifications of a typical industrial robot

As depicted in Fig. 2.7 a given vector of reference data $[u_1, u_2, u_3]^T$, P controller generates corresponding velocity input, accounting the last configuration vector of the joints as specified by position sensors and consequently fed it to servo controller for servo operation of robot actuators. The software and coding architecture explain the control of a single decoupled servo joint in detail and Table 2.1 shows the set of control parameters for Performer MK3 robot. For simplicity, second order model for servo system has been assumed to illustrate the software servo architecture, but it is not necessarily be the second order model (please refer following sections of the thesis for details).

For the mathematical model of the servo system in the block diagrams of Fig. 2.8 and Fig. 2.9, the position feedback and velocity feedback are generally considered. The current feedback is simply assumed as the output of the power amplifier. In addition to that most software servo control system comprises the torque quantization with A/D, D/A conversion, as a problem, is expressed according to the quantization term in Fig. 2.8 and general external profile picture is given as in Fig. 2.9.

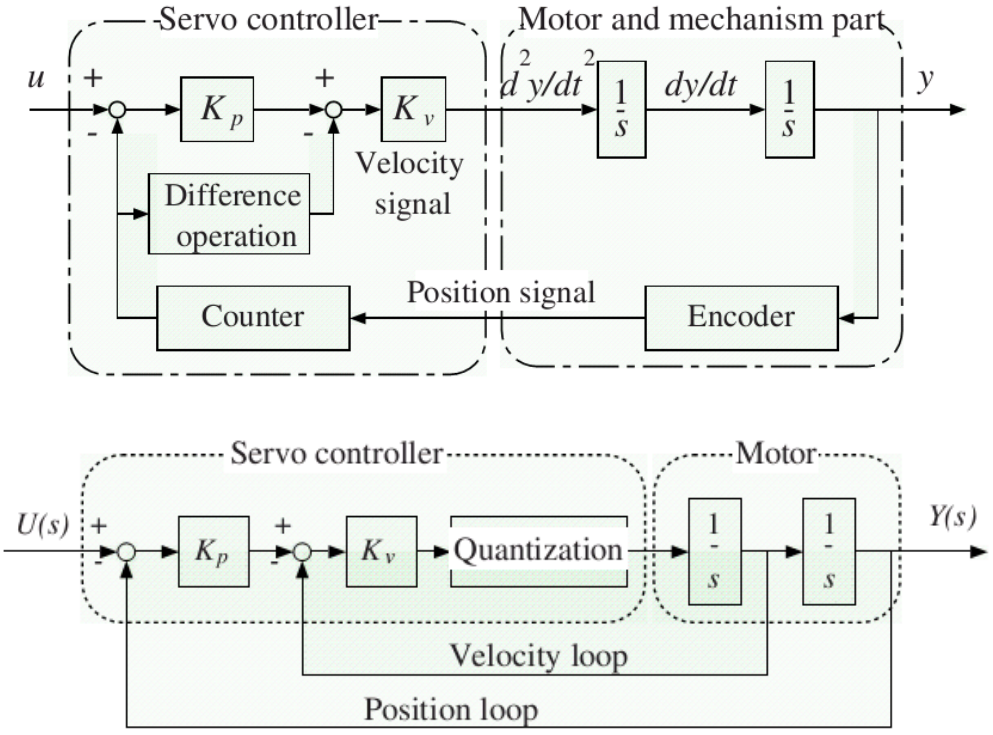

Figure 2.8: The 2nd Order Model of Software Servo System Including Quantization

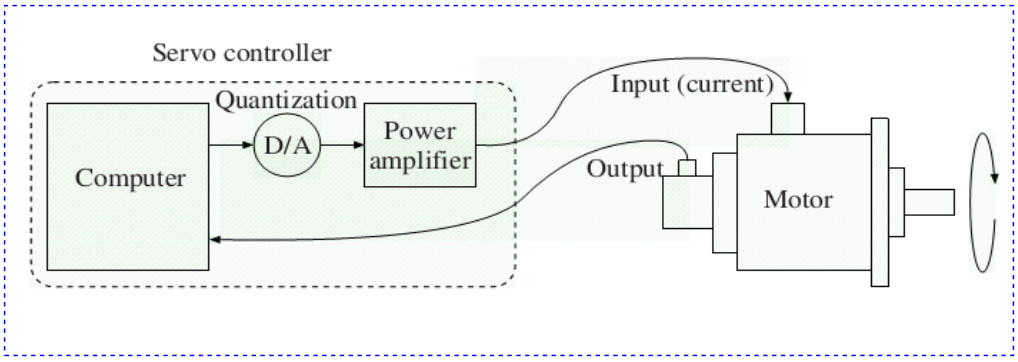

Figure 2.9: Software Servo Motor Mechatronic Control System

Table 2.1: Control System Parameters for Servo Control for Performer MK3s Robot Arm

Parameter	Denotation	Value
Shaft encoder resolution	N	8192[pulse/rev]
Gear ratio @joint 1	N_1	120
Gear ratio @joint 2	N_2	160
Gear ratio @joint 3	N_3	160
Conversion factor of velocity pulse to voltage for joint 1	R_1	0.000015161 [volt/(rad/s)]
Conversion factor of velocity pulse to voltage for joint 2	R_2	0.000012484 [volt/(rad/s)]
Conversion factor of velocity pulse to voltage for joint 3	R_3	0.000012169 [volt/(rad/s)]

Industrial robot manipulators are designed to meet the performance level required by the application such as welding, cutting, part handling, etc. The specifications in general are limited only to a certain degree of accuracy, velocity, and complexity. Therefore, most industrial robot manipulators are designed with linear proportional-integral-derivative (PID) servo controllers with current limiting power amplifiers [19]. This saturating current determines the acceleration limit of the joint. Furthermore, joints are independently controlled, whereas unknown inertia torques, coriolis and centrifugal torques, and torques due to friction and gravity are treated as disturbances to be rejected by the controller. To support this assumption, manipulator links are designed with low inertia, and joints are driven through high gear reductions (Sage et. al. 1999) given in [70]. These controllers are simple, and also provide sufficient robustness. Figure 2.7 illustrates three degree of freedom decoupled joint dynamic model of an industrial manipulator.

2.2.4 Software implementation architecture of a revolute joint

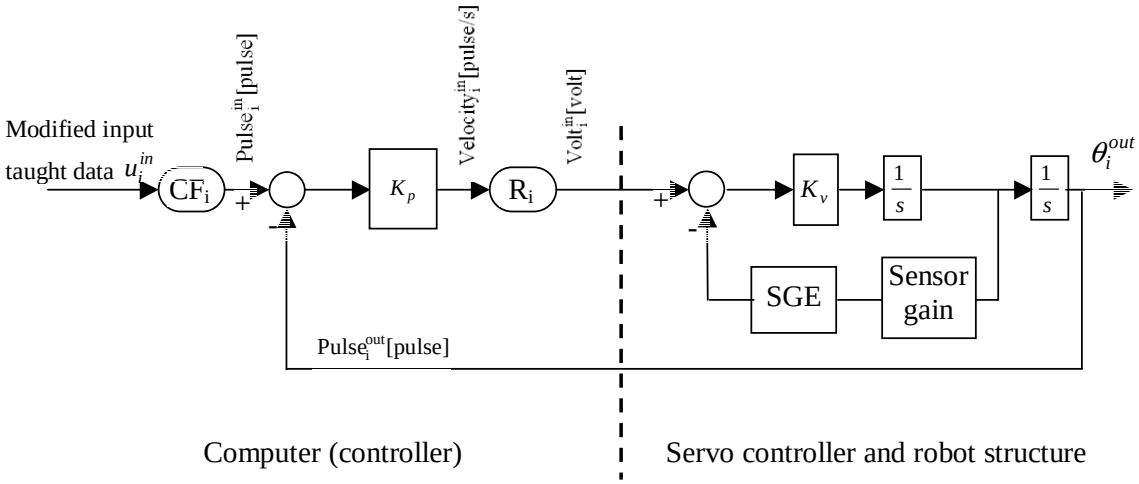

Figure 2.10: Software Architecture of a Single Decoupled Servo Joint Method: A

2.2.4.1 Method A The input position data u_i^{in} [rad] is converted to $Pulse_i^{in}$ [pulse] by conversion factor CF_i [pulse/rad] for the i^{th} joint. The most of the control actions take place in pulse form to comply with the existing pulse counter. The reference pulse input $Pulse_i^{in}$ [pulse], is compared with the reading of the pulse counter $Pulse_i^{out}$ [pulse] so as to generate position error. The position loop gain of the i^{th} joint transforms this position error into velocity input $Velocity_i^{in}$ expressed in pulse per second. The coefficient R_i converts $Velocity_i^{in}$ into a quantity in voltage $Volt_i^{in}$ [volt], which lies within the acceptable bounds of input to the servo pack.

Velocity sensor connected to the i^{th} joint reads the output velocity of the joint and sensor gain enhancer (SGE) conditions this signal to be compatible with voltage input $Volt_i^{in}$ [volt], so that the difference could be used to generate the velocity error at joint i. Velocity loop gain transforms velocity error into acceleration and two successive integrators convert acceleration into output position of joint i, θ_i^{in}.

The value of the conversion factor CF_i corresponding to i^{th} joint governs as

$$CF_i = \frac{N * N_i}{2\pi} \tag{2.4}$$

where N and N_i take the usual meaning as specified in Table 2.1.

2.2.4.2 Method B Method B is slightly different version of method A described in the above. Some changes of implementation architecture can be identified when comparing both schematic diagrams in Figs. 2.11 2.11 subjected to method A and Method B.

The details of a single decoupled servo joint are given in Fig. 2.11. Details are given including the control loop dynamics, working coordinate conversion methods and servo system parameters. These details are very important for those who doing designs or algorithm developments on software based servo architectures, robotics researchers and practitioners must have these internal constructional details to develop control strategies. The method is described below as per illustrated in Fig. 2.11.

The reference input θ_{in} [rad] is converted to $PULS_{in}$ [pulse] by conversion factor CF_i [pulse/rad]. Most control actions take place in pulse form in order to comply with the "pulse counter". The reference input $PULS_{in}$ is compared with actual output $PULSE_{Out}$ to get the position error. Then position error is multiplied by K_p [1/s] to get a velocity input VEL_{in} [pules/s]. Similarly, velocity input VEL_{in} is multiplied by conversion factor R to determine the control input $VOLT_{in}$ [Volt] to the servo controller. Respective gear reduction ratios are also used to convert link coordinates to motor shaft coordinates. Resolution of the pulse counter is applied to convert motor shaft coordinates to pulse numbers. Sensing reading is also used and conversion is made, convert it to physical quantities by using entities of R and RR commonly.

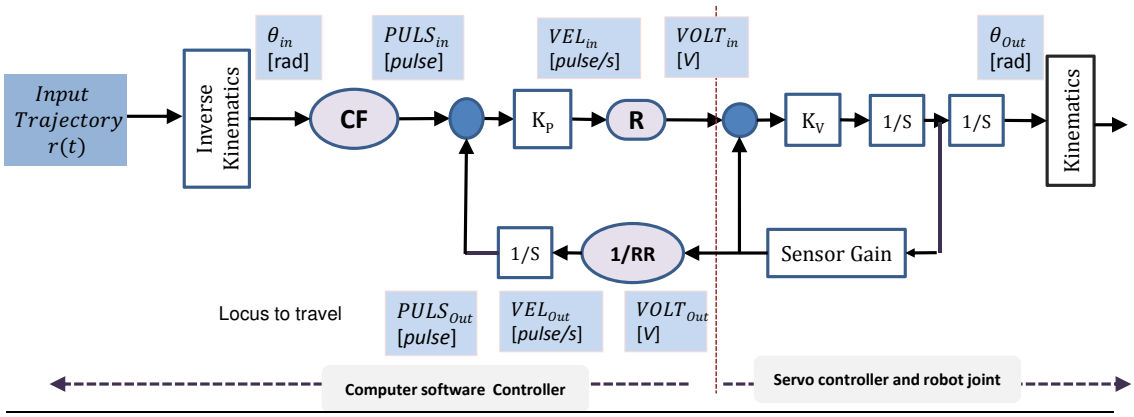

Control loop Dynamics			Control system parameters
θ_{in}	=> from traj. Planning	[rad]	N = 8192 pulse/Revolution
$PULS_{in}$ [*pulse*]	= θ_{in} * CF	[pulse]	N1,N2,N3 = 120,160,161 gear
VEL_{in} [*pulse/s*]	= K_p * ($PULS_{in}$ - $PULS_{Out}$)	[pulse]	reduction ratios of joint 1,2 and 3
$VOLT_{in}$ [*V*]	= R* VEL_{in}	[Volt]	CF1, CF2,CF3, = NN1/2Pi, NN2/2Pi, NN3/2Pi [pulse/rad]
VEL_{Out} [*pulse/s*]	= 1/RR * $VOLT_{Out}$	[pulse/s]	R1,R2,R3 = 0.000015161, 0.000012484, 0.000012169 [volt/rad/s]
$PULS_{Out}$ [*pulse*]	= $PULS_{Out}$ + VEL_{Out} * ts	[pulse]	RR = 0.0000366 [volt/rad/s]
Conversion to working co-ordinate system			
Velocity [rad/s] = Velocity [Volt/s] / (RR*CF_i) , Acceleration [rad/s^2] = Acceleration [Volt/s^2]/(RR*CF_i)			

Figure 2.11: Software Architecture of a Single Decoupled Servo Joint Mothod: B

Chapter 3

Evaluation of Force-free Control Models and Strategies

Model construction, evaluation and analysis of the two different strategies of force-free control (FFC) based on Lagrangian dynamics of industrial type robot arm are mainly discussed and presented in this chapter. Subsequently, detailed construction of dynamic properties of the FFC with relative mathematical models is illustrated with consistent simulations according to the real robot parameters. In addition to that comparison of force-free control (FFC) implemented using "Mass-point model" against an impedance control (IC) method in cartesian space is presented with comprehensive model based analysis and simulations for identifying unique characteristics of FFC against common impedance control method. The study of interaction forces between a robot arm and the environment is carried out. First, robot arm dynamic model for two link model and basic structure of force-free control method are described. Then two different force-free control architectures are illustrated. Two different force-free control strategies are force-free control by dynamic external torque (FFC-ET) and force-free control by dynamic torque independent compensation (FFC-TIC), respectively. Analysis of the each type of force-free control strategy is carried out for the single link and two links perspectives of industrial robot arm configurations by means of simulations under Matlab/Simulink environment. The model characteristics of the force-free control are exploited to discuss the application scenarios. Moreover, analysis of the force-free control dynamics is carried out by using real robot parameters throughout the simulations. Since, the force-free control deals with external forces applied on the robot arm, it can be used to illustrate the interactive and cooperative force control between a human and a robot arm by passive motion over an external force.

Further, simulation and analysis of the dynamic force-free control of robot arm based on revolute joints (articulated type) are presented through this chapter.

The model characteristics of the force-free control is utilized to demonstrate the autonomous safety action being taken by the robot arm in particular instances such as; when the robot insisting on an undesirable operation or a collision with an obstacle or an unusual dragging along the working objects. In each case, simulation results are obtained by adopting the force-free control on robot arms with industrial mechatronics controllers. Moreover, an analysis based on simulations is carried out by using real robot parameters in each scenario of interest.

This chapter also extended to presents the comparison of Force-Free Control (FFC) against an Impedance Control (IC) method in cartesian space. The study of interaction forces between a robot arm and an environment is carried out. Main objective of this investigation is to find how to regulate and tune force-free control for safe and feasible operation. And how proposed force-free control compliances against an external force given from the environment, and compares the behavior with general impedance control method. A concise description of analyzing procedure is given for modeling and simulation of a robot arm and also how it interacts with environment under force-free and impedance controls schemes. The modeling and comparison are made by adopting Matlab/Simulink environment. Furthermore, the intention is also focused to make use of actual industrial robots whose factory fitted dynamical control loops are not accessible.

3.1 Introduction

In the current context of designing control systems and robotics use of computers are unavoidable. Therefore, best and acceptable approach to use proper tools which can assist designers and engineers is to improve their creativity and efficiency. Hence, modeling and simulation have been recognized as a vital tool in designing systems including fields of robotics, mechatronics, automation etc. [72]. Simulation inherently allows user to investigate and analyze the structure, functions and characteristics of the system at different levels of the parameters and details [73].

However, tools can have different capabilities according to the level of requirement. And also we know that when complexity of the system under investigation increases the level of role and responsibility of the simulation become more critical. Industrial robot control systems are quite complex in nature. Hence, simulation tools mostly increase efficiency and accuracy throughout the cycle of the system development.

Through this chapter, author focuses on modeling and analysis of the force-free control (FFC) system by adopting Matlab/Simulink as a simulation tool. The importance of FFC is that it can be used to generate the flexible motion of the robot arm by applying an external force. It creates passive motion according to the applied force.

In [12] gives details of the FFC by using compensation coefficients approach which is only tested under experimental robot and no simulation studies are carried out to analyze the system behavior in detail.

Generally, robot arms are used in various fields of industries for many purposes, and the rigidity of robots must be kept and adaptive to a purpose. For instance, in

case of cutting and welding, the rigidity of robot arm must be kept high, because high accuracy is needed for the locus of a tip of the robot arm [17, 19, 75]. However, in some cases such as grinding or assembly operations rigidity of robot arms must be kept lower, because the flexible motion by external force is required [47, 66]. In general, industrial articulated robot arms however are designed with the high rigidity for application convenience of accurate positioning and contouring, those robot arms are not adaptable to flexible motion requirements such as grinding and assembling with pulling work out cases.

To realize flexible motion of robot arms in industries, a flexible device is attached to the tip of the robot arm, or a torque limit is induced to the joint actuator, which is named as "servo float method" [67, 68]. The servo float method is not so convenient to be realized in the industrial articulated robot arms as it needs to change the factory fitted servo controllers of robot arms. The other established force control methods such as impedance control and compliance control have been proposed to reduce the rigidity of robot arms are also described in [66, 69]. However, those methods are relatively complex and also required additional changes to the existing controllers of industrial robots.

By considering the above difficulties, applicability of FFC has been described by the several experimental cases in [74]. Gravity-free and friction-free conditions are desirable for implementation of the FFC on industrial robot arms. Under these conditions, the robot arm is actuated appropriately by an external force given by the operator or by the contact object. Therefore, realization of such conditions is the key point for implementing FFC. Hence, FFC has been realized by calculating objective joint positions according to the ideal motion activated by an external force. In the FFC, a robot arm is actuated as if it would be moved by an external force under zero-gravity and zero-friction conditions. In this chapter, first, detail theoretical explanation of the FFC and modeling and analysis of FFC are given by using simulation approach. Validity of the simulation is verified according to the theoretical development of the FFC and its different implementation paradigms.

3.1.1 Force-free control strategies based on Lagrangian dynamic models

This chapter merely dedicated on simulation and analysis of the force-free control (FFC) system by adopting Matlab/Simulink as a simulation tool [73]. The importance of the FFC is that it can be used to generate the flexible motion of the robot arm by applying an external force. It creates passive motion according to the applied force.

In [74] and references therein gives details of the FFC by using compensation coefficients approach which is only tested under experimental robot and no simulation studies are carried out to develop and evaluate the system behavior in detail.

Generally, robot arms are used in various fields of industries for many purposes, and the rigidity of robots must be needed and adaptive to a specific requirement. For instance, in case of cutting and welding, the rigidity of robot arm must be higher, because high accuracy is needed for the locus of a tip of the robot arm [17, 19]. However, in some cases such as grinding or assembly operations rigidity of robot arms must be maintained to be lower, because the flexible motion by external force is

required [66]. In general, industrial articulated robot arms are designed with the high rigidity for application convenience of accurate positioning and trajectory tracing, those robot arms are not adaptable to flexible motion requirements such as grinding and assembling with pulling work out cases as its original configuration. To realize the flexible motion of robot arms in industries, a flexible device is attached to the tip of the robot arm, or a torque limit is brought to the joint actuator also described in [67, 68]. Those torque limit or servo float method is not so convenient to be realized in the industrial articulated robot arms as it needs to change the factory fitted configurations of servo controllers. The other established force control methods such as impedance control and compliance control are proposed to reduce the rigidity of robot arms are similarly described in [66, 69]. But, those methods are relatively complex and also required additional changes to the existing controllers of industrial robots.

By considering the above difficulties and need of keeping original servo controller as it is, FFC is introduced by using several experimental cases in [12]. Two different implementation strategies of FFC are illustrated here, force-free control by external torque (FFC-ET) and force-free control by torque independent compensation (FFC-TIC), respectively. Zero-gravity and zero-friction conditions are desirable for implementation of FFC on industrial robot arms. Under these conditions, the robot arm is actuated properly by an external force given by the operator or by the contact object. Therefore, realization of such conditions is the key point for implementing FFC.

Hence, FFC is realized by calculating objective joint positions according to the ideal motion actuated by an external force. In both form of FFC, a robot arm is actuated as if it would be moved by an external force under zero-gravity and zero-friction conditions. This chapter also describes the details of theoretical explanation of FFC and the analysis of both forms of FFC strategies by using simulation over Matlab and Simulink. Validity of the each strategy based on simulation is verified according to the theoretical development of the respective FFC strategy.

3.1.2 Comparison of force-free control by a mass point concept model vs impedance control model

This chapter is also extended to describe a study on force-free control compared with an impedance control to find the control feasibility of the interaction forces of a simulated two link planar arm. The study of interaction forces between a robot arm and the environment is carried out. Main objective of this investigation is, how to regulate and tune force-free control for safe and feasible operation. And how proposed FFC compliances against an external force given from the environment [12], and also compare the behavior with general impedance control method [47]. Several historical reviews of the impedance control techniques are given in [77].

Modeling and simulation of a robot arm and how it interacts with the environment under force-free and impedance controls schemes are described concisely by analyzing the given procedures. The modeling and comparison are made by adopting Matlab/Simulink environment [73]. This research intention also focuses to make

use of actual industrial robots whose factory fitted dynamical control loops are not accessible, relevant details of the industrial type mechatronics servo controllers are illustrated in [19] .

In contrast with direct force control methods which can be used in practice where the maximum or threshold value of force to be exerted is known in advance [78], an indirect force control techniques can be found their way more attractive when it comes to scenario like unexpected collisions or contacts [47, 69]. It means that the robot and the environment should be able to protect themselves by compliance with each other. In most of the industrial robot applications main control action is given to the positioning of the end effector of the robot, however, it also important to control the interaction forces to ensure the safe and correct contacts with working objects. In this section, we concern about the impedance control as an established indirect force control method to compare the FFC method by adopting similar dynamical and external conditions. Impedance control focuses to control the dynamic behavior of the robot arm when contacting the environment [47]. Since, impedance control (IC) does not try to control the exact contact forces, it controls the properties of contact such as controls the stiffness and the damping of the interaction and desired steady-state force can also be set to a feasible maximum level [78]. In impedance control actually creates virtual new impedance for the robot arm.

With the FFC non-friction and non-gravity motion of the industrial arm can be realized and it also illustrated in [12, 76]. Non-friction merely refers to that friction forces included by motors and gears of each joint of the manipulator during operation are compensated as if it is mounted on a friction-less bearing. Non-gravity means that influence of the gravity to the dynamic model and the motion of the manipulator is compensated as if it would be in the space. However, FFC does not need the environment properties as impedance control so that model of an environment is not required, and also while controlling an external force, robot tool end can be assigned to a desired path to be moved during an external force applies from the environment.

The following steps are followed to achieve the above target. First, a mechanical model of the robot structure is created using Matlab/Simulink [73]. Then model based controller is created, which needs the correct mathematical model of the mechanical system in order to use with the decoupled and linearized version of the control system [45]. Thereafter, when the system is made to be linear, simple linear PD controllers can be adopted for joint control of the robot arm [45, 46]. And for impedance control implementation, a mathematical model of the environment is created to control the forces exerted on the manipulator [78].

To verify and test the system and control behavior, same input trajectory is referenced to the robot arm for each control method. That intentionally let the robot arm to hit the wall in both impedance and FFC scenarios. In this research, mass point type FFC method is used and the experimental scenario of the mass point type FFC is given in [79]. Finally, performance of the system and dynamic behaviors are observed while the robot arm is interacting with an external force. Each of the simulation and modeling task is carried out under Matlab/Simulink environment by considering total dynamics with gravity effect and friction for 2DOF 2-link planar

type robot arm [24].

The remaining sections of this chapter are organized as follows. In the next section, general characteristics of the dynamics and kinematics of industrial articulated type robot arms are presented. The dynamic equations are given for a two link revolute joint type robot arm. Then, general concept of the FFC is illustrated and subsequent section is given to explain the theoretical model of the FFC-ET and the FFC-TIC by including their individual properties. Afterward, the section is devoted to explain the simulation and analysis of each of the two FFC models under Matlab/Simulink integrated environment. And next some of the possible applications of the FFC and a complete section on comparison studies of FFC and IC are stated at last, and finally discussion is given followed by the conclusions at the end.

3.2 Force-free control and flexible motion realization

Control of a contact force is required in order to carry out assembling, handling, pulling and grinder operations. Although, it is difficult to control the contact force if the robot arm possesses the high rigidity. In this view, the property of the low rigidity for the industrial robot arms is required to control the contact force.

Similarly, flexible motion is also required for the safety operation such as control contact forces between the robot and human operator. Generally, an emergency shutdown switch is built in to the servo controller. If the operator happened to be trapped in-between the tip of the robot arm and the surrounding, then an emergency halt would be impossible or more danger. If the robot arm can be actuated with flexibility, the operator would be able to release from the danger occurrences.

In general, most of the industrial robot arms are manufactured for general purpose category due to cost aspects rather than special purpose custom designs. Therefore, some of the above flexibility requirements are to be accomplished by means of user made changes on industrial robots. However, such changes to the factory settings would be very expensive or at times need major technical guidance from the manufacturer as well. Therefore, the FFC control is suggested to realize flexible motion control of industrial robot arms without make changes to the existing controllers. The flexible motion is actuated by the external force given to the robot arm and of cause; force can be given by the human operator for safety purpose if needed. This chapter is basically concern about FFC and flexible motion for safety first and foremost.

A number of force control methods for the change of rigidity of robot arms are developed such as impedance control [67], compliance control [69], servo float method [68] which have been mainly listed as established proposed approaches. These methods are apparently good enough torque to the robot arm, respectively. However, to apply these methods in industry, there are technically difficult problems to be solved. For general purpose robots including the servo controller, most of these methods require changes of the control strategy in the servo controller. Most of the available methods for realization of flexible contact between the tip of the robot arm and the environment are almost carried out by attaching a flexible device on the tip of the robot arm.

In Yaskawa Co. servo float method is developed to realize flexible contact force

without flexible devices. The method limits the torque of each joint by setting the contact force. In the servo float method, the setting of the contact force is also depended upon applications. In addition, realization of servo float method modifies the factory fitted servo controller; hence the system change cost is rather high.

This section defines the modeling and simulation of FFC for flexible motion of general purpose industrial articulated robot arms without modification of the servo controller. The specified FFC is also applied to realize the desired vertical moment against the external force under Matlab/Simulink simulated environment by adopting exact real world parameters, and it is one of the expected flexible works.

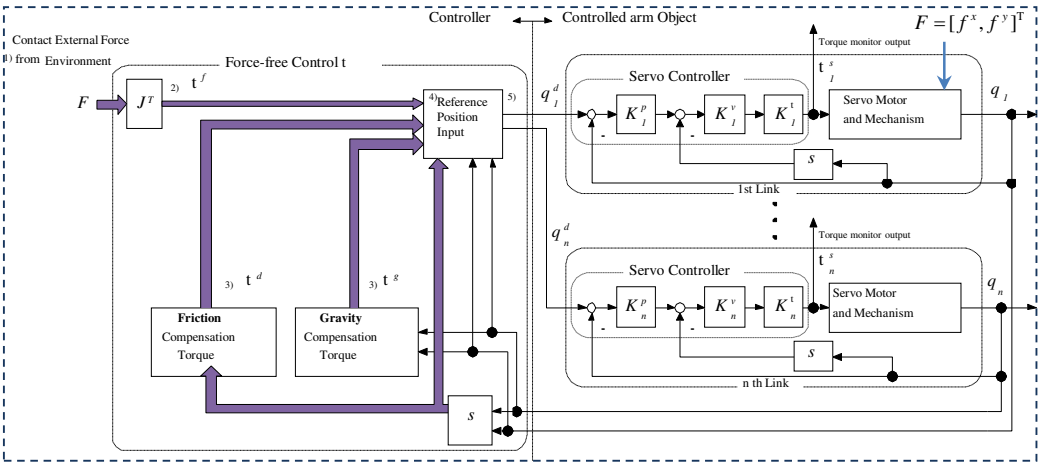

Figure 3.1: Schematic Diagram of Industrial Articulated Robot Arm with Force-free Controller.

3.2.1 Development of FFC concept and background

FFC can realize non-gravity and non-friction motion of industrial articulated robot arms. Since the robot arm is actuated by the attached motor, the robot arm behaves directly as it works under the external force.

In general "Impedance Control" is used in order to realize objective contact force [47]. It is constructed based on mechanical impedance which virtually exists between tip of the robot arm and external object. Therefore, impedance control mainly considers tip's flexibility of the robot arm. The FFC refers to total exerted force to the robot arm by use of torque monitor [12]. Therefore, FFC theoretically realizes more flexible motion on the robot arm compared with impedance control. In this research work, an external force is always considered to be applied on the tip of the robot arm for simulations. Mathematical explanation of FFC is described below.

3.2.2 FFC mathematical model using Lagrange dynamics

As illustrated in Fig. 3.1 the industrial articulated robot arm comprises of the articulated robot arm mechanism and the servo controller. Complete functional and implementation flow of FFC is cascaded in Fig. 3.2. The servo controller parameters

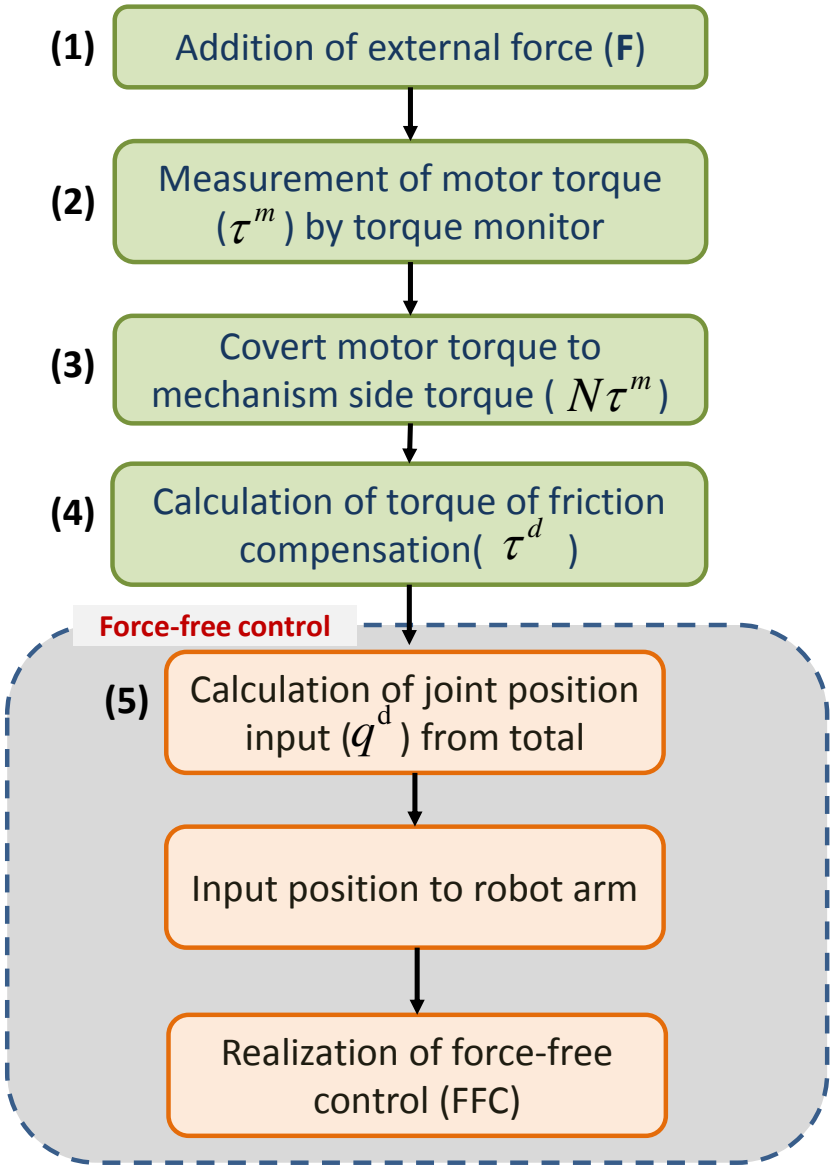

Figure 3.2: Functional and Implementation Flow Diagram of a Torque Monitor Based Force-free Controller.

K_i^p, K_i^p and K_i^p $(i = 1, ..., n)$ are position loop gain, velocity loop gain and torque constant, respectively [46].

The parameters q_i^d, q_i and τ_i^s $(i = 1, ..., n)$ are the inputs of joint angle, output of joint angle and input torque generated by the servo controller, respectively. The letter i is given for the link number. The general dynamic equation of the industrial type articulated robot arm including the servo controller is given by [47]

$$\mathbf{H}(\mathbf{q})\ddot{\mathbf{q}} + \mathbf{D}(\dot{\mathbf{q}}) + \mu\,\mathrm{sgn}(\dot{\mathbf{q}}) + \mathbf{h}(\mathbf{q},\ \dot{\mathbf{q}}) + \mathbf{g}(\mathbf{q}) = \mathbf{K}^{\tau}[\mathbf{K}^{v}\{\mathbf{K}^{p}(\mathbf{q}^{d} - \mathbf{q}) - \dot{\mathbf{q}}\}] \tag{3.1}$$

where $\mathbf{H}(\mathbf{q})$ is the inertia matrix, $D(\dot{\mathbf{q}})$ and $\mu\,\mathrm{sgn}(\dot{\mathbf{q}})$ are viscous and coulomb friction terms, $\mathbf{h}(\mathbf{q},\ \dot{\mathbf{q}})$ is the coupling nonlinear term and $\mathbf{g}(\mathbf{q})$ is the gravity matrix term [47], $\mathbf{q} = [q_1, ..., q_n]^T$ is the joint angles. Besides, $\mathbf{K}^p$ is a diagonal matrix of K_i^p and $\mathbf{K}^v$, $\mathbf{K}^{\tau}$ are diagonal matrices of K_i^v and K_i^{τ}, respectively. The input vector of joint angle $\mathbf{q}^d = [q_1^d, ..., q_n^d]^T$ is obtained in order to realize FFC by solving the right side of equation (3.1) as;

$$\mathbf{q}^d = (\mathbf{K}^p)^{-1}\big\{(\mathbf{K}^v)^{-1}(\mathbf{K}^{\tau})^{-1}(\boldsymbol{\tau}^f + \boldsymbol{\tau}^g + \boldsymbol{\tau}^d) + \dot{\mathbf{q}}\big\} + \mathbf{q}. \tag{3.2}$$

Where $\tau^f (= [\tau_1^f, ...\tau_n^f]^T)$ is the joint torque corresponding to the external force on the tip of the robot arm, $\boldsymbol{\tau}^g (= [\tau_1^g, ...\tau_n^g]^T)$ is the gravity compensation torque and $\boldsymbol{\tau}^d (= [\tau_1^d, ...\tau_n^d]^T)$ is the friction compensation torque. The joint torque corresponding to the external force is obtained by [46, 66]

$$\boldsymbol{\tau}^f = \mathbf{J}^T\mathbf{F} \tag{3.3}$$

where $\mathbf{F}$ is the external force vector and $\mathbf{J}^T$ is the Jacobian matrix. The friction compensation torque $(\boldsymbol{\tau}^d)$ is calculated by obtaining coefficients of viscous damping and coulomb static friction as;

$$\boldsymbol{\tau}^d = \mathbf{D}(\dot{\mathbf{q}}) + \mu\,\mathrm{sgn}(\dot{\mathbf{q}}) \tag{3.4}$$

where D is coefficients of viscous damping matrix, μ is coefficient of coulomb friction. The gravity compensation torque $(\boldsymbol{\tau}^g)$ is obtained by calculating from an instant posture and joint position of the robot arm by;

$$\boldsymbol{\tau}^g = \mathbf{g}(\mathbf{q}). \tag{3.5}$$

The FFC concept is that the flexible motion of the industrial articulated robot arm is realized by inputting the joint position $(\mathbf{q}^d)$ to the servo controller.

The inverse matrices $(\mathbf{K}^p)^{-1}$, $(\mathbf{K}^v)^{-1}$ and $(\mathbf{K}^{\tau})^{-1}$ are used as same value as inverse of servo gains $\mathbf{K}^p$, $\mathbf{K}^v$ and $\mathbf{K}^{\tau}$ of the servo controller. However, a manipulator's action can be affected if servo gains of either FFC or/and a servo controller are changed. The following steps described the sequence flow of the FFC algorithm.

1) External contact force $\mathbf{F} = [f^x,\ f^y]^T$ is detected by the force sensor.

2) Detected force is converted to joint torque by solving equation (3.3).

3) The friction compensation torque $(\boldsymbol{\tau}^d)$ and the gravity compensation torque $(\boldsymbol{\tau}^g)$ are calculated from position output and velocity output of servo mechanism by equations (3.4) and (3.5).

4) Position input ($\mathbf{q}^d$) is generated by the solving equation (3.2).

5) Finally, the position input ($\mathbf{q}^d$) is brought as the reference input for the servo controller.

That sequence flow is expressed for the FFC also briefs in the abstract. However, in real situations applied torque ($\boldsymbol{\tau}^s$) can be directly measured by use of a torque monitor device.

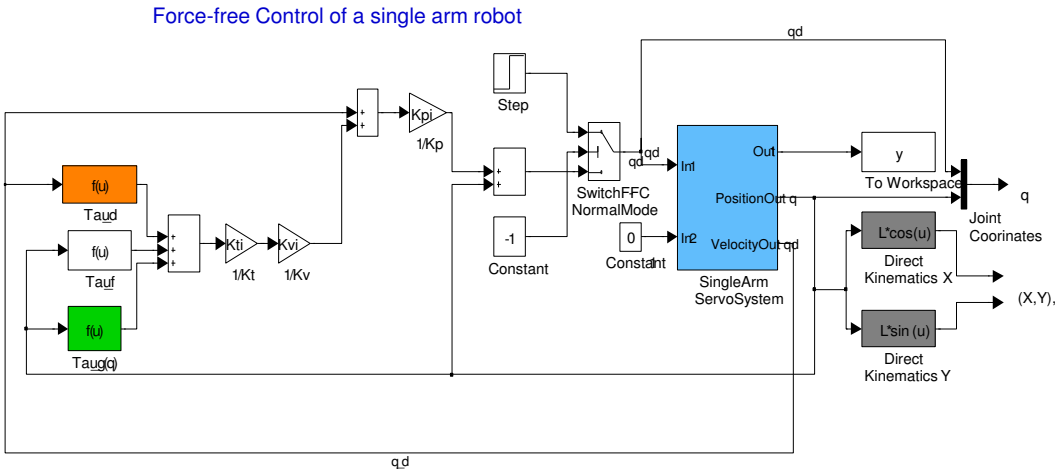

Figure 3.3: Diagram of Matlab/Simulink Model for Single Arm Robot with FFC.

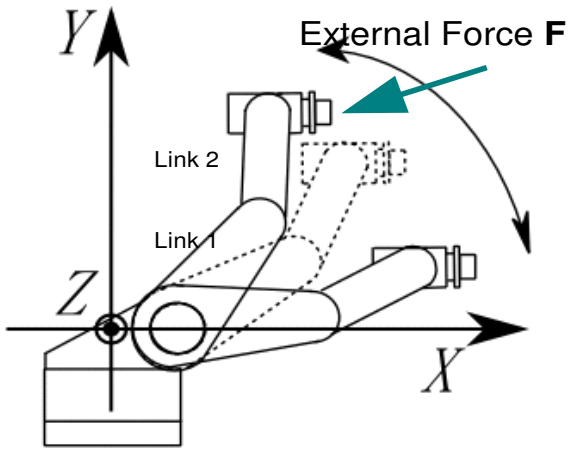

Figure 3.4: Schematic Diagram of the Robot Arm for FFC.

3.2.3 General FFC function and properties

The above mentioned procedure is generally used to realize the FFC conceptually. The basic idea behind the FFC method is the realization of the FFC by giving appropriate

position to the servo controller without modification of the original servo controller. Moreover, the robot arm would realize the desired motion by an external force because the inertia of the robot arm can be changed by modifying the reading of the torque monitor output. The FFC also controls the inherit stiffness of the robot arm same as that of appearing in the impedance control, which generates a control input to realize an ideal mechanical impedance model. In case of force-free control, a servo motor generates a torque equivalent to the external force by performing opposite operation of servo system. Figure 3.3 shows the implementation of the FFC under Matlab/Simulink environment.

In addition to that gravity compensation torque and friction compensation torque are added to the FFC block to achieve the torque equivalent to the external force. Therefore, FFC and established stiffness control algorithms are shown similar behaviors and action outputs, though they differ from the algorithm and the conceptual architecture from each other.

3.3 Simulations of force-free control technique

The entire simulation is carried out to mimic an actual articulated type robot arm (Performer-MK3s, YAHATA Electric Machinery MFG, CO., LTD.). A structure of an industrial articulated robot arm for the experiment is shown in Fig. 3.4. The simulation studies are carried out for active single arm (1-Link) and 2-DOF 2-Link cases. First, modeling and simulation are carried out for single arm case to verify the concept of FFC under Matlab/Simulink integrated environment by adopting real robot parameters. Then, simulation is accomplished for 2-link planar robot arm to observe and analyze the FFC for given external force, in which FFC flexible motion is confined only to the objective path of vertical 'Y'-direction by introducing constrain to the 'X'-direction.

3.3.1 Condition parameters for simulation

The articulated robot arm's physical parameters are set for the simulation consist of following specifications as; link lengths $l_1 = 0.25$[m], $l_2 = 0.215$[m] and masses of the links $m_1 = 2.86$[kg], $m_2 = 2.19$[kg]. The servo controller parameters are given as follows: The sampling interval set for simulation under Simulink ΔT =0.04 [s], simulation time is 5[s], position loop gains were $\mathbf{K}_1^p = \mathbf{K}_2^p = 25$[1/s], velocity loop gains were $\mathbf{K}_1^v = \mathbf{K}_2^v = 150$ [1/s], torque constants are $\mathbf{K}_1^\tau = 0.1045$ [Nm/(rad/s^2)], $\mathbf{K}_2^\tau = 0.0605$ [Nm/(rad/s^2)], friction coefficients of viscous damping are $D_1 = 4.68$ [Nms/rad], $D_2 = 2.72$[Nms/rad], coefficients of coulomb friction are μ_1= 0.5 [Nm], μ_2 = 0.5 [Nm]. Coefficients of viscous damping and coefficients of coulomb friction are taken from the Performer MK3s parameters. Gear ratios are used as $Gr_1 = 160$ and $Gr_2 = 160$ for link 1 and 2, respectively as per Performer MK3s robot.

3.3.2 Simulation results of basic FFC for 1-link robot arm scenario

Modeling and simulation of general FFC algorithm and behavior are the main aspect in this section. Therefore, validation of the FFC algorithm is verified by using 1-link robot arm which comprises of real industrial type parameters. Different kinds of

external force scenarios are applied to analyze the output of the FFC implementation. Figure 3.3 also illustrates the switching of position control and FFC. Initially, step reference is applied then, at the time of 2[s], an external force is applied as in Fig. 3.5 in order to analyze the simulation in Matlab/Simulink for the single arm robot case. Furthermore, research is carried out for 2-link case to illustrate the application of FFC for achieving safety by reducing stiffness under danger circumstances. In such case, passive movement is achieved the robot arm by applying an external force to desired direction.

Simulation result of 1-link robot arm is shown in Figs. 3.5 and 3.6. According to the total system diagram shown in Fig. 3.3, the joint torque is calculated from equation (3.3) as external force components, joint torque is generated according to the external force. The friction compensation and gravity compensation torques are obtained with respect to the equations (3.4) and (3.5) respectively. The concept of the FFC and the passive motion under an external force are calculated using equation (3.2). Figure 3.5 shows simulation result obtained from the 1-link robot arm under FFC activated after 2[s].

Position variation according to the external force can be seen in the X-Y plot against time. Figure 3.5 realizes the FFC algorithm by simulation. Figure 3.6 shows the robot joint position against input joint angle under FFC after 2[s] in the total time. A continuous step type external force is given to the robot arm; hence FFC algorithm generates the required joint position in order to execute the flexible motion and movement of the robot arm is realized as shown in Fig. 3.7 as X vs Y graph.

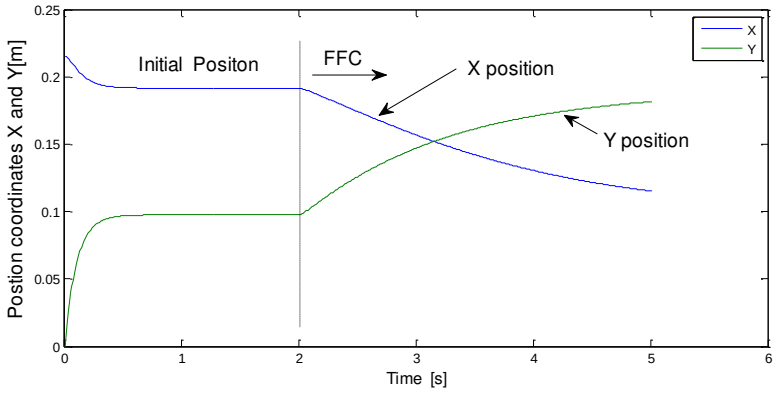

Figure 3.5: Flexible Motion Due to FFC.

3.3.3 Simulation force-free control (FFC) for 2-link robot arm scenario

Figures 3.8 to 3.10 illustrate the simulations carried out on the 2-link robot arm under FFC applied on impact type external force. Figure 3.8 shows the case of sudden applied external force and corresponding torques generated on respective joints. Figure 3.9 is given for joint angle trajectory generated by FFC and corresponding robot joint angles and control toque generated by the robot controller under the action of

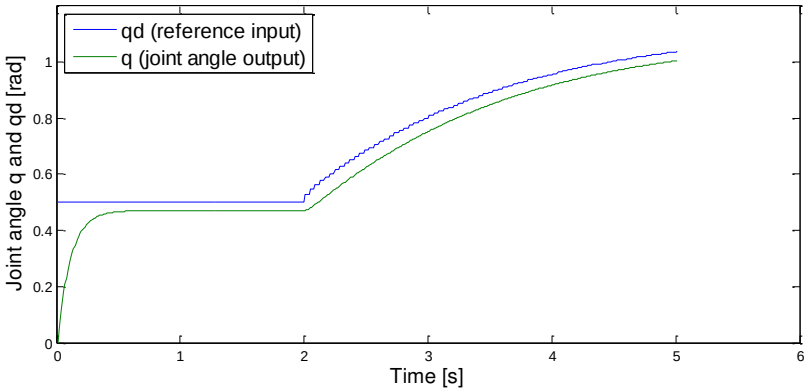

Figure 3.6: Reference Position and Joint Position.

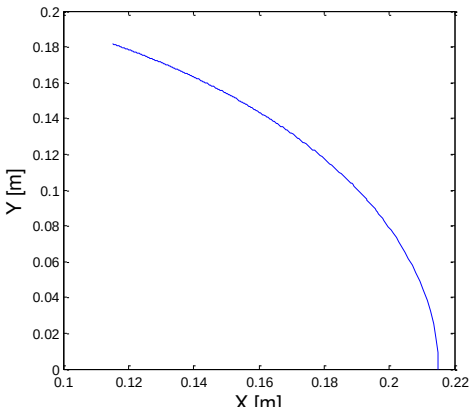

Figure 3.7: Position Plot X and Y.

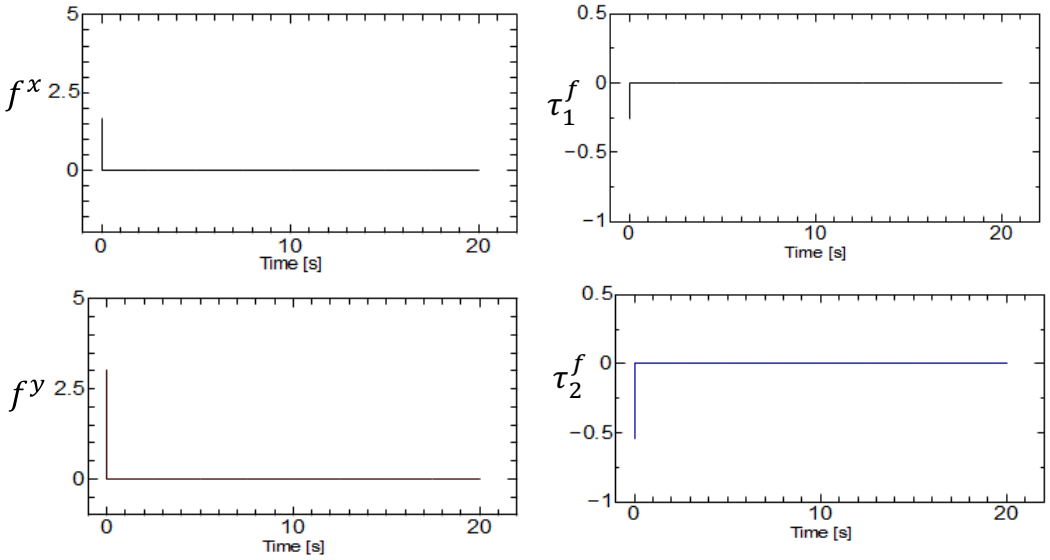

Figure 3.8: External Force ($\mathbf{F}$) and Generated Torque ($\boldsymbol{\tau}^f$).

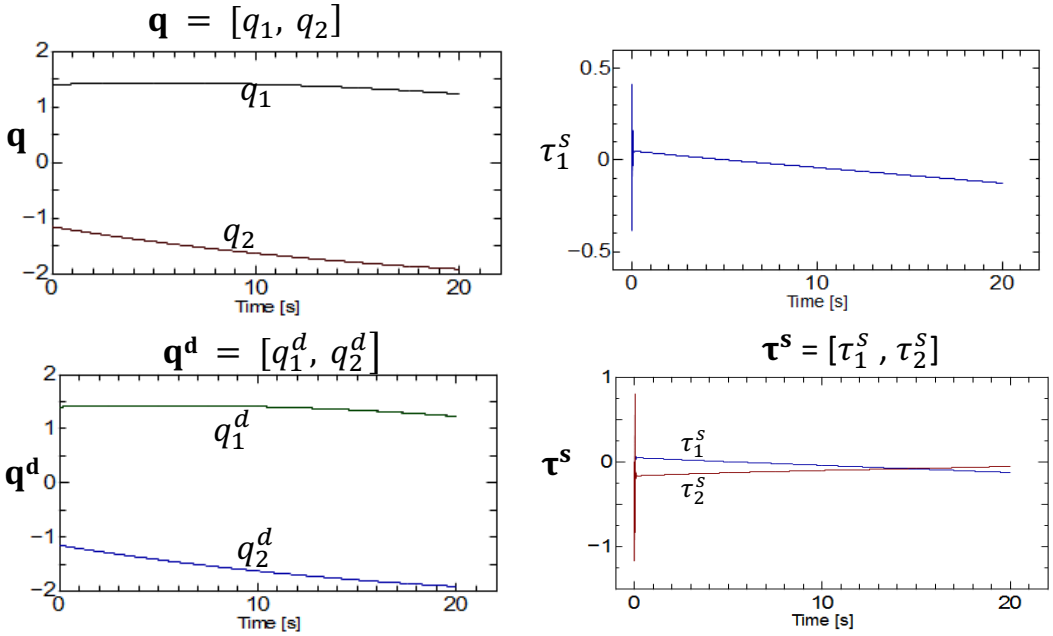

Figure 3.9: Joint Angles ($\mathbf{q}, \mathbf{q^d}$) and Generated Torque ($\boldsymbol{\tau}^s$).

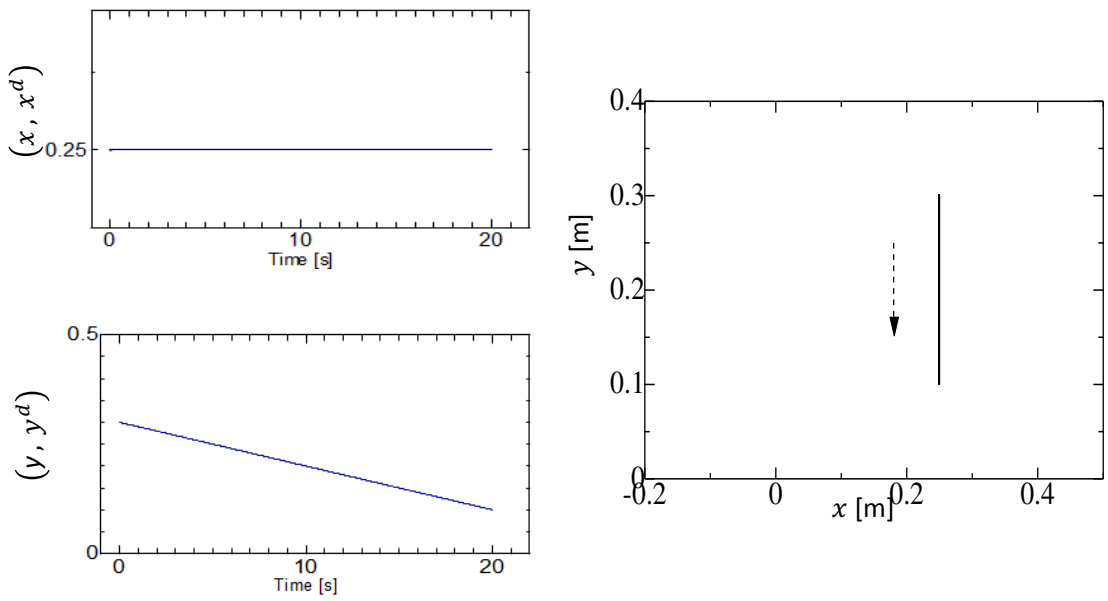

Figure 3.10: Time Trajectory and $(x,\ y)$ Plot of the Tip Position.

FFC. Figure 3.10 indicates the result trajectory of the tip position of the robot arm by applying FFC technique for desired vertical direction and hence, movement of X-direction is constrained. Therefore, FFC is verified for passive motion for desired direction. Then it is given the idea of adaptability of safety under undesirable operating circumstances such as; user might be trapped between the robot arm and the fence wall. Hence, user can apply an external force to part of the robot body to move away it from the user if the FFC is implemented for safety purposes by providing consistent switching mechanism.

3.4 Dynamics and derivations of two different force-free control strategies

In this section a brief overview of the robot kinematics, dynamics and also the required mathematical representation models are presented. Equations are given for two link articulated type robot arm. Two distinct approaches of FFC, force-free control by external torque (FFC-ET) and force-free control by torque independent compensation (FFC-TIC) concepts are described in subsequent sections in which mathematical models of the each type of FFC are explained, including distinguish and highlighted properties of which some of them already explained in section 3.2.2.

3.4.1 Derivation of force-free control mathematical models

In general, dynamic equation of the industrial articulated robot arms is given as in section 3.2.2:

$$\mathbf{H}(\mathbf{q})\ddot{\mathbf{q}} + \mathbf{h}(\mathbf{q},\ \dot{\mathbf{q}}) + \mathbf{D}\dot{\mathbf{q}} + \mu\,\mathrm{sgn}\,(\dot{\mathbf{q}}) + \mathbf{g}(\mathbf{q}) = \boldsymbol{\tau}^s \tag{3.6}$$

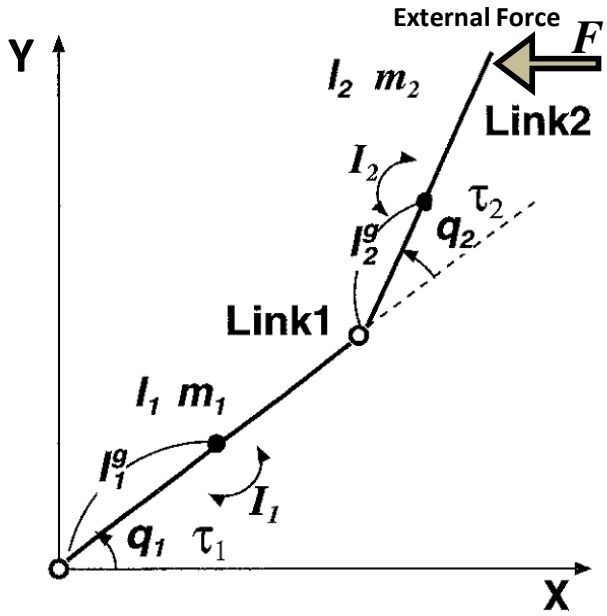

Figure 3.11: Schematic Diagram of 2-link Articulated Type Robot Arm

where $\mathbf{H}(\mathbf{q})\ddot{\mathbf{q}}$ is the inertia matrix, $\mathbf{D}\dot{\mathbf{q}}$ and $\mu\,\mathrm{sgn}\,(\dot{\mathbf{q}})$ are viscous and coulomb friction terms, $\mathbf{h}(\mathbf{q},\ \dot{\mathbf{q}})$ is the coupling nonlinear term (Coriolis and centrifugal force vector), $\mathbf{g}(\mathbf{q})$ is the gravity matrix term, $\boldsymbol{\tau}^s$ is the input torque to the robot arm joints and $\mathbf{q}$ is the joint position vector [47]. An industrial articulated robot arm comprises of the articulated robot arm mechanism and the servo controller. The servo controller parameters ${K_i}^p$, ${K_i}^v$ and ${K_i}^\tau$ $(i = 1, \cdots, n)$ are position loop gain, velocity loop gain and torque constant, respectively [10, 19, 46]. A schematic diagram of a 2-link revolute joint type robot arm is shown in Fig. 3.11. The parameters ${q_i}^d$, q_i and ${\tau_i}^s$ (or ${t_i}^s$) $(i = 1, \cdots, n)$ are the inputs of joint angle, output of joint angle and input torque generated by the servo controller as in Fig. 3.12, respectively. The letter i is given for the link number of the robot.

Therefore, from section 3.2.2 general dynamic equation of the industrial type articulated robot arm including the servo controller is given by equation (3.7) and then relationship is obtained as equation (3.8), describes in [19].

$$\mathbf{H}(\mathbf{q})\ddot{\mathbf{q}} + \mathbf{D}(\dot{\mathbf{q}}) + \mu\,.\mathrm{sgn}(\dot{\mathbf{q}}) + \mathbf{h}(\mathbf{q},\ \dot{\mathbf{q}}) + \mathbf{g}(\mathbf{q}) = \mathbf{K}^\tau[\mathbf{K}^v\{\mathbf{K}^p(\mathbf{q}^d - \mathbf{q}) - \dot{\mathbf{q}}\}] \tag{3.7}$$

$$\boldsymbol{\tau}^s = \mathbf{K}^\tau[\mathbf{K}^v\{\mathbf{K}^p(\mathbf{q}^d - \mathbf{q}) - \dot{\mathbf{q}}\}] \tag{3.8}$$

A simple conceptual explanation of FFC is shown in Fig. 3.13. In Fig. 3.13, left-hand side shows the ideal scenario of FFC where a virtual robot arm is connected to a zero-friction bearing in zero-gravity space. The right-hand side of Fig. 3.13 shows an actual robot arm which is driven by a motor in normal space under the influence of gravity and friction. On the left-hand side, when an external force is applied at the tip of the virtual robot arm, it rotates like on the friction-free bearing. However,

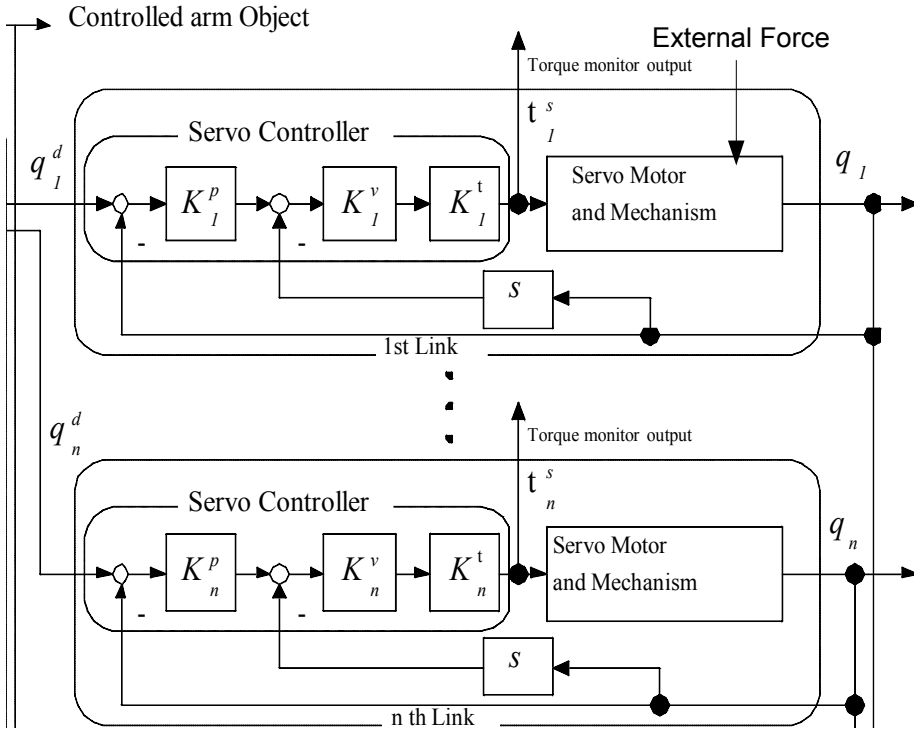

Figure 3.12: Industrial Type Servo Controllers for n-link Robot Arm

on the right hand side, the actual robot arm is not actuated by an external force because it is connected to a motor axis through a gear under gravity and friction. By FFC, motion data on the left-hand side are sent to the motor on the right-hand side. Hence, the actual robot arm on the right-hand side is moved as if it would be actuated by an external force under zero-gravity and zero-friction conditions.

The FFC concept is then derived theoretically by applying gravity and friction compensation torques to the servo controller, $\boldsymbol{\tau}^g$ $(= [{\tau_1}^g, \cdots, {\tau_n}^g]^T)$ is the gravity compensation torque and $\boldsymbol{\tau}^d$ $(= [{\tau_1}^d, \cdots, {\tau_n}^d]^T)$ is the friction compensation torque.

The friction compensation torque $(\boldsymbol{\tau}^d)$ is calculated by adopting coefficients of viscous damping and coulomb static friction as,

$$\boldsymbol{\tau}^d = \mathbf{D}(\dot{\mathbf{q}}) + \mu\,\mathrm{sgn}(\dot{\mathbf{q}}) \tag{3.9}$$

where $\mathbf{D}$ is coefficient of viscous damping matrix, μ is coefficient of coulomb friction. The gravity compensation torque $(\boldsymbol{\tau}^g)$ is obtained by calculating from the instant posture and joint position of the robot arm by,

$$\boldsymbol{\tau}^g = \mathbf{g}(\mathbf{q}) \tag{3.10}$$

Thus the FFC concept is that flexible motion of the industrial articulated robot arm is realized by entering the joint position $(\mathbf{q}^d)$ to the robot servo controller as the reference position input. Therefore, corresponding joint position is calculated by taking inverse effect of the servo controller.

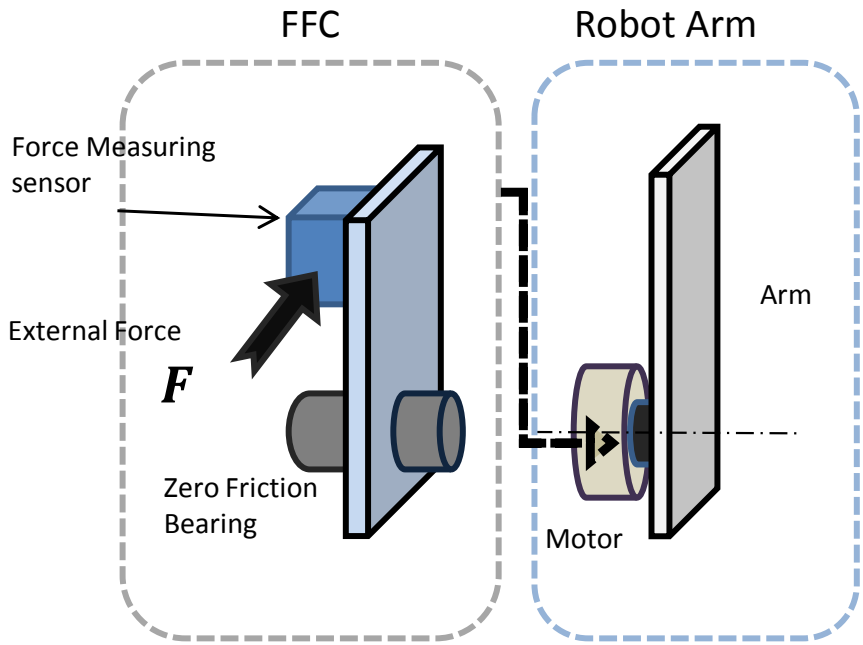

Figure 3.13: Conceptual Illustration of Force-free Control Principle

The inputs of joint angles $\mathbf{q}^d$ $(= [{q_1}^d, \cdots, {q_n}^d]^T)$ are obtained in order to realize FFC by solving the right side of equation (3.8) as already described in section 3.2.2;

$$\mathbf{q}^d = (\mathbf{K}^p)^{-1}(\mathbf{K}^v)^{-1}(\mathbf{K}^\tau)^{-1}(\boldsymbol{\tau}^f + \boldsymbol{\tau}^g + \boldsymbol{\tau}^d) + \dot{\mathbf{q}} + \mathbf{q} \tag{3.11}$$

where $\boldsymbol{\tau}^s = (\boldsymbol{\tau}^f + \boldsymbol{\tau}^g + \boldsymbol{\tau}^d)$ and $\mathbf{q}$ $(= [q^d, \cdots, {q_n}^d]^T)$ is the joint angles. Besides, $\mathbf{K}^p$ is a diagonal matrix of ${K_i}^p$ and $\mathbf{K}^v$, $\mathbf{K}^\tau$ are diagonal matrices of ${K_i}^v$ and ${K_i}^\tau$, respectively.

3.4.2 FFC-ET type structure and properties

The base equations of the FFC-ET type control strategy are equations (3.1), (3.7), (3.8) and (3.11). Therefore, FFC-ET control scheme can be reduced to an ideal characteristic form as:

$$\mathbf{H}(\mathbf{q})\ddot{\mathbf{q}} + \mathbf{h}(\mathbf{q},\ \dot{\mathbf{q}}) = \boldsymbol{\tau}^f. \tag{3.12}$$

Ideal scenario describes, the inertial torque compensation is done by means of the external toque due to applied external force. Following steps explain the implementation flow of the FFC-ET strategy.

1) Contact force $(\mathbf{F} = [f^x,\ f^y]^T)$ is detected by the force sensor.

2) Detected force is converted to the joint torque $(\boldsymbol{\tau}^f)$ by using the Jacobian matrix as equation (3.18).

3) The friction compensation torque $(\boldsymbol{\tau}^d)$ and the gravity compensation torque $(\boldsymbol{\tau}^g)$ are calculated from position output and velocity output of the servo motor by

equation (3.9) and (3.10).

4) Position input ($\mathbf{q}^d$) is generated by solving equation (3.11).

5) Finally, the position input ($\mathbf{q}^d$) is brought in as the reference input for the servo controller.

3.4.3 FFC-TIC type structure and properties

This category of FFC is derived similarly by using general dynamics equations described as in above sections with an external force added is given by,

$$\mathbf{H}(\mathbf{q})\ddot{\mathbf{q}} + \mathbf{D}(\dot{\mathbf{q}}) + \mu\,\mathrm{sgn}(\dot{\mathbf{q}}) + \mathbf{h}(\mathbf{q},\ \dot{\mathbf{q}}) + \mathbf{g}(\mathbf{q}) = \boldsymbol{\tau}^s + \boldsymbol{\tau}^f. \tag{3.13}$$

The servo controller torque is modeled as;

$$\boldsymbol{\tau}^s = \mathbf{K}^\tau[\mathbf{K}^v\{\mathbf{K}^p(\mathbf{q}^d - \mathbf{q}) - \dot{\mathbf{q}}\}] + \boldsymbol{\tau}^{\mathbf{d}} + \boldsymbol{\tau}^{\mathbf{g}} - \boldsymbol{\tau}^{\mathbf{f}}. \tag{3.14}$$

The total dynamic equation of an industrial articulated robot arm including the servo controller is given by substituting equations (3.13) and (3.14),

$$\mathbf{H}(\mathbf{q})\ddot{\mathbf{q}} + \mathbf{h}(\mathbf{q},\ \dot{\mathbf{q}}) = \mathbf{K}^\tau[\mathbf{K}^v\{\mathbf{K}^p(\mathbf{q}^d - \mathbf{q}) - \dot{\mathbf{q}}\}]. \tag{3.15}$$

FFC-TIC means that the effect of inertia, friction and gravity to the robot arm motion can be assigned as linear combinations with arbitrary coefficients; see [12] and references there in. Details of algorithm and implementation flow is given in Fig. 3.14. Therefore, dynamics of FFC-TIC is described by;

$$\mathbf{H}(\mathbf{q})\ddot{\mathbf{q}} + \mathbf{h}(\mathbf{q},\ \dot{\mathbf{q}}) = \sigma^f\,\boldsymbol{\tau}^f + \sigma^d\,\boldsymbol{\tau}^d + \sigma^g\,\boldsymbol{\tau}^g \tag{3.16}$$

where σ^f, σ^d and σ^g are coefficients of independent compensation. From equations 3.14 and 3.15, it can be shown that following relationship exists;

$$\boldsymbol{\tau}^f = -\{\boldsymbol{\tau}^s - \boldsymbol{\tau}^d - \boldsymbol{\tau}^g - (\mathbf{H}(\mathbf{q})\ddot{\mathbf{q}} + \mathbf{h}(\mathbf{q},\ \dot{\mathbf{q}}))\}. \tag{3.17}$$

High level Matlab/Simulink diagram is given in Fig. 3.15 in which FFC-ET and FFC-TIC modules are presented with the single arm industrial servo controller model.

3.5 Simulation of force-free control (FFC) strategies

3.5.1 Simulation setup for FFC-ET and FFC-TIC

Simulation is carried out to by using actual articulated type robot parameters (Performer-MK3s, YAHATA Electric Machinery MFG, CO., LTD.). A detailed structure of an industrial articulated robot arm mechanism with a servo controller is given in Fig. 3.12. The simulation studies are carried out for an active single arm and a 2 DOF 2-Link cases. First, modeling and simulation are carried out for single arm case to verify the concept of FFC under Matlab/Simulink integrated environment by adopting real robot configuration and parameters. Then, simulation is accomplished for 2-link planar robot arm to observe and analyze both form of FFC for the given external force, in which FFC flexible motion is obtained for 'X' and 'Y' directions.

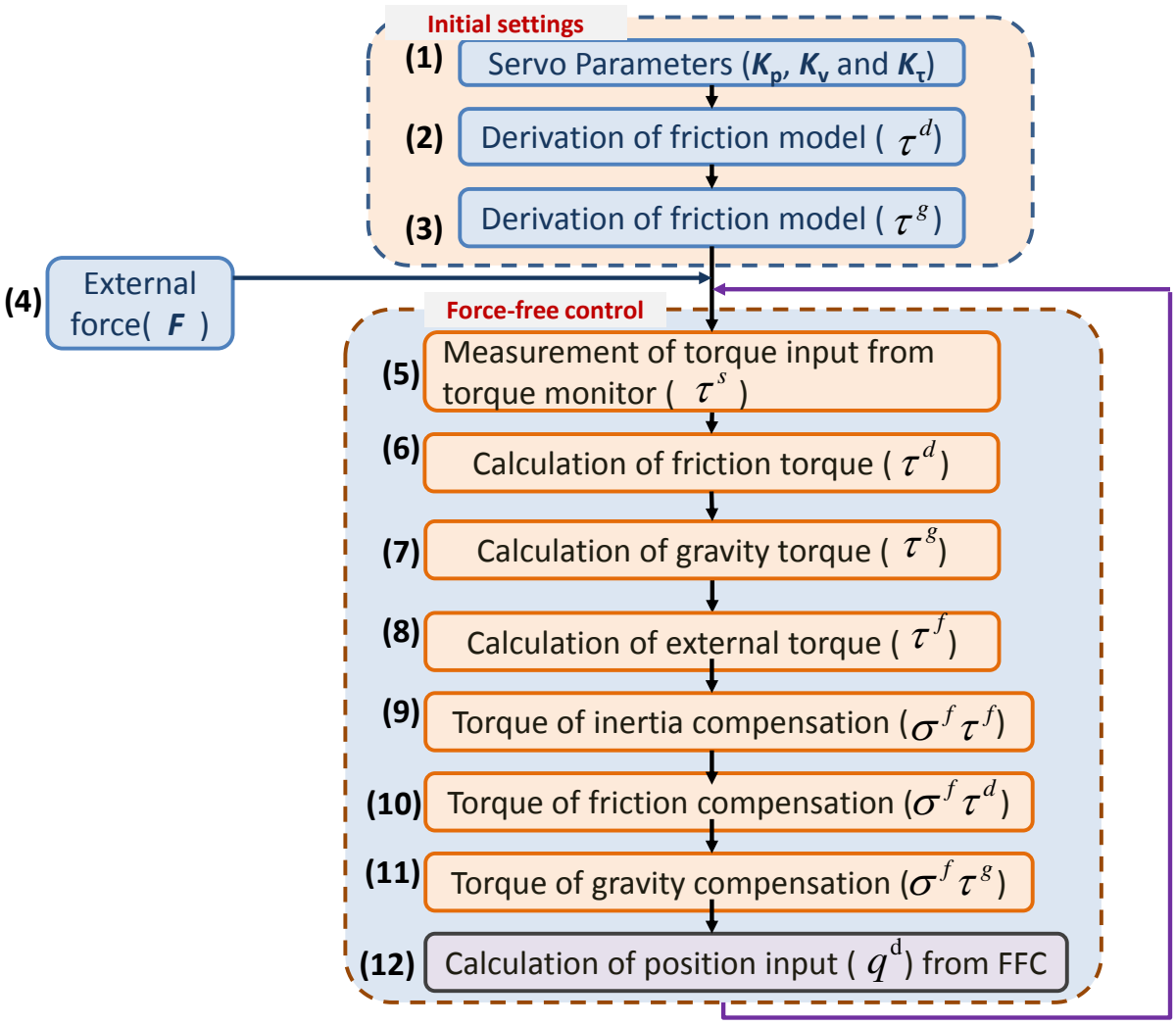

Figure 3.14: Algorithm with Implementation Flow Diagram of FFC-TIC

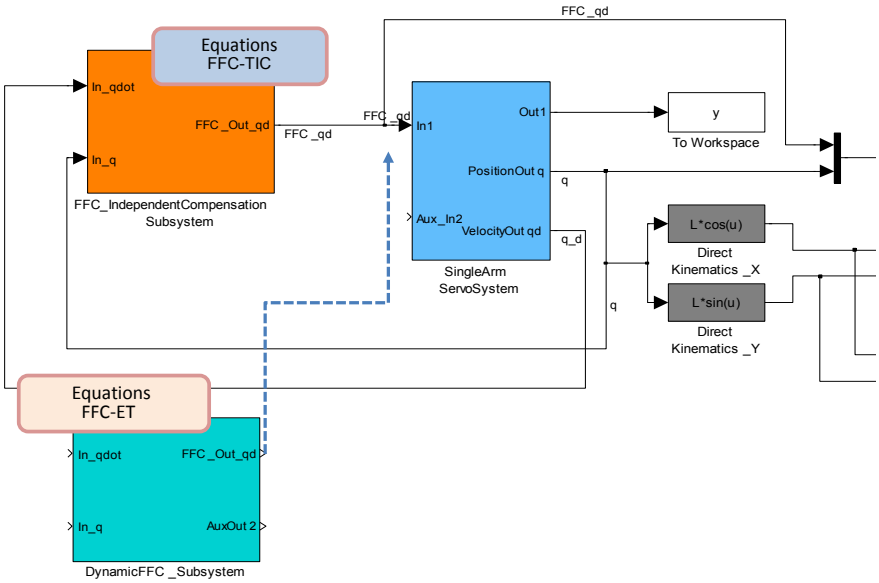

Figure 3.15: Simulink High Level Model Diagram of FFC-ET and FFC-TIC

The schematic view example of an articulated type robot arm with 2-links having two degrees of freedom is shown in Fig. 3.11. The required matrix vector parameters are obtained as follows:

$$\mathbf{H}(\mathbf{q}) = \begin{bmatrix} H_{11} & H_{12} \\ H_{21} & H_{22} \end{bmatrix}$$

$$\begin{aligned} H_{11} &= m_1(l_1^g)^2 + m_2\{(l_1)^2 + 2l_1 l_2^g \cos q_2 + (l_2^g)^2\} + I_1 + I_2 \\ H_{12} &= m_2 l_1 l_2^g \cos q_2 + m_2(l_2^g)^2 + I_2 \\ H_{21} &= I_2 + m_2\{(l_2^g)^2 + l_1 l_2^g \cos q_2\} \\ H_{22} &= m_2(l_2^g)^2 + I_2 \end{aligned}$$

$$\mathbf{h}(\mathbf{q}, \dot{\mathbf{q}}) = \begin{bmatrix} -m_2 l_1 l_2^g \{2\dot{q}_1\dot{q}_2 + (\dot{q}_2)^2\} \sin q_2 \\ m_2 l_1 l_2^g \dot{q}_1 \dot{q}_2 \sin q_2 \end{bmatrix}$$

$$\mathbf{g}(\mathbf{q}) = \begin{bmatrix} m_1 g l_1^g \cos q_1 + m_2 g\{l_1 \cos q_1 + l_2^g \cos(q_1 + q_2)\} \\ m_2 g l_2^g \cos(q_1 + q_2) \end{bmatrix}$$

$$\mathbf{D} = \begin{bmatrix} D_1 & 0 \\ 0 & D_2 \end{bmatrix} \qquad \mu = \begin{bmatrix} \mu_1 & 0 \\ 0 & \mu_2 \end{bmatrix}$$

The $\boldsymbol{\tau}^f$ $(= [{\tau_1}^f, \cdots, {\tau_n}^f]^T)$ is the joint torque corresponding to the external force $\mathbf{F}$ acting on the tip of the robot arm. The joint torque corresponding to the external force is obtained as follows [46]:

$$\boldsymbol{\tau}^f = \mathbf{J}^T \mathbf{F} \tag{3.18}$$

$$\mathbf{J}(\mathbf{q}) = \begin{bmatrix} l_1 \sin q_1 - l_2 \sin(q_1 + q_2) & -l_2 \sin(q_1 + q_2) \\ l_1 \cos q_1 + l_2 \cos(q_1 + q_2) & l_2 \cos(q_1 + q_2) \end{bmatrix}$$

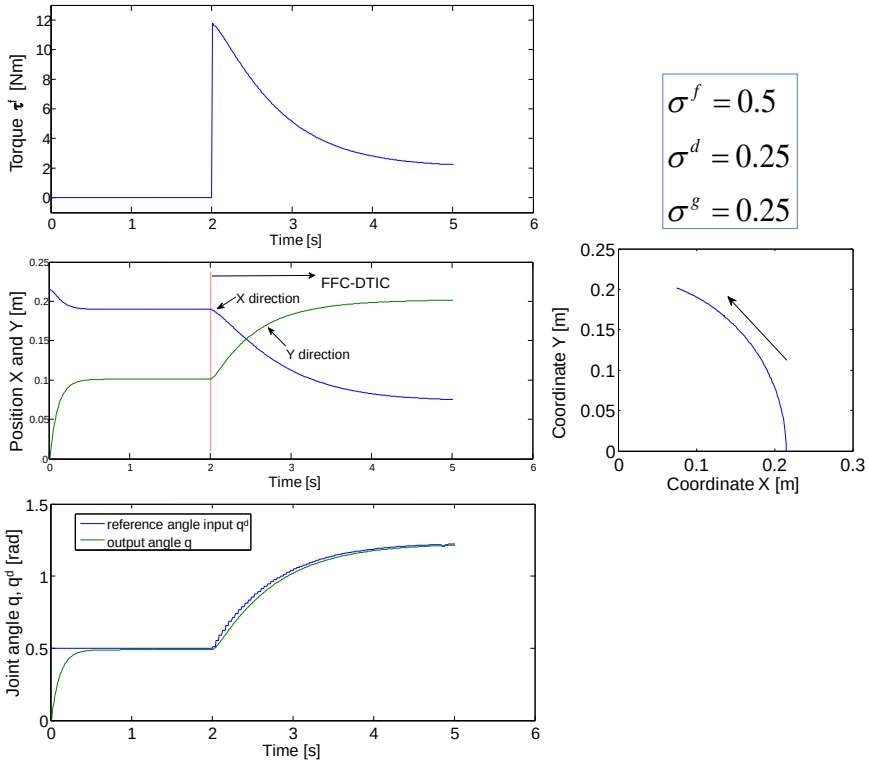

Figure 3.16: Simulation Results for FFC-TIC, External Force ($\mathbf{F} = [\mathbf{15}, \mathbf{70}]^{\mathbf{T}}$N)

where $\mathbf{F}$ is the external force vector and $\mathbf{J}$ is the Jacobian matrix. The articulated robot arm's physical parameters set for the simulation have following specifications as; link lengths $l_1 = 0.25$ [m], $l_2 = 0.215$ [m], ${l_1}^g = (1/2)\, l_1$, ${l_2}^g = (1/2)\, l_2$ and masses of the links $m_1 = 2.86$ [kg], $m_2 = 2.19$ [kg]. I_1 and I_2 are moment of inertia along the center of gravity of link 1 and 2. The servo controller parameters are given as follows: The sampling interval set for simulation under Simulink $\Delta t = 0.04$ [s], simulation time is 5[s], position loop gains are ${K_1}^p = {K_2}^p = 25$ [1/s], velocity loop gains are ${K_1}^v = {K_1}^v = 150$ [1/s], torque constants are ${K_1}^\tau = 0.1045$ [Nm/(rad/s2)], ${K_2}^\tau = 0.0605$ [Nm/(rad/s2)], friction coefficients of viscous damping are $D_1 = 4.68$ [Nms/rad], $D_2 = 2.72$ [Nms/rad] and coefficients of coulomb friction are $\mu_1 = 0.5$ [Nm], $\mu_2 = 0.5$ [Nm]. Coefficients of viscous damping and coefficients of coulomb friction are taken from the Performer MK3s parameters. Gear ratios are used as $Gr_1 = 160$ and $Gr_2 = 160$ for link 1 and 2, respectively as per Performer MK3s robot.

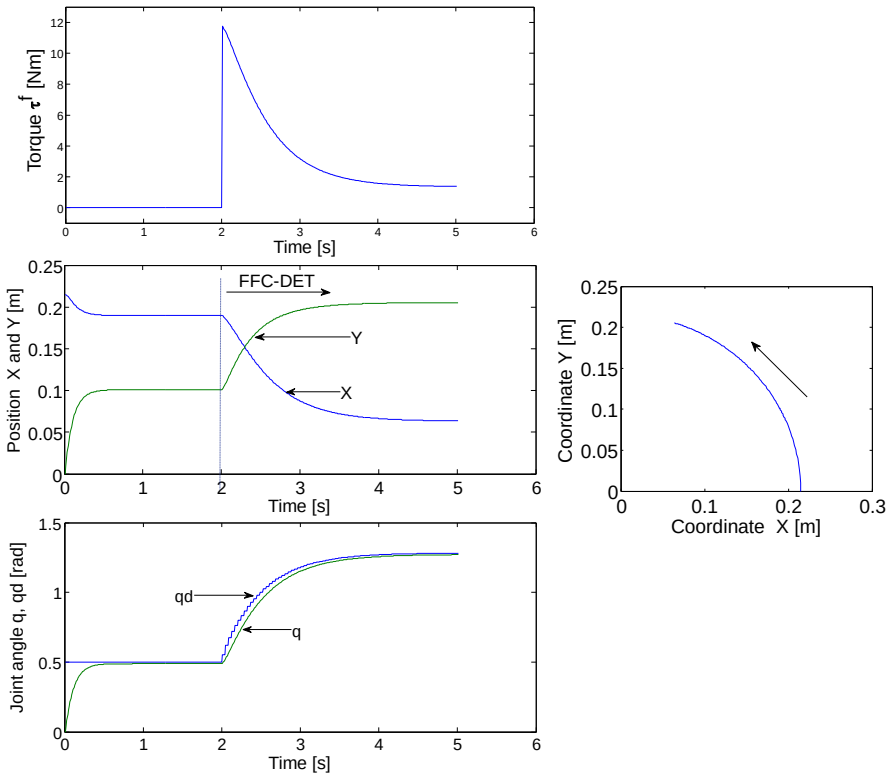

Figure 3.17: Simulation Results for FFC-ET, External Force ($\mathbf{F} = [\mathbf{15}, \mathbf{70}]^{\mathbf{T}}$N)

3.5.2 Simulation results of FFC-ET and FFC-TIC

Simulation and analysis of the two different FFC algorithms are the main aspect in current section. Therefore, validation of the each FFC algorithm is verified by using single arm robot which comprises of real industrial type parameters. For single link simulation, link 2 parameters of the Performer MK3s are taken. Different kinds of external force scenarios are applied to analyze the output of expected passive movement with respect to the external force for each FFC strategy.

Initially, step reference is applied and then, at the time of 2 [s], an external force is applied as in Figs. 3.16 and 3.17 in order to analyze the behavior of FFC via simulation in Matlab/Simulink for each FFC models with the same robot arm parameters and servo configurations. Furthermore, simulation research is also carried out for 2-link case to illustrate the non-linear behavior for both FFC-ET and FFC-TIC strategies and results are illustrated in Figs. 3.18 and 3.19. External force signal is generated by means of Matlab/Simulink signal generator block with added 1% random noise.

3.5.3 Important characteristics of simulation results

In 2-link robot arm scenario, passive motion based on external forces under FFC can be configured to an objective trajectory. Therefore, FFC-ET and FFC-TIC can be

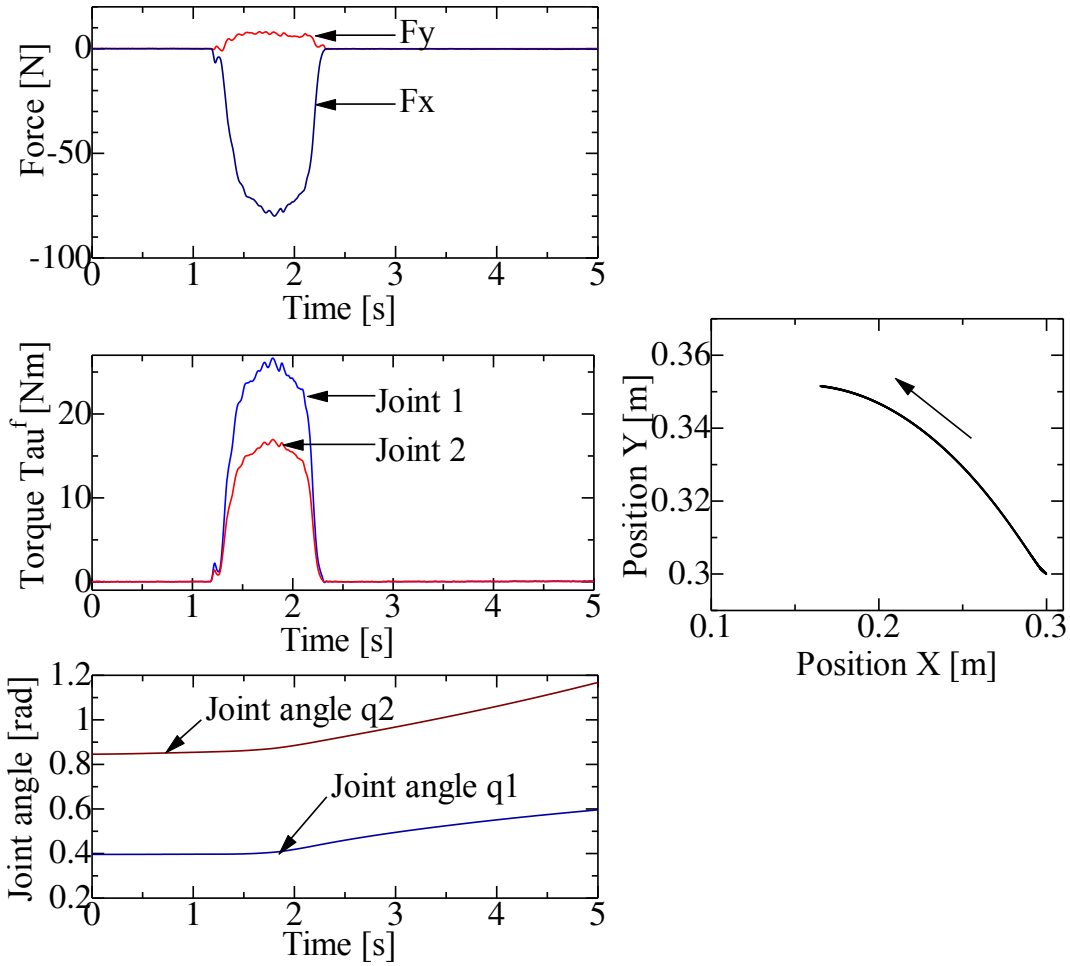

Figure 3.18: Simulation Results for 2-link Robot of FFC-TIC for Varying External Torque

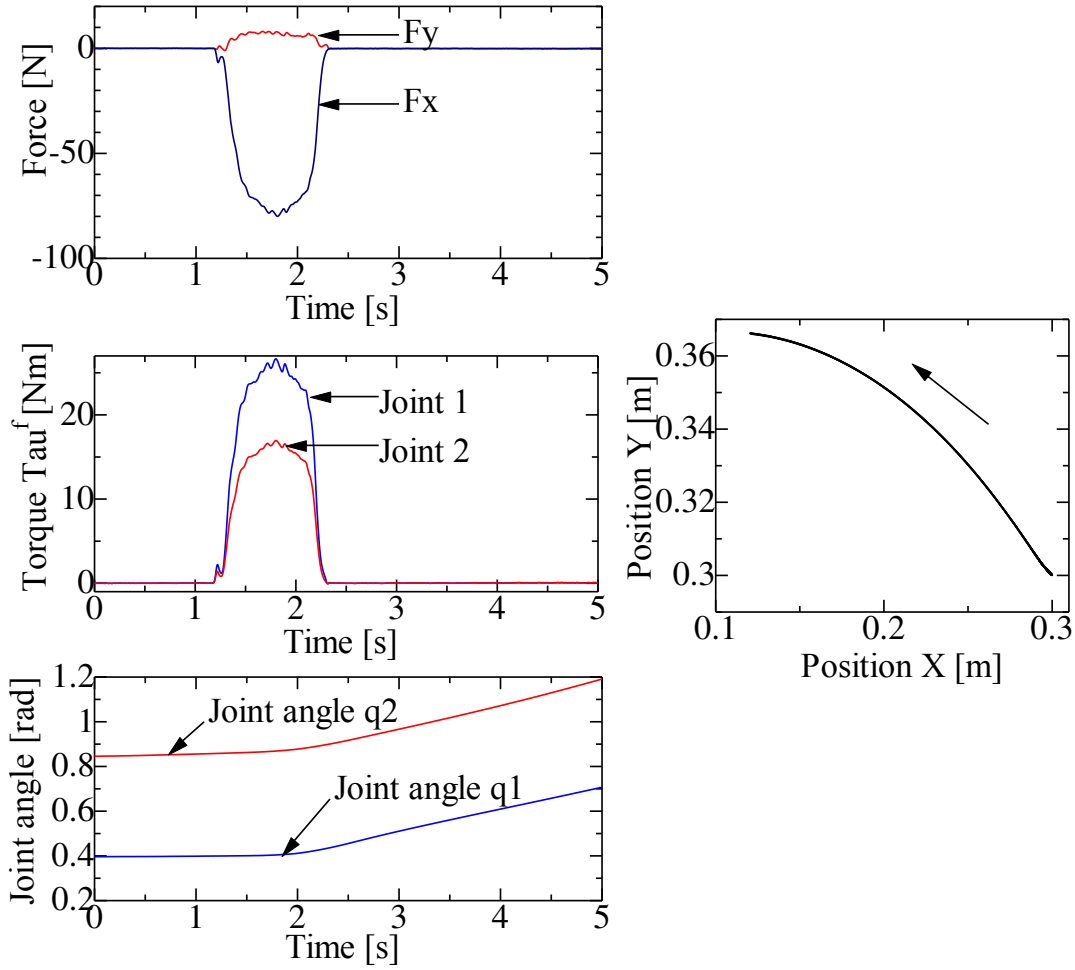

Figure 3.19: Simulation Results for 2-link Robot of FFC-ET for Varying External Torque

applied to the industrial type servo mechanisms which need to follow desired trajectories or assist to move towards the desired locations, for example, FFC application on teleoperation of the robot arms is discussed in [76].

In single link robot arm simulation scenario, robot arm only has 1-DOF so that, end effector always follows the locus of an arc of the circle with radius of link length. However, it is observed in Figs. 3.16 and 3.17 small differences in arc lengths for FFC-ET and FFC-TIC cases. For 2-links robot arm cases, end effector has freedom to travel in planar paths of 2-DOF.

Therefore, Figs 3.18 and 3.19 show the free movements due to FFC and then again we observe slightly different movements for FFC-ET and FFC-TIC cases. Since, 2-links robot arm has freedom to travel planar paths, passive motion against external force by FFC can also be configured to travel assigned end effector path.

Another, possible scenario is of achieving safety by reducing stiffness under danger circumstances. In such case, passive movement of the robot arm is accomplished by applying an external force to desired direction. Switching between the positioning / contouring control and the FFC for the same task execution is also feasible.

3.6 Analysis of force-free control and general type impedance control

3.6.1 Robot mechanical model

Before considering dynamics of FFC and impedance control (IC), our initial step is to create a mechanical model of a basic type 2-link planar robot arm to investigate the each of the force control approach. Figure 3.11, shows the schematic diagram of the mechanical model of the 2-link robot arm illustrated with Matlab/Simulink environment. The model comprises of two revolute joints and two linear bodies. The mechanical model is given torques as inputs and it outputs joint angles, torques and end-effector position in joint and Cartesian coordinates. For the sake of eliminating the complexity, link masses are considered to be concentrated at the center of each link and links are also linear, that will also simplify the modeling tasks without much affect to the objective. The following section describes the dynamics of the respective 2-link planar arm.

3.6.2 Dynamic model and equations

The respective dynamic model of the system is non-linear and also highly coupled. Therefore, such control system can either to use non-linear control techniques or to linearize the system and apply commonly use linear control techniques. The second option is adopted and will be used herein. Better explanation is given how to linearize and decouple the system in [45, 46]. The method makes use of the dynamic model of the system, and accuracy of the dynamic model is highly determined by liberalization and decoupling process and its dynamic control approach. The dynamic model of a robot manipulator describes the forces acting on the mechanical structure with the resulting displacements, velocities and accelerations. The acting forces are given

by different elements and sources. The torques are delivered by the motors, the inertia of the mechanical links, non-linear Coriolis and centripetal forces, the gravity, the friction forces and the forces exerted by the environment on the robot. The importance of the dynamic model is, if given an initial state of the robot links and the time history of torques $\tau(t)$ acting at joints, the direct dynamic model allows to predict the resulting motion $q(t)$, $\dot{q}(t)$, $\ddot{q}(t)$ in joint space. Hence, by using the direct kinematic model, a prediction of the trajectory $x(t)$, $y(t)$ in Cartesian form can be calculated. The dynamic model of an n-joint robot manipulator can be obtained in the Lagrangian form [46] as described in sections 3.2.2 and 3.4.1.;

$$\mathbf{H}(\mathbf{q})\ddot{\mathbf{q}} + \mathbf{C}(\mathbf{q},\ \dot{\mathbf{q}}) + \mathbf{V}(\dot{\mathbf{q}}) + \mathbf{G}(\mathbf{q}) = \boldsymbol{\tau} \tag{3.19}$$

where $\mathbf{q}$ is the joint variable vector for n-joints and $\boldsymbol{\tau}$ is the vector of generalized forces acting on the robot manipulator. $\mathbf{H}(\mathbf{q})$ is the inertia matrix, $\mathbf{C}(\mathbf{q},\ \dot{\mathbf{q}})$ is the non-linear Coriolis-centripetal force, $\mathbf{V}(\dot{\mathbf{q}})$ is the friction force and $\mathbf{G}(\mathbf{q})$ is the gravity vector. In equation (3.20) we are taking into account the friction torques as viscous friction that are always to be found in a real robot manipulators. The dynamic model of the 2-link planar robot arm illustrated in section 3.4.1 of Fig. 3.11, following the Lagrangian form is given as described in section 3.4 and more details are given in [45];

$$\mathbf{H}(\mathbf{q})\begin{bmatrix}\ddot{q}_1 & \ddot{q}_2\end{bmatrix}^T + \mathbf{C}(\mathbf{q},\ \dot{\mathbf{q}}) + \mathbf{V}(\dot{\mathbf{q}}) + \mathbf{G}(\mathbf{q}) = \begin{bmatrix}\tau_1 & \tau_2\end{bmatrix}^T \tag{3.20}$$

$$\mathbf{H}(\mathbf{q}) = \begin{bmatrix} H_{11} & H_{12} \\ H_{21} & H_{22}\end{bmatrix} \tag{3.21}$$

$$\begin{aligned}
H_{11} &= m_1(l_1^g)^2 + m_2\{(l_1)^2 + 2l_1l_2^g\cos q_2 + (l_2^g)^2\} + I_1 + I_2 \\
H_{12} &= m_2l_1l_2^g\cos q_2 + m_2(l_2^g)^2 + I_2 \\
H_{21} &= I_2 + m_2\{(l_2^g)^2 + l_1l_2^g\cos q_2\} \\
H_{22} &= m_2(l_2^g)^2 + I_2
\end{aligned}$$

$$\mathbf{V} = \begin{bmatrix} D_1 & 0 \\ 0 & D_2\end{bmatrix} \tag{3.22}$$

$$\mathbf{C}(\mathbf{q},\dot{\mathbf{q}}) = \begin{bmatrix} -m_2l_1l_2^g\{2\dot{q}_1\dot{q}_2 + (\dot{q}_2)^2\}\sin q_2 \\ m_2l_1l_2^g\dot{q}_1\dot{q}_2\sin q_2\end{bmatrix} \tag{3.23}$$

$$\mathbf{G}(\mathbf{q}) = \begin{bmatrix} m_1gl_1^g\cos q_1 + m_2g\{l_1\cos q_1 + l_2^g\cos(q_1+q_2)\} \\ m_2gl_2^g\cos(q_1+q_2)\end{bmatrix} \tag{3.24}$$

where $\mathbf{q} = [q_1 \quad q_2]^T$ is the joint angle vector, l_1, l_2 the length of link 1 and link 2, m_1, m_2 the mass of link 1 and link 2, l_1^g, l_2^g the center of gravity of link 1 and link 2, I_1, I_2, the moment of inertia along center of gravity of link 1 and 2, respectively and D_1 and D_2 the coefficient of viscous damping of link 1 and link 2, respectively, and $\boldsymbol{\tau} = [\tau_1 \quad \tau_2]^T$.

3.6.3 Kinematics

Typically kinematics analysis includes inverse forward analysis and kinematics analysis. Forward analysis converts joint variables to end-effector variables and it only has unique end-effector solution. It is used for simulation and find the workspace of manipulators. Otherwise, inverse kinematics converts end-effector variables to joint variables, and typically it has multiple joint angle solutions. In most of the industrial manipulators, the possibility of sending torque commands directly to the robot is not available. To simplify the tasks industrial robots usually include an internal joint controller together with the necessary inverse kinematics algorithms. In other words, the designer can choose either to send direct joint angle commands to the robot or an end-effector position command in Cartesian coordinates.

In our case and in order to be able to easily port some of the results of this simulation to an industrial manipulator, an inverse kinematics module is also integrated. For that, the mechanical model of the manipulator, the dynamic model-based controller and the inverse kinematics module can be considered the "black box" for most of the industrial robots. From this point on, our strategies can build up outer control loops that will be easily tested on a real manipulator by concentrating on Cartesian ICs and position loop FFC rather than on internal joint/velocity controllers. According to the Fig. 3.11 corresponding inverse kinematics equations can be derived for 2-link planar case as follows:

$$\begin{cases} q_2^d(k) = \pi - \cos^{-1}\left(\frac{l_1^2+l_2^2-\gamma^2}{2l_1l_2}\right) \\ q_1^d(k) = \tan^{-1}\left\{\frac{y^d(k)}{x^d(k)}\right\} - \sin^{-1}\left\{\frac{l_2 \sin q_2^d(k)}{\gamma}\right\} \end{cases} \tag{3.25}$$

where, $\mathbf{q}^d(k) = [q_1^d(k),\ q_2^d(k)]^T$, and $q_1^d(k),\ q_2^d(k)$ are the joint positions of link 1 and link 2, respectively, k is the sample step number and $\gamma = \sqrt{x^d(k)^2 + y^d(k)^2}$. Then $\mathbf{q}^d$ is brought to the servo controller of the industrial articulated robot arm.

3.6.4 Controller model

This section describes now the technique use to linearize and decouple the system. We can define a controller such as;

$$\mathbf{P}\mathbf{u}^c + \mathbf{Q} \tag{3.26}$$

where $\mathbf{u}^c$ is the new control input, and can be defined as;

$$\mathbf{P} = \mathbf{H}(\mathbf{q}) \tag{3.27}$$

$$\mathbf{Q} = \mathbf{C}(\mathbf{q},\ \dot{\mathbf{q}}) + \mathbf{V}(\dot{\mathbf{q}}) + \mathbf{G}(\mathbf{q}) \tag{3.28}$$

By connecting the controller with the dynamic model $\mathbf{H}(\mathbf{q})\ddot{\mathbf{q}} + \mathbf{C}(\mathbf{q},\ \dot{\mathbf{q}}) + \mathbf{V}(\dot{\mathbf{q}}) + \mathbf{G}(\mathbf{q}) = \mathbf{P}\mathbf{u}^c + \mathbf{Q}$ and hence, control input is reduced to form of,

$$\ddot{\mathbf{q}} = \mathbf{u}^c. \tag{3.29}$$

This control input is linear and then simple model as well. This type of controller can work as long as it is possible to accurately represent and implement parameters $\mathbf{P}$

and **Q**. Simulations in Matlab/Simulink, the analytical solution for **P** and **Q** matches precisely the dynamics described by the mechanical model in equation 3.20. Therefore it can be then easily implemented as a typical PD controller as follows [46]:

$$\mathbf{u}^c = -\left\{\mathbf{K}_p(\mathbf{q}^d - \mathbf{q}) + \mathbf{K}_v(\dot{\mathbf{q}}^d - \dot{\mathbf{q}})\right\} \tag{3.30}$$

Hence, equations (3.27) and (3.28) describe a dynamic model-based controller for the manipulator that will be used to cancel the non-linearities of the manipulator in order to achieve a model to control a double integrator given in equation (3.29). The general detailed structure of the dynamic model-based controller can be seen in [45, 46].

The parameters $\mathbf{K}_p$ and $\mathbf{K}_v$ are found empirically but it is easy to demonstrate how to choose them depending on the desired dynamical response. If the error is defined as $e = (q^d - q)$, then the systems error equation is a second order system with the format of $s^2 + 2\zeta w_n + {w_n}^2 = 0$ where the resonant frequency w_n and the damping coefficient ζ are computed as $w_n = \sqrt{(K_p)}$ and $\zeta = K_v/2\sqrt{(K_v)}$. Therefore, after canceling the non-linearities of the mechanical model with the use of the model-based part of the controller, we can tune the PD parameters to achieve the desired performance of the system.

3.6.5 Modeling of the wall environment

To deal with the robot interaction with the environment or external forces act on the robot, correct model of the acting forces is vital factor when designing robot applications. Therefore, a model of the environment is included in our system whose interaction force will act on our robot tool end. Usually, a simple linear spring model is used as model for the environment as $f_x = K_e(x - x_e)$, where f_x is the contact force, K_e is the stiffness of the environment, x is the end-effector position at the contact point and x_e is the static position of the environment.

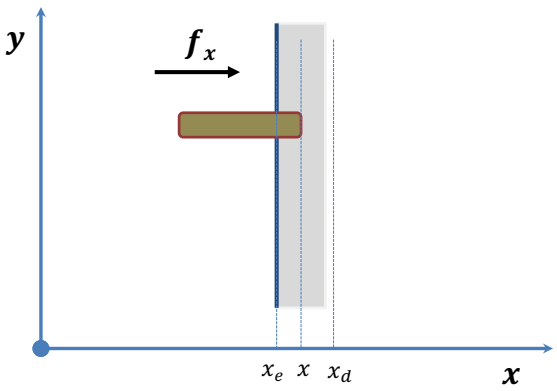

Figure 3.20: Manipulator in Contact with the Environment.

Figure 3.20 depicts the conceptual spring damper model of the contact environment with parameters, where a manipulator contacts the environment at position x_e

trying to reach the desired end-effector position x_d. In this simulation, we include a damping coefficient B_e such that environment is then modeled as;

$$f_x = K_e(x - x_e) + B_e(\dot{x} - \dot{x}_e). \tag{3.31}$$

3.6.6 Modeling of contact force by Jacobian

The dynamic equation describing the behavior of 2-link robot arm which is used here is defined in (3.20). For that, τ is considered to include the effects of all the generalized forces acting on the robot, i.e. also the external contact forces. Therefore, we can modify equation to show the effect of those forces and also compensate in the model. Hence modified dynamic equation governing the robots behavior is now defined as:

$$\mathbf{H}(\mathbf{q})\ddot{\mathbf{q}} + \mathbf{C}(\mathbf{q},\ \dot{\mathbf{q}}) + \mathbf{V}(\dot{\mathbf{q}}) + \mathbf{G}(\mathbf{q}) = \tau_{\mathbf{s}} - \mathbf{J}^T\mathbf{F}_{ext} \tag{3.32}$$

where $\boldsymbol{\tau}_s$ can be defined as the driving torques and the term $\mathbf{J}^T\mathbf{F}_{ext}(\mathbf{q})$ translates the task-space forces $\mathbf{F}_{ext}$ acting on the end-effector to the joint space by adopting transpose of the Jacobian. Hence, Simulink model based on equation (3.32) is applied in order to include the contact forces in the dynamic response. In the case of a two-link planar arm, and knowing that the relation between torques and forces is defined as $\tau_f = \mathbf{J}^T\mathbf{F}_{ext}$, then respective equations can be written as:

$$\tau_{f1} = J_{11}f_x + J_{21}f_y$$
$$\tau_{f2} = J_{12}f_x + J_{22}f_y$$

where $\tau_{f1},\ \tau_{f2}$ are the torque due to contact, J_{ij} are the elements of the transpose of the (2×2) Jacobian matrix and $\mathbf{F}_{ext} = [f_x,\ f_y]$ forces along the X and Y directions, respectively. Since we assume that no forces are acting along the Y axis, because its path in this direction is free and we don't consider friction forces, However, in our simulation contact force is assumed to be parallel to X-axis therefore, $f_y = 0$ so that $\tau_{f1} = J_{11}f_x$ and $\tau_{f2} = J_{12}f_x$.
Hence, torque due to external contact forces are to be included in equation (3.32).

3.6.7 Modeling of impedance controller

In this section we describe how to design a controller that regulates the interaction when the robot contacts the external environment. The simple scenario can be described as follows: at present, if the robot follows a defined trajectory that finds on its way to an object, and then will collide with it, then again trying to reach the final end position of the given trajectory, and hence, likely to be exerting large forces into the contact environment, therefore, that would likely to have high degree of damages to a real robot and/or the object of collision. To avoid such massive impact forces, an impedance controller is introduced [47].

In IC, input is the reference trajectory at each time step. The measured contact forces will be supplied to the IC module so as to get an immediate feedback of the contact state. The output is a modified trajectory that handles the contact forces. Moreover, if there are no forces are sensed, then desired trajectory will be followed

always . Otherwise, if forces are measured, by means of the IC trajectory is modified in order to limit the maximum steady-state forces. And also IC is designed to achieve dynamic behavior of the the mass-spring-damper system described in the control law given in [47] and illustrated in Fig. 3.21. Thus the impedance controller is modeled as follows;

$$M_t\ddot{e}_{trj} + D_t\dot{e}_{trj} + K_t e_{trj} = (f_x, f_y) \tag{3.33}$$

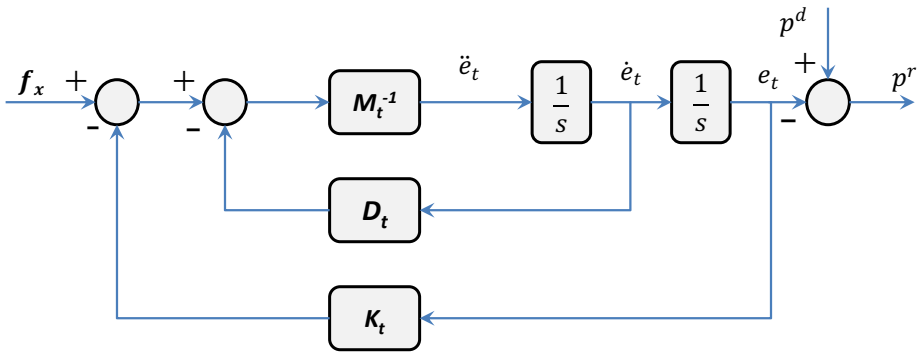

Figure 3.21: Block Diagram of Impedance Controller.

where M_t, D_t and K_t are the inertia, damping and the stiffness coefficients, respectively. An e_{trj} is the trajectory error, defined as $e_{trj} = (p^d - p^r)$ where p_d is the desired trajectory input and p^r is the reference trajectory for the inverse kinematics model. M_t, D_t and K_t are defined the dynamic behavior of the robot that could be compared to the effect of including physical springs and dampers on the robot. Figure 3.21 shows the architecture of the impedance controller which is used here.

3.6.8 Modeling of force-free control (FFC)

In this simulation study we focus to model the mass point type FFC method. Initially, mass point type FFC is derived as follows:

Mass point type FFC is constructed by a translational motion model of the mass point which is assumed as a tip of a 2-DOF robot arm as shown in Fig. 3.22. When the force is applied to the mass point F from the external environment, it is generally moved to the same direction of the applied external force. The concept of FFC is the realization of zero-friction and zero-gravity motion. However, in practical situation a friction term is required for positioning the mass point actually. Therefore, the translational motion model of the mass point includes the friction term. Moreover, the motion of the mass point is applied for the motion of the tip of the robot arm. However, mass point motion can also be assigned to a desired locus if it is required as function $f(x)$.

When it maintains zero-gravity condition, the equation of motion of the mass

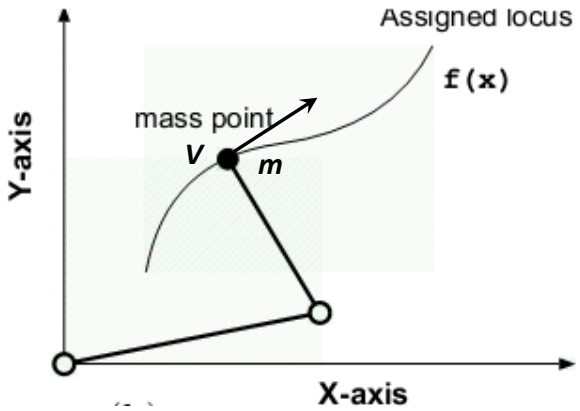

Figure 3.22: Schematic of Mass Point Orientation.

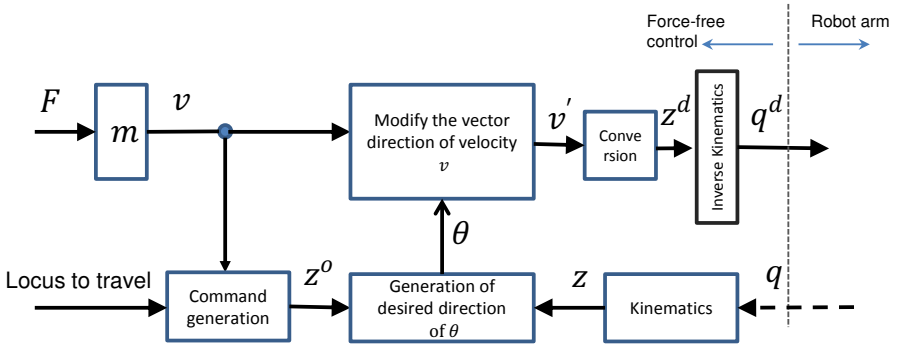

Figure 3.23: Block Diagram of Mass Point Type FFC.

point by added force $\boldsymbol{F}$ can be shown as;

$$\mathbf{F}(t) = m\ddot{\mathbf{z}}(t) + d_v\dot{\mathbf{z}}(t) \tag{3.34}$$

where, $\mathbf{F}(t) = [f_x(t) \;\; f_y(t)]^T$, $\mathbf{z}(t) = [x(t) \;\; y(t)]^T$, and $f_x(t)$, $f_y(t)$ are the forces along the direction of X-axis and Y-axis, respectively, and $x(t)$, $y(t)$ are the displacement of the direction of X-axis and Y-axis, respectively, and m is the mass of the mass point at the end of robot arm, d_v is the coefficient of viscous friction. To make discrete form of equation 3.34, velocity $\mathbf{v}$ and position $\mathbf{z}$ are obtained as:

$$\mathbf{v}(k) = \frac{\Delta t}{m}\mathbf{F}(k) + \left(1 - \frac{d}{m}\Delta t\right)\dot{\mathbf{z}}(k) \tag{3.35}$$

$$\mathbf{z}^d(k+1) = \alpha\mathbf{F}(k)\Delta t^2 + \beta\dot{\mathbf{z}}^d(k)\Delta t + \mathbf{z}^d(k) \tag{3.36}$$

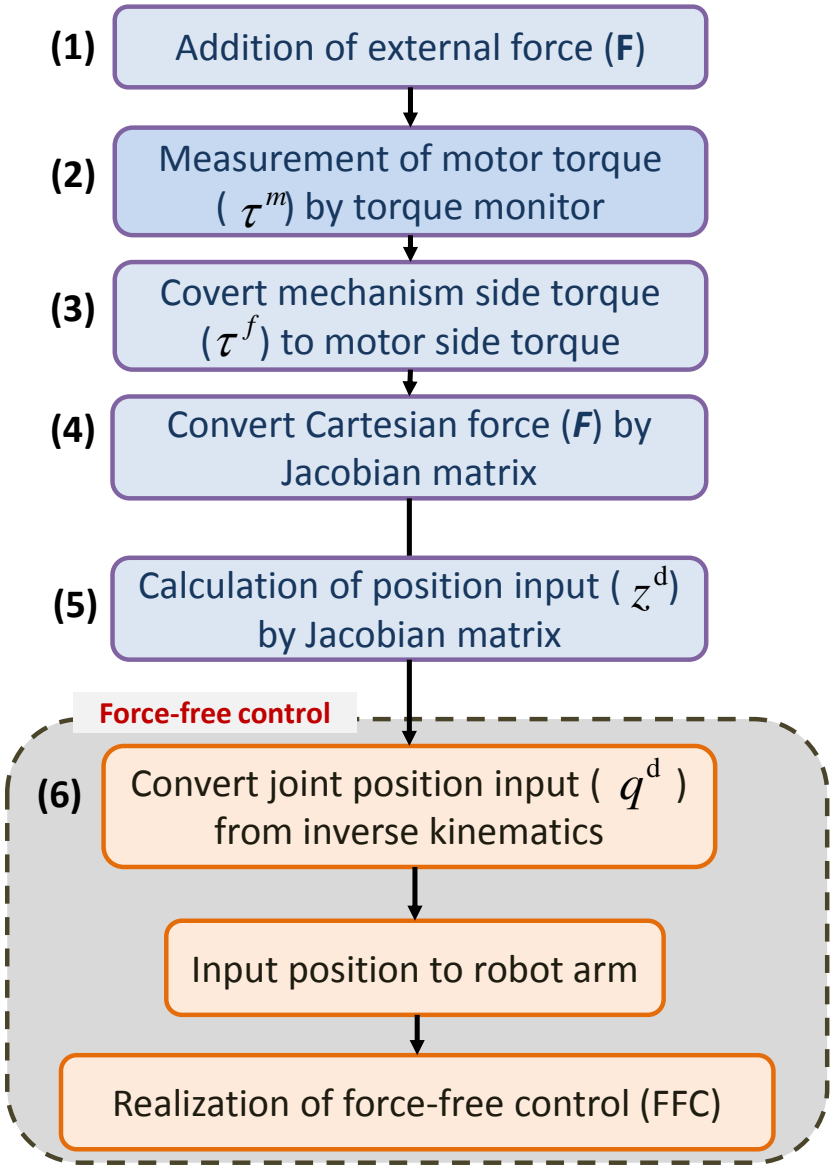

Figure 3.24: Functional and Implementation Flow Diagram of a Mass-point Considered Force-free Controller.

where Δt is the sampling interval, k is the sample step number of control, $\alpha = 1/(m + \Delta t \cdot d_v)$, $\beta = m\alpha$ and $\mathbf{z}(k) = \mathbf{z}^d(k) = [x^d(k) \quad y^d(k)]^T$. $\mathbf{z}^d(k)$ is converted to the objective joint position $\mathbf{q}^d(k)$ by inverse kinematics.

The schematic diagram of the mass point type FFC algorithm is shown in Fig. 3.23. From the FFC, reference input is given to the robot servo controller and z^o is objective position if locus is predefined and θ is angle between x-axis and vectorial direction of the mass point for FFC. Therefore, $\mathbf{q}^d$ is brought to the servo controller of the industrial articulated robot arm. Since the robot arm is actuated by the added force $\mathbf{F}$ with flexibility, then the tip of the robot arm moves in the direction of the added force $\mathbf{F}$. This phenomena of control is called mass point type FFC.

3.6.9 Simulation of force-free control vs typical impedance control

3.6.9.1 Simulation setup Figure 3.25 shows the complete Matlab/Simulink model of the simulation system. It includes the mechanical model of 2-link planar robot arm, the dynamic model-based controller, the model of the environment (wall), the impedance controller and the mass point type FFC. Simulation is done based on IC and FFC, each controller is selected for simulation by using a switch and rest of the system remains unchanged for both IC and FFC cases. Comparison in terms of functions and properties are listed in Table 3.1.

In order to identify the behaviors and performances of both force control techniques, robot is given a same input trajectory for the IC and FFC. The input for the X axis is a ramp starting at X = 0.8 [m] with slope = 0.02 [m/s]. The reference for the Y-axis is a ramp starting a Y = 1.3 [m] with slope = -0.015 [m/s]. The wall is located at X = 1.12 [m] and it is modeled as defined in equation (3.31) with K_e = 600000 [N/m] and $B_e = 0.12$ [N (s/m)]. Figure 3.26 shows the response of the system when contacting the environment. It also shows the wall contact point X = 1.12 [m], y = 1.00 [m] and the contact force F_{ext}. Length of the each arm for simulation is take as 0.72 [m]. The controller parameters for impedance controller scenario are $M_t = 3$ [kg], $D_t = 750$ [N (s/m)], $K_t = 8.5$ [N/m] and link mass is chosen as 6 [kg] for each link. For the mass point type FFC, mass of the mass point is taken as $m = 0.75$ [kg]. Moreover, model based robot controller parameters are taken as $K_p = 9000$ [N/m] and $K_v = 80$ [N ms/rad].

3.6.9.2 Simulation results The simulations of the FFC and IC control algorithms that are carried out for horizontal direction of contact force (x-direction) are shown in Figs. 3.26 and 3.27. In IC, when robot collides on the wall controller compensate the impact force by stopping movement in x-direction by limiting to a lower steady-state force defined in the IC . In FFC, collision is compensated by smooth and curvier backward movement of the tool end. The controller without force control shows, the robot tool end move towards the wall by generating hard contact forces. Moreover, the theoretical comparison against the impedance control is clearly observed as in Fig. 3.27 with same environmental interactions. We can also see the results of the same simulation case without using force controllers, in which, robot arm tries to

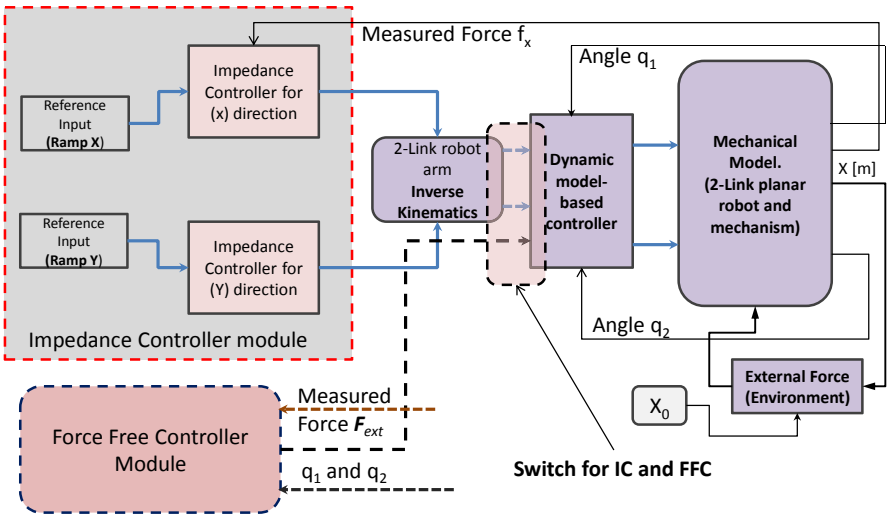

Figure 3.25: Complete System Block Diagram for Simulation of IC and FFC in Matlab/Simulink.

follow the given input trajectory and after hitting the wall surface, the contact forces must be increased immensely according to the equation (3.31) as the robot travels inside the wall. In this simulation, FFC also shows the acceptable theoretical behavior compared with commonly use IC technique. Besides, FFC shows backward movement of the robot tool end against contact position whereas, IC limits the contact force to a lower value and contact point of the tool end remains the same position.

3.7 Concluding Remarks

In sections 3.2 to 3.3 presents the simulation with analysis of FFC for single arm case of an industrial type arm and its possible applicability for safety is also discussed for 2-links scenario. Simulation results indicate the realization of theoretical model of the FFC for different kinds of external force conditions and applicability for safe operation under a being danger circumstance due to high rigidity of industrial robots is also tested and verified by realistic and parameterized simulations.

Simulation and analysis of the two FFC strategies are given as FFC-ET and FFC-TIC in sections 3.4 and 3.5, exclusively. Each type is investigated under Matlab/Simulink integrated environment. For each model, single and 2-links cases of the industrial type robot arms with real parameters are investigated. Possible application scenarios are also discussed as per feasible future developments. Simulation results indicate the possible realization of the theoretical models of two different FFC strategies under real values of friction and gravity effects.

Moreover, section 3.6 is initially devoted to discusses the use of Matlab/Simulink as a tool to model the mechanics of the robot arm and also the possibility to verify model-based control algorithms. Thereafter, process of modeling a 2-link planar robot

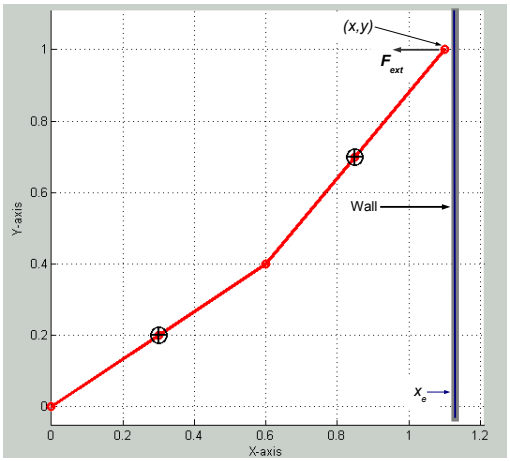

Figure 3.26: Robot Orientation of Hitting Wall at (x,y).

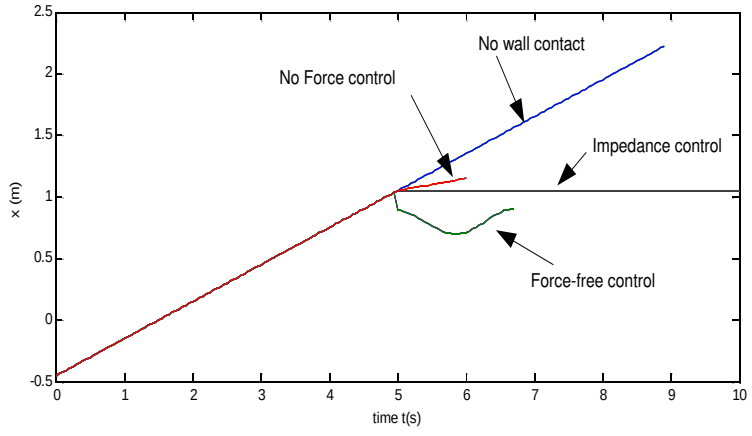

Figure 3.27: Simulation Results of Tool-end Position After Hitting the Wall for FFC, IC and without Force Controller.

Comparison with Impedance Control

	Forcefree control	Impedance control
Objective	Free motion by external force	Desirable mechanical impedance
Model	Dynamics of industrial articulated robot arm	Mechanical impedance between tip arm and object
Motion	Passive motion against external force	Active motion to realize assigned force
Rigidity	Zero	Setting by virtual spring
Inertia	Setting by the coefficient of inertia	Setting by virtual mass
Friction	Setting by the coefficient of friction	Setting by virtual damper
Gravity	Setting by the coefficient of gravity	Compensation
Target	Industrial articulated robot arm	Articulated robot arm
Coordinates	Joint coordinates	Cartesian coordinates
Command	Position command	Torque command, Position command

Table 3.1: High Level Comparison of FFC and IC According to Properties and Functions.

arm with correct mechanical model, and its interaction with the environment are also carried out. With the help of simulation, the ability of the algorithm to match the real model can easily be identified.

Finally, comparison studies of FFC with respect to commonly use impedance control (IC) technique are mainly focused and detailed in the latter part of section 3.6, in which, both techniques are implemented in an integrated simulation environment. Based on the results, the uses of FFC and IC show that capability of controlling the robot-environment interaction, especially in those applications where the environment is completely or partially unknown. Simulation output also shows that similar to the IC, the property of compliance the external forces rather than controlling the exact forces exerted into the environment is also shown to be inherited by the FFC.

Chapter 4

Teleoperation of Industrial Robot Arms Using a Visual Servo Technique

This chapter discusses the development of a teleoperation system to control robot arms remotely combined with a vision system module. In fact, force-free control and template matching techniques are applied to control the motion of industrial robot arms via network communication. The system has two motion control schemes; rough motion of the robot arm is handled through teleoperation by using force-free control technique, and accurate motion is implemented by visual template matching. Switching between two control schemes is carried out from one to another appropriately to achieve the desired motion control. The effectiveness of the methodology is verified by the experimental results.

4.1 Teleoperation and visual servo control

4.1.1 Introduction

In last two decades conventional robot arms are heavily used in industrial applications [80]. In the recent years, computer vision attached, network and teleoperation of robotics [81, 82, 83], have been paid much attention by researchers especially in emerging areas like telemedicine [84], telesurgery [85, 86], remote controlled robots in hazardous operations, undersea operations, nuclear or high radioactive rich environments [87], high temperature environments, space or planetary explore operations [88] etc.

This chapter mainly focuses on the accurate remote control of the motion of robot arm via network. Time delays and data losses during the remote communication are two constrains to be discussed in this chapter. On the other hand, the proposed control strategy is applied without any changes to the existing factory fitted controllers of robot arms. The force-free control and template matching are two

separate modules and externally attached to the factory fitted components of the robot. The proposed solution has a real time control behavior, which is implemented on real-time operating system environment.

Considering the industrial robot arms in general it is difficult to move freely by applying external force (passive motion) since the servo controller behavior itself prevents the robot arm movement against the external force. In order to restrain the inherent behavior of the built-in servo controller, the technique called force-free control (FFC) was described by one of the authors in [20]. One of the most important behavior of FFC is that it would not involve any changes to the existing controller (factory fitted hardware or software) for the robot arm.

On the other hand, computer vision techniques with required control methodologies have been consistently studied [88, 89], and widely used among the researchers in various fields including robot vision and visual servo control systems. Template matching is known as one of applicable techniques widely used in vision control applications, and shows reasonable accuracy with the speed [90, 91], although the speed, accuracy and robustness depend on the hardware and the complexity of the algorithm expected to be used. However, template matching is currently a consistent method and proved to be a reliable derivation of visual servo applications. Therefore, this chapter is based on the remote control of the robot arm by using FFC and visual template matching schemes.

The problem of accurate teleoperation of industrial robot arms has been studied by the researchers mostly in the last two decades. However, most of the researches were based on provision of less autonomy to the remote working side (slave side) robot. And also, an important noticeable difference is that the related researches did not use or seldom used the industrial robot arms for the operational side (master side) manipulations. In most cases, virtual tool or a small joy stick type manipulator were used instead, to give control commands to the slave side. Therefore, those related researches focused and directed to handle the important issues on time delays contracted in the communication channels between master and slave sides.

In [92], a method to deal with teleoperated surgery in kinematic restricted environments was proposed. However, the described system depends on the master side to make reactions to dynamic changes in the environment. The virtual force feedback approach for teleoperation without coupled visual aid was presented in [93]. In this approach, the system is assumed to be limited to the direct communication without considering time delays and data losses during telesurgical training practices. A useful contribution to solve the problem of assuring stability of the teleoperation due to time delay was presented in [94]. A method to assist the human operator semi-autonomously by using virtual tool dynamics was also rendered in [95]. However, the accurate motion highly relies on the master side control commands.

As mentioned above, most of the researches rely on the master side control actions on teleoperation. Then, it creates traffic on the communication channels and makes definite burden to the timely information processing. In addition, most

researches of the teleoperation are also highly sensitive to master side mistakes which can be expected in any human control involvement. In [71], a new enhancement for the time-delayed systems was introduced. It also can only be shown the given results as long as the delays are finite constants and an upper bound for the round-trip delay is known. Another issue of the above approaches is that in real operations time delay adversely affected on control actions given from the master side untimely and inefficiently. To address the above problems, in our approach, autonomous image processing based visual servo control is adopted on the slave side.

In [97], the teleoperation implementation proved the applicability of FFC through network, and the experiments were carried out to verify the technique. However, the movement of robot arm tip was restricted only to the vertical direction movement of robot arm tip, and also the vision system behavior policy was not implemented. The control scheme described in this chapter, is also applicable for the horizontal accurate motion of the tip of the robot arm. Moreover, vision system behavior policy is also illustrated, and two experiments were carried out to show the repeatability and applicability of the promising approach.

Experimental setup comprises of a SCARA-type robot manipulator for the operational side to generate reference position manually through rough motion using FFC by a human operator, and a PUMA-type industrial articulated robot arm is used for the working side to obtain the accurate motion autonomously by means of template matching [90] upon visual servo control. The effectiveness is verified by experimental results obtained from different sets of trials.

The rest of this chapter is organized as follows: Next section, total system is explained with details of concept and configurations of FFC and template matching. Section 4.3 is devoted to the validation of the proposed system. Then, conditions of the experimental setup and outcome of the experiments are also given. Section 4.4 discusses the proposed system from the viewpoints of the maneuverability and network delays cum data losses. Finally, the discussion of this paper is given followed by a summary.

4.2 Teleoperation System by force-free control and template matching

4.2.1 Concept and overview of the system

Figure 4.1 illustrates the schematic diagram of the described teleoperation control system. The system consists of two main modules as shown in the block diagram in Fig. 4.2: (i) robot arm and (ii) two reference generation mechanisms.

Figure 4.1 shows the detailed implementation of rough motion and accurate motion. Upper portion gives the idea of teleoperation using FFC, where human operator manipulates the operational side robot arm in order to get the target within the view of the camera fixed on the working side robot. Lower portion illustrates the accurate motion after detecting the target object. The position commands for the

accurate motion are given by the camera side computer which is connected to the working side robot locally.

Figure 4.2 also shows the block representation of the operational, working and camera sides in order to provide a clear view of the functions of the teleoperation system. It also describes how external force creates the reference position and sends the generated reference position via network channel to the working side robot. Also the camera side uses the template matching technique to detect the target position within the camera view and it generates the required reference position and sends it to the working side position controller.

The computers are interconnected through network, and TCP/IP socket communication [98] is used for both operational and working sides of the system. Rough motion is obtained manually with the aid of an external force from a human operator in the operational side by FFC, and accurate motion in working side is governed autonomously by the visual template matching method. The change of mechanisms between remote control for rough motion and visual servo control for accurate motion is handled by the vision system.

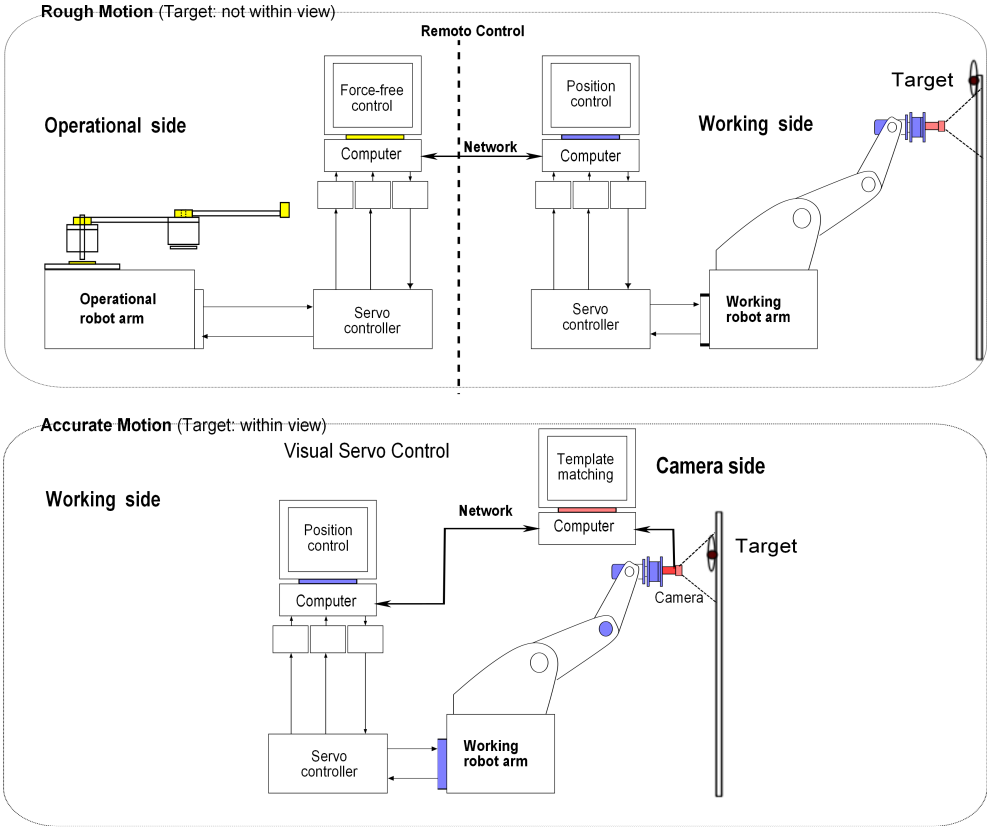

Figure 4.1: Schematic Overview Diagram of the Teleoperation System

The human operator manipulates the robot arm in the operational side in order

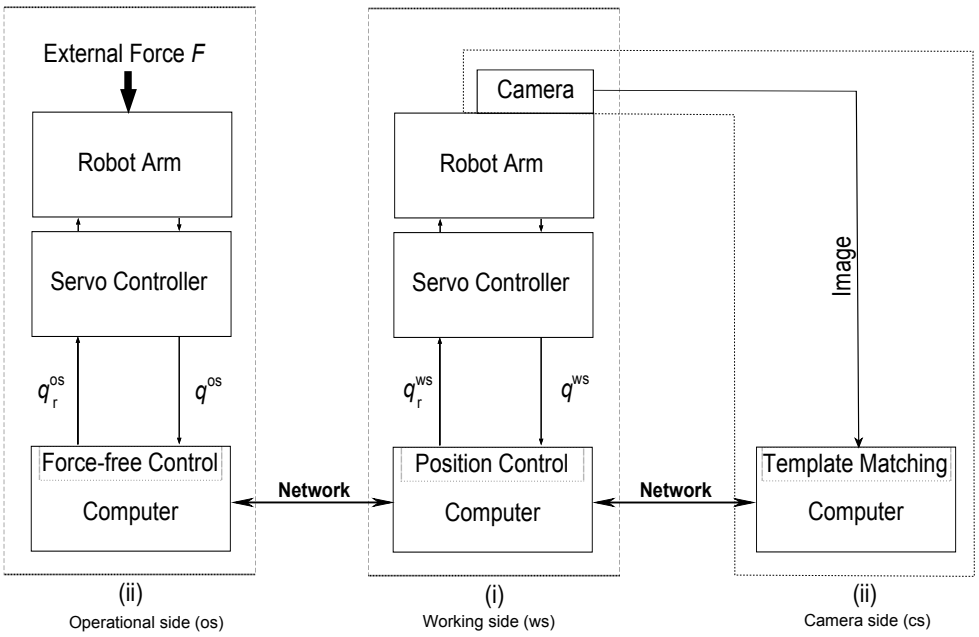

Figure 4.2: Block Diagram of the Proposed Teleoperation Mechanism

to move the robot arm in the working side. FFC [20] is applied to the robot arm in the operational side, so that its passive motion according to the external force can be realized. The reference position of the robot arm generated by the manipulation in the operational side is sent to the working side through the network. Hence, the rough motion of the robot arm can be realized in the working side by the remote control.

The camera side of the system analyzes images obtained by the camera, and the reference position for the robot arm in the working side is calculated. Then, the reference position is sent to the working side via network. Thereafter, accurate motion of the robot arm in the working side can be realized through the visual servo control.

The servo controller of the robot arm in the working side is adopted as the position control. Hence, the position control realizes the following motion of the reference position of the robot arm in the working side. In the case of rough motion, the position reference is generated by the remote control module, whereas for the accurate motion, the position reference is determined by the vision system.

In the following subsections, configuration of the teleoperation setup (i.e., the remote control setup of the operational side, the visual servo control and template matching in the working side and the switching mechanism between remote control and visual servo control) is explained in detail.

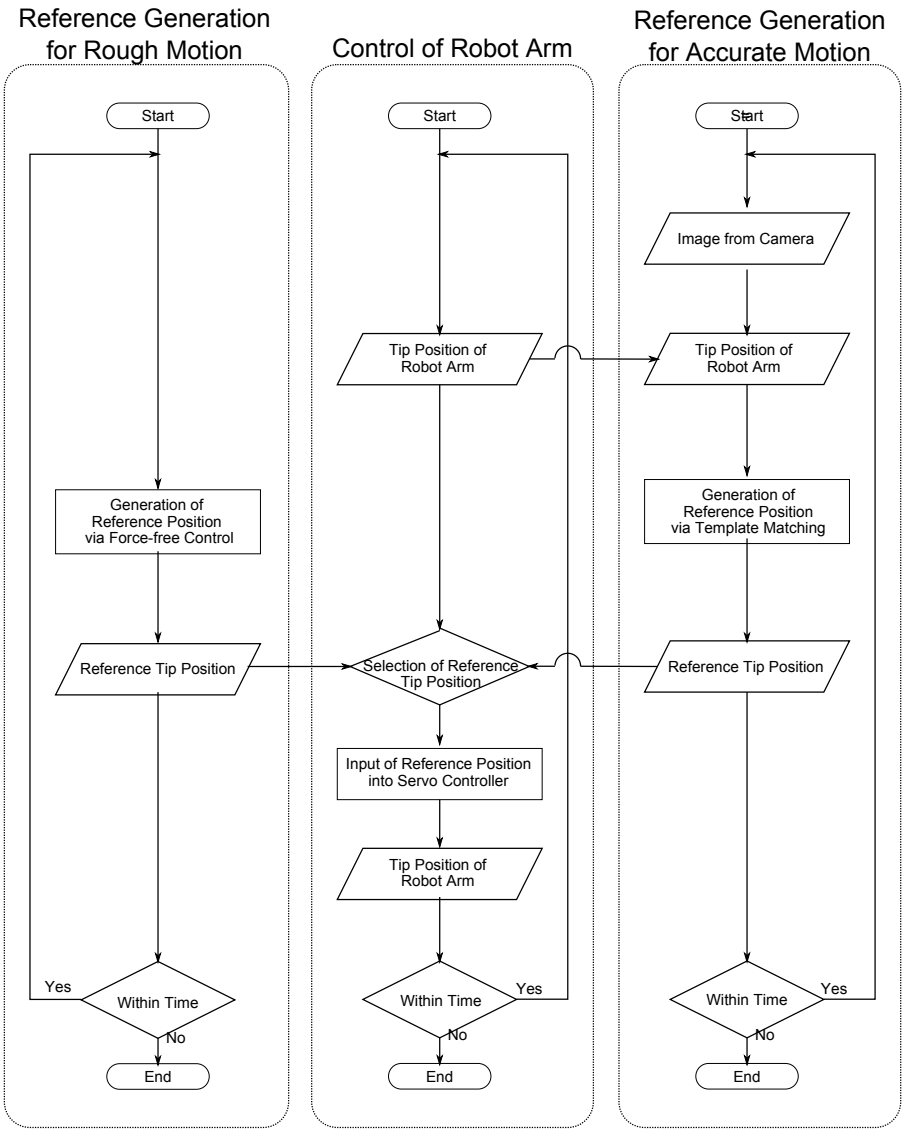

Figure 4.3: Overall Flow Chart of the Teleoperation System

4.2.2 Configuration of the teleoperation system

Figure 4.2 shows the total mechanism chart of the proposed system. The robot arm in the operational side is used to generate the reference position. The vision system in the camera side is used for detecting the target position and determining the reference position.

Figure 6.2 shows the total flow chart of the teleoperation mechanism. The robot arm is controlled according to the reference tip position received from the reference generation mechanisms. The position control can be achieved by two kinds of motions for the reference position of the robot arm, i.e., the rough motion and the accurate motion. For the rough motion, the reference position is generated manually by using the force-free control. On the other hand, for the accurate motion, the reference position is generated automatically by using the vision system based on the template matching technique. In order to generate the reference position of the robot arm for the accurate motion, the image obtained from the Universal Serial Bus (USB) camera is analyzed and processed. The vision system attached to the camera side is responsible for detecting the target position. The position data for the robot arm are sent through the network.

4.2.2.1 Operational side (Remote control behavior) The FFC is adopted in order to realize the passive motion of the robot arm. In FFC [20], the robot arm moves passively according to the external force as if it were under the circumstances of zero friction and zero gravity. In general, dynamics of industrial robot arm is described in details under **Chapter 3***(please refer for more illustrations)* as given by

$$\mathbf{H}(\dot{\mathbf{q}})\ddot{\mathbf{q}} + \mathbf{D}\dot{\mathbf{q}} + \mathbf{N}_{\mu}\mathbf{f}_{\mathbf{s}}(\dot{\mathbf{q}}) + \mathbf{h}(\dot{\mathbf{q}}, \ddot{\mathbf{q}}) + \mathbf{g}(\mathbf{q}) = \boldsymbol{\tau}_{\mathbf{s}} + \boldsymbol{\tau}_{F}, \tag{4.1}$$

where $\mathbf{q}$ is the output vector of the joint angle, $\mathbf{H}(\dot{\mathbf{q}})$ is the inertia matrix, $D\dot{\mathbf{q}} + N_{\mu}f_{s}(\dot{\mathbf{q}})$ denotes compound friction term, $\mathbf{h}(\dot{\mathbf{q}}, \ddot{\mathbf{q}})$ is the coupling non-linear term, $\mathbf{g}(\mathbf{q})$ gives the gravity term, τ_{s} is the torque input to the robot arm and τ_F is the torque caused by the external force [46, 91].

The ideal dynamics of the robot arm in the operational side applied FFC is given as; (refer **Chapter 3** for more details)

$$\mathbf{H}^{\mathrm{os}}(\mathbf{q}^{\mathrm{os}})\ddot{\mathbf{q}}^{\mathrm{os}} + \mathbf{h}^{\mathrm{os}}(\mathbf{q}^{\mathrm{os}}, \dot{\mathbf{q}}^{\mathrm{os}}) = \boldsymbol{\tau}_{F}^{\mathrm{os}}, \tag{4.2}$$

where $\mathbf{q}^{\mathrm{os}}$ is the position vector of joint angle, $\mathbf{H}^{\mathrm{os}}(\mathbf{q}^{\mathrm{os}})$ is the inertia matrix, $\mathbf{h}^{\mathrm{os}}(\mathbf{q}^{\mathrm{os}}, \dot{\mathbf{q}}^{\mathrm{os}})$ is the coupling nonlinear term, τ_F^{os} is the joint torque generated the external force $\mathbf{F}$ on the tip of the robot arm in the operational side.

The dynamic of the robot arm in the operational side including the servo controller is given by

$$\mathbf{H}^{\mathrm{os}}(\mathbf{q}^{\mathrm{os}})\ddot{\mathbf{q}}^{\mathrm{os}} + \mathbf{h}^{\mathrm{os}}(\mathbf{q}^{\mathrm{os}}, \dot{\mathbf{q}}^{\mathrm{os}}) = \mathbf{K}_{\tau}^{\mathrm{os}}[\mathbf{K}_{\mathrm{v}}^{\mathrm{os}}\{\mathbf{K}_{\mathrm{p}}^{\mathrm{os}}(\mathbf{q}_{\mathrm{r}}^{\mathrm{os}} - \mathbf{q}^{\mathrm{os}}) - \dot{\mathbf{q}}^{\mathrm{os}}\}], \tag{4.3}$$

where $K_{\mathrm{p}}^{\mathrm{os}}$, $K_{\mathrm{v}}^{\mathrm{os}}$ and K_{τ}^{os} are position loop gain, velocity loop gain and torque constant of built-in servo controller of the robot arm in the operational side, respectively and $\mathbf{q}_{\mathrm{r}}^{\mathrm{os}}$ is the reference position of joint angle.

In order to realize the ideal dynamics (4.2) of the industrial robot arm, the reference $\mathbf{q}_{\mathrm{r}}^{\mathrm{os}}$ for the robot arm is selected as

$$\mathbf{q}_{\mathrm{r}}^{\mathrm{os}} = (\mathbf{K}_{\mathrm{p}}^{\mathrm{os}})^{-\mathbf{1}}\{(\mathbf{K}_{\mathrm{v}}^{\mathrm{os}})^{-\mathbf{1}}(\mathbf{K}_{\tau}^{\mathrm{os}})^{-\mathbf{1}}\boldsymbol{\tau}_{F}^{\mathrm{os}} + \dot{\mathbf{q}}^{\mathrm{os}}\} + \mathbf{q}^{\mathrm{os}}. \tag{4.4}$$

The joint torque $\boldsymbol{\tau}_{F}^{\mathrm{os}}$ corresponding to the external force $\mathbf{F}$ on the tip of robot arm is assumed to be

$$\boldsymbol{\tau}_{F}^{\mathrm{os}} = -(\boldsymbol{\tau}_{\mathrm{s}}^{\mathrm{os}} - \boldsymbol{\tau}_{\mathrm{d}}^{\mathrm{os}} - \boldsymbol{\tau}_{\mathrm{g}}^{\mathrm{os}}), \tag{4.5}$$

where $\boldsymbol{\tau}_{\mathrm{d}}^{\mathrm{os}}$ and $\boldsymbol{\tau}_{\mathrm{g}}^{\mathrm{os}}$ are described by

$$\boldsymbol{\tau}_{\mathrm{d}}^{\mathrm{os}} = D^{\mathrm{os}}\dot{\mathbf{q}}^{\mathrm{os}} + N_{\mu}^{\mathrm{os}} f_{s}^{\mathrm{os}}(\dot{\mathbf{q}}^{\mathrm{os}}), \tag{4.6}$$

$$\boldsymbol{\tau}_{\mathrm{g}}^{\mathrm{os}} = \mathbf{g}(\mathbf{q}^{\mathrm{os}}), \tag{4.7}$$

and $\boldsymbol{\tau}_{\mathrm{s}}^{\mathrm{os}}$ is the output of the torque monitor. The abbreviations "os", "ws" and "cs" mean "operational side", "working side" and "camera side" respectively.

For three modules communication protocol is TCP/IP, and therefore, the Internet technology is used as the communication platform of the teleoperation system. The Internet is commonly used as a standard platform so that our implementation is adapted easily without changing the existing hardware and/or software [97]. The socket communication via TCP/IP is applied for communication technique of the teleoperation system. The transmitted data from the operational side to the working side are the reference position of the robot arm in the working side, and the received data of the operational side from the working side are inputs to the servo controller for the robot arm in the working side as the reference command.

The robot arms both of the operational side and of the working side are controlled by the real time tasks at the constant sampling interval. Since the real time task behavior can not be fulfilled by the socket communication via TCP/IP, the communication must be handled by the non real time task.

The reference position generated in the operational side is transmitted to the working side via network communication. After receiving the reference position, the information is sent to the real time task of the robot arm control in the working side. Then, the robot arm in the working side is moved according to the received reference position. Therefore, even if the time intervals between the successively received reference position in the working side vary due to the undesirable effects such as communication delays, the remote control system works well.

The sequential flow of the remote control system is explained as follows:

1. The start command is transmitted from the operational side to the working side through the socket communication via TCP/IP.

2. In the operational side, the robot arm is controlled by FFC scheme at the constant sampling time interval.
3. At the operational side, the position request is sent to the real time task. Then, the position response of the robot arm in the operational side is received.
4. Subsequently at the operational side, the reference position of the working side is calculated from the position response of the robot arm in the operational side.
5. Next reference position of the working side is transmitted from the operational side to the working side through the Socket communication via TCP/IP.
6. In the working side, the received reference position is sent to the real time task of the robot arm controller, and the robot arm is controlled at the constant sampling time interval.
7. The above process from 1. to 6. continues until the mechanism switches to the visual servo control.

4.2.2.2 Working side (Position control behavior) The dynamics of the robot arm in the working side with the servo controller is expressed by

$$\mathbf{H}^{\mathrm{ws}}(\mathbf{q}^{\mathrm{ws}})\ddot{\mathbf{q}}^{\mathrm{ws}} + \mathbf{h}^{\mathrm{ws}}(\mathbf{q}^{\mathrm{ws}}, \dot{\mathbf{q}}^{\mathrm{ws}}) = \mathbf{K}_{\tau}^{\mathrm{ws}}[\mathbf{K}_{\mathrm{v}}^{\mathrm{ws}}\{\mathbf{K}_{\mathrm{p}}^{\mathrm{ws}}(\mathbf{q}_{\mathrm{r}}^{\mathrm{ws}} - \mathbf{q}^{\mathrm{ws}}) - \dot{\mathbf{q}}^{\mathrm{ws}}\}], \tag{4.8}$$

where $\mathbf{H}^{\mathrm{ws}}(\mathbf{q}^{\mathrm{ws}})$ is the inertia matrix, $\mathbf{h}^{\mathrm{ws}}(\mathbf{q}^{\mathrm{ws}}, \dot{\mathbf{q}}^{\mathrm{ws}})$ is the coupling nonlinear term, $\mathbf{q}^{\mathrm{ws}}$ is the position of joint angle, $K_{\mathrm{p}}^{\mathrm{ws}}$, $K_{\mathrm{v}}^{\mathrm{ws}}$ and K_{τ}^{ws} are position loop gain, velocity loop gain and torque constant for the robot arm in the working side, respectively.

The tip position $\mathbf{p}^{\mathrm{os}}$ of the robot arm in the operational side is calculated from the joint position output $\mathbf{q}^{\mathrm{os}}$ as

$$\mathbf{p}^{\mathrm{os}} = \mathbf{f}^{\mathrm{os}}(\mathbf{q}^{\mathrm{os}}), \tag{4.9}$$

where f^{os} means the forward kinematics of the robot arm in the operational side.

4.2.2.3 Camera side (Visual servo control by template matching) The template matching is applied to images obtained from the USB camera at each sampling time. The template matching is carried out by using the image for the target object obtained in advance. Both images for the target object and the image obtained from the camera are converted into gray-scale versions. The gray-scale image for the target object is resized according to the distance between the camera and the target object. Then, the target position in the image is obtained by the template matching, where the direction is conducted by using an appropriate criterion such as the sum of squared differences of the brightness between two images [90]. The reference position vector from the camera side (cs), $\mathbf{p}^{\mathrm{cs}}$ is determined in such a way that the center position of the target is coincided with that of the image obtained from the camera by using the distance calculation between the two center positions.

The target position is determined as follows:

1. Images are taken from the USB camera at each sampling time.

2. To process the image, acquired image is converted from *jpeg* format to *RGB* format.
3. Template matching method is used to determine the target position.
4. The detected target position is sent to the operational side through socket communication by using TCP/IP.

4.2.2.4 Switch from remote control to visual servo control Figure 4.4 shows the flow diagram of the switching mechanism from remote control to visual servo control. The rough motion is handled by the remote control upon FFC scheme. If the USB camera detects the target followed by sequential template matching [90], the working side robot arm moves to the target position by using the visual servo control. In this approach, reference position $\mathbf{p}^{\mathrm{cs}}$ is selected if there is the target object in the image detected and obtained from the camera. If not, the reference position $\mathbf{p}^{\mathrm{os}}$ is selected,

$$\mathbf{q}_{\mathrm{r}}^{\mathrm{ws}} = \begin{cases} (f^{\mathrm{ws}})^{-1}(\mathbf{p}^{\mathrm{os}}) & (\text{if } \mathbf{p}^{\mathrm{os}} \text{ is selected}) \\ (f^{\mathrm{ws}})^{-1}(\mathbf{p}^{\mathrm{cs}}) \ , & (\text{if } \mathbf{p}^{\mathrm{cs}} \text{ is selected}) \end{cases} \tag{4.10}$$

where f^{ws} and $\mathbf{q}_{\mathrm{r}}^{\mathrm{ws}}$ stand for the kinematics of the robot arm to be controlled and reference of joint angles, respectively. Target detection from the camera image is carried out by using the method of setting threshold criterion in term of the brightness values [90, 91]. In our experiments, constant light conditions are assumed.

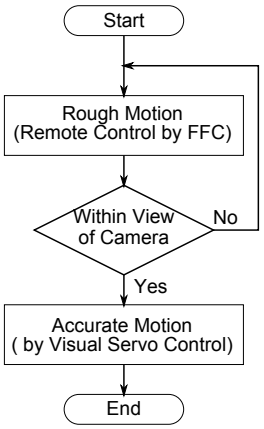

Figure 4.4: Concept Flow Chart of Switching of Remote Control to Visual Servo Control

4.3 Validation of the teleoperation system

4.3.1 Experimental condition

The effectiveness of the proposed teleoperation system is assured by experiments. The experimental study was carried out using actual robot arms connected with LAN. Figure 4.5 shows the diagram of experimental setup for the given teleoperation system.

A vertical articulated robot arm, Performer MK3s *(Yahata Electric Machinery Mfg. Co. Ltd.)* was used for the robot arm in the working side, and a SCARA was used for the robot arm in the operational side. The parameters of these robots are shown in Table 4.1. The position loop gain was given as $K_{\mathrm{p}}^{\mathrm{ws}} = 25I$ [1/s] and the velocity loop gain was given as $K_{\mathrm{v}}^{\mathrm{ws}} = 150I$ [1/s] for Performer MK3s, and the position loop gain was given as $K_{\mathrm{p}}^{\mathrm{os}} = 2I$ [1/s] and the velocity loop gain was given as $K_{\mathrm{v}}^{\mathrm{os}} = 120I$ [1/s] for SCARA. The real time behavior for both position and force-free control was established by the RT-Linux environment. The sampling interval of the real-time task for the robot arm control was 4 [ms], the time interval of the reference position generation in the non-real time task of the operational side was approximately 50 [ms], and the time interval of visual servo control was approximately 200[ms]. For SCARA, Link 2 and Link 3 were used. For Performer MK3s, Link 1, Link 2, Link 3 and Link 4 were used. This means that we can achieve the accurate motion for not only y-direction but also z-direction. Then, Link 4 is controlled so as to maintain the direction of the camera horizontally.

The following assumptions and conditions are made for the given teleoperation system and for all the experiments.

1. The changes of external environment factors such as illumination level of the working area are assumed to be negligible.
2. Skills and cognitive factors of the human operator are remained unchanged throughout the experiments.
3. Locations of the master and slave robots are fixed and also network traffic on communication channels, therefore, time delays and data loses are assumed to be constant for given experimental results.
4. The template matching technique used in the experiments is sum of square difference (SSD). We assume SSD accuracy to remain unchanged during all the experiments.
5. The SSD is known as light weight algorithm, so that computational burden issues are homogeneous and assumed to be minimal throughout the experiments.

Table 4.1: Parameters of Performer MK3s and SCARA Robot

	MK3s	SCARA
Resolution	8192	8000
Gear ratio of Link 1	120	-
Gear ratio of Link 2	160	50
Gear ratio of Link 3	160	50
Gear ratio of Link 4	100	-
Length of Link 1 [m]	0.36	-
Length of Link 2 [m]	0.25	0.3
Length of Link 3 [m]	0.215	0.315

The USB camera used (we used a general purpose web-cam for this experiment) during the experiments is MiniCam2 *(V-Gear, Asiamajor Inc.)*. The proposed system

claims to be able to work with any type of USB camera which merely depends on the degree of accuracy needed. Therefore, the robot manipulator at the working side will be able to operate with any type of plug and play camera after applying a few changes on settings if necessary. However, our experimental setup for these experiments was confined to the local area network on TCP/IP. Since our teleoperation system carries out the control of the robot arm through the Internet, the working side can be located in either a distant location of the local country or different geographical location anywhere in the world.

Before experiments, we need to give the threshold value for the template matching algorithm. The sum of squared differences was adopted as the index to evaluate the brightness of images. The pre-requisite experiment was carried out to find the average value for the threshold upon the same environmental conditions and same target button. In the experiment, we took the readings as follows:

1. Size of the template image was configured as 74×72 [pixels] and camera image size was configured as 288×352 [pixels].
2. Read the SSD value when the USB camera detects the target button, was approximately 7000.
3. Again read the SSD value when the USB camera is away from the view of the target button, was approximately 22000.
4. The average 14500 of both readings for template matching algorithm was selected as the threshold.

The robot arm in the operational side is moved passively according to the external force applied by a human hand. Therefore, robot arm, Performer MK3s will have to be controlled as to bring the tip of the robot arm to reach the target position.

4.3.2 Experimental results by actual industrial robot arms

The experimental outcome was obtained from a series of experiments. The experiments were carried out using actual robot arms. For the illustration, two of them are described in this paper. The effectiveness of the teleoperation system is assured by comparison of them. The outcome from the two different trials are illustrated in Figs. 4.6 and 4.9. The actual robot arms were connected via LAN including the mounted USB camera on the working side Performer-MK3s robot. Figures 4.6 and 4.7 are given by the reference positions for rough motion and accurate motion, respectively. Figure 4.8 shows the time evolution of the robot arm tip position and the corresponding reference position of the working side robot arm tip. Figure 4.9 shows sequential plots of the locus of the tip position and symbol '$\times$' indicates the switching point from rough motion to the accurate motion for each experiments.

Notations for the experiment result graphs are as follows: Tables 4.2 and 4.3 denote data format and the notations of the experiments. In Fig. 4.6, $\mathbf{p}^{\mathrm{os}} = (\mathbf{x}^{\mathrm{os}}, \mathbf{y}^{\mathrm{os}})$ is the reference position sent from the operational side (os) for x-direction and y-direction, and in Fig. 4.7, $\mathbf{p}^{\mathrm{cs}} = (\mathbf{y}^{\mathrm{cs}}, \mathbf{z}^{\mathrm{cs}})$ is the reference position sent from the camera side (cs) for y-direction and z-direction.

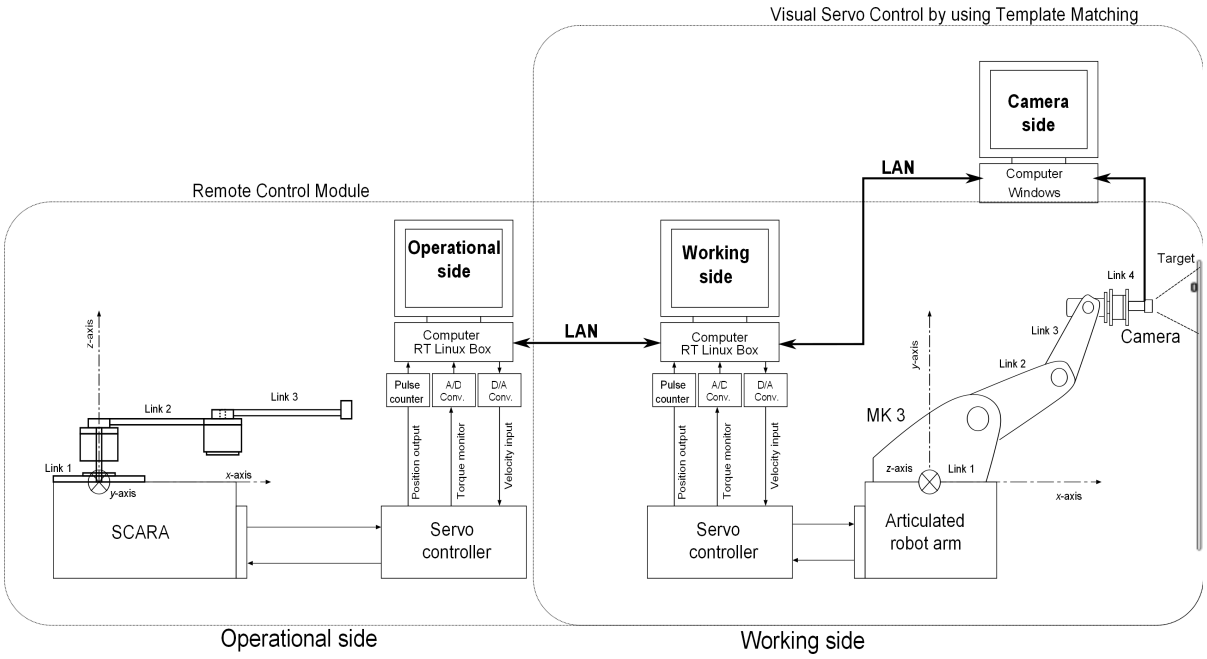

Figure 4.5: Experimental Setup Diagram of the Proposed Teleoperation System

The tip positions of the robot arm in the working side behaved according to the reference position in the operational side until 4.32 [s] for the experiment (1) and 3.30 [s] for experiment (2), respectively. Then, the control strategy was changed from the remote control to the visual servo control. The tip position was closed to the camera side reference position. Finally, the tip position of the robot arm in the working side reached the target position, where target was created by using a round black button of 0.02 [m] diameter, fixed on the board as shown in Fig. 4.5. Target was fixed for both experiments, and located at 0.51 [m] away from the x axis, 0.64 [m] high from the y axis and 0.05 [m] from z axis of the robot base in the working side. The results show that the teleoperation system combined with the remote control and the visual servo control can be successfully operated.

Table 4.2: Communication Data Format for Operational Side (os) to Working Side (ws)

Transmit data	Time[s]	Position reference x^{os}[m]	Position reference y^{os}[m]
Received data	Time[s]	Position output $x_{\mathrm{r}}^{\mathrm{ws}}$[m]	Position output $y_{\mathrm{r}}^{\mathrm{ws}}$[m]

Table 4.3: Communication Data Format for Camera Side (cs) to Working Side (ws)

Transmit data	Time[s]	Position reference y^{cs}[m]	Position reference z^{cs}[m]
Received data	Time[s]	Position output $y_{\mathrm{r}}^{\mathrm{ws}}$[m]	Position output $z_{\mathrm{r}}^{\mathrm{ws}}$[m]

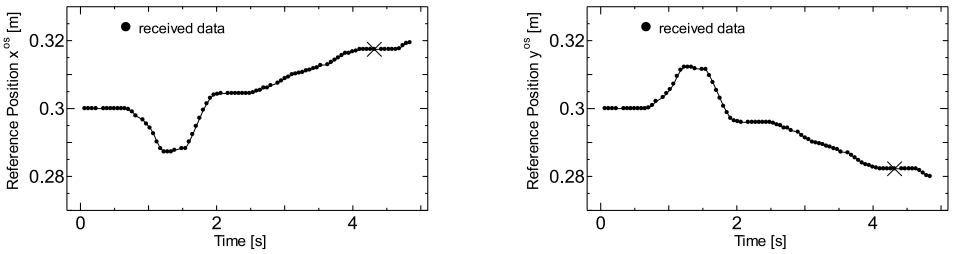

(a) Experiment 1

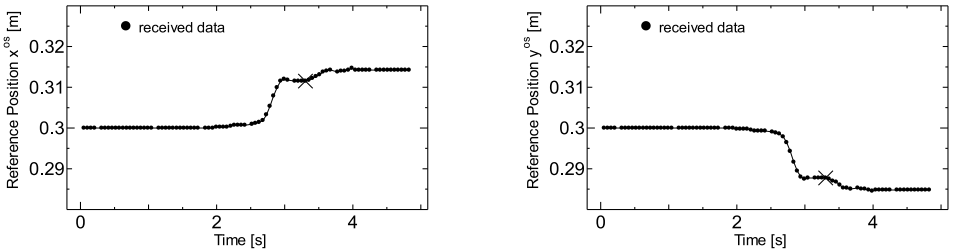

(b) Experiment 2

Figure 4.6: Reference Position Generation with Time by Force-free Control for Experiment Number 1 (Top) and 2 (Bottom)

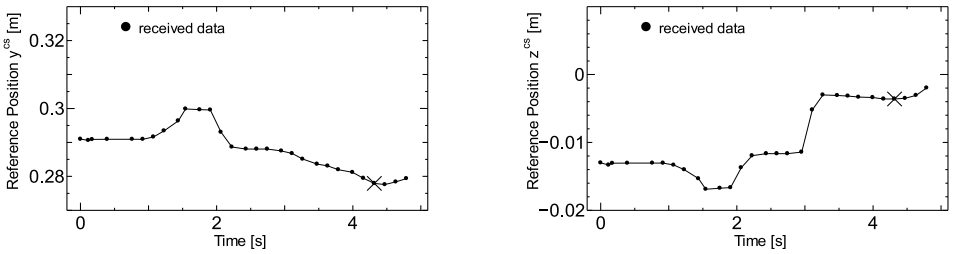

(a) Experiment 1

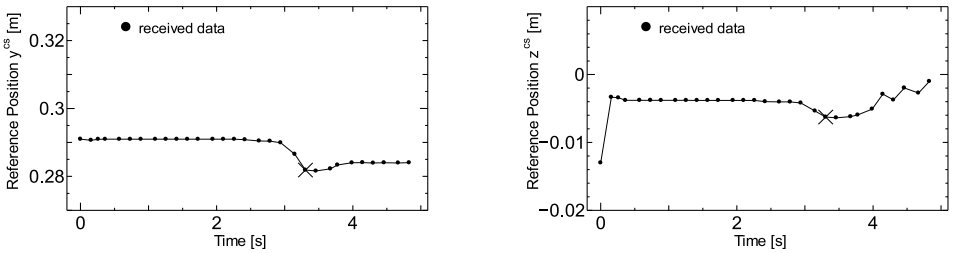

(b) Experiment 2

Figure 4.7: Reference Position Generation with Time by Template Matching for Experiment Number 1 (Top) and 2 (Bottom)

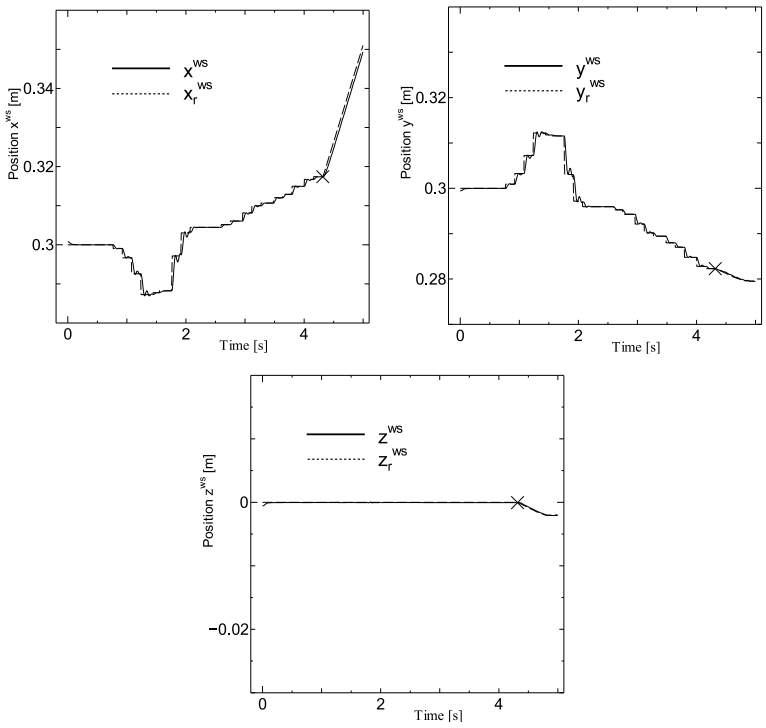

(a) Experiment 1

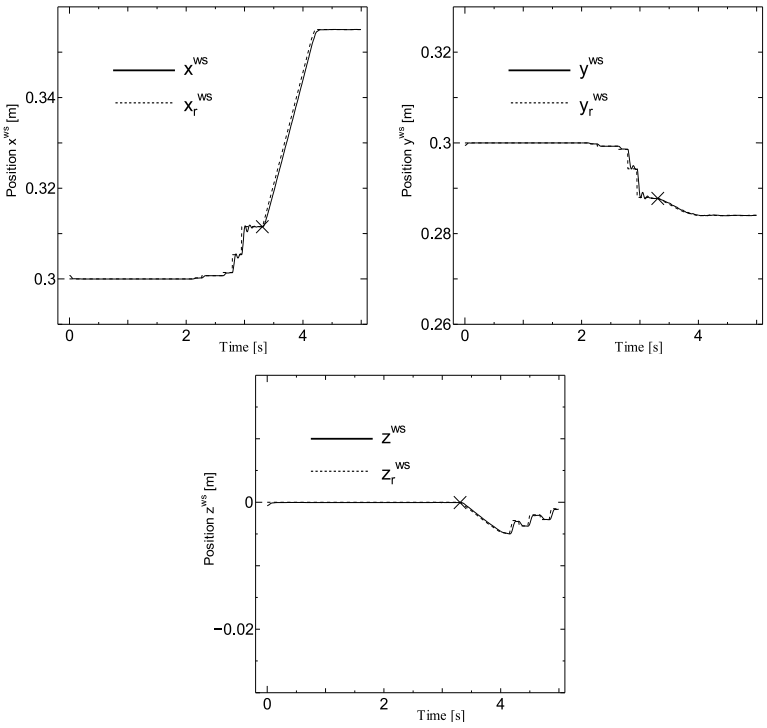

(b) Experiment 2

Figure 4.8: Tip Position of the Robot Arm in the Working Side

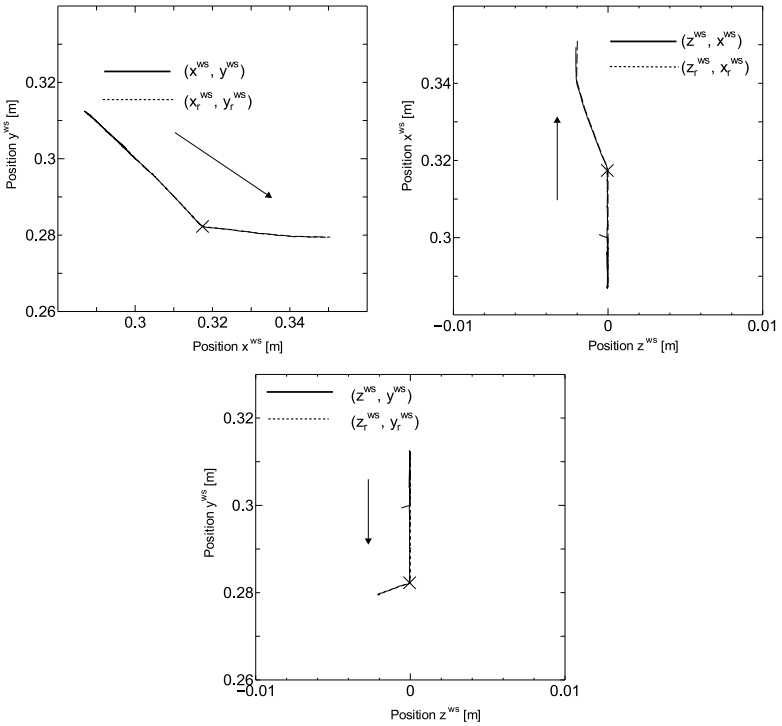

(a) Experiment 1

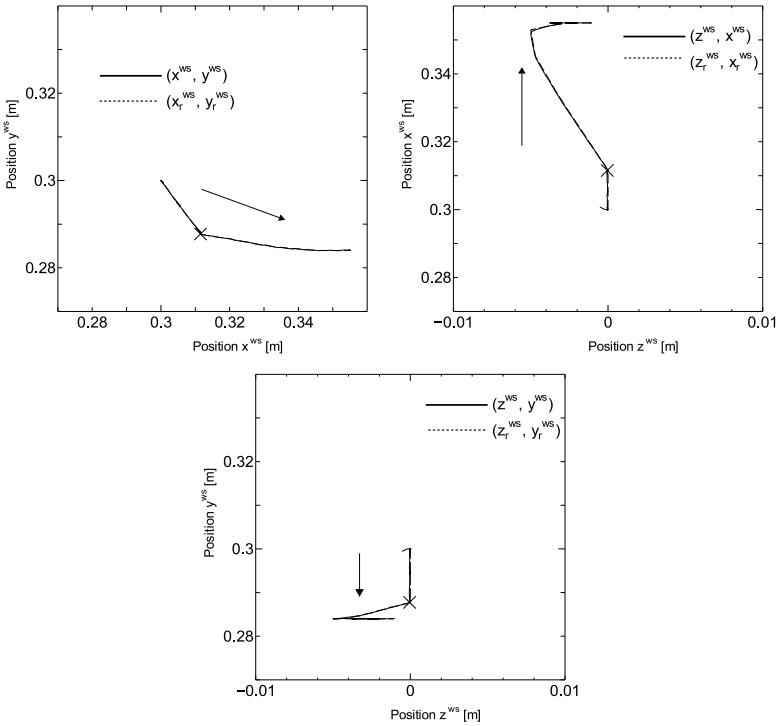

(b) Experiment 2

Figure 4.9: Locus of the Tip Position of the Working Side

4.4 Discussion

4.4.1 Maneuverability

Although, in the proposed system, human operator is required to operate the robot arm in the working side by means of force-free control, it handles only the rough motion through the remote control. Then, after receiving the reference position from the operational side, the accurate motion of the robot arm in the working side can be initiated autonomously by using the template matching cum visual servo control. Besides, the behavior of our teleoperation system has two motion steps to reach the desired target of working side robot arm to move. Therefore, requirement of the human operator is to move the robot arm in the operational side whose operation will be reflected in the working side (where the target is located) within the frame of the USB camera mounted on the robot arm in the working side. Thus, the handleability of the proposed teleoperation system is high enough to execute more complex movements as per the operator's expectations.

The most important aspect is that, we can use servo controller of the industrial robot arm, without changing the factory fitted configurations. Therefore, any robot arm can be used for this application theoretically. The additional software of the force-free control and communication program is enough for the realization of the teleoperation system. In addition, a common type of USB camera with a computer to process the images can be attached to the robot arm separately in the working side to acquire the accurate target position control. The advantage of the above brings flexible teleoperation system configuration by use of the appropriate mechanism selection of FFC followed by visual servo control for the operational side and for the working side.

4.4.2 Accountability of network delays and data losses

Our aim is to make a teleoperation robot control system that will work between two geographical locations in any part of the world. Therefore, the Internet technology is identified as a readily available and suitable communication platform to be used for the proposed system. The socket communication via TCP/IP may include communication delay and data losses which may also create inconsistency when transferring data. With respect to the communication delay, the influence may appear as a delay of the robot arm motion in the working side from the motion in the operational side because the reference position generated in the operational side is transmitted to the working side, and the robot arm in the working side is moved according to the received reference position with communication delay. Due to the lack of required data of corresponding reference positions, the consequence of data losses may be reflected as an awkward or an undesirable robot arm movements in the working side. By considering the remote control behavior, communication delay obviously defects the maneuverability of the teleoperation system. Although, in this research, communication delay may also be incurred to our teleoperation system, communication delay is caused to the rough motion behavior of the robot arm in the working side. Hence, the communication delay is not going to be a critical factor to be handled for the cited system as accurate motion is totally carried out by the working side visual

servo control under real time conditions.

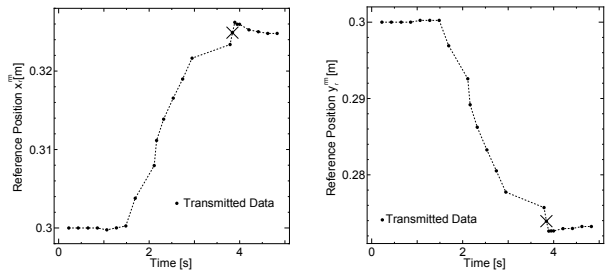

(a) Experiment No. 1

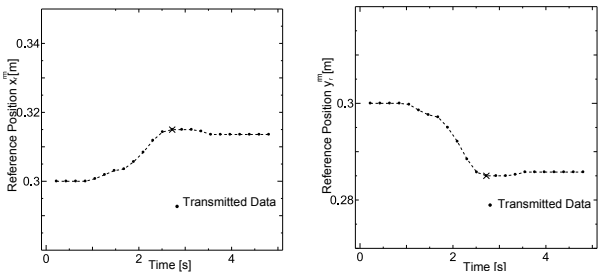

(b) Experiment No. 2

Figure 4.10: Reference Position Generation by FFC for Experiment No. 1 and No. 2

Following control experiments are carried out to illustrate the presence of delayed and loss of data during operation and transmission. We can clearly see the data loses in the Figs. 4.10 and 4.11 of the experiment No. 1. The reference position graphs, in the experiment No. 1 dots are missing with respect to the time intervals and experiment No. 2 no data loses can be seen. Since, both cases proposed control system make robot arm to reach to the target position, we can accept the systems fault tolerance on data loses during the transmission. Thus, during an operation remote control communication delay can also be occurred. Since, the communication delay is caused to the rough motion behavior of the robot arm in the working side, undesirable movements is not going to be created by communication delay or random data losses. Therefore, it reflects to the conclusion that fault tolerant capability of the given system for presence of data loses and communication delays has been inherited.

4.4.3 Practical usability and advantages

The teleoperation system was tested using actual industrial type robot arms in both master and slave sides. The results show the accurate motion of the working robot that brings the tip of the robot arm to the desired target position. Our motivation is to implement teleoperation system without changing existing servo controllers of the industrial robots used in both master and slave sides. The proposed system was achieved by introducing external control software modules for FFC and visual servo control including a low cost USB camera. In our specific approach, the idea of using an industrial type robot arm in the operational side stems from the fact that, in the present time, industrial robot arms are commonly available in most of the countries.

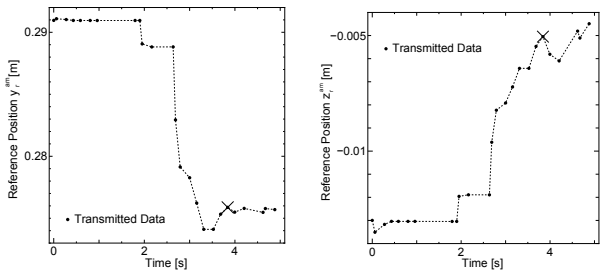

(a) Experiment No. 1

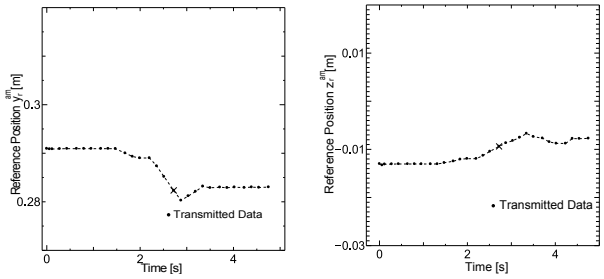

(b) Experiment No. 2

Figure 4.11: Reference Position Generation by Template Matching for Experiment No. 1 and No. 2

We found that it is highly versatile if one can varify an accurate teleoperation by using existing robots without major changes to their controllers. In practice, the proposed teleoperation system can be verified with an addition of extra software modules along with a few required configuration changes and an available low cost Internet communication channel. The above capability proves that in any situation like hazardous or an emergency, the proposed system can be applied even if the working robot is located in a remote location. By adopting the Internet technology, it can accurately be controlled remotely by using an industrial type robot arm located anywhere by means of minor configuration changes and human operator assistance. Moreover, it is important to state that the operation side industrial robot arm need not to be so accurate or precise in operation so that a low cost or an old robot arm can be used in the operational side as it is used only to provide rough motion reference position for the slave robot. Therefore, we also contribute to provide a low cost teleoperation system by means of integrating FFC and visual servo control techniques, where the proposed system can be configured for the existing industrial robots when teleoperation needs to be performed.

The teleoperation system provides an accurate motion control autonomously in the working side robot. Therefore, the system would compensate burdens due to the master control time delays and human operator mistakes to greater extent. The above facts give evidence to the fact that proposed teleoperation system has been a significant alternative solution to handle the existing problems of time delays, data losses and irregular communications of the current context of teleoperation. To

accomplish the solution, the system needs a few command data from the master side as supervisory control. The high degree of slave side autonomy feature for accurate control scheme brings the system tradeoff by reducing processing complexities and computational and communication burdens.

4.5 Summary with concluding remarks

In this chapter work, teleoperation of robot arm by means of force-free control and visual template matching was described. The reference position of the working side robot arm was generated by two control schemes, called rough motion and accurate motion. Two control schemes were executed; the remote control was achieved by means of force-free control, and visual servo control scheme was developed using template matching. The effectiveness of the above approach was verified by the experiments. Indeed, two sets of experimental results were provided to assure the repeatability of the proposed system. Additional control experiments were carried out to justify the claim of fault tolerance against data losses and delays during data communication via network. At this stage, since each of the experiments were conducted without changing light, glare, illumination conditions, these result are not assured and guaranteed to be used under different environment conditions. Some of the possible deviations due to an environment and a human factor changes were analyzed for different lighting level variations and different human operator perceptions, an exclusive description for the analysis given in next chapter.

Chapter 5

Evaluation of the Teleoperation System for Human Operator Perceptions

This chapter is dedicated to illustrate that an extension to investigate research considers the teleoperation of an articulated robot arm by means of force-free control and visual servo control (VSC) over communication channels using the Internet technology. A semi-autonomous type teleoperation system contains a human supervisory control and VSC schemes and switches one scheme to another for accomplishing the required task accurately. The main investigation is carried out to find how it effectively improves the accuracy and the effectiveness of the tele-operation after provision of a visual feedback channel to the system. The system accuracy, effectiveness, repeat-ability and handleability based on the human operators skills and operators cognitive aspects are evaluated using experimental results and statistical data analysis. Effectiveness of the statistical analysis is assured by increasing the number of experiment data and assuming environmental factors, and implicit variables maintain to be unchanged. Correlation coefficients are calculated to find out how controlled input parameters are related to the successful output given by the system.

5.1 Introduction

In many years, telerobotics has been a major concern among researchers. It becomes more focused and justified for space and undersea operations, fire-fighting and rescue operations in battlefronts and disasters, and also for training and entertainment activities. Teleoperation is of utmost importance, when the working site is hazardous, such as nuclear plant activities, land-mine extraction, toxic chemical plant activities and so forth. In recent two decades, Internet has been much popular infrastructure for the communication activities and therefore, researchers use Internet for telerobotic applications as consistent communication platform. The TCP sockets have also been

consistently used in many areas in telecommunication so that it gives past track records to be guaranteed as reliable communication with flow control, sequencing and re-transmitting of lost data [104]. The first Internet based telerobotics started as *Goldberg* [105] connecting a SCARA and ASEA IRb-6 type robots to the Internet in 1994. Since then, more researchers found their interest to use Internet for the development of advanced robot teleoperation applications, and remarkable early stage developments are published in [106, 107, 108].

However, the major concern in Internet technology based teleoperation is that an uncertain transmission delay between human operator in the master side and the teleoperated robot in the slave side. Major contributions to overcome such transmission issues are given in [109]. The *Sheridan's* supervisory control [82] was proposed and it was appreciated in view of stable teleoperation. Supervisory control approach implements an autonomous local feed back loop at the slave manipulator. Remote human operator needs only to send key parameters or few required data to initiate and the slave manipulator, of what just slave manipulator required for planing the trajectories and controlling the manipulator. This research is also based on a human supervisory control approach.

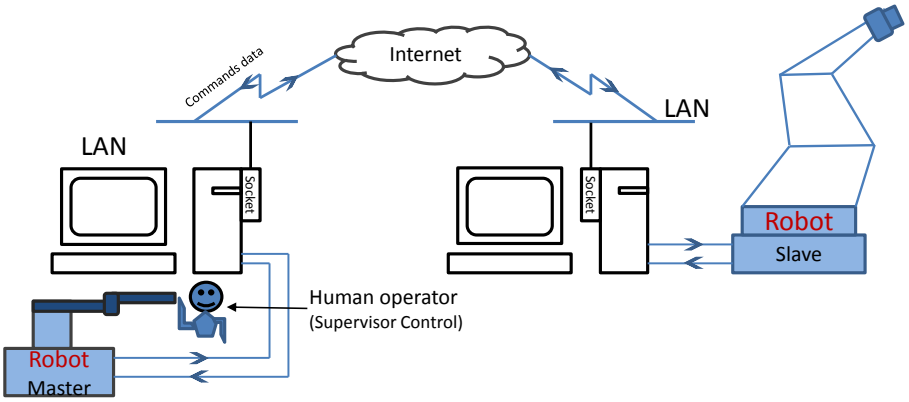

Figure 5.1: Schematic Diagram of General Supervisory Controlled Semi-autonomous Teleoperation System.

Figure 5.1 shows the schematic model representation of an Internet-based supervisory controlled teleoperation system. It also illustrates the main components and the terminologies in the context of a teleoperation systems. In our research, we adopted the same base architecture for experimental teleoperation setup. Moreover, the applicability and effectiveness of the supervisory control in teleoperation is highly depended and affected by the capability of the supervisory control in the master side as well as the local controller of the slave side. The investigation is based on the

evaluation of the human operator's skills and cognitive factors on a supervisory control. And how those factors can correlate with an effectiveness of the investigated teleoperation system.

The teleoperation system of this investigation comprises of two different techniques which are attached in to different modules. First one is the force-free control (FFC) which is used to realize the passive motion of robot arm for given external force by human operator. The details of FFC are described in [12] and references therein. The second one is the image processing module in which template matching (TM) techniques are used to carry out the accurate motion control by means of visual servo control [89]. Experiments were carried out by selecting operators appropriately corresponding to the following three kinds of experiments:

1. Providing camera view feedback to the operator.
2. Giving a guided map including desired path of the target.
3. Both map and visual feedback provided.
4. No additional aid provide (by seeing remote location robot from operational point).

5.2 Teleoperation by force-free conrol and visual servo control

Please refer chapter **4** for more details, in which full description of teleoperation system is given. Our teleoperation system consists of two different motion control mechanisms. First is to accomplish remote control action by means of human operator assistance, in which FFC method is used. The details of the mechanisms and functions are described in author's work [76]. Figure 5.2 shows the detailed schematic presentation of the teleoperation system and Fig. 5.3 gives the details of the data communication paths. The position control can be achieved by two kinds of motions for the reference position of the robot arm, i.e., the rough motion and the accurate motion. For the rough motion, the reference position is generated manually by using FFC. Second is to accomplish the accurate motion where the reference position is generated automatically by using the vision system based visual servo control (VSC). In order to generate the reference position of the robot arm for the accurate motion, the image obtained from the USB camera is analyzed and processed. The vision system attached to the camera side is responsible for detecting the target position. The reference position data for the robot arm are sent through the network as illustrated in Figs. 5.2 and 5.3.

After receiving reference position data from the master control, slave robot in the working side moves accordingly as "rough motion." The human operator moves the master robot arm manually until the camera mounted on the working side robot captures the image of the target object. Then system switches to the second control scheme for "accurate motion."

5.2.1 Force-free control (FFC)

The FFC realizes the passive motion of the robot arm due to external force so that the robot arm can move freely according to the external force. In this teleoperation system FFC control plays an important role by generating reference positions when human

operator executes the desired movement on the operational side robot. The generated reference position data is sent to the working side robot via network by using the socket communication TCP/IP [98]. The FFC for passive motion of the robot arm is applied without changes to the robot manufacturer's hardware configurations [97].

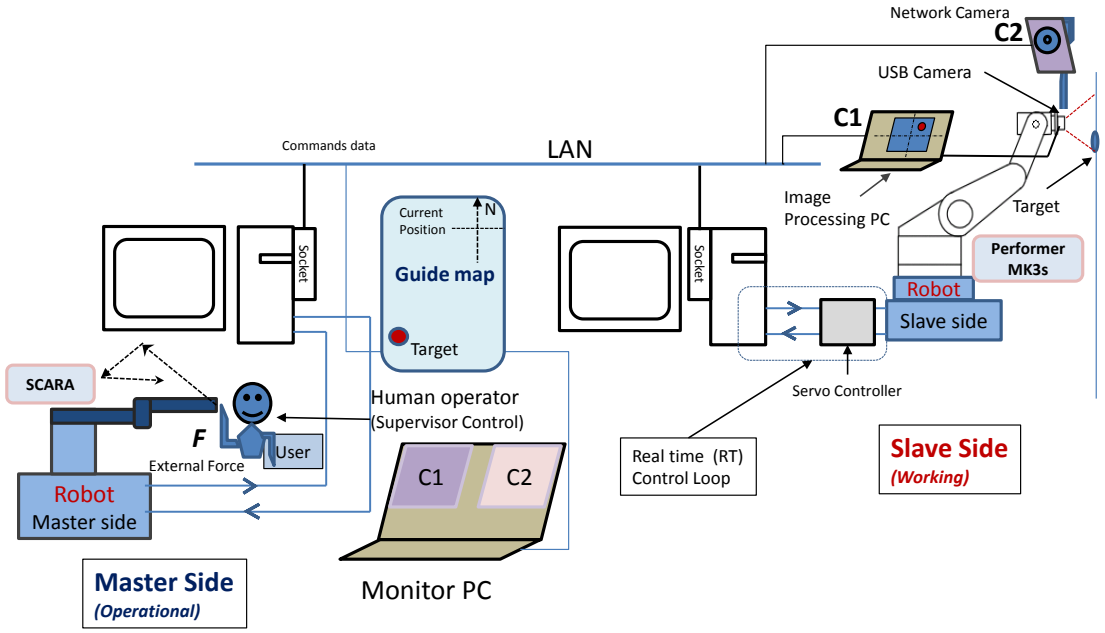

Figure 5.2: Schematic Diagram of the Investigated Teleoperation System with Visual Feedback

5.2.2 Visual servo control (VSC)

In our teleoperation system, VCS [89] plays an important role by helping working side robot arm to reach the target, after switching from the "rough motion." A general USB camera can be used in the VSC. At each sampling time, image is sent to the image processing in the camera side computer.

The image analysis is done by using template matching (TM) techniques [103, 101], in which, it calculates the position of the target inside the image. Then, system calculates the corresponding reference position and send it to the working side robot. To apply the template matching algorithm, camera image must be processed at a each sampling so that, robot can reach to the target position. The center of the camera view and the target object at a particular instance of the VSC are calculated in each sampling. And continuously, image is processed and applied the template matching until target would coincides with the center of the camera view.

5.3 Human operator's perception

The main objective of this research to investigate the applicability of the system by using different users and scenarios. Therefore, this research is focused on some aspects

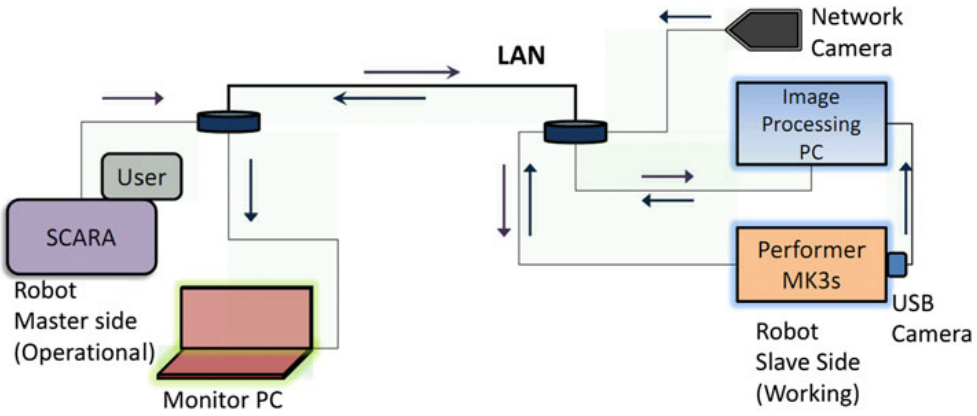

Figure 5.3: Communication Network and Data Flow Directions

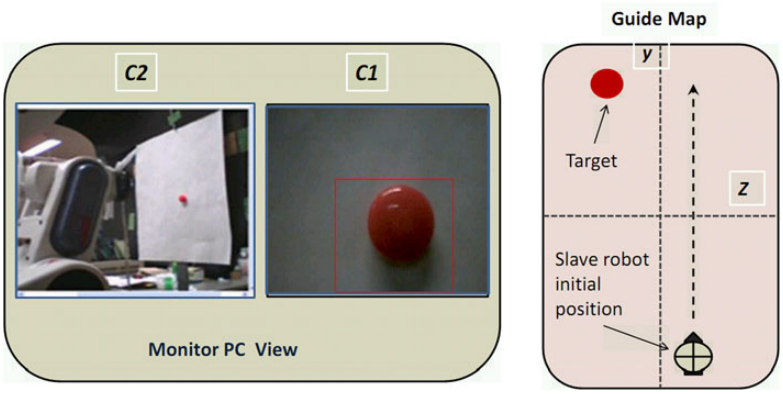

Figure 5.4: Monitor PC User View and Guide Map

Table 5.1: Experiment Data and Results for Teleoperation Using Different Users

Exp. No.	User No. (Operator)	Skill / Experience. Level	Results (Success or Failed)				Remarks Age-Field of Study (Related or Not)
			Direct View	Guide Map	Camera View	Guide & Camera View	
1	User No.1	High	Success	Success	Success	Success	23 - Related
2	User No.2	High	Success	Success	Success	Success	23 - Related
3	User No.3	High	Success	Success	Success	Success	34 - Related
4	User No.4	Low	Success	Failed	Success	Success	21 - Related
5	User No.5	Low	Success	Failed	Failed	Success	22 - Related
6	User No.6	New	Failed	Failed	Failed	Failed	20 - Non Related
7	User No.7	New	Success	Success	Success	Success	20 - Related
8	User No.8	New	Success	Failed	Success	Success	21 - Non Related
9	User No.9	New	Success	Failed	Failed	Success	21 - Non Related
10	User No.10	New	Success	Success	Success	Success	21 - Non Related
11	User No.11	New	Success	Success	Success	Success	23 - Non Related
12	User No.12	New	Failed	Success	Success	Success	23 - Non Related
13	User No.13	New	Success	Failed	Success	Success	20 - Related
14	User No.14	New	Failed	Failed	Failed	Failed	20 - Related
15	User No.15	New	Failed	Failed	Success	Success	21 - Non Related
16	User No.16	New	Success	Success	Success	Success	21 - Related
17	User No.17	New	Success	Failed	Failed	Success	20 - Non Related
18	User No.18	New	Success	Failed	Success	Success	20 - Non Related
19	User No.19	New	Success	Failed	Success	Success	20 - Related
20	User No.20	New	Success	Failed	Success	Success	21 - Non Related
21	User No.21	New	Success	Success	Success	Success	21 - Non Related
22	User No.1-R	High	Success	Success	Success	Success	23 - Related
23	User No.4-R	Low	Success	Success	Failed	Success	21 - Related
24	User No.9-R	New	Success	Failed	Success	Success	21 - Non Related
25	User No.19-R	New	Failed	Failed	Success	Failed	20 - Related
26	User No.20-R	New	Success	Failed	Failed	Success	21 - Non Related

NB:User No.X-R means Repeat by same user

of the system especially for accuracy, effectiveness, repeatability, handleability and so forth.

In a practical situation no one can guarantee that high skill exclusive operator would be available in all time. Therefore, teleoperation system design is focused to make it as simple to operate even by the average user who does not have prior experience or special skills of operating the system. And also it can be operated with the minimum guidance as shown in Fig. 5.2. the system would provide the operational assistance by means of online camera views ("C1" and "C2" in Figs. 5.2, 5.4) and the guide map of the target location.

The human operator's responsibility is to manipulate the robot arm in the operational side as to give "rough motion" to the working side robot that would catch the target within its camera view. To investigate the ability of applying the supervisory action by the general user, a larger number of experiments were carried out by providing different means of aid to human user and also sample of users were selected with irrespective of experience, age, field of studies and anthropometry of the body [113].

In general, each human has different levels of cognitive power, persistence, reactive or response time, level of skill for particular area, level of experience, prior knowledge of a particular subject etc. Therefore, any system with human involvement subjects to above mentioned aspects [114]. Due to above mentioned reasons, system is designed in such way that it should be identified the tolerances of those aspects if the system is intended to be applied in real practice.

5.4 Experimental results

Figure 5.2 is illustrated the experimental setup, the robot arm named Performer MK3s with attached USB camera in working side was controlled by the reference position generated in the operational side using SCARA robot. The SCARA is manually operated by a human operator until the target was included in the view of the camera. Then, Performer MK3s is controlled autonomously by the reference position generated in the camera side. As in Fig. 5.2, target object is located in the slave side. A network camera is used to capture the view of the target area and it will give the video feed back to the monitor PC as a camera view "C2" in Fig. 5.3. The SCARA and the MK3s robots are connected to the computers in the master side and the slave side respectively. Image processing is done in the image processing pc "C1" in the slave side of the system. The arrow marks are given to show the movements of the SCARA robot which are performed by a human operator.

In this experiment, each of the experiments was done by volunteer users as listed in the Table 5.1. The experiments were arranged to get four readings from each user. Users skill level is defined based on the past experience of using the system and ranked them as "High", "Low" and "New" as in Table 5.1. Four reading were taken form different scenarios of the experiments as listed in Table 5.1 as follows:

1. "Direct View" is given for an operator manipulate the robot arm by looking at

the master side robot directly and no any other aid is given.
2. "Guide Map" is given for an operator manipulates the robot arm by only looking at the site map of the target position as shown in Fig. 5.2.
3. "Camera View" is given for an operator manipulates the robot arm by looking at the computer monitor which has camera view of the target location of the working side as shown in Figs. 5.2 and 5.4 .
4. "Guide and Camera View" is given when operator has both aids of guide map and camera view feed back. Figure 5.4 illustrates the "Monitor PC" view provided to the user.

However, communication delays contracted in the system are assumed to be constant for all the scenarios and effects of them are not taken into the account.

The results showed that visual feed back improved the effectiveness of the total teleoperation cycle in regardless of the age and level of experience. However, communication delay on video stream can degrades the decision taking time for performing desired movements by applying external force. Statistical data analysis using the "probability and correlation coefficients" are carried out to verify the results based on how effectively target is reached on different experiment scenarios by different human operators as shown in Tables 5.2 and 5.3. The "success level" gives the probability of success in each category.

To identify a feasibility of the use of the teleoperation system by different users with different perceptions, thorough investigation are carried out by using unbiased sample of human users. In this investigation, we used 26 different trials of experiments as given in Table 5.1 which denotes the abstract and final information about the total investigation. User age and user's field of studies whether it related to the teleoperation or not are also given under remarks. From the research, we draw main objective that how effectively new user having different perspectives can operate the teleoperation system by using different visual aids such as a video feed back or/and a guide map of the target location.

In addition, a new user was given an introduction prior to begin his trials of experiment. It was found that certain either new or experience users shown energetic and confident interest, and also they wanted to perform more and more trials, however, few of them were found an uncomfort feeling and were lethargic during their turns. Hence, the effectiveness of the supervisory action also depends upon operators instantaneous condition and cognitive aspects of their mind or/and their perspectives regardless of their experience or skills at the time of an experiment [115].

Table 5.2: Correlation Variations with Skill Level

	Category	Correlation with skill level	Remarks
1	Direct View	-0.2218	Negative
2	Guide map Only	0.1379	Positive
3	Cameras Only	-0.1011	Negative
4	Cameras & Guide	-0.1136	Negative

Table 5.3: Probability of Success Level Variation With Category

	Category	Success level %	Remarks (Skilled user)
1	Direct View	80.77	all success
2	Guide map Only	42.31	2 failed
3	Cameras Only	73.1	2 failed
4	Cameras & Guide	88.46	all success

5.5 Discussion

According to Table 5.2, the guide only scenario has shown positive correlation with skill level. However, in all other scenarios, correlation with skill level and success rate has negative correlation. Also it is observed that negative correlation decreases with introduction of camera view, this indicates that giving online visual feedback with instructions to the users gives better performance. Moreover, it can be stated that skill level and guide only scenario indicate stronger linear relationship than that of skill level and camera view scenario. Table 5.3 shows the success probability variation for each category.

The results show positive increment on system effectiveness by introducing online camera feedback, regardless of a user being experienced or not. Since a large number of new users are involved in this investigation, we can conclude that introducing visual aid directly increases the effectiveness as shown in Table 5.3 of probability of success. However, in most cases experienced users of the system have shown that they can handle the system successfully even without an online visual feedback. Moreover, certain amount of users found difficult to use and manipulate the teleoperation system; results show that success percentage varies when category changes. It is also observed that certain number of users could not be able to operate the master robot arm as then moving the working robot on desired rough motion towards the target.

However, in their second attempt, same users could get succeeded. Therefore, we conclude that system operational functions can easily be understandable for a general user who did not have either any previous interactions or experience on using the system. Since the sample of users used for the investigation does not include

female users, correlation results might have a high possibility of variation if sample includes female users.

5.6 Summary with concluding remarks

In this contribution, an investigation is carried out for the teleoperation system to find out how human factors with cognitive aspects affect the system effectiveness and performance when it applies in practice. It is essential that we must test the system with large number of real scenarios to validate the applicability, if the teleoperation system claims to be used in real application. Moreover, especially if a system has human user involvement and which is a critical factor for a fulfillment of final objectives then a sample of users should be selected with a high degree of variation and the sample amount must also be higher.

The relevance of the real world application of the teleoperation system, particularly in case of human supervisory involvement, is highlighted herein. Finally, provision of a visual feedback channel for the human user effectively increased the applicability and success rate (effectiveness) of the teleoperation system regardless of users skills, age and relevance to their major field of study. By considering the results, if number of users in the sample or number of experiments is increased then the regression analysis also can be carried out using a fitted probability model for the experimental results.

Chapter 6

Analysis of Teleoperation System for Lighting Variations

In this chapter, the evaluation criteria for teleoperation system described in the chapters 4 and 5 is investigated by the viewpoint of variation of lighting conditions on different image processing algorithms. For all cases, communication channels are established by using the Internet technology. The teleoperation system is almost similar to that of chaper 4 and 5 which comprises of two different techniques. One is the force-free control (FFC), which is used to realize the passive motion of the robot arm for an external force. The other is an image processing component in which template matching (TM) techniques are adopted to realize the accurate motion by means of visual servo control. Since the template matching technology plays a vital role in our teleoperation system, it is important to investigate the behavior according to varying lighting levels. The experiments were performed to investigate the influence of lighting conditions by using actual robot arms with vision system. Two main template matching algorithms are illustrated in order to make clear understanding of applying the teleoperation system appropriately for different lighting conditions.

6.1 Introduction

Teleoperation via Internet technology is an important research topic in robotics. This has been an emerging topic in recent years, is a means of rendering demanding services in hazardous environments, space exploration, mining, maintenance and hazard handling of nuclear plants, surgery and deep sea explorations with under water maintenance [87, 88, 95]. However, in conventional approaches (e.g., direct manipulation from the master side control with human interference [82]), the self-adaptive capability of the slave manipulator (in this context slave side referred as"working side") is limited. In addition, in conventional methods, the time delay in communication is a

considerable problem. Therefore, self-adaptive or autonomous capability on the slave robot arm is important because teleoperation is often performed in dangerous (e.g., nuclear, hazardous chemical environments, high temperature areas) or partially uncertain (e.g., unexpected changes in environmental conditions such as glare, shading, sudden drops of sunlight and reflections) environments. In such situations, control ability from the master side is limited and slave side control should handle the robot control autonomously.

However, vision systems are generally sensitive to the changes of lighting levels of the surrounding environment. It must be eagerly vital to investigate the behavior of the vision system according to the variation of lighting conditions before applying to the practical usage.

In [99], investigations on the effect of lighting variation on template matching are elaborated, where lighting invariant matching algorithms are also discussed in order to make concise comparisons. The ability to tolerate brightness variations with different template matching techniques and their applicability were studied in [100, 101].

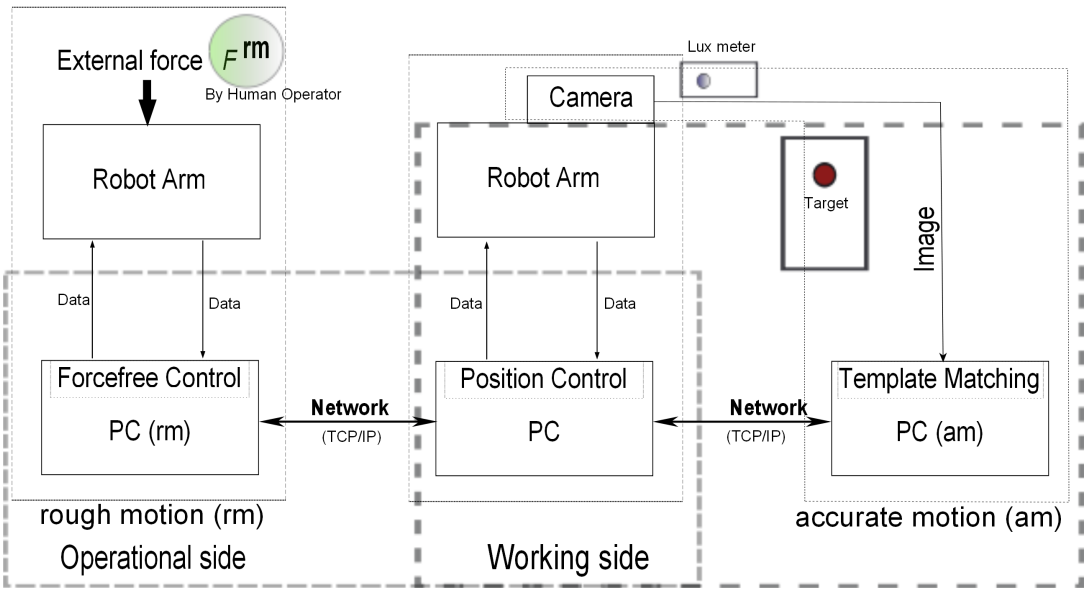

Figure 6.1: Schematic Diagram of the Teleoperation System

Due to obvious communication delays and uncertainty limitations, the accurate manipulation from the master side by human operator is highly impossible (In this context, master side referred to as "operational side."). Therefore, the operational side performs initial movements to the robot and then the working side robot moves accordingly. It always shows such movements are not so accurate due to communication delays and human and internal uncertainties involved (teleoperation until camera detects the target is said to be "rough motion"). The rough motion is enough for

working side robot to move towards the target manually by human operator however, it is difficult to reach the exact desired target position. To reach the exact target position visual servo control is used where camera guided vision system is implemented (where image processing is done referred as "camera side"). The camera side operation has the responsibility of moving working side robot to the exact target position autonomously (in these cases, movement of robot since camera detects the target and until it reaches to the target referred as "accurate motion"). In fact, by applying appropriate switching of two control schemes, it can be compensated the uncertainty errors involve in cause of human and communication delays [98].

Table 6.1: Recommended Standards Levels of Indoor Lighting for Industrial and Laboratory Work

Place or area	**Activity type**	**brightness** (Illuminance [Lux])
General Laboratories	Doing Experiments	700 - 1500
Office Environment	General work stations	1500 - 3000
Industrial Factories/Labs.	Production area/ Laboratory work	1500 - 3000
	Electrical cabinet	1500 - 3000

The recommended standards for lighting levels depend upon the type of the work being done. Table 6.1 shows some of the recommended lighting ranges for experiments and indoor industrial operations [102].

In this research, industrial type robot arms are used in the experiments. In general, it is difficult to move the robot arms freely by applying external force (passive motion). To restrain from such difficulty, the force-free control (FFC) technique is used. The FFC is used in operational side to execute desired movements when applying an external force by the human operator. The details of the implementation of FFC for teleoperation system is given in [97] and references therein. The details and current status of the teleoperation system which is used to investigate and describe in this context are given in [76, 111, 112].

Figure 6.1 shows the schematic diagram of the investigated teleoperation system. In "operational side," robot arm is manipulated by a human operator giving an external force 'F^{rm}' to the robot arm. Then, according to that movement, the robot arm in the working side moves until the camera mounted on the working side robot arm's tool end detects the target object. In each experiment, lighting level is measured by using the "lux-meter" fixed at the working side.

To investigate the lighting conditions, experiments using actual robot arms with vision system were carried out for different lighting levels. And those experiments were carried out by using the same parameters and target position except the lighting level. The target position was set in advance and fixed throughout the experiments.

Moreover, it is found that small change of lighting level is affected in vision system parameters, hence, it affects to the visual servo control behavior of the teleoperation system. The results also illustrate that color of the target has a considerable effect to achieve the desired behavior of our teleoperation system. Finally, to create concrete investigations, multiple experiments were performed for each lighting level and hence, repeatability of the teleoperation system is justified. The operation repeatability is also an important parameter when the system is claimed to be applicable in operation. To study the same in operation, investigations were carried out based on lighting variations towards finding the lighting level for the accurate operation, in which correlation of the color variation of the target object was also observed. The experimental results are also described the effectiveness and the accuracy of the system under different lighting conditions.

6.2 Overview of main system components

To understand the operation, it is required to identify the main parts of the system, so that this section briefly introduces the roles of the force-free control and the template matching technique with visual servo control. Please refer Chapters 3 and 4 for full details of FFC and an adapted teleoperation system.

6.2.1 Force-free control

The idea of the FFC is to realize the passive motion of the robot arm due to external force so that the robot arm can move freely according to the external force. In this teleoperation system FFC control plays an important role by generating reference positions when human operator executes the desired movement on the operational side robot. The generated reference position data is sent to the working side robot via network by using the socket communication TCP/IP [98]. After receiving reference position data, robot in the working side moves accordingly as "rough motion." The human operator should move the robot arm manually until the camera mounted on the working side robot captures the image of the target object. Until this stage, we call such motion as "rough motion," and then system switches to the second control scheme for "accurate motion."

In the FFC control concept, the passive motion of the robot arm by the external force under zero friction and zero gravity conditions. The FFC for passive motion of the robot arm is applied without changes to the robot manufacturer's hardware configurations, so that FFC is coupled as separate control module to built in servo controller of the robot arm [12].

6.2.2 Visual servo control

Visual servo control [89] plays an important role by helping working side robot arm to reach the target, after switching from the rough motion. This component consists of a general USB camera which is used to capture the target. And at each sampling time image is sent to the image processing unit in the camera side computer. Figure 6.2 illustrates the flow diagram of switching between rough motion to accurate motion.

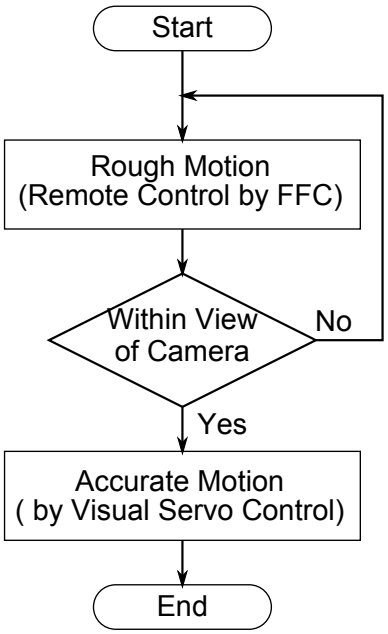

Figure 6.2: Flow Chat of the Motion State Switching

The image analysis is done by using template matching (TM) techniques [103, 116], in which correlation between images taken in each sample and the predefined template image of the target is calculated. Then, it calculates the position of the target inside the image. Thereafter, it calculates the corresponding reference position and send it to the working side robot.

Sum of Square Differences SSD and Normalized Cross Correlation Matching NCC algorithms [90, 91] are used to match the template and hence, used to calculate the position of the target within the camera view, in which "SSD" has higher sensitivity on lighting changes whereas NCC has less sensitivity though, high computational complex instead. The accuracy of expected results of the experiment and speed of the TM output depend on the algorithm [101]. Due to our requirement of online and fast object tracking, histogram technique of using 'H' of "HSV" has been rejected. At early stage spot tests also given poor computational speeds and poor efficacy during very low lighting levels for 'H' component based tracking. Therefore, we use SSD and NCC to gain the faster response.

To apply the template matching algorithm, camera image must be processed

at each sampling so that, robot reaches the correct target position. In order to coincide the target to the center of the camera image (an instantaneous position of the robot arm tip) the center should be moved towards the target position which is being detected by the template matching. The center of the camera view and the target object at a particular instance of the visual servo control are calculated in each sampling. And then image must be processed and applied the template matching until target would coincides with the center of the camera image view. The processing time of the template matching also depends upon the selected TM algorithm [101].

6.2.3 Lighting level measurements

The lighting level measurement of the working environment is an uncertain task because, in practical scenarios frequent lighting level changes can be observed. However, our investigation is based on the indoor working conditions of the robot so that uncertain light condition changes are expected. Therefore uncertainty of the light must be assumed in advance to justify the uncertain measurements. We assume, the variations of the sun light component is negligible. Throughout the experiments, light is given from both indoor sunlight and artificial florescent light sources fixed along the roof board. Since the sun light has a considerable amount of the total light measurement and also if the sun light from the outdoor drops or jumps, that would again have a high chance to vary the indoor light level. However, the above variations are assumed to be included under possible uncertainties of the measurements. We found that lighting variations and also projection perspectives of images are likely to be an indeterministic (stochastic) in nature. However, as an initial step we concentrated only on stochastic nature of light level variations while assuming orthogonal perspectives of the images.

The light level measurements are done by using the Lux meter. The measurement are taken under 3 different lighting levels as low, normal and high, under each category three different color target objects are used as red, blue and white. Two template matching algorithms are used to investigate the lighting conditions under each category.

6.3 Experimental evaluation

We need to evaluate the system accuracy, effectiveness and operation repeatability of teleoperation based on lighting conditions or level variations of the working environment.

6.3.1 Experimental setup

The robot arm named Performer MK3s (an articulated type robot arm, we called it as MK3s in short) with USB camera in working side is controlled by the reference position generated in operational side using SCARA type robot. The SCARA is manually controlled by a human operator until the target is included in the camera image. Then, MK3s is controlled autonomously by the reference position generated in camera side. General purpose USB cameras are not always directly supported on

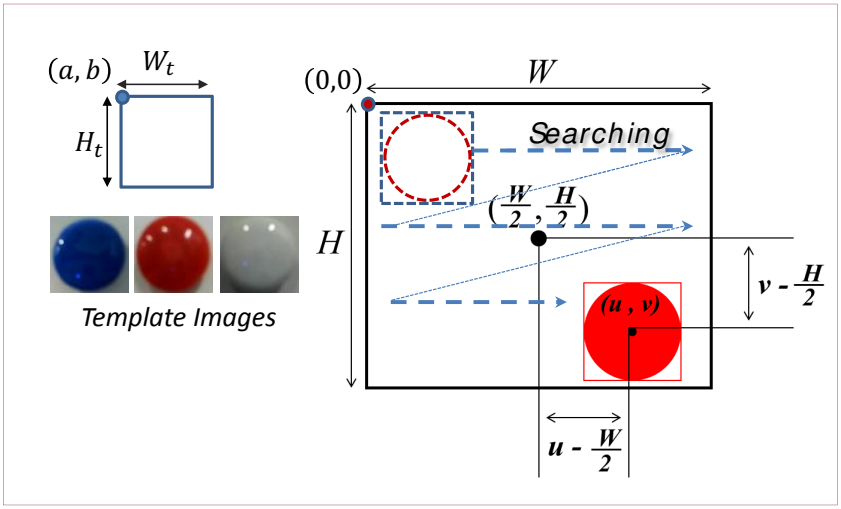

Figure 6.3: Schematic Diagram of Template Matching Technique

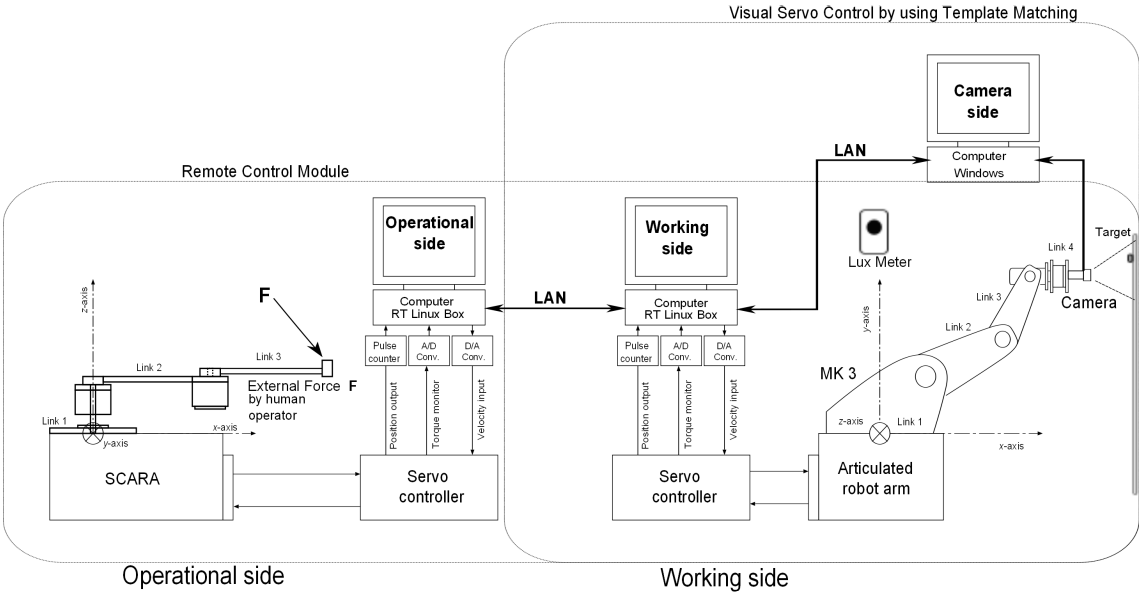

Figure 6.4: Pictorial View of the Experimental Setup

UNIX based real-time OS, therefore, we configured Microsoft Windows based system for image processing and connected via LAN. Figure 6.3 shows the schematic view of the TM, where W_t and H_t are width and height of the template image which is used in the experiment and W and H are the width and height of the camera image respectively. Center of the camera image is shown as $(W/2,\ H/2)$ and $(u,\ v)$ given the position of the target object located in the camera image. $(a,\ b)$ is the corner coordinates of the target template included in the camera view, where range is defined as $(a,\ a + W_t/2)$ and $(b,\ b + H_t/2)$.

Figure 6.4 shows the schematic diagram of experimental setup (cf. [12]). The experiments were carried out by using the same parameters and target position except the lighting level. The target position was set as $(x, y, z) = (0.635, 0.465, 0.003)$ [m] and fixed throughout the experiments. As the target, round shape buttons with diameter 0.02 [m] were used and fixed on the white color board. Three different color targets (red, blue and white) were used for experiments under three different lighting conditions; low, normal and high (light intensity is changed by adding more florescent bulbs and changing room exposer to sun light) as shown in Tables 6.2 and 6.3. Lighting conditions were measured using a "Lux Meter" *(Accuracy: Illumination* 5%*)* which was fixed near to the target as shown in Fig. 6.4.

Before it starts the image processing, required parameters must be initialized. As shown in Fig. 6.3, First, camera image frame size is given as $(W,\ H) = (352,\ 288)$ [pixels]. For all the template images, size is predefined as $(W_t,\ H_t) = (72,\ 72)$ [pixels]. Then, for each experiment, "average value" is calculated by doing pre-requisites tests by using same target object as shown in Tables 6.2 and 6.3 and we measured the illumination level by using Lux-meter with the illumination measurement accuracy of $\pm 5\%$. Thereafter, experiment is done for particular TM and the target assuring illumination level should be unchanged in order to obtain correct correlation values against predefined threshold. And also glare effects, shading, reflections and natural micro variations are assumed to be negligibly small and considered as avoidable effects. The above process was carried out for each experiment as listed in Tables 6.2 and 6.3.

6.3.2 Experimental results and discussion

The experiments were carried out for each lighting level under SSD and NCC of TM algorithms, and the results for SSD algorithm are illustrated in Table 6.2 and for NCC in Table 6.3.

In the described teleoperation system, the calculation of the threshold value for TM is required in advance. The procedure is summarized as follows: First, the value of TM (SSD/NCC) algorithm is calculated when the camera image contains the target, where the values are shown in Tables 6.2 and 6.3 as "Lower." Second, the value of SSD/NCC is computed when the camera image does not include the target, where the values are shown in Tables 6.2 and 6.3 as "Upper." Finally, the average of the lower and upper values to adopt as the threshold value for TM is calculated, the observed values are shown in tables as "Average."

It is found that change of lighting level is highly affected on SSD average value, and results also verify that it reflects to the visual servo control behavior of our teleoperation system. The results also illustrate that color of the target also has a considerable effect to achieve the desired behavior of our teleoperation system based on TM, where "succeeded" in Tables 6.2 and 6.3 means that the USB camera of the robot arm MK3s captured the target and then, tip of the MK3s reached to the target. The term "Succeeded-smoothly" was given in that, robot reached to the target after it detects by the camera view without showing trembling or jerks. However, NCC has an inherit attribute that it requires very similar image of target as the template, where as SSD perform well even if the template color intensity different from the actual target.

Further, it is seen from the Tables 6.2 and 6.3 that "Lower" values calculated for "red" and "blue" buttons have shown noticeable differences. The red button used in the experiments had shiny light-red in color surface, so that color contrast between white board and the button was lower and also reflection and glare effects incurred might be higher. The blue button was dark-blue in color, and the color contrast between white board was higher. Therefore, TM algorithm had given better threshold values for blue color one, and therefore, teleoperation experiment was successfully conducted.

Despite of the higher sensitivity on lighting conditions, SSD can be used when lighting levels are managed approximately in between $300 - 650$ [Lux] and provided the color contrast between target and background is higher. Moreover, NCC shows an acceptable output when system operate at lower lighting levels around $90 - 650$ [Lux] as shown in Table 6.3.

Table 6.2: Summary of Experimental Data and Results for SSD Type

Light [Lux]	Target Color	Exp. No.	Threshold value cal.(SSD)			Experiment Result
			Lower	Upper	Average	
Low (90-100)	Red	1	340	760	550	Not succeeded
	Blue	2	410	760	585	Not succeeded
	White	3	580	750	670	Not succeeded
Normal (330-340)	Red	4	10500	24500	17500	Succeeded
	Blue	5	6500	24500	15500	Succeeded-smoothly
	White	6	18500	24500	21500	Not succeeded
High (620-630)	Red	7	14300	31730	23015	Succeeded-smoothly
	Blue	8	8650	31730	20190	Succeeded-smoothly
	White	9	24400	31730	28065	Not succeeded

6.4 Concluding remarks

The investigations are carried out for the teleoperation system by considering the system behavior due to varying lighting conditions. The evaluated system has a

Table 6.3: Summary of Experimental Data and Results for NCC Type

Light [Lux]	Target Color	Exp. No.	Threshold value cal.(NCC)			Experiment Result
			Lower	Upper	Average	
Low (90-100)	Red	1	0.860	0.940	0.900	Succeeded
	Blue	2	0.740	0.940	0.840	Succeeded
	White	3	0.983	0.986	0.984	Not-Succeeded
Normal (330-340)	Red	4	0.866	0.914	0.890	Succeeded
	Blue	5	0.780	0.920	0.800	Succeeded-smoothly
	White	6	0.984	0.987	0.985	Succeeded
High (620-630)	Red	7	0.880	0.924	0.902	Succeeded
	Blue	8	0.796	0.946	0.871	Succeeded-smoothly
	White	9	0.985	0.988	0.986	Succeeded

module to make an accurate motions in which, TM techniques were used to aid the visual servo control, and two different type of TM algorithms are used in the the investigations. Therefore, it is revealed that system performance and behavior are highly depend upon light intensity around robot working space as well as the color contrast between the target and the target background.

From the results, it is verified that, lower lighting conditions NCC has shown accurate template matching performance when color contrast between the target object and the background is higher. However, the illumination level is higher than 330 [Lux] both TM algorithms are shown accurate results by reaching target in each experiment. So in practice, we need to setup an appropriate selection of the algorithm if the lighting levels likely to be changed during the operations. However, throughout the investigation glaring effects, sunlight to florescent light ratio, lighting reflections due to surround objects and so forth are taken as homogenous and constant effects.

Chapter 7

Force Compliance Passive Motion Control Implemented Using AI Techniques

This chapter is mainly collaborated with the detailed evaluation of lightweight compliance force control synthesis for commonly use industrial type robot arms. In order to apply for the safety cum fault tolerance implications in industrial operating conditions, the proposed control scheme uses different theoretical approaches depending on the output/input constrains and the level of access of the servo controller parameters of the target robot arm. Therefore, four different implementations of the proposed compliance controller are defined and two of them which adapt genetic algorithm and neural network are mainly analyzed and simulated under the research since the other two are investigated in our previous states of the sequence of work which have been carried so far. In general, changing of existing configurations of the industrial robot servo parameters and hardware setups are really a tedious task for the user due to high technical and cost factor considerations and also most cases older versions could not be supported in technical means by the manufacturer itself. This chapter also comprehends and suggests a solution by adapting the controller module as a plug-in which needs only minute changes to the existing setup by free of cost and risk.

7.1 Introduction and background

In current context most industrial countries use robots in higher number in various fields including manufacturing, medical, military welfare, amusement and so forth. This chapter is merely focused on robots belong to the industrial manufacturing and also we found that current industrial type robot population has exceeded 1.5 million around the world (cited from IEEE spectrum 2012). However, higher number of industrial robots are manufactured as general purpose versions in order of to make

them in higher numbers with lower cost whereas, the special purpose robots are available lower numbers at extremely high cost. Therefore most of the industrial users adopt general purpose industrial robots in their production lines and workshops to achieve maximum profit with lower costs.

Nowadays, people seek higher degree of safety in workplaces as well as industrial environments so that higher priority must be given on the safety concerns over operation of the robots as well. By considering above facts, authors have identified that most commonly use industrial robots inherit higher rigidity due to a higher precision requirements [16, 70], and hence, found following three common problems that are to be solved to proliferate the safety and the production process for both robots and human users/workers. First, robot can have a chance to collide undesirably with an object or a human operator during operations at dynamic and uncertain conditions. If any collision could have occurred that would cause to damage both the robot and the object or the human since industrial robots are transferred very high inertia at the tool end [47, 69, 116]. Second, if a robot is needed to be calibrated to perform tasks that require lower rigidity and higher flexibility such as grinding, welding, sealing, pull-out work pieces and so forth, robot controller should be altered to handle the flexibility of those operations [68].

Number of different solutions have been proposed and most of them are currently in practice at industrial production systems. However, most solutions are required considerable changes to the existing hardware and servo parameters and also those approaches need manufacturer involvement for complex low-level configuration changes which cost very high in nature, some of such solutions are illustrated in [47, 67, 78]. Third is to handle the scenario like, if robot could have been mistakenly performed undesirable operation or malfunctioning on the target object with higher rigidity that may cause to high losses. In such cases, we believe, being acted on instantaneous flexibility at the robot tool-end and by quick switching to the compliance controller, may keep lesser damage to the both sides by making controller behave to be fault tolerant and hence which can revoke losses.

In order to provide a global solution to the above circumstances, industrial robot arms should perform passive motion against; any undesired impact, collision with an obstacle, shear forces or any other external disturbance forces. It means, remedial concept is provided by keeping flexible motion realization against external forces, as we proposed under previous states of the research named as force-free control (FFC) which is extensively described in [116, 117] and references therein.

However, in [68] restricting torque implementation is given for realization of flexible motion though it can not be performed motion against external force on free space. And also impedance and compliance control strategies provide similar flexibility based on contact forces [47, 67] yet, they can not perform flexible motion on space as given by FFC [118]. Moreover, FFC and impedance control merely compliance against external contact forces [69][76] rather than controlling exact force exerted by environment [77, 78].

In this chapter, we address on first and third problems described in the above. Two profiles of "Force Compliance Passive Motion Control (FCPMC)" is proposed to provide the solution for industrial robot safety and fault tolerance requirements. Our previous approaches FCPMC method is described under two folds based on the application requirement; first is called as "force-free control by external torque (FFC-ET)" [76] and second is named as "force-free control by torque independent compensation (FFC-TIC)" [116, 117, 119]. In this chapter, we refer FCPMC as an abbreviation for the proposed controller from here onwards. This also describes, FCPMC implements under two categories, one is former FFC-TIC is improved by using genetic algorithm based optimization technique to evaluate more accurate compensation coefficients [120, 121, 122], and second is FCPMC is synthesized using artificial neural network to compensate the uncertainties involved [123, 124]. Both methods are evaluated by comprehensive simulation studies under Performer MK3s real industrial robot parameters for which identical model has been created using Matlab/Simulink-Simmechanics of the same robot [19, 73].

Following section describes overview of the industrial robot architecture including details of the most common servo controller representations. Then principles and development of FCPMC with former implementations of FFC-ET and FFC-TIC are illustrated in brief. An improved version of FCPMC based on the former FFC-TIC optimized by genetic algorithm is derived. A neural network implementation of the FCPMC is explained in details as more accurate version of the FCPMC to overcome the uncertain parameter estimation issues incurred in the previous FFC-ET version. Finally, possible applications on safety and fault tolerance are discussed with appropriate scenarios for the new FCPMC profiles including simulation results for verifying the applicability cum effectiveness of the FCPMC.

7.2 Particulars of industrial type robot arms: an overview

7.2.1 System architecture

An articulated type general industrial robot system is shown in Fig. 7.1-(a). A reference input generator normally generates the sampled Cartesian trajectory and transforms it into sampled joint trajectories. Sampled joint trajectories are written onto the servo controller in real-time operation [19]. The servo controller joint trajectory data drive to actuates joint motors accordingly [126]. According to Fig. 7.1-(b), two-degree-of-freedom configuration is selected for illustration and clear understanding, it also uses to derive the proposed force compliance algorithms. The robot arm parameters are given in the figure as: $K_p(\text{or } K^p)$, $K_v(\text{or } K^v)$, ΔT, $\theta_i(\text{or } q_i)$ $i = 1 \cdots 3$, l_j, m_j $j = 1, 2$, $h_{r,p}$ and r; position and velocity loop gains, reference input sampling time, joint angles of the robot, link length and mass of corresponding 2 and 3 links of the performer MK3s robot shown in Fig. 7.1-(a), zero order hold and reference input, respectively.

Figure 7.1-(b) shows a two-dimensional (2-DOF) global coordinate system along with a wire-frame of the robot links orientation. Industrial robot arms are devised by

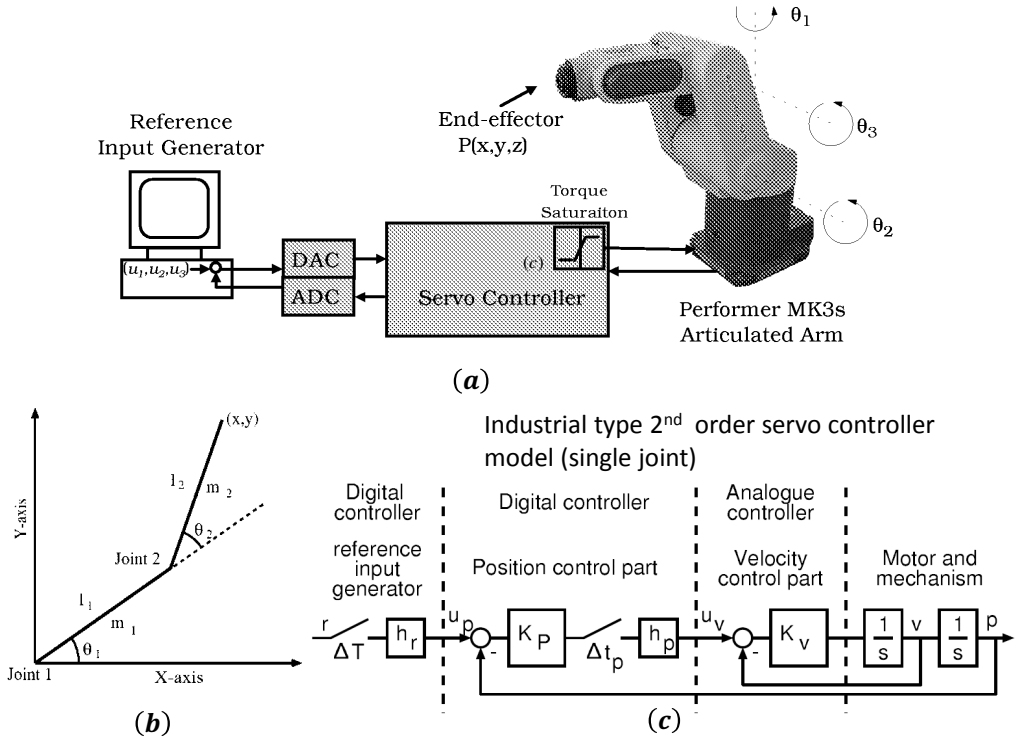

Figure 7.1: (a): Performer MK3s Robot and Data Flow Directions (b): Wire Frame Diagram of Two Links of an Articulate Robot Arm (c): Mechatronic Servo Controller Block Diagram for Single Joint Motor

independent joint controllers based on the decoupled joint dynamics, and driven by PID servo systems. Servo systems comprises of joint servomotors, which are actuated with current or voltage controllers to govern torque control of joint servomotors as in [127].

7.2.2 Kinematics of a robot arm

Typically kinematics includes forward and inverse analysis. Forward kinematic converts joint variables to end-effector variables and it only has unique end-effector solution. It is used for simulation and find the workspace of manipulators. Forward kinematic equations determine Cartesian position (x, y) and orientation of the end-effector, given the arm configuration in joint coordinates $(q_1(k), q_2(k))$. Kinematics reduces to a unique solution as given by

$$\begin{cases} x = l_1 \sin q_1 + l_2 \sin(q_1 + q_2) \\ x = l_1 \cos q_1 + l_2 \cos(q_1 + q_2). \end{cases} \tag{7.1}$$

Inverse kinematics converts end-effector variables to joint variables, and typically inverse case denotes multiple joint angle solutions as well [128]. Inverse transformation method [46] is a general solution for inverse kinematics and it is extremely

time consuming, hence, troublesome in real-time implementations. It further requires alternative decision equations to eliminate redundancy. Based on "Denavit-Hartenberg" representation *(D-H)* [45], Paul et al. [128] proposed an explicit closed form arm solution for simple robot arms. The simplest geometric approach proposed by Lee et al. [129] which could be applied to most industrial robot arms in the form of an explicit solution. For the robot arm illustrated in Fig. 7.1, inverse kinematics is given by

$$\begin{cases} q_2(k) = \pi - \cos^{-1}\left(\frac{l_1^2+l_2^2-\gamma^2}{2l_1l_2}\right) \\ q_1(k) = \tan^{-1}\left\{\frac{y(k)}{x(k)}\right\} - \sin^{-1}\left\{\frac{l_2 \sin q_2(k)}{\gamma}\right\} \end{cases} \tag{7.2}$$

where, $\mathbf{q}(k) = [q_1(k),\ q_2(k)]^T$, and $q_1(k),\ q_2(k)$ are the joint positions of link 1 and link 2, respectively, k is the sample step number and $\gamma = \sqrt{x(k)^2 + y(k)^2}$. Then $\mathbf{q}$ or generally given as $\mathbf{q}^d$ is brought to the servo controller of the industrial articulated robot arm as reference input.

7.2.3 Dynamics properties of industrial robot arm

Dynamic equation *(please refer Chapter 3 for detailed explanation of the dynamic equations of industrial type robot arms)* of the articulated robot arms is given by

$$\mathbf{H}(\mathbf{q})\ddot{\mathbf{q}} + \mathbf{h}(\mathbf{q},\ \dot{\mathbf{q}}) + \mathbf{D}\dot{\mathbf{q}} + \mu \operatorname{sgn} \dot{\mathbf{q}} + \mathbf{g}(\mathbf{q}) = \boldsymbol{\tau}^s \tag{7.3}$$

where $\mathbf{H}(\mathbf{q})\ddot{\mathbf{q}}$ is the inertia matrix, $\mathbf{D}\dot{\mathbf{q}}$ and $\mu \operatorname{sgn} \dot{\mathbf{q}}$ are viscous and coulomb friction terms, $\mathbf{h}(\mathbf{q},\ \dot{\mathbf{q}})$ is the coupling nonlinear term (Coriolis and centripetal force vector), $\mathbf{g}(\mathbf{q})$ is the gravity matrix term, $\boldsymbol{\tau}^s$ is the input torque to the robot arm joints and $\mathbf{q}$ is the joint angle position vector [46, 47].

If $\boldsymbol{\tau}^f$ $(= [{\tau_1}^f, \cdots, {\tau_n}^f]^T)$ is the joint torque corresponding to the external force $\mathbf{F}$ acting on the tip of the robot arm, then joint torque corresponding to the external force is obtained as follows [46]:

$$\boldsymbol{\tau}^f = \mathbf{J}^T \mathbf{F} \tag{7.4}$$

where $\mathbf{F}$ is the external force vector and $\mathbf{J}$ is the Jacobian matrix.

However, industrial robot arms are employed in predetermined operations and, therefore, the nonlinear torque disturbances such as centripetal and Coriolis torques, friction torque and also gravity effects can be estimated. Nonlinearities are usually minimize by appropriate mechanical design along confined operational specifications, usually for velocity and acceleration. In industrial robot arms, inertia change due to the varying arm configuration is not considered significant. Hence, a linear relationship of joint torque and joint acceleration is assumed.

7.2.4 Industrial robots servo controller properties

Figure 7.1(c) indicates the schematic representation of digital form of a single industrial robot servo motor controller. Figure 7.2 shows a joint dynamic controller model

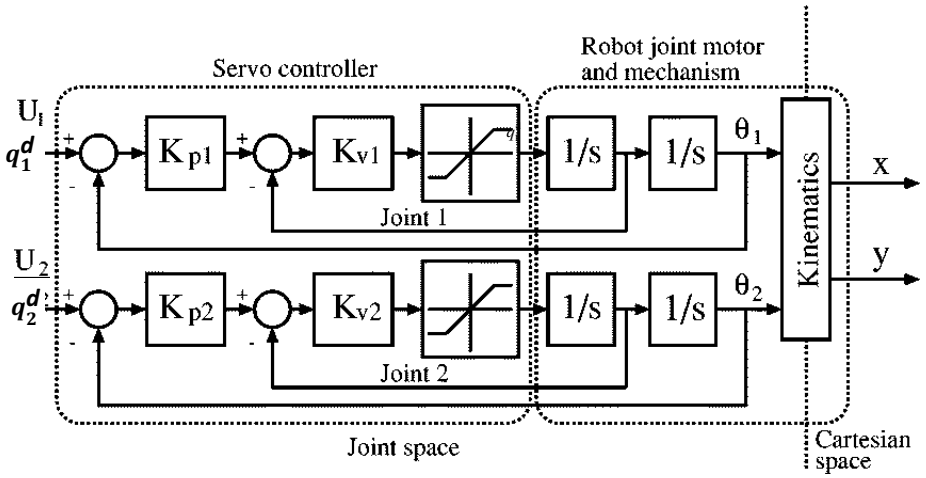

Figure 7.2: Block Representation of Common Industrial Servo Controller for Two Active Joints

of a two-link industrial robot arm. Kinematic control of industrial robot arms is based on the decoupled, linear servo model, which is widely used in todays robotic applications. A comprehensive details with analysis and examples of this model can be found in [19]. The two-link version of this dynamic model is also given in Fig. 7.2. Joint dynamics is governed by the two servo parameters. These parameters are named in industry as gains of position loop and velocity loop, respectively. The determination procedures of these parameters can be found in [19, 130]. Referring to this model, linear joint dynamics $G_j(s)$ is given by

$$G_j(s) = \frac{\Theta_j(s)}{U_j(s)} = \frac{K_j^p K_j^v}{s^2 + K_j^v s + K_j^p K_j^v} \tag{7.5}$$

where, $\Theta_j(s)$ and $U_j(s)$ are Laplace transforms of $\theta_j(t)$ (or $q_j(t)$) and $u_j(t)$ (or $q_j^d(t)$), respectively. From equation 7.5, linear joint dynamics in time domain can be written as

$$\ddot{\theta}_j(t) = K_j^v \left\{ K_j^p \left(u_j(t) - \theta_j(t) \right) - \dot{\theta}_j(t) \right\} \tag{7.6}$$

in that $\ddot{\theta}_j(t)$ (or $\ddot{q}_j(t)$) and $\dot{\theta}_j(t)$ (or $\dot{q}_j(t)$) are acceleration and velocity of joint variables $\theta_j(t)$ in j^{th} joint.

Moreover, each joint operates independently and coupling between links is neglected, are generally assumed. Also Coriolis and centripetal torques are neglected, which cause significant contributions to contouring performance only at high speeds [16, 19]. The corresponding joint dynamic model of industrial robot arm is shown in Fig. 7.2.

7.3 Force compliance passive motion control (FCPMC) strategies

FCPMC or previously FFC (force-free control) can be defined as flexible motion of an industrial robot arm accomplish in the form of passive motion against an external force applied to the robot arm, it moves passively against the external force as if robot would be in a non-gravity and non-friction condition. A full details of the former force-free control development and two different implementations can be found in our previous work as listed in following sub sections *7.3.1* and *7.3.2*. All cases FCPMC can be applied without modifications to the existing controllers whereas, most of the solutions found for the same problem need costly changes on hardware, software and manufacturer consultation.

7.3.1 External torque method

This section is given to describe former implementation of FFC-ET method in brief and Fig. 7.3 (a) represents the schematic of the FFC-ET and full details of this type can be viewed in [119, 131]. FFC-ET method needs an accurate force sensor to measure the applying external force, however, most of the industrial robots are not equipped with an accurate force sensor originally. For that reason, our next implementation was developed so that it can be used without force sensor, it needs embedded torque monitor instead, and also following section *7.3.2* details the same in brief.

The FFC concept is then derived theoretically by applying gravity and friction compensation torques to the servo controller for n joints , $\boldsymbol{\tau}^g$ $(= [{\tau_1}^g, \cdots, {\tau_n}^g]^T)$ is the gravity compensation torque and $\boldsymbol{\tau}^d$ $(= [{\tau_1}^d, \cdots, {\tau_n}^d]^T)$ is the friction compensation torque,

$$\boldsymbol{\tau}^d = \mathbf{D}(\dot{\mathbf{q}}) + \mu \operatorname{sgn}(\dot{\mathbf{q}}) \tag{7.7}$$

$$\boldsymbol{\tau}^g = \mathbf{g}(\mathbf{q}) \tag{7.8}$$

where $\mathbf{D}$ is coefficients of viscous damping matrix, μ is coefficients of coulomb friction. The gravity compensation torque $(\boldsymbol{\tau}^g)$ is obtained by calculating from the instant posture and joint position of the robot arm. The inputs of joint angles $\mathbf{q}^d$ $(= [{q_1}^d, \cdots, {q_n}^d]^T)$ are obtained in order to realize FFC-ET as [131];

$$\mathbf{q}^d = (\mathbf{K}^p)^{-1}\{(\mathbf{K}^v)^{-1}(\mathbf{K}^\tau)^{-1}(\boldsymbol{\tau}^f + \boldsymbol{\tau}^g + \boldsymbol{\tau}^d) + \dot{\mathbf{q}}\} + \mathbf{q} \tag{7.9}$$

where $\boldsymbol{\tau}^s = (\boldsymbol{\tau}^f + \boldsymbol{\tau}^g + \boldsymbol{\tau}^d)$ and $\mathbf{q}$ $(= [q^d, \cdots, {q_n}^d]^T)$ is the joint angles. Besides, $\mathbf{K}^p$ is a diagonal matrix of ${K_i}^p$ and $\mathbf{K}^v$, $\mathbf{K}^\tau$ are diagonal matrices of ${K_i}^v$ and ${K_i}^\tau$ respectively. The FFC-ET control scheme can be reduced to an ideal characteristic form as exclusively described under Chapter 3:

$$\mathbf{H}(\mathbf{q})\ddot{\mathbf{q}} + \mathbf{h}(\mathbf{q},\ \dot{\mathbf{q}}) = \boldsymbol{\tau}^f. \tag{7.10}$$

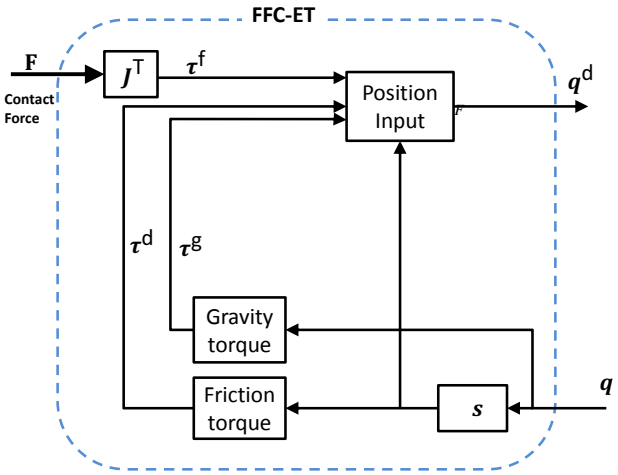

(a)

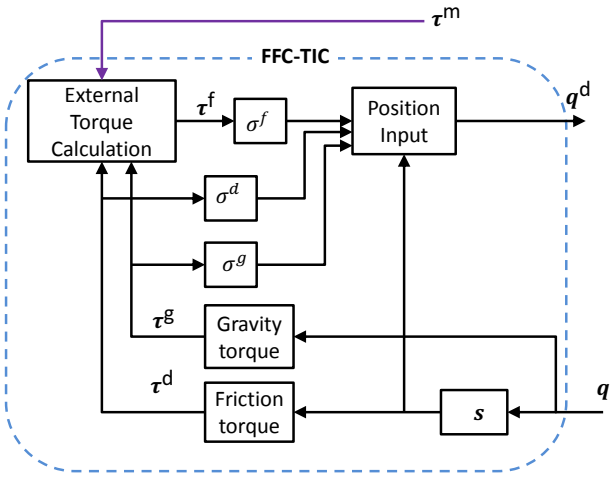

(b)

Figure 7.3: (a): Block Diagram of FFC-ET and (b): Block diagram of FFC-TIC

7.3.2 Torque independent compensation method

FFC-TIC is given when absence of the force measurement available and the robot arms with very large inertial torques. Most of the industrial robots in operation include a toque monitor, from that external torque is derived. Full details of this implementation can be found in [117] and [132] and block diagram is depicted in Fig. 7.3 (b). However, finding compensation coefficient of σ^f (or σ^s), σ^d and σ^g should be trial and error which could be costly in time and needed more experience and heuristics to decide correct values. For that reason, we propose the following optimization approach of which the above coefficient are evaluated based on the specific requirements

by using a reliable genetic algorithm.

Basic governing equations for FFC-TIC type is listed below. FFC-TIC means that the effect of inertia, friction and gravity to the robot arm motion can be assigned as linear combinations with arbitrary coefficients; see [117] and references there in. Then, dynamics of FFC-TIC is described by;

$$\mathbf{H}(\mathbf{q})\ddot{\mathbf{q}} + \mathbf{h}(\mathbf{q},\ \dot{\mathbf{q}}) = \sigma^f\,\boldsymbol{\tau}^f + \sigma^d\,\boldsymbol{\tau}^d + \sigma^g\,\boldsymbol{\tau}^g \tag{7.11}$$

where σ^f, σ^d and σ^g are coefficients of independent compensation and

$$\boldsymbol{\tau}^f = -\{\boldsymbol{\tau}^s - \boldsymbol{\tau}^d - \boldsymbol{\tau}^g - (\mathbf{H}(\mathbf{q})\ddot{\mathbf{q}} + \mathbf{h}(\mathbf{q},\ \dot{\mathbf{q}}))\} \tag{7.12}$$

is obtained. However, by considering low speed and higher gear ratios noted in [117]; $\mathbf{H}(\mathbf{q})\ddot{\mathbf{q}} + \mathbf{h}(\mathbf{q},\ \dot{\mathbf{q}}) \approx 0$ is assumed. Although, $\boldsymbol{\tau}^f = -\{\boldsymbol{\tau}^s - \boldsymbol{\tau}^d - \boldsymbol{\tau}^g\}$ is used in this approach, low speeds and high gear assumptions always being an uncertain and an explicit property as well and it must be a demerit in this approach and degrade the same as well. For the same reason also causes to develop the following optimization approach. Further, following section describes the fair explicit algebraic solution to the arguable zero dynamic assumption made by early developments.

7.3.3 New algebraic solution to the contradictory zero dynamics assumption

This is to explain a better approximation for FFC-TIC method, an algebraic and an explicit mathematical model to describes the dynamics of the FFC-TIC. Hence, we named this as; Extended FFC-TIC of (EFFC).

The problem emerges when it adopts the torque monitor to measure and estimate the external force which acts on robot end-effector. Full details of derivation is given in *Appendix B*.

Problem was found that removing inertial and non-linear terms by assuming very slow operating speed in the equation (7.12).

Proposed algebraic approach, the dynamic equation (7.12) taken as it is, and then applies mathematical reduction of algebra to obtain the relationship given below as equation (7.14).

Lets take Γ to represent the inertia and non-linear terms of the dynamic equation as equation (7.13);

$$\Gamma = \mathbf{H}(\mathbf{q})\ddot{\mathbf{q}} + \mathbf{h}(\mathbf{q},\ \dot{\mathbf{q}}). \tag{7.13}$$

$$\Gamma = \frac{\sigma^f + \sigma^d}{1 - \sigma^f}\,\boldsymbol{\tau}^d + \frac{\sigma^f + \sigma^g}{1 - \sigma^f}\,\boldsymbol{\tau}^g - \frac{\sigma^f}{1 - \sigma^f}\,\boldsymbol{\tau}^s \tag{7.14}$$

Therefore, we can take σ^f, σ^d and σ^g as constant parameters to represent coefficients as given in above.

Hence, we can simplify the relationships of coefficients with new constant parameters as;

$\frac{\sigma^f+\sigma^d}{1-\sigma^f} \Longrightarrow k^d$, $\frac{\sigma^f+\sigma^g}{1-\sigma^f} \Longrightarrow k^g$ and $\frac{(-)\sigma^f}{1-\sigma^f} \Longrightarrow k^s$

where k^d, k^g and k^s are new constant parameters. However, due to denominator constraint, new coefficient parameters should be taken by assuring the condition, $(1-\sigma^f) \neq 0$.

Therefore,

$$\Gamma = k^d\,\boldsymbol{\tau}^d + k^g\,\boldsymbol{\tau}^g + k^s\,\boldsymbol{\tau}^s. \tag{7.15}$$

Thus, the final representation of new extended force-free control (EFFC) input can be obtain as equation (7.16)

$$\mathbf{q}^d = (\mathbf{K}^p)^{-1}\{(\mathbf{K}^v)^{-1}(\mathbf{K}^\tau)^{-1}(k^d\,\boldsymbol{\tau}^d + k^g\,\boldsymbol{\tau}^g + k^s\,\boldsymbol{\tau}^s) + \dot{\mathbf{q}}\} + \mathbf{q} \tag{7.16}$$

.e: extended FFC by independent compensation can be realized proper selection of new compensation coefficients k^d, k^g and k^s.

7.3.4 Optimized coefficient of torque method (OCT)

This section describes the new approach to determine the coefficients of independent compensation given in the above subsection *7.3.3*. The all governing equations and concepts described in the above two sections are concerned here as well, though this will be given as alternative and improved version of the second method. This method is named as force compliance passive motion control by optimized coefficients of torque, abbreviated as FCPMC-OCT for convenient.

In this method first we need to create data for the objective function to be minimized and hence find the required coefficient under minimum error condition. Creating data can be from either data from tracking temporal data in each sampling interval of previous experiments or from artificially generated data from generated programs. In the second kind, there is a possibility to create an output trajectory to be a defined one i.e. it can be formed as a desired passive motion path to be followed when external force is applied. However, configuring larger deviations of the normal passive motion is not guaranteed when defining custom passive motion path by creating artificial data for GA.

The FCPMC-OCT is developed around the equation given in under FFC-TIC. Therefore, the objective function is defined to apply the genetic algorithm (GA) [122, 133] and is given by

$$\boldsymbol{\Phi} = \{(\mathbf{H}(\mathbf{q})\ddot{\mathbf{q}} + \mathbf{h}(\mathbf{q},\ \dot{\mathbf{q}})) - (\sigma^f\,\boldsymbol{\tau}^f + \sigma^d\,\boldsymbol{\tau}^d + \sigma^g\,\boldsymbol{\tau}^g)\}. \tag{7.17}$$

From this, we need to minimize the the function given in $\boldsymbol{\Phi}^T\boldsymbol{\Phi}$ for a defined time period with define total number of samples take as N and hence, total time span

can be taken as t_N. Therefore, optimization is accomplished using GA to determine the values of the parameters σ^f, σ^d and σ^g, when the final minimum value of the cost function $\mathbf{\Delta}$ is reached, and cost function or fitness function [122] defined as;

$$\mathbf{\Delta} = \frac{1}{t_N} \sum_{i=0}^{N} \left\{ \mathbf{\Phi}^{\mathrm{T}} \mathbf{\Phi} \cdot \left(1 + 10 \cdot (\sum_{j=0}^{m} g_j) \right) \right\} \tag{7.18}$$

$$g_j = \begin{cases} g_j & \text{if } g_j > 0 \\ 0 & \text{if } g_j \leq 0 \end{cases}$$

where m denotes total number of constrains imply to the objective function, g_j is given for j^{th} constrain and $\mathbf{q} \in \Re^{\mathbf{2}}$.

7.3.5 Neural network based force compliance method

In this approach, our main concern is to achieve more precise FCPMC with improved robustness even the presence of existing dynamic modeling errors, uncertainties and possible unknown factors involved and so forth. A Gaussian type neural network (GNN) is proposed to realize the FCPMC (or FFC-ET) as shown in Fig. 7.4, hence new controller is named as "FCPMC-GNN".

Fig. 7.4 shows the block representation of developed architecture, and GNN is used to provide controller action given by equation 7.9. Therefore, following accumulated joint torque input is realized by using GNN in order to get rid of deterioration of control performance caused by modeling errors in K^p, K^v, K^τ, unknown factors in D and μ and uncertainty in torque measurements $\boldsymbol{\tau}^f = \alpha\, \boldsymbol{\tau}^m$ where α is an uncertainty factor of torque measurement. GNN is trained by using data created based on the specific scenario with typical "Back-propagation learning algorithm"

$$\mathbf{f}_{GNN} = \{\alpha\, \boldsymbol{\tau}^m + \mathbf{D}\dot{\mathbf{q}} + \mu\, \mathrm{sgn}(\dot{\mathbf{q}}) + \mathbf{g}(\mathbf{q})\}. \tag{7.19}$$

The adapted GNN is define as follows:
If z is defined to represent each element of the input layer, then the output can be evaluated based on single hidden layer architecture as:

$$\begin{cases} f_i(z) = \exp\left[-(z-\mu_i)^2/\{2(\sigma_i)^2\}\right] \quad (i = 1 \ldots 10) \\ \phi_i(z) = \sum_{i=0}^{10} w_i\, f_i(z) \end{cases} \tag{7.20}$$

where w_i and $\sigma_i\,(=\sigma)\,(i = 1 \ldots 10)$ denote weight, mean and marginal deviation of the i^{th} Gaussian node of the network, respectively. Calculation methods and finding initial parameters of GNN and derivation and simplification details of the equations are also published in [123, 125] and references therein.

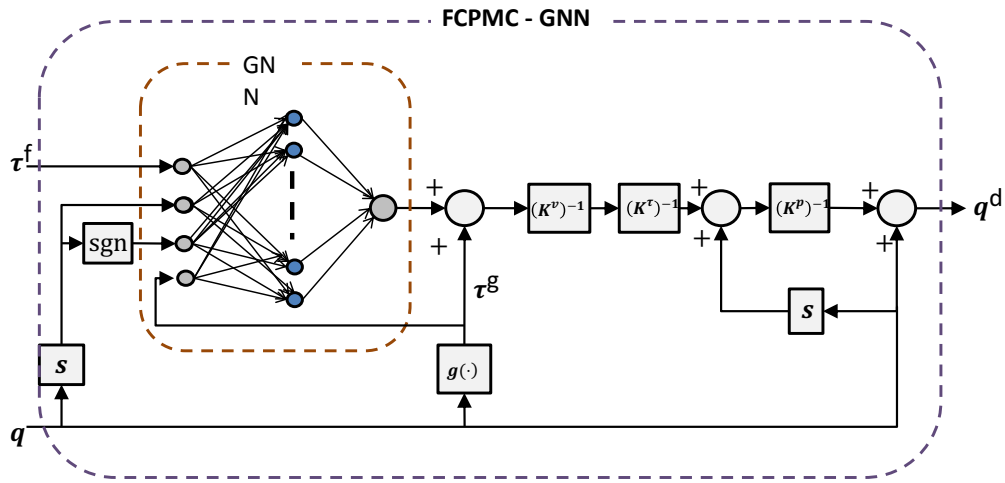

Figure 7.4: Gaussian Neural Network Model Representation for New FCPMC

7.4 Evaluation of proposed control methodology

7.4.1 Simulation setup and conditions

The articulated robot arm's physical parameters set for the simulation have following specifications; link lengths $l_1 = 0.25$ [m], $l_2 = 0.215$ [m] and masses of the links $m_1 = 2.86$ [kg], $m_2 = 2.19$ [kg]. I_1 and I_2 are moment of inertia along the center of gravity of link 1 and 2. The servo controller parameters are given as follows: The sampling interval set for simulation $\Delta t = 0.04$ [s], simulation time is 5 [s], position loop gains are ${K_1}^p = {K_2}^p = 25$ [1/s], velocity loop gains are ${K_1}^v = {K_1}^v = 150$ [1/s], torque constants are ${K_1}^\tau = 0.1045$ [Nm/(rad/s^2)], ${K_2}^\tau = 0.0605$ [Nm/(rad/s^2)], friction coefficients of viscous damping are $D_1 = 4.68$ [Nms/rad], $D_2 = 2.72$ [Nms/rad] and coefficients of coulomb friction are $\mu_1 = 0.5$ [Nm], $\mu_2 = 0.5$ [Nm]. Coefficients of viscous damping and coefficients of coulomb friction are taken from the Performer MK3s parameters. Gear ratios are used as $Gr_1 = 160$ and $Gr_2 = 160$ for link 1 and 2, respectively as per Performer MK3s robot.

For FCPMC-OCT, population size is taken as 24 for three variables to be calculated, and 0.05 mutation rate is selected and crossover is 0.9. For FCPMC-GNN, learning rate is taken as $\eta = 0.008$ and momentum is selected as 0.01. Number of data is selected for training GNN by using sampling interval Δt of 0.004 for 4 [s].

7.4.2 Simulation results

The FCPMC-OCT method calculates the coefficients of independent compensation by using GA according to the cost function defined in equation (7.18) as: $\sigma^f = 1.34, \sigma^d = 0.36$ and $\sigma^g = 0.43$ with rounded figures to nearest second decimal point. Figure 7.5 shows the result obtained from the simulation by applying above parameter

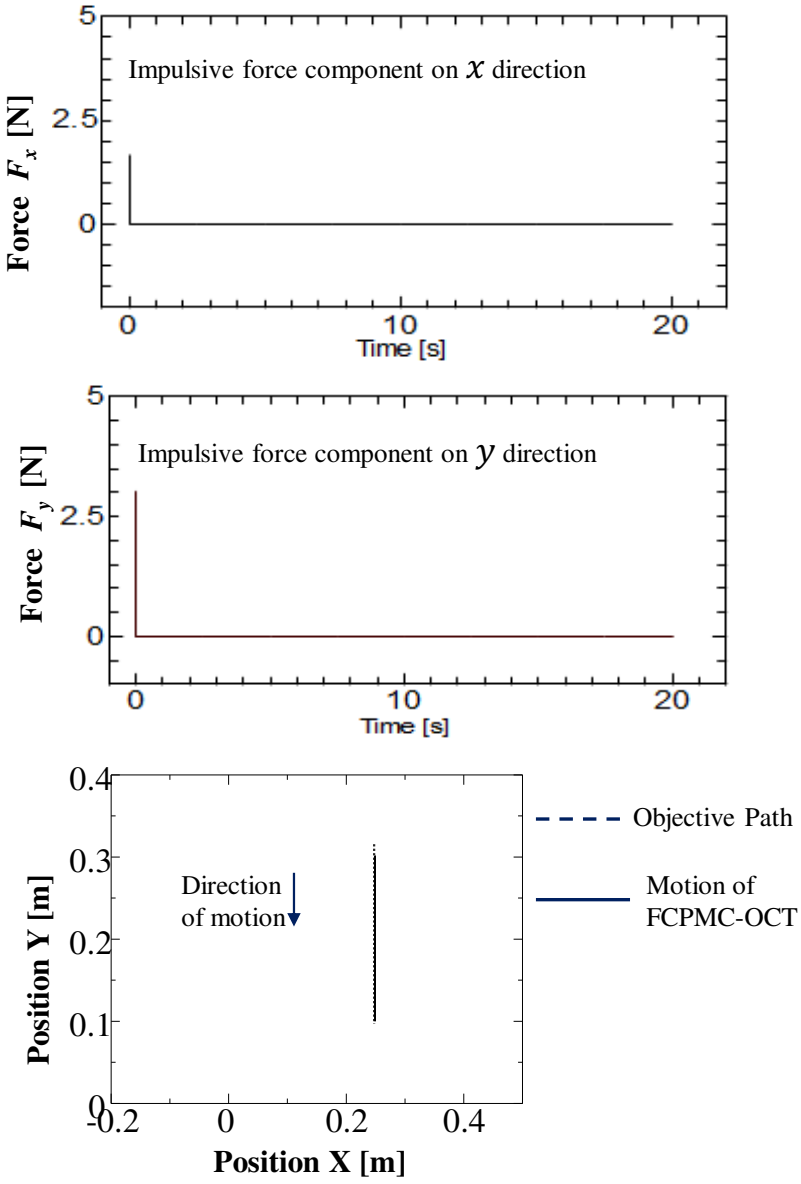

Figure 7.5: Results of FCPMC-OCT Method for Passive Motion Against Defined Locus in y-direction with Restricted x

values. For FCPMC-GNN case, results is illustrated in Fig. 7.6 against former FFC-ET method.

7.4.3 Discussion

In correct context, most of the industrial applications are sought better safety and fault tolerance in greater degree by any means of less overheads and upgrade costs involve. In this effort, we are eagerly trying bring a solution to above safety and fault tolerance issues on existing commonly used industrial robots. Our solution has a lower

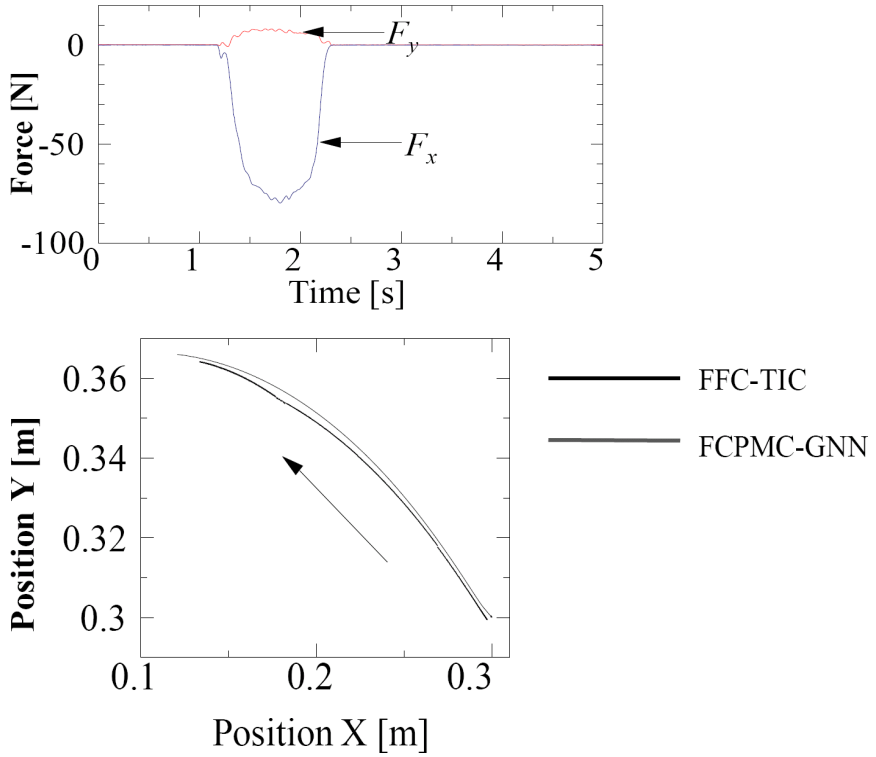

Figure 7.6: Results of FFC-TIC Vs FCPMC-GNN Method for Same Input External Force

cost and risk property and it also comes as a plug-in to the existing systems without interfering existing operating conditions. Results taken from the two types of FCPMC simulations (on real robot dynamics and servo parameter values as given in Performer MK3s version) are accordance with our expectations from the each methodology at a higher satisfaction. Result for FCPMC-OCT in Fig. 7.5 shows robot followed a pre-defined desired locus without any ripples or jerky effects by applying a known primitive type external force.

Moreover, result of FCPMC-GNN method in Fig. 7.6 is also brought high motivation about realization of the method in actual robot working in a real production facility or a workshop. Further, authors are hoping to conduct analysis of proposed two methods in next step based on: the cross validations and correlations of data for two optimization methods for larger number of different application scenarios, robustness and reliability checks on long run; to justify and emphasize the statistical validations for of the FCPMC concepts given in this instinct approach. Therefore, that will make sense industrial parties to show their interest.

7.5 Concluding remarks

Two new improved versions of FCPMC have beed proposed and named as FCPMC-OCT and FCPMC-GNN, respectively. The FCPMC-OCT is proposed based on GA to avoid ad-hog parameter estimation and implicit assumptions based upon former FFC-TIC, and FCPMC-GNN is derived to eliminate uncertainty and incorrect modeling effects of former FFC-ET. The proposed FCPMC can be configured easily and it can also be easily plug-in to the existing systems. Therefore, cost and risk free implementation brings high demand of industrial implications.

Chapter 8

Discussion and Conclusions

8.1 General discussion and conclusions

This chapter mainly describes the overall and abstract high-level discussion of the thesis. Since, an each chapter consists of a specific discussions and concluding remarks at the end, most of the inside details would not be included as an abstracted view by avoiding duplication of the same entries as well. Thesis has made a focused attempt to contribute in some important areas of passive motion controls (named as FFC or FCPMC) against external forces acting on industrial robots. Some conceptual ideas are presented and a considerable attempt is made to back them up with experimental results. The work done may open numerous avenues for further work especially competitive with impedance and admittance type approaches of force control strategies. However, the limitation in time and resources imposed a great pressure to make experimental validation as brief as possible. Therefore, the objective of this chapter is to discuss the positive as well as the negative aspects of the work presented in the above respective chapters. Finally, suggestions regarding future directions are made in brief.

This thesis starts with general introduction chapter followed by **Chapter 2**, which is entirely devoted to described necessary theoretical, experimental and mathematical preliminaries that are used throughout the research. Kinematics, dynamics and control properties of industrial robot arms and actuators are described with relative mathematical and architectural view points. And logical arguments with manifests are highlighted in appropriate locations and which are sometimes necessary to be adapted in practice. General industrial robotics and its intuitive control strategies are also given in brief. Real time discrete time software based control architecture

is also illustrated. Throughout the thesis, same software architecture and technique have been used during experiments.

Chapter 3 described the core concepts of FFC which is illustrated as in sequential step development approach. Initially, mathematical background is depicted. Then modeling of FFC and how it combines to the existing velocity controllers of an industrial robot are shown. Integrated full fledged simulation environment has been given with comparative descriptions under each respective location. This chapter also presents the simulation with analysis of FFC for single arm case of an industrial type arm and applicability for safety is also tested for 2-link case. Simulation results indicate the realization of theoretical model of FFC for different kinds of external force conditions. And an applicability for safe operation under danger due to high rigidity of industrial robots is also analyzed and verified adaptability of the same for safety implication through simulation outcomes.

This chapter also move forward to presents the simulation and analysis of the two FFC strategies FFC-ET and FFC-TIC. Each type is investigated under Matlab/Simulink integrated environment. Simulations are carried out for two FFC models, for each the model, single and 2-links cases of the industrial type robot arms with real parameters are investigated. Possible application scenarios are also discussed as per feasible future developments.

The process of modeling a 2-link planar robot arm with correct mechanical model, and its interaction with the environment are also carried out at the latter part of the chapter. With the help of simulation, the ability of the algorithm to match the real model can easily be identified. The comparison studies of FFC with respect to an impedance control (IC) technique are also a main aspect of this paper. Therefore, both techniques are implemented in an integrated simulation environment. Based on the results, the uses of FFC and IC show that capability of controlling the robot-environment interaction, especially in those applications where the environment is completely or partially unknown. Simulation output also shows that similar to that of IC, the property of compliance the external forces rather than controlling the exact forces exerted into the environment is also inherited in FFC but in different manner.

In **Chapter 4**, remote control of a robot arm by means of force-free control and visual template matching is investigated. The reference position of the working side robot arm is generated by two control schemes, called rough motion and accurate motion. The remote control was achieved by means of force-free control and visual servo control scheme was developed using a template matching algorithm. Experimental results indicate effectiveness of the proposed approach. Fault tolerant capability for the data loses and communication delays also illustrated by conducting two experiments. First experiment is carried out with data loses and second experiment is without data loses, and irrespective of the data loses and delays, both cases proposed and clarified that remote control system has been performed well.

Chapter 5 is a subsequent branch for evaluating the system described in Chapter 4. This is devoted for an investigation is carried out for the teleoperation system to find out how human factors with cognitive aspects affect the system effectiveness and performance when it applies in practice. It is essential that we must test the

system with large number of real scenarios to validate the applicability, if the teleoperation system claims to be used in real application. Moreover, especially if a system has human user involvement and which is a critical factor for fulfillment of final objectives then a sample of users should be selected with a high degree of variation and the sample amount must also be higher. The relevance of the real world application of the teleoperation system, particularly in case of human supervisory involvement, is highlighted in this paper. Finally, provision of a visual feedback channel for the human user effectively increased applicability and success rate (effectiveness) of the teleoperation system regardless of users skills, age and relevance to their major field of study.

The another system performance evaluation study carried out as extension to the chapter 4, has been described in **Chapter 6**. The evaluated system has a module to make accurate motions in which, Template Matching (TM) techniques were used to aid the visual servo control. In which, two different types of TM algorithms are used in the investigation. Therefore, it is revealed that system performance and behavior are highly depend upon light intensity around robot working space as well as the color contrast between the target and the target background. From the results, it is verified that, lower lighting conditions NCC has shown accurate template matching performance when color contrast between the target object and the background is higher.

Two new improved versions of FFC alias here as FCPMC have been proposed in **Chapter 7** which are named as FCPMC-OCT and FCPMC-GNN, respectively. The FCPMC-OCT is proposed based on genetic algorithm (GA) to avoid ad-hog parameter estimation and implicit assumptions based upon former FFC-TIC. And FCPMC-GNN is derived to eliminate uncertainty and incorrect modeling effects of former FFC-ET. The proposed FCPMC can be configured easily and it can also be easily plug-in to the existing systems. Therefore, cost and risk free implementation would bring high demand of industrial implications.

8.2 Future directions

There are open problems to be solved before applying FFC and its derivative control strategies to real robots which are currently being executed in production floors. Here, I would like to encourage an incremental approach where the robots start with a comprehensive set of practical safety objectives. In that case, possibly preventing unexpected collisions between industrial robot and human operators or other dynamic objects. And for which, one can start to develop its own passive motion behaviors to employ its end effectors to realize situation dependant behaviors. That must agree with safety objectives to be expected by implementing FFC on existing robots.

At times, robots with higher degree of freedom to be handled, for which, further exploration of specific technology for redundancy resolution of robot manipulators are needed. Because of morphological advantage of them to realize FFC for safety objectives is invaluable. Redundancy gives room to have many joint velocity vectors lying in the null-space of the end-effector. This means that there can be infinitely many joint configurations for a given end-effector configuration. Therefore, adapting

FFC control for each joint actuators independently would be an over design and hence it might impair for profit oriented businesses. Therefore, redundancy can sometimes be seen as a morphological resource to realize safety by attaching FFC on industrial robots, where less number of independent FFC units in a robot might be enough to achieve required passive motions against undesired collisions. However, robots with redundant actuators have never been analyzed or experimented during this research.

An important aspect not discussed in this thesis is proposing an appropriate switching mechanism between proposed FFC and a original robot controller. It is a must have entity because, non of FFC development would not be impled in real industrial environment if robot would not be able to automatically switched from normal operation to FFC when it could face an illegal touch or collision during an operating session. It will be fascinating if the robots have intelligent switching mechanism and coupled vision ability along with FFC. In fact, hence robot can mimic the humans to adapt and decide when to proceed switching to a safety scheme if robot facing a threat. An extension would be an application of Neuro-fuzzy based FFC in which, advices/experiences of human operators and by fusing them appropriately whenever necessary through fuzzy rules. That is also hand to evolve a synergetic reasoning engine for reducing possible uncertainty/noise of friction, interference and other modeling parameters.

One other important feature would be to have is, mechatronic actuator back-drivability, in which rigid actuator can be move by applying external forces. In most actuator-gear systems being subjected to the static and dynamic friction, even though, some applications need those actuators to be back-drivable under small external contact toques or forces. Most rehabilitation type robots need to be more flexible by making those actuators back-drivable. Thereby, FFC of intelligent kind would be a good future choice for taking care of those kind of requirements. Because, neural network based FFC can be altered to handle the different levels of friction smoothly hence, choice of which would have higher implication potential for future extensions.

Appendix A

Digital Control Analysis

A.1 DC motor for robotic systems

A.1.1 Equation of motion

Figure A.1: (a)shows schematic diagram of a motor, gear, wheel and chassis.

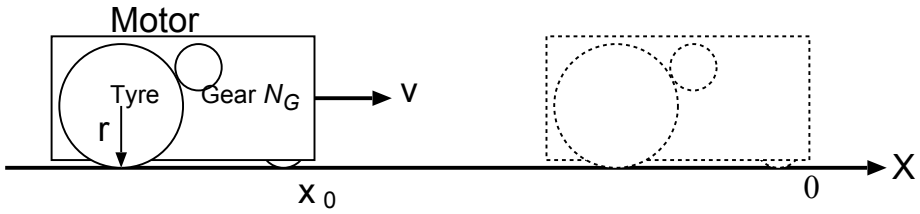

(a) Structure of robot.

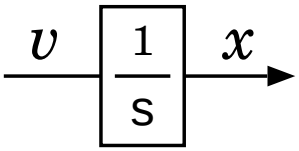

(b) Simple model of a robot

Figure A.1: Mobile Robot Model

Let's take DC motor input voltage e_a [V], angular velocity of the rotor ω_M [rad/s] and voltage constant of the motor K_e, then following relationship can be expressed.

$$\omega_M = \frac{e_a}{K_e} \tag{A.1}$$

And, if radius of the tyre r [m] and moving speed of the robot v [m/s], then distance traveled in time t [s], x [m] is given by

$$v = r\omega_M = \frac{r}{K_e} e_a \tag{A.2}$$

$$x = vt = \frac{r}{K_e} t e_a \tag{A.3}$$

In Fig. A.1 (b) distinguish the block model of the mobile robot in simplified form.

A.1.2 Feed back control

As in Fig. A.1 robot starts from x_0 [m] and stop at 0 [m] position by controlling velocity, hence, velocity v can be written as $v = x_o/\Delta, T$, where Δ, T is fixed sampling time. However, if velocity is not zero at the end position it should be force to zero to stop the robot movement. To achieve control property, we introduce control parameter K_p and by $v = -K_p, x$ we could be able to control the robot $v = 0$ [m/s]. From that variable mobile robot can be moved with desired speed to the desired destination. If $\Delta, T = 0$ then model can be shown as Fig. A.2 (b).

(a) Robot digital control (b) If sampling time is very small ($\Delta T \simeq 0$)

Figure A.2: Mobile Robot Controller

Let's take initial position x_o [m], starting velocity v_o [m/s] and one sample time ΔT, robot will reach to the new position x_1 [m] then, it can be given by

$$x_1 = x_0 + v_0 \Delta T = (1 - K_p \Delta T) x_0 \tag{A.4}$$

and from position x_1 if new velocity is given by v_1 then $v_1 = -K_p x_1$ that is,

$$x_2 = x_1 + v_1 \Delta T = (1 - K_p \Delta T) x_1 = (1 - K_p \Delta T)^2 x_0. \tag{A.5}$$

Therefore, general relationship can be obtain if sampling time is constant for entire process, and again $v = -K_p x$ exists.It can be shown as

$$x_i = (1 - K_p \Delta T)^i x_0 \tag{A.6}$$

s.t.

$$|1 - K_p \Delta T| < 1 \tag{A.7}$$

When $i \to \infty$, $(1 - K_p \Delta T)^\infty = 0$ as $x_i|_{i \to \infty} = 0$, but on the other hand if $|1 - K_p \Delta T| > 1$ then oscillations will occur which is caused to instability, even if varying the K_p. Therefore, it should be prevented to reach the $K_p = 1/\Delta T$.

A.1.3 Changing proportional gain K_p

Following cases are illustrated in Fig. A.3, as (a) $K_p < 0$ and not satisfy the condition in A.7, (b) $K_p < 1$ it satisfies the A.7, (c) $K_p > 1$ and then satisfies A.7 and (d) $K_p > 2$ while satisfying A.7; all cased ΔT is maintained to be 0.1 [s].

Graphs are given for each of the above cases, where $x_0 = -1$ [m] and simulation time t [s] is for all cased 0.65 [s]. Controller is given as $v = K_p x$.

(a) For any of the three values of K_p, responses are not reach to the desired input value 0 [m] level.

(b) In this case, K_p is selected as comply with A.7.

(c) Overshoot occur in each of the depicted graphs in A.3 (c) and increasing K_p tends to unstable the system response.

(d) Overshoot occurs for all cases and increasing K_p oscillation amplitude also increasing which creates controller unstable.

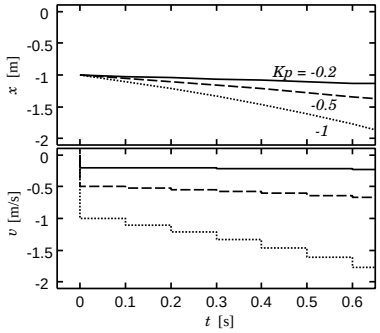

(a) $K_P = -1$(doted), -0.5(dashed), -0.2(line)

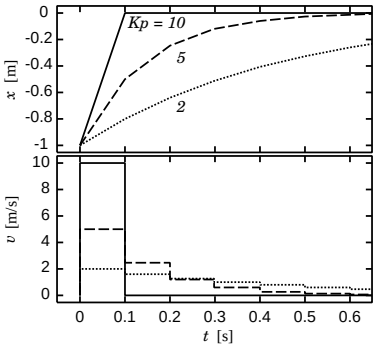

(b) $K_P = 2$(doted), 5(dashed), 10(line)

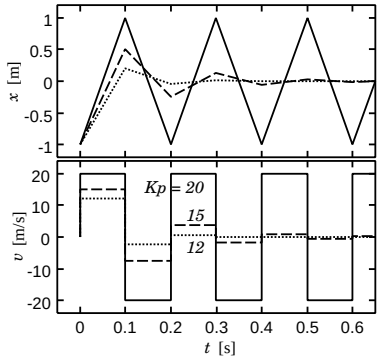

(c) $K_P = 12$(doted), 15(dashed), 20(line)

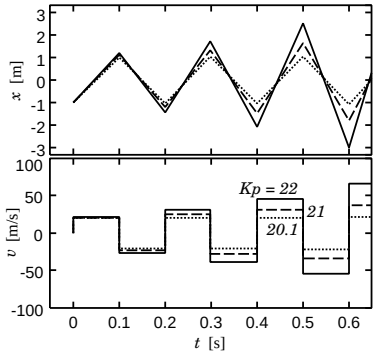

(d) $K_P = 20.1$(doted), 21(dashed), 22(line)

Figure A.3: Simulation of Mobile Robot,($\Delta T = 0.1$ [s])

A.1.4 Changing sampling time ΔT

Simulations are carried out by keeping constant $K_p = 10$ while varying sample time. Results are given in Fig. A.4 (a) and (b), it is very clear that better controller action

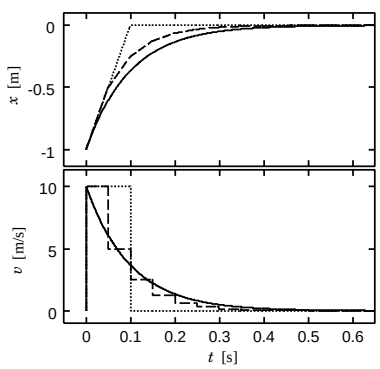

(a) $\Delta T = 1$[ms](line), 50[ms](dashed), 100[ms](doted)

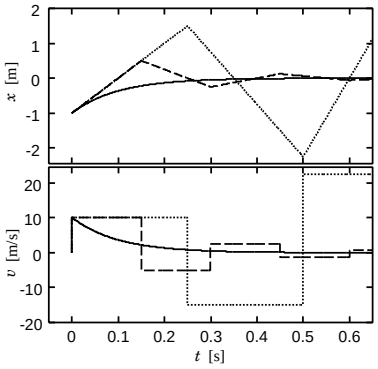

b) $\Delta T = 1$[ms](line), 150[ms](dashed), 250[ms](doted)

Figure A.4: Simulation of Mobile Robot, ($K_P = 10$)

can be achieved when lower the sampling time at 1 [ms] level, and tracking is highly undesirable for higher sampling time cases which are shown in highly oscillatory responses.

A.1.5 Simulation for motor properties

Motor properties are given in A.3, is simulated under two conditions which are also shown in Fig. A.5 (a)voltage and speed and (b)transient properties.

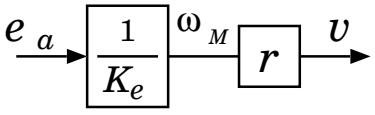

(a) Motor voltage and speed relationship model

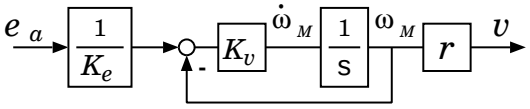

(b) Model of transient property

Figure A.5: Motor Model

Here by taking $r/K_e = 1$ as Fig. A.2 (b) and Fig.A.6 (a) can be shown as

$$\frac{X(\mathtt{s})}{U_x(\mathtt{s})} = \frac{K_p K_v}{\mathtt{s}^2 + K_v \mathtt{s} + K_p K_v} \tag{A.8}$$

where four set of conditions are interested $K_v = 40$, $K_p < 4K_v$, $K_p > 4K_v$ and $K_p = 4K_v$ simulations are given in A.6 (b).

A.1.6 Digital representation of a motor controller model

In practice ΔT is always difficult to control because if it will cause to create faster system responses, therefore when decreasing K_p will again cause to increase the settling time hence tendency of adding noise is greater. Therefore, 2nd order systems can not be controlled with single controller parameter K_p for appropriate sampling time, as in Figs. A.7 and A.8.

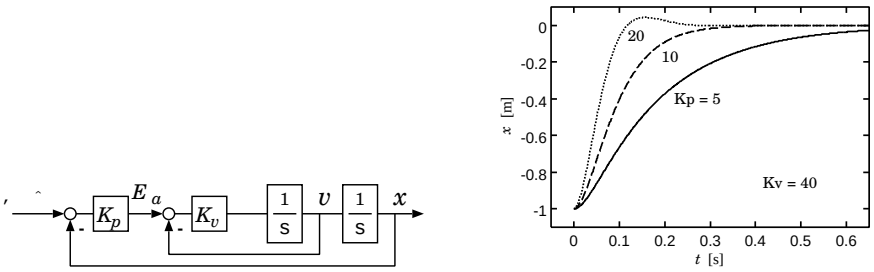

(a) 2nd order block model (b) 2nd order response plots

Figure A.6: 2nd Order Model of a Mobile Robot

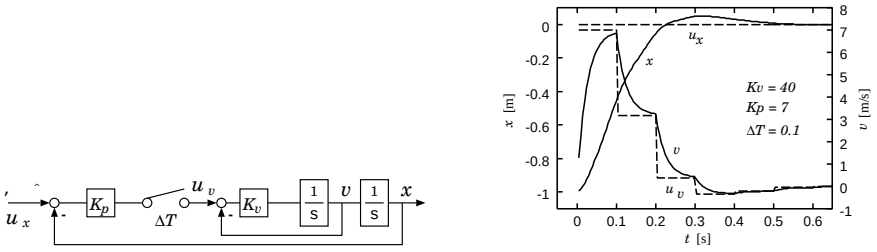

(a) 2nd order block model (b) 2nd order response plots

Figure A.7: Digital Control Model

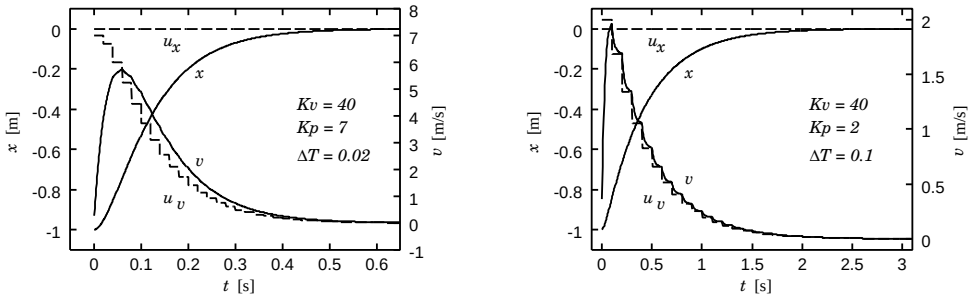

(a) $K_v = 40$, $K_p = 7$, $\Delta T = 0.02$ [s] (b) $K_v = 40$, $K_p = 2$, $\Delta T = 0.1$ [s]

Figure A.8: Overshoot Varying Characteristics of a Digital Control

Appendix B

Motor Anatomy and Digital Architecture

B.1 DC Motor Characteristics

According to the laws of physics we derive the equations of motion of the DC motor, an then derive the transfer function. In addition, here we ignore the friction in the analysis.

B.1.1 Analysis of the DC motor

The DC motor, as shown in Fig. B.1: Rotor, armature, magnet, commutator, brush from coil wound with wire to the core is constructed. Here, B [Wb/m^2] is magnetic flux density in, n is the number of turns of the coil, l [m] is the length of the coil across the magnetic field, diameter of the coil is D [m], current to flow through the coil is I_a [A], J_M [kg m^2] is moment of inertia of the armature.

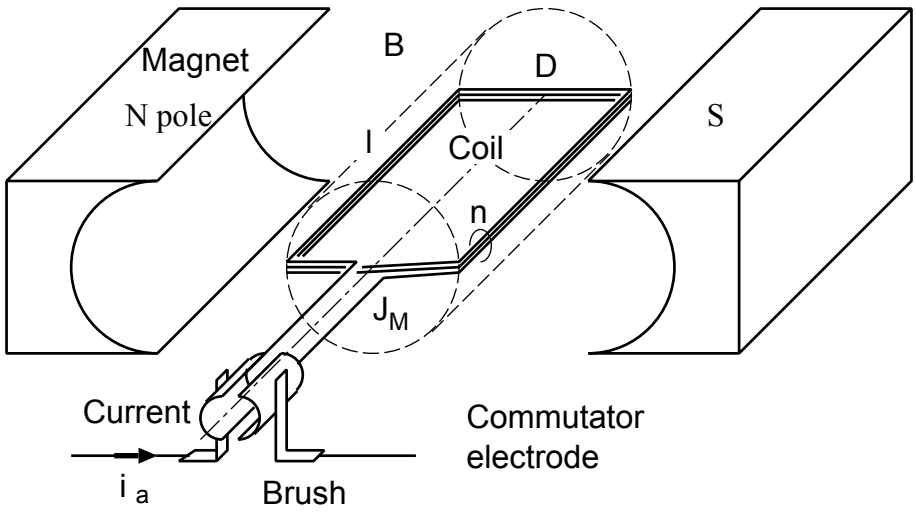

Figure B.1: Configuration of the DC motor

B.1.2 Angular acceleration and rotational force of the armature by electromagnetic force

Cross-sectional view thereof given in Fig. B.2

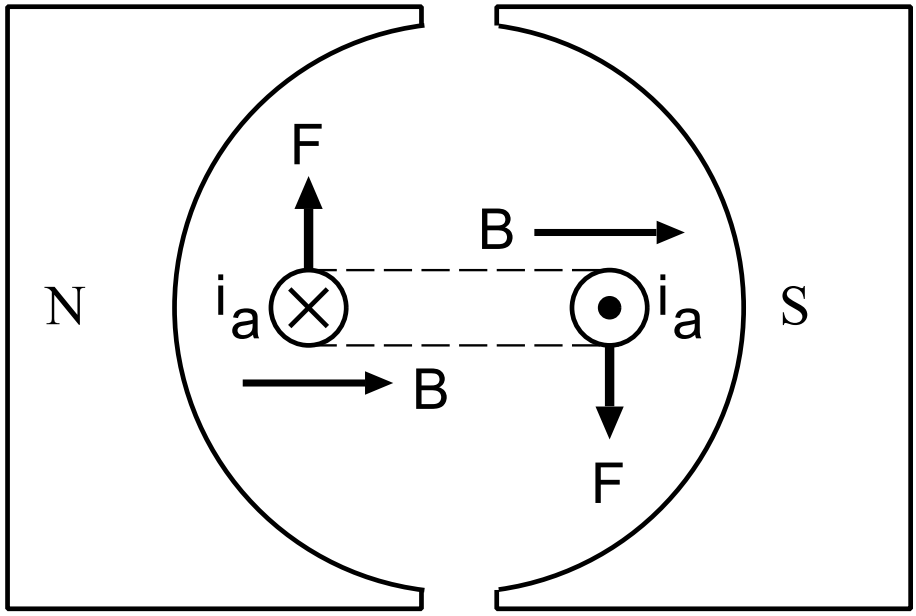

Figure B.2: Cross-sectional view of the DC motor

Current of the magnetic field in the electromagnetic force F [N]

$$F = l\,B\,i_a \tag{B.1}$$

That means, if you produce electromagnetic force at both ends of the coil, torque T_M [Nm] is generated by rotational force in the armature.

$$T_M = F \times D/2 \times 2 = n\,l\,D\,B\,i_a = K_T i_a \tag{B.2}$$

$$K_T = n\,l\,D\,B \tag{B.3}$$

Here, K_T [Nm/A] is a torque constant. This torque, generates angle acceleration in armature $\dot{\omega}_M$ [rad/s^2] as given below.

$$\dot{\omega}_M = \frac{d}{dt}\omega_M = \frac{T_M}{J_M} = \frac{K_T}{J_M} i_a \tag{B.4}$$

B.1.3 The counter-electromotive force by electromagnetic induction

Rotation speed of the motor (angular speed) ω_M [rad/s] obtained by integrating the angular acceleration,

$$\omega_M = \int \frac{T_M}{J_M} dt. \tag{B.5}$$

This angular velocity of the coil results

$$v_M = \frac{D}{2}\omega_M \tag{B.6}$$

tangential velocity v_M [m / s]. Since the coil across the magnetic field as shown in Fig. B.3, induced electromotive force $e = l\,B\,v_M$ [V] is generated by electromagnetic induction, .

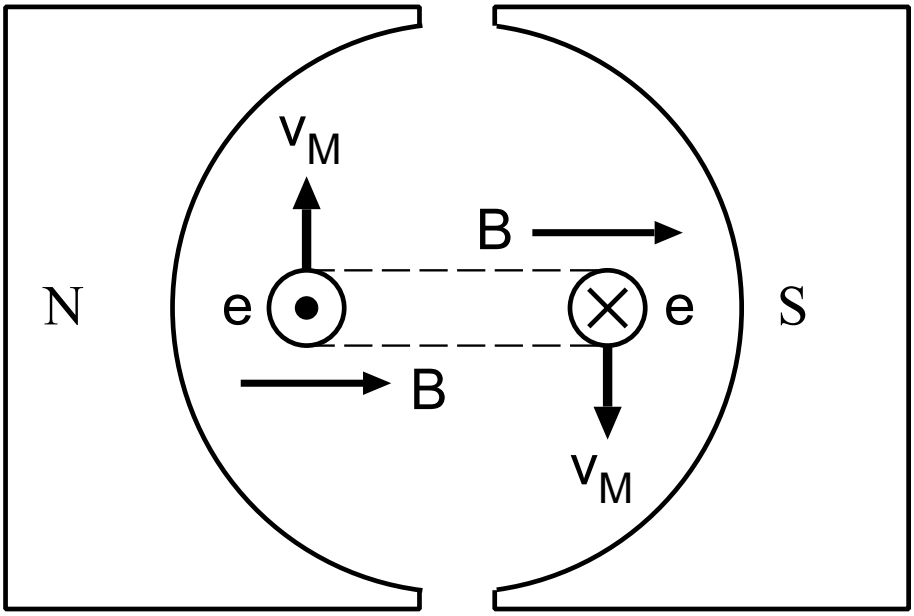

Figure B.3: Generation of induced electromotive force

e_e [V] was the total induced electromotive force of all, due to the back EMF.

$$e_e = e \times 2 \times n = n\,l\,D\,B\,\omega_M = K_e\omega_M \tag{B.7}$$

$$K_e = n\,l\,D\,B \tag{B.8}$$

K_e [Vs/rad] is the induced voltage constant, induced voltage constant and torque constant are equal.

B.1.4 Electrical circuit of DC motor

Voltage to be applied to the armature e_a [V], R_a [Ω] is the electrical resistance of the coil, L_a [H] is the inductance shown in Fig B.4, then current i_a [A] flowing through the armature given as;

$$L_a\frac{d}{dt}i_a + R_a i_a = e_a - e_e = e_a - K_e\omega_M. \tag{B.9}$$

Here, T_e [s] the electrical time constant given as follows,

$$T_e = \frac{L_a}{R_a}. \tag{B.10}$$

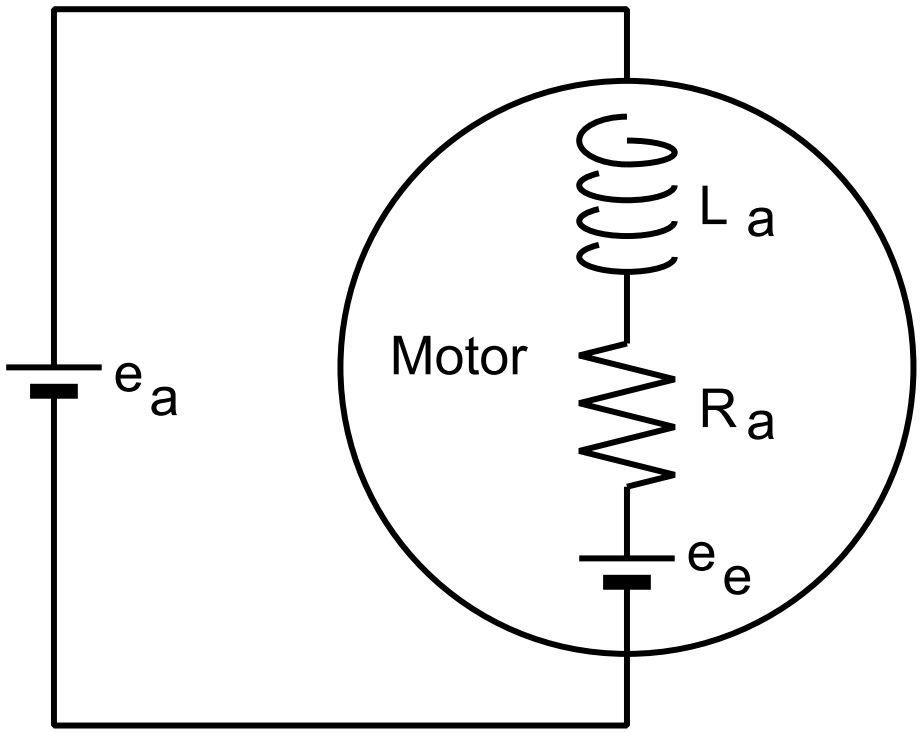

Figure B.4: Electrical circuit diagram of the motor

B.1.5 Equation of motion of the DC motor

Enter the current of the armature i_a, equation of motion of the motor to the output rotational force T_M and it will be evaluated from (B.4),

$$T_M = K_T i_a. \tag{B.11}$$

In addition, $i_a = J_M \dot{\omega}_M / K_T$ can be obtained from equation (B.9) by substituting the expression (B.4):

$$\frac{L_a J_M}{K_T}\ddot{\omega}_M + \frac{R_a J_M}{K_T}\dot{\omega}_M + K_e \omega_M = e_a \tag{B.12}$$

This is the input voltage e_a applied to the armature,the obtained a differential equation becomes the equation of motion of the DC motor and output (number of revolutions) ω_M is angle of the armature.

From this equation of motion, block diagram of the motor as Fig. B.5 then, the number of transfer $G_M(\mathtt{s})$ is expressed as;

$$G_M(\mathtt{s}) = \frac{\omega_M(\mathtt{s})}{E_a(\mathtt{s})} = \frac{K_T}{L_a J_M \mathtt{s}^2 + R_a J_M \mathtt{s} + K_T K_e} \tag{B.13}$$

If the constant T_s is sufficiently small electrical time, i.e. in the case of $L_a \simeq 0$, Fig. B.6 it could also be written as in Fig. **??**, hence, the transfer function $G_s(\mathtt{s})$ is given as;

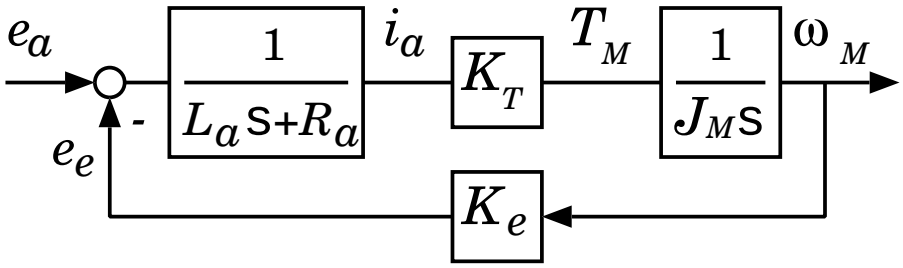

Figure B.5: Block diagram of the DC motor

$$G_s(\mathtt{s}) = \frac{\omega_M(\mathtt{s})}{E_a(\mathtt{s})} = \frac{K_T}{R_a J_M \mathtt{s} + K_T K_e}. \tag{B.14}$$

The mechanical time constant of the motor constant T_s [s] expressed when the step response of this system as follows;

$$T_s = \frac{R_a J_T}{K_T K_e}. \tag{B.15}$$

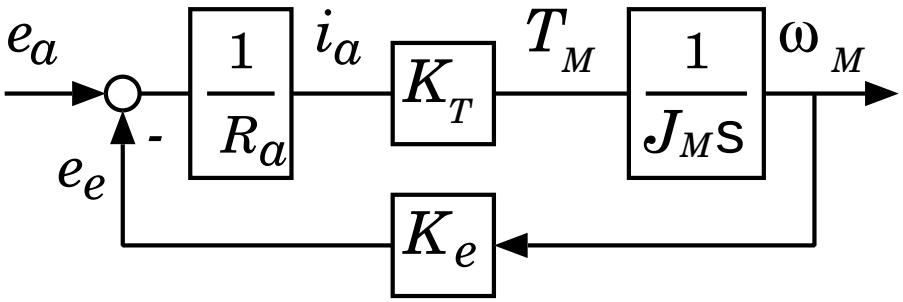

Figure B.6: Block diagram of the case constant smaller electrical time

B.2 Rigid coupling with the two mass model

B.2.1 Connection of the motor mechanism

FigureB.7 the motor as shown does not used alone, mechanism and motor are used in connected via a gear.

Here, The J_M [kg m^2] is the moment of inertia of the armature, N_G reduction ratio of the gear, K_L [N m] spring constant of the mechanism,, J_L [kg m^2] moment of inertia of the mechanism, D_L [N ms] is the viscous friction coefficient of the mechanism.

Block diagram of a two mass model is illustrated in Fig. reffig motor-8 then

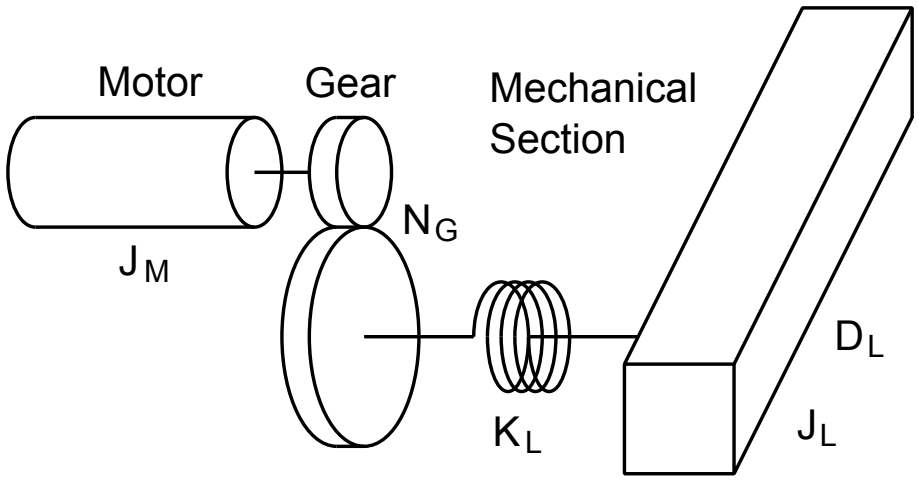

Figure B.7: Connection of the motor mechanism

transfer function of the two mass model and represented as $G_2(\mathrm{s})$.

$$\begin{aligned} G_2(\mathrm{s}) &= \frac{\omega_M(\mathrm{s})}{E_a(\mathrm{s})} \\ &= K_T(J_L\mathrm{s}^2 + D_L\mathrm{s} + K_L)/\left[L_aJ_MJ_L\mathrm{s}^4 + J_M(L_aD_L + R_aJ_L)\mathrm{s}^3\right. \\ &\quad + \left\{L_aK_L(J_M + J_L/N_G^2) + R_aJ_MD_L + J_LK_eK_T)\right\}\mathrm{s}^2 \\ &\quad + \left\{L_aK_LD_L/N_G^2 + R_aK_L(J_M + J_L/N_G^2) + D_LK_eK_T)\right\}\mathrm{s} \\ &\quad \left. + K_L(R_aD_L/N_g^2 + K_TK_e)\right] \end{aligned} \tag{B.16}$$

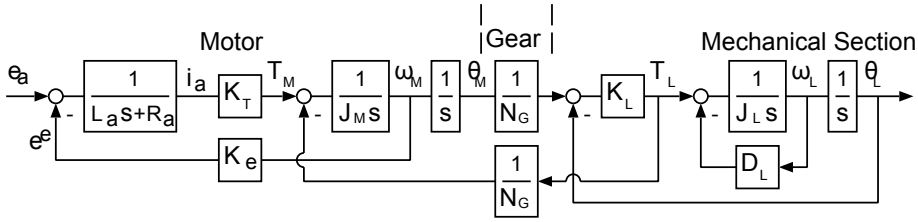

Figure B.8: Block diagram of the two mass model

B.2.2 œRigid body combined model

If it can be approximated mechanism and motor shown in Fig. B.9 and is rigid bonded, mass model it becomes rigid binding model that set with infinite spring constant K_L.

Here, The moment of inertia of the composite armature $J_T(= J_M + J_L/N_G^2)$ [kg m^2], and $D_T(= D_L/N_G^2)$ [N m s] is a viscous friction coefficient of the composite armature of mechanism and gear.

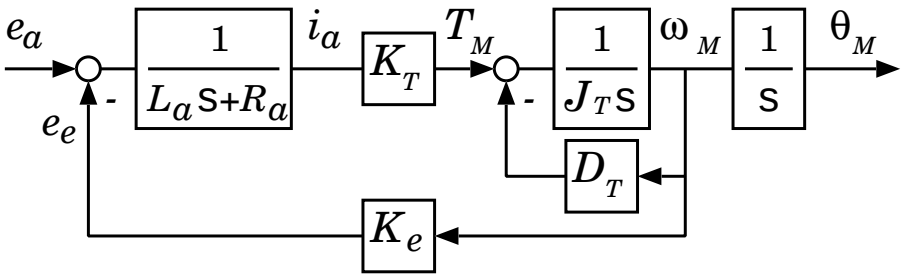

Figure B.9: Block diagram of the rigid body binding model

The transfer function $G_1(\mathtt{s})$ of rigid body binding model of two mass model of equation(ref eq: G2)and by placing the infinity the transfer function $G_2(\mathtt{s})$ represented with K_L .

$$G_1(\mathtt{s}) = \frac{K_T}{L_a J_T \mathtt{s}^2 + (L_a D_T + R_a J_T)\,\mathtt{s} + R_a D_T + K_T K_e} \tag{B.17}$$

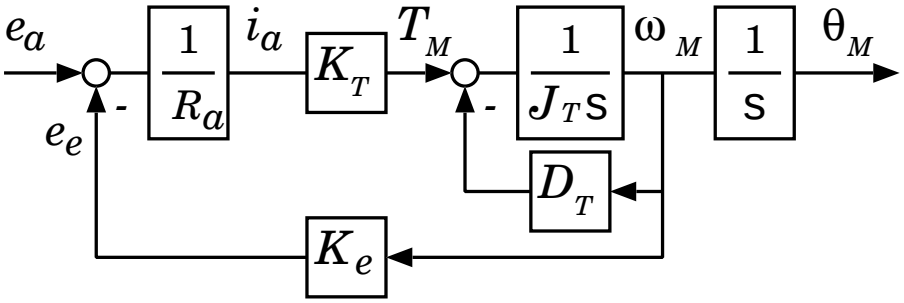

Figure B.10: Block diagram of the rigid coupling simple model

In addition, if constant T_s is sufficiently small electrical time, i.e. in the case of $L_a \simeq 0$, Fig. B.9 and B.10 be rewritten as the transfer function $G_T(\mathtt{s})$ is as;

$$G_T(\mathtt{s}) = \frac{\omega_M(\mathtt{s})}{E_a(\mathtt{s})} = \frac{K_T}{R_a J_T \mathtt{s} + R_a D_T + K_T K_e}. \tag{B.18}$$

B.3 Measurement of the parameters of the DC motor

The measurement parameters is performed using a rigid coupling simplified model of the transfer function shown in Fig. B.10. From Equation (refeq:GT), parameters of mechanism and motor R_a, K_T, K_e, J_T, and D_T, are measured in this order.

A circuit diagram for the measurement is shown in Fig. B.11. Here, R_s [Ω] is electrical resistance of the armature current measurement, (example 1[Ω],10[W]), voltage amplification gain of the amplifier is A_{V1}. relationship voltage applied voltage amplification gain of A_{V2} , the motor and output voltage from the D/A converter on

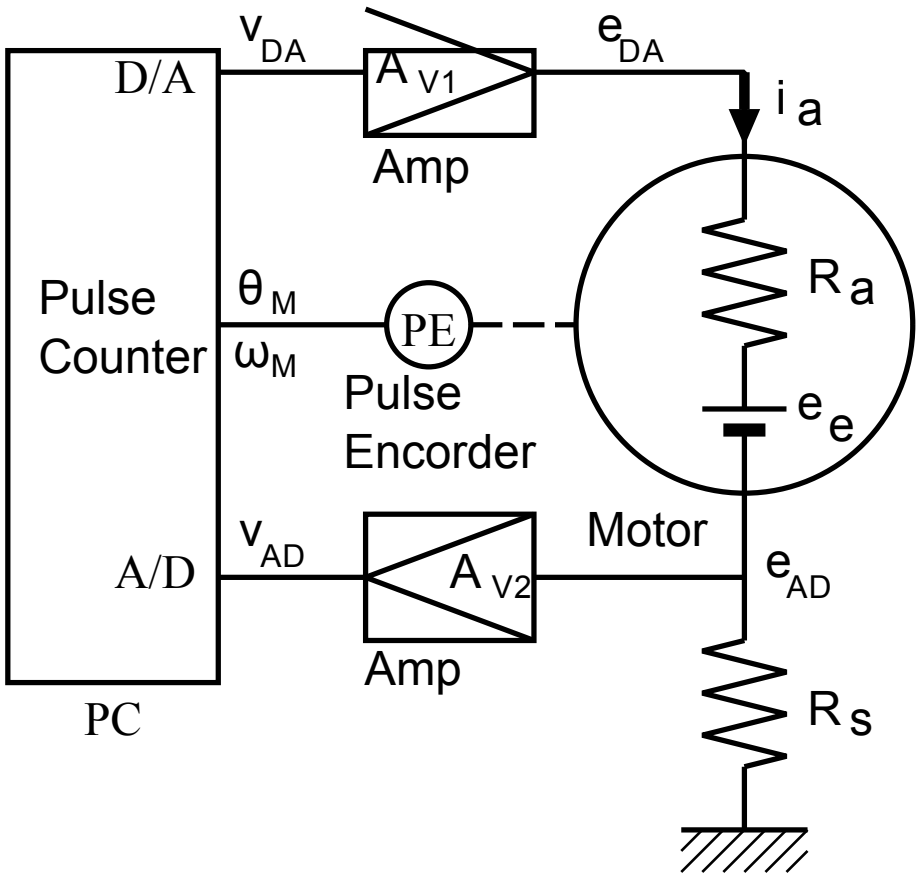

Figure B.11: Circuit diagram for the measurement

the PC with the v_{DA} is $e_{DA} = A_{V1}v_{DA}$, relationship of v_{AD} input voltage to the A/D converter and PC e_{AD} voltage measurement is $v_{AD} = A_{V2}e_{AD}$, if I want to measure the angle θ_M angular velocity and ω_M of the motor by a pulse counter.

Therefore, it is armature current i_a shown calculation and armature voltage e_a is given below.

$$e_a = e_{DA} - e_{AD} = A_{V1}v_{DA} - v_{AD}/A_{V2} \tag{B.19}$$

$$i_a = \frac{e_{AD}}{R_s} = \frac{v_{AD}}{R_s A_{V2}} \tag{B.20}$$

Next, Fig. **??** depicted the step response of the motor when it is a E_a magnitude is measured.

The response, it is substituting step input $\frac{E_a}{\mathtt{s}}$ to the expression: (B.18).

$$\omega_M(\mathtt{s}) = \frac{K_T}{R_a J_T \mathtt{s} + R_a D_T + K_T K_e} \cdot \frac{E_a}{\mathtt{s}} \tag{B.21}$$

$$\omega_M(t) = \left(1 - e^{-\frac{R_a D_T + K_T K_e}{R_a J_T} t}\right) \frac{K_T E_a}{R_a J_T} \tag{B.22}$$

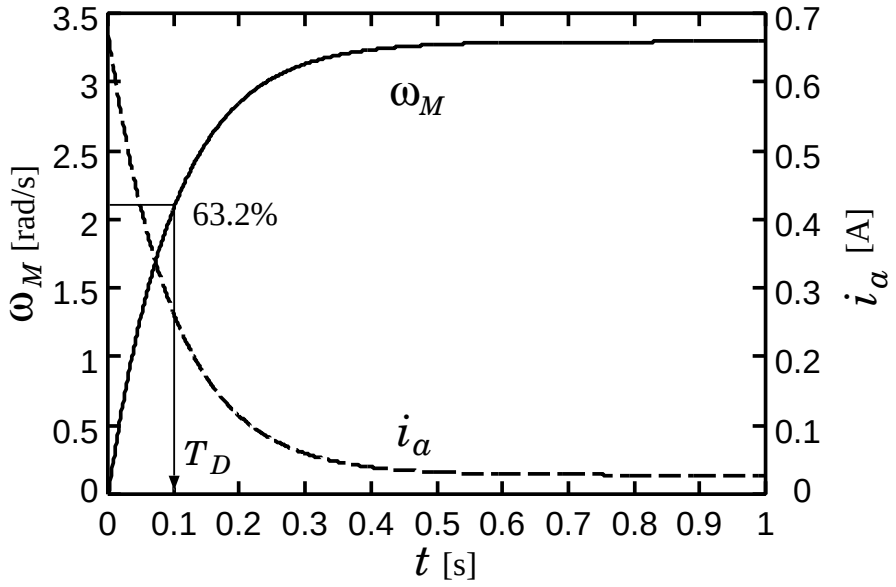

Figure B.12: Step response of the DC motor

B.3.1 Total armature resistance

The armature resistance R_a, i.e. counter-electromotive force e_e is 0 when the angular velocity $\omega_M = 0$ Motor to prevent rotation so that, it can be determined and by measuring the armature current i_a when gave armature voltage e_a

$$R_a = \frac{e_a}{i_a} \tag{B.23}$$

Resistance varies depending on the state of the brush and commutator, It is necessary to measure in several places.

B.3.2 Measurement of the induced voltage constant torque and constant

First, Fig.B.12 using the step response of, to obtain the induced voltage constant K_e torque and constant K_T. Fig. B.10, the back EMF e_e so $K_e\omega_M$, armature current i_a is expressed by

$$i_a = \frac{e_a - e_e}{R_a} = \frac{e_a - K_e\omega_M}{R_a}. \tag{B.24}$$

Thus, the induced voltage constant K_e torque and constant K_T, is measured armature current $i_a a(\infty)$ when the step response has a steady angular velocity ω_M and ∞),

$$K_T = K_e = \frac{e_a - R_a i_a(\infty)}{\omega_M(\infty)} \tag{B.25}$$

B.3.3 œMeasurement of the moment of inertia (inertia)

Moment of inertiaJ_T is and we put $t \to \infty$ in the step response by the formula (B.22),

$$\omega_M(\infty) = \frac{K_T E_a}{R_a J_T} \tag{B.26}$$

From

$$J_T = \frac{K_T E_a}{R_a \omega_M(\infty)} \tag{B.27}$$

it can be determined.

B.3.4 Measurement of viscous friction coefficient

The viscous friction coefficient D_T, time constant T_D [s], step response is determined by the formula (B.22)

$$T_D = \frac{R_a J_T}{R_a D_T + K_T K_e} \tag{B.28}$$

from the following equation

$$D_T = \frac{R_a J_T - K_T K_e T_D}{R_a T_D} = \frac{J_T}{T_D} - \frac{K_T K_e}{R_a} \tag{B.29}$$

B.4 Control of the DC motor

In order to control the DC motor, and a position loop for controlling the angle θ_M is to be constructed. As a minor loop, velocity loop for controlling the angular velocity ω_M, further, there is a case to construct a current loop to control the armature current i_a.

B.4.1 Configuration of the current loop

I configured the current loop as Fig. B.13, i.e. the amplification gain of the amplifier is K_1 and K_a^g is the current gain.

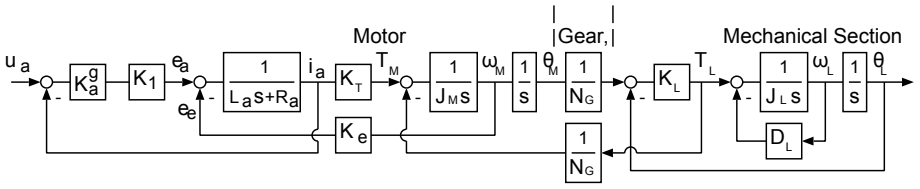

Figure B.13: Transfer function of the current loop

Further, in order to analyze the motor alone, removed the mechanism as shown in: Fig. B.14. When back EMF $e_e \simeq 0$, i.e. relationship of i_a for 0 small angular velocity $\omega_M \simeq 0$ and u_a is denoted by;

$$\frac{I_a(\mathtt{s})}{U_a(\mathtt{s})} = \frac{K_a^g K_1}{L_a \mathtt{s} + K_a^g K_1 + R_a} \tag{B.30}$$

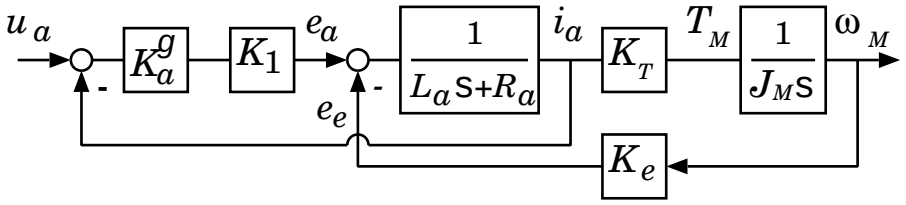

Figure B.14: The current loop in the motor

Because it is constant, T_{ea} electrical time of a current loop is formed when;

$$T_{ea} = \frac{L_a}{K_a^g K_1 + R_a} < T_{ea}. \tag{B.31}$$

The relationship of ω_M and u_a is given by;

$$\frac{\omega_M(\mathtt{s})}{U_a(\mathtt{s})} = \frac{K_a^g K_1 K_T}{(K_a^g K_1 + R_a) J_M \mathtt{s} + K_T K_e} \tag{B.32}$$

Which requires a constant mechanical time T_{sa} when I formed a current loop is given as;

$$T_{sa} = \frac{(K_a^g K_1 + R_a) J_M}{K_T K_e} = T_s + \frac{K_a^g K_1}{K_T K_e} > T_s. \tag{B.33}$$

Therefore, when form a current loop, reducing the electrical time constant, to increase the mechanical time constant there is work to be done, it is possible that $L_a \simeq 0$ is regarded.

When it was carrier frequency of the PWM is low and the number of KHz, motor to vibrate at that frequency, Since the noise is generated, install the external inductance as a low-frequency filter had. Therefore, current response was so worse, the current loop for the compensation was crossed. However, the carrier frequency of the PWM is increased at present, the external inductance by eliminating the need to install is exhausted, it can be thought of as a $L_a \simeq 0$, and do not have to form a current loop.

Therefore, it is assumed that $L_a \simeq 0$ is later, a configuration that does not bear current loop.

B.4.2 Configuration of the velocity loop

The configuration of the velocity loop in rigid upon binding is shown in Fig. B.15 Here, Speed gain is the integral time of the control T_I to K_v^g is given as;

$$T_M = K_T i_a = K_T e_{AD} / R_s. \tag{B.34}$$

Relationship of ω_M and u_v is given as

$$\begin{aligned} \frac{\omega_M(\mathtt{s})}{U_v(\mathtt{s})} &= \frac{(T_I \mathtt{s} + 1) K_v^g K_T}{T_I R_a J_T \mathtt{s}^2 + T_I (R_a D_T + R_a K_T K_e + K_v^g K_T)\mathtt{s} + K_v^g K_T} \\ &= \frac{K_v^g K_T}{R_a J_T \mathtt{s} + R_a D_T + R_a K_T K_e + K_v^g K_T - R_a J_T / T_I + \frac{R_a (D_T + K_T K_e - J_T / T_I)}{T_I \mathtt{s} + 1}} \end{aligned} \tag{B.35}$$

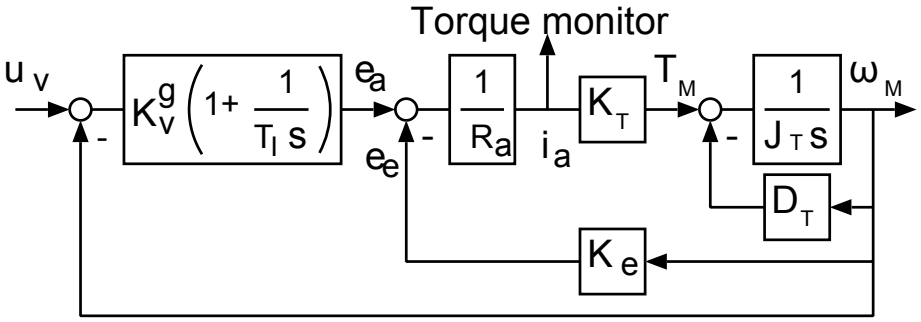

Figure B.15: The velocity loop in rigid upon binding

Here, the integration time T_I is shown

$$T_I = \frac{D_T + K_T K_e}{J_T} \tag{B.36}$$

The ability to adjust and as in Fig. B.17 it can be as simple as that of Fig. B.16. However,J_T, D_T from change depending on the state of the mechanism, and , be careful the approximate and an adjustment, because it can only be approximately represented.

$$\frac{\omega_M(\mathtt{s})}{U_v(\mathtt{s})} = \frac{K_v^g K_T}{R_a J_T \mathtt{s} + K_v^g K_T} = \frac{\frac{K_v^g K_T}{R_a J_T}}{\mathtt{s} + \frac{K_v^g K_T}{R_a J_T}} = \frac{K_v}{\mathtt{s} + K_v} \tag{B.37}$$

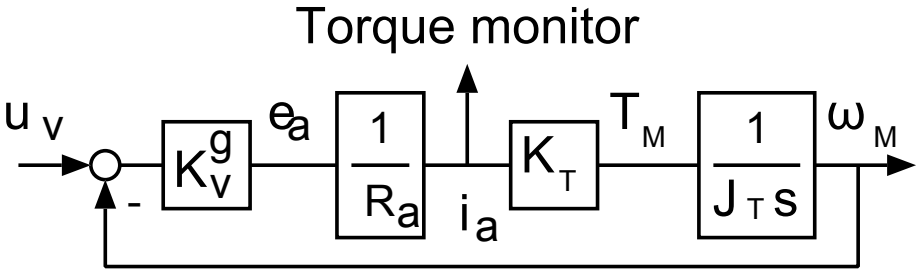

Figure B.16: Approximate model of the speed loop

B.4.3 Structure of the position loop

The structure of the position loop in rigid upon binding is shown in Fig. B.18. Here, T_I has been adjusted properly, as in Fig.B.16, and can be represented by the approximation model, K_p^g is a position gain.

The relationship of θ_M and u_p is determined by following equation and it can be represented by the quadratic approximation model shown in Fig. B.19.

$$\frac{\theta_M(\mathtt{s})}{U_p(\mathtt{s})} = \frac{K_p^g K_v^g K_T}{R_a J_T \mathtt{s}^2 + K_v^g K_T \mathtt{s} + K_p^g K_v^g K_T} = \frac{\frac{K_p^g K_v^g K_T}{R_a J_T}}{\mathtt{s}^2 + \frac{K_v^g K_T}{R_a J_T}\mathtt{s} + \frac{K_p^g K_v^g K_T}{R_a J_T}} = \frac{K_p K_v}{\mathtt{s}^2 + K_v \mathtt{s} + K_p K_v} \tag{B.38}$$

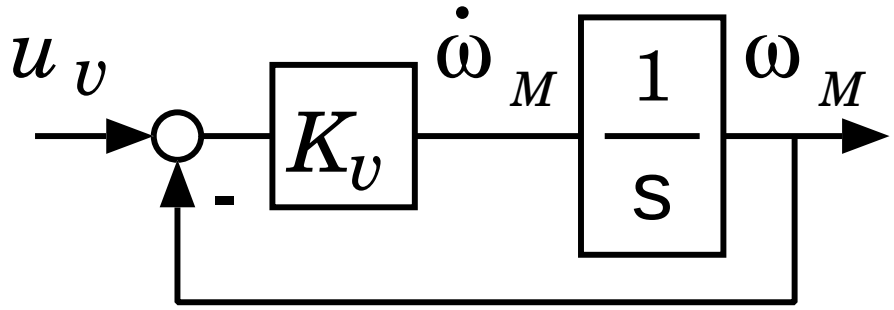

Figure B.17: Simple approximate model of the speed loop

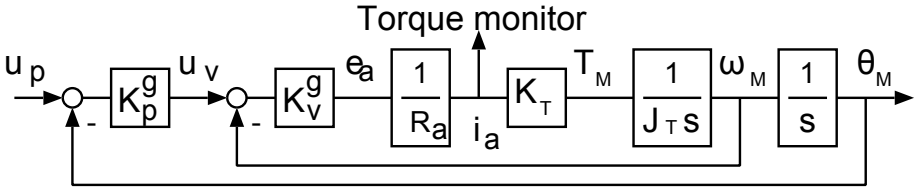

Figure B.18: The position loop in rigid upon binding

Response becomes oscillatory be insufficient braking if $K_v < 4K_p$, you can adjust the K_p to be a $K_v \geq 4K_p$. In this case, since it is a response similar to the primary model, it is regarded as a $K_v \gg 4K_p$, it may be represented in the first approximation model that is approximated by a first-order model and as shown in Fig. B.20.

$$\frac{\theta_M(\mathtt{s})}{U_p(\mathtt{s})} = \frac{K_p}{\mathtt{s} + K_p} \tag{B.39}$$

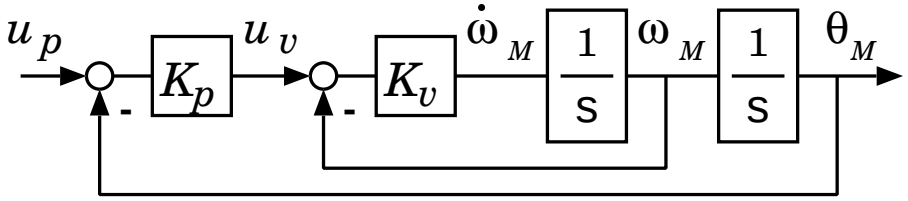

Figure B.19: 2-order approximation model

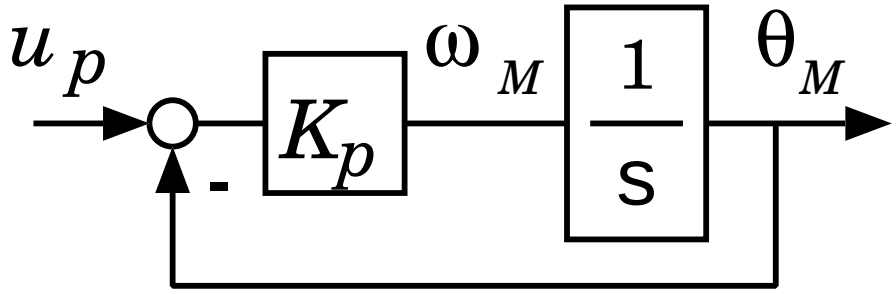

Figure B.20: First approximation model

B.4.4 Connection to the PC controller

Here we will explain how to connect to a PC's controller. I carried out it and it is connected as in Fig. B.11.

It is shown in Fig. B.21 when building the current loop.

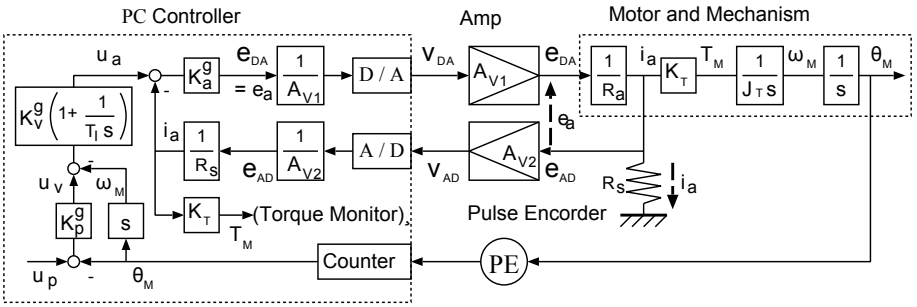

Figure B.21: System configuration diagram for building the current loop

Next, we show a case where not having a current loop. If you use a torque monitor, it is necessary to correct voltage drop of the current detection resistor $e_{AD} = R_s i_a$. A shown in Fig. B.22, $(1 + R_s/R_a)e_a$ current-sensing resistor R_s minute the system block diagram of a case of correcting using the e_{AD} that measured is shown in Fig. B.23 the system configuration diagram of a case of correcting.

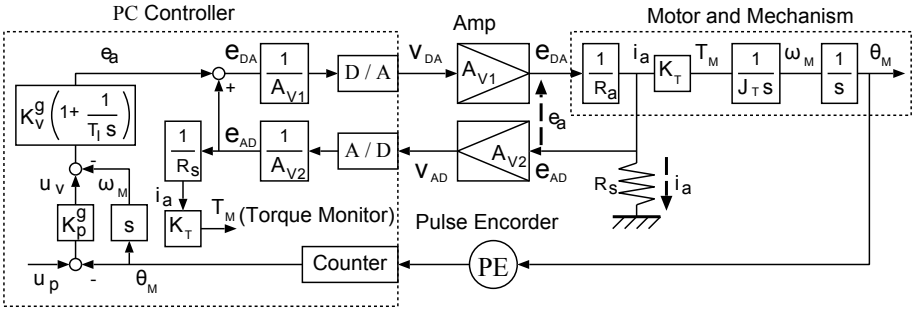

Figure B.22: Mobile Robot Model

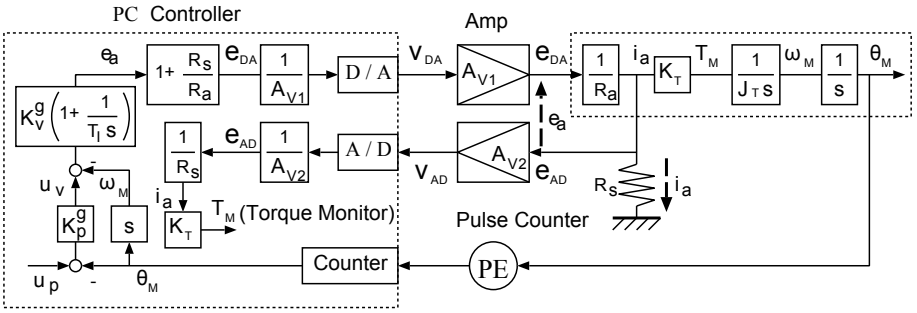

Figure B.23: (Part 1) system configuration diagram in the case of using a torque monitor

If you do not use a torque monitor, the case of calculating from $T_M = J_T\omega_M$ torque T_M is shown in Fig. B.24.

The system described above, will be selected as required.

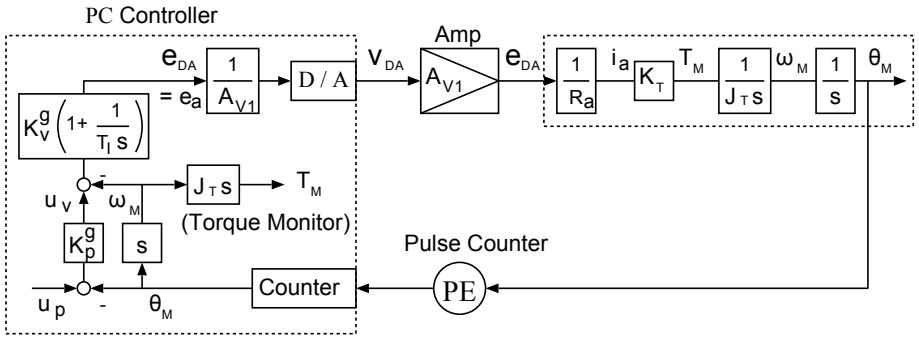

Figure B.24: System configuration diagram of the case of not using the torque monitor

Publications

A. Refereed International Journal Papers

1. A. Pallegedara, Y. Matsuda, T. Matsumoto, K. Tsukamoto N. Egashira and S. Goto, "Teleoperation of Robot Arms Using Force-Free Control and Template Matching," *International Journal of Innovative Computing*, Information and Control IJICIC 2012, ISSN 1349-4198, Volume 8, Number 10, pp. 6869-6884, October 2012.
2. A. Pallegedara, Y. Matsuda, N. Egashira, T. Sugi and S. Goto, "Experimental Evaluation of Teleoperation System with Force-free Control and Visual Servo Control by Human Operator Perception," *Artificial Life and Robotics*, ISSN 1433-5298, Volume 17,Combined 3-4,pp. 388-394, ISAROB November 2012.

B. Proceedings of International Conferences

1. A. Pallegedara, Y. Matsuda, T. Matsumoto, K. Tsukamoto N. Egashira and S. Goto, "Remote Control of Robot Arms via Network by Force-Free Control Followed Template Matching," Proceedings of the SICE Annual Conference 2011, (IEEE explorer), pp. 940-945, September 13-18, Tokyo, (Japan) 2011.
2. A. Pallegedara, Y. Matsuda, N. Egashira, T. Sugi and S. Goto, "Investigation of Lighting Conditions for Teleoperation of Robot Arms by Image Processing and Force-free Control," Proceedings of the 43rd ISCIE International Symposium on Stochastic Systems Theory and Its Applications, pp. 198-203, Oct. 28-29, Shiga, (Japan), 2011.
3. A. Pallegedara, Y. Matsuda, T. Matsumoto, K. Tsukamoto N. Egashira, T. Sugi and S. Goto, "Evaluation of the teleoperation system based on force-free control and visual servo control by using different human operator perception: evidence verified by experiments and statistical analysis," The Seventeenth International Symposium on Artificial Life and Robotics 2012 (AROB 17th '12), (IEEE explorer), pp. 1089-1094, January 19-21, B-Con Plaza, Beppu, Oita, (Japan), 2012.
4. A. Pallegedara, Y. Matsuda, N. Egashira, T. Sugi and S. Goto, "Comparison of Interaction Forces of Robot Arm on Force-free Control and Impedance Control by Model Based Simulations," Proceedings of the SICE Annual Conference 2012, (IEEE Explorer), pp. 1695-1700, August 20-23, Akita, (Japan), 2012.
5. Achala Pallegedara, Yoshitaka Matsuda, Naruto Egashira, Takenao Sugi and Satoru Goto, "Simulation and Analysis of Dynamics of the Force-free Control for Industrial Robot Arms," 12th International Conference on Control, Automation and Systems (ICCAS 2012), (IEEE explorer), pp. 733-738 Oct. 17-21, ICC Jeju

Island, (Korea), 2012.

6. Achala Pallegedara, Yoshitaka Matsuda, Naruto Egashira, Takenao Sugi and Satoru Goto, "Development and Evaluation of Simulation Model for Force-free Control Strategies," IEEE 6th International Conference on Information and Automation for Sustainability (ICIAfS 2012), (IEEE Explorer), pp. 147-152, September 27,28 & 29, Beijing, (China), 2012.

References

[1] Joseph F. Engelberger, *Robotics in Service*, First MIT Press Edition, 1989.

[2] Programmed Article Transfer, US Patent No. 2988237, 1961.

[3] H.A. Ernest, "A-Computer Controlled Mechanical Hand," Sc.D thesis, Massachusette Institute of Technology, Cambridge, 1961.

[4] R. Kelly "A tuning procedure ofPID control for robot manipulators". *Robotica*, Vol. 13, pp. 141-148, 1995.

[5] T.,Arimoto & F.,Miyazaki, "Stability and Robustnessof PID Feedback Control for Robot Manipulators of Sensory Capability," In:Robotics Research, M.Brady and R.Paul (Ed.), *MIT Press, Cambridge*, pp.783-799, 1984.

[6] D. E. Whitney, "Resolved Motion Rate Control of Manipulators and Human Prostheses", *IEEE Transactions on Man-Machine Systems*, vol. MMS-10, no. 2, 1969.

[7] R. P. Paul, "Manipulator Cartesian Path Control", *IEEE Transactions on Systems, Man, and Cybernetics*, vol. SMC-9, pp.702 -711, 1979.

[8] J. Y. S. Luh, M. W. Walker and R. P. Paul, "Resolved Acceleration Control of Mechanical Manipulators", *IEEE Transactions on Automatic Control*, vol. AC-25, pp.468 -474 1980.

[9] R. P. Paul, *Robot Manipulators: Mathematics, Programming, and Control*, M.I.T. Press, 1981.

[10] K. S. Fu, R. C. Gonzalez and C. S. G. Lee, *Robotics Control, Sensing, Vision, and Intelligence*, McGraw-Hill Inc., Singapore, pp. 82-144, 1987.

[11] A. J. Koivo and T. H. Guo, "Adaptive linear controller for robotic manipulators", *IEEE Trans. Automat Control*, vol. AC-28, pp.162 -171, 1983.

[12] S. Goto, M. Nakamura and N. Kyura, "Accuract contour control of mechatronic servo systems using gaussian networks," *IEEE Trans. Ind. Electron.*, vol. 43, pp. 469-476, 1996.

[13] G. Feng, "A new stable tracking control scheme for robotic manipulators", *IEEE Trans. Syst., Man, Cybern.*, vol. 27, pp.510 -516, 1997.

[14] Y. Gao, M. J. Er, and S. Yang, "Adaptive fuzzy neural control of robot manipulators", *IEEE Trans. Ind. Electron.*, Vol. 48, pp.1274 -1278, 2001.

[15] J.Y.S. Luh, "An anatomy of industrial robot and their controls", *IEEE Trans. Automat. Control*, Vol. AC-23, no. 2, pp.133-153, 1983.

[16] F. Caccavale, S. Chiaverini, B. Siciliano, "Second-order kinematic control of robot manipulators with Jacobian damped least-squares inverse: Theory and experiments", *IEEE/ASME Transactions on Mechatronics*, Vol. 2, pp. 188-194, 1997.

[17] K. G. Shin and N. D. McKay "A dynamic programming approach to trajectory planning of robotic manipulators", *IEEE Trans. Autom. Control*, Vol. AC-31, no. 6, pp.491 -500, 1986.

[18] M. Spong, J. Thorp and J. Kleinwaks, "The control of robot manipulators with bounded input", *IEEE Transactions on Automatic Control*, Vol. 31, Issue: 6, pp. 483 - 490, 1986.

[19] M. Nakamura, S. Goto, and N. Kyura, *Mechatronic Servo System Control: Problems in Industries and their Theoretical Solutions*, Springer, Chap. 1,2 and 3, 2004.

[20] S. Goto, M. Nakamura, and N. Kyura, "Modified taught data method for industrial mechatronic servo-controller to achieve accurate contour control performance," *IEEE/ASME Int. Conf. Advanced Intelligent Mechatronics (AIM)*, Waseda Univ., Tokyo, Japan, June 14, 1997.

[21] S. R. Munasinghe, M. Nakamura, S. Goto, and N. Kyura, "Precise control of industrial robot arms considering trajectory allowance under torque and speed constraints," *in Proc. IEEE Int. Conf. Robotics and Automation*, pp. 39493954, May 2001.

[22] S. R. Munasinghe, M. Nakamura, S. Goto, and N. Kyura, "Optimum contouring of industrial robot arms under assigned velocity and torque constraints," *IEEE Trans. Syst., Man, Cybern.*, vol. 31, pp. 159167, May 2001.

[23] C. H. An, C. G. Atkeson and J. M. Hollerbach, "Estimation of Internal Parameters of Rigid Body Links of Manipulators", *Artificial Intelligence Memo 887*, MIT Artificial Intelligence Laboratory, 1986.

[24] H. Kawasaki and K. Nishimura, "Terminal Link Parameter Estimation of Robotic Manipulators," *IEEE Trans. on Robotics and Automation*, pp.485490, 1998.

[25] C. J. Wu and C. H. Huang, "Back-Propagation Neural Networks for Identification and Control of a Direct Drive Robot," *Journal of Intelligent and Robotic Systems, 16(1)*, pp. 4564, 1996.

[26] C. Kwan, F. L. Lewis and D. M. Dawson, "Robust Neural-Network Control of Rigid-Link Electrically Driven Robots," *IEEE Trans. on Neural Networks, 9(4)*, pp. 481488, 1998.

[27] L. Behera, M. Gopal and S. Chaudhury, "On Adaptive Trajectory Tracking of a Robot Manipulator Using Inversion of Its Neural Emulator," *IEEE Trans. on Neural Networks,7(6)*, pp. 14011414, 1996.

[28] C. Y. Su, Y. Stepanenko and S. Dost,"Hybrid Integrator Back stepping Control of Robotic Manipulators Driven by Brushless DC Motors," *IEEE/ASME Trans. on Mechatronics,1(4)*, pp. 266277, 1996.

[29] H. Searaji M. K. Long and T. S. Lee, "Motion Control of 7-DOF Arms: the Configuration Control Approach," *IEEE Trans. on Robotics and Automation, 5(4)*, pp. 125139, 1993.

[30] P. Fiorini, H. Seraji and M. L. Long, "A PC-Based Configuration Controller for

Dexterous 7-DOF Arms," *IEEE Robotics and Automation Magazine, 4(3)*, pp. 3038, 1997.

[31] J. Wang, Q. Hu and D. Jiang, "A Lagrangian Network for Kinematic Control of Redundant Robot Manipulators," *IEEE Trans. on Neural Networks, 10(5)*, pp. 11231131, 1999.

[32] C. C. Cheah, S. Kawamura and S. Arimoto, "Feedback Control for Robotic Manipulator with Uncertain Kinematics and Dyanamics," *Proc. of IEEE International Conference on Robotics and Automation*, pp. 36073612, 1998.

[33] G. Liu, K. Iagnemma, S. Dubowsky and G. Morel, "A Base Force/Torque Sensor Approach to Robot Manipulator Inertial Parameter Estimation," *Proc. of IEEE International Conference on Robotics and Automation*, pp. 33163321, 1998.

[34] M. R. Emami, A. A. Goldenberg and I. B. Turksen, "Fuzzy-Logic Dynamics Modeling of Robot Manipulators," *Proc. of IEEE International Conference on Robotics and Automation*, pp. 25122517, 1998.

[35] J. Swevers, C. Ganseman, X. Chenut and J. C. Samin, "Experimental Identification of Robot Dynamics for Control," *Proc. of IEEE International Con-ference on Robotics and Automation*, pp. 241246, 2000.

[36] A. Jain and G. Rodriguez, "Computational Robot Dynamics Using Spatial Operators," *Proc. of IEEE International Conference on Robotics and Automa-tion*, pp. 843849, 2000.

[37] R. Featherstone and D. Orin, "Robot Dynamics: Equations and Algorithms," *Proc. of IEEE International Conference on Robotics and Automation*, pp. 826834, 2000.

[38] D. K. Pai, U. M. Ascher and P. G. Kry, "Forward Dynamics Algorithms for Multi-body Chains and Contact," *Proc. of IEEE International Conference on Robotics and Automation*, pp. 857863, 2000.

[39] F. Sun, Z. Sun, K. I. Kim, Y. Zhu and L. Wenjuan, "Stable Neuro-Adaptive Control for Robot with Unknown Dynamics," *Proc. of IEEE Interna-tional Conference on Robotics and Automation*, pp. 18061811, 1999.

[40] T. Zhang, "High precision contour control of industrial articulated robot arm by Gaussian neural network," PhD dissertation submitted to Saga University Japan, September 2002.

[41] C. J. Lin and C.T. Lin, "Reinforcement Learning for an ART-Based Fuzzy Adaptive Learning Control Network," *IEEE Trans. on Neural Networks,* **7***(3)*, pp. 709–731, 1996.

[42] J.S. Gu and C.W. de Silva, "Development and implementation of a real time open architecture control system for industrial robot systems," *Engineering applications in Artificial Intelligence*, Vol. 17,pp. 469483, 2004.

[43] B. Siciliano, L. Sciavicco, L. Villani and G. Oriolo, *Robotics Modelling, Planning and Control*, Springer, London, UK, 2009.

[44] S.R. Munasinghe, M. Nakamura, S. Goto, and N. Kyura, "Pole Selection of Feed Forward Compensators Considering Bounded Control Input of Industrial

Mechatronic Systems," in *IEEE Transaction on Industrial Electronics*, vol. 50, pp. 1191-1206, 2003.

[45] J. J. Craig, *Introduction to Robotics Mechanics and Control*, Pearson Education Int. 3rd Edition, 2005.

[46] L. Sciavicco and B. Siciliano, *Modeling and control of robot manipulators*, London: Springer, Chap. 2-7, 2000.

[47] N. Hogan, "Impedance Control of Industrial Robots," *IEEE Transaction on Robotics Computer Integrated Manufacturing*, Vol. 1, Issue 1, pp. 97-113, 1984.

[48] T. Endo and F. Matsuno, "Force control and exponential stability for one-link flexible arm," *Proceedings of the 16th IFAC World Congress* 2005.

[49] S. Chiaverini, L. Sciavicco, "The parallel approach to force/position control of robotic manipulators," *IEEE Transactions on Robotics and Automation, 9*, 361373, 1993.

[50] O. Rohani, A. Yousefi-Koma, A. Rezaeeian and A. Doosthoseini, "ANFIS Modeling and Feedforward Control of Shape Memory Alloy Actuators." *International Journal of Mathematical Models and Methods in Applied Sciences*, Vol.2, pp.22835, 2008.

[51] J. Roy and L. L. Whitcomb, "Adaptive Force Control of Position/Velocity Controlled Robots: Theory and Experiment," *IEEE Transactions on Robotics and Automation*, Vol. 18, pp. 12137, 2002.

[52] C. H. S. Chiu and K. Y. Lian, "Adaptive motion/force tracking control of holonomic constrained mechanical systems: A unified viewpoint." *International Journal of Adaptive Control and Signal Processing*, Vol. 21, 41533, 2007.

[53] R. G. Landers, A. G. Ulsoy and Y. H. Ma, "A comparison of model-based machining force control approaches." *International Journal of Machine Tools and Manufacture*, Vol. 44, pp. 73348, 2004.

[54] V. Parra-Vega, A. Rodrguez-Angeles and G. Hirzinger, "Perfect position/force tracking of robots with dynamical terminal sliding mode control," *Journal of Robotic Systems*, Vol. 18, pp. 51732, 2001.

[55] L. Birglen and C. M. Gosselin, "Fuzzy Enhanced Control of an Underactuated Finger Using Tactile and Position Sensors," *Proceedings of the IEEE International Conference on Robotics and Automation*, pp. 23205, 2005.

[56] K. Burn, M. Short and R. Bicker, "Adaptive and Nonlinear Fuzzy Force Control Techniques Applied to Robots Operating in Uncertain Environments," *Journal of Robotic Systems*, Vol. 20, pp. 391400, 2003.

[57] A. Fanaei and M. Farrokhi, "Robust adaptive neuro-fuzzy controller for hybrid position/force control of robot manipulators in contact with unknown environment," *Journal of Intelligent and Fuzzy Systems*, Vol. 17, pp. 125144, 2006.

[58] C. K. Loo, R. Mandava and M. V. C. Rao, "A hybrid intelligent active force controller for articulated robot arms using dynamic structure neural network," *Journal of Intelligent and Robotic Systems: Theory and Applications*, Vol. 40, pp. 11345, 2004.

[59] V. Mallapragada, D. Erol and N. Sarkar, "A new method of force control forunknown environments," *Proceedings of the IEEE/RSJ International Conference on Intelligent Robots and Systems*, pp. 450914, 2006.

[60] P. B. Goldsmith, B. A. Francis and A. A. Goldenberg, "Stability of hybrid position/force control applied to manipulators with flexible joints," *International Journal of Robotics and Automation*, Vol. 14, pp. 14660, 1999.

[61] C. Q. Huang, S. J. Shi, X, G. Wang and W. K. Chung, "Parallel Force/Position Controls for Robot Manipulators with Uncertain Kinematics," *International Journal of Robotics and Automation*, Vol. 20, pp. 15868, 2005.

[62] G. Ziliani, A. Visioli and G. Legnani, "Gain Scheduling for Hybrid Force/Velocity Control in Contour Tracking Task," *International Journal of Advanced Robotic Systems*, Vol. 3, pp. 36774, 2006.

[63] H. T. Cho, P. Jeon and S. Jung, "Implementation and control of a roadway crack tracking mobile robot with force regulation," *Proceedings of the IEEE International Conference on Robotics and Automation*, Vol. 3, pp. 24449, 2004.

[64] C. Pholsiri, D. Rabindran, M. Pryor and C. Kapoor, "Extended generalized impedance control for redundant manipulators," *Proceedings of the 42nd IEEE Conference on Decision and Control*, Vol. 4, pp. 33316, 2003.

[65] C. Ott, R. Mukherjee, and Y. Nakamura, "Unified impedance and admittance control," *Proceedings of the IEEE International Conference on Robotics and Automation*, pp. 554561, 2010.

[66] E. Freund and J. Pesara, "High-bandwidth force and impedance control for industrial robots," *Robotica*, Vol. 16, pp. 75-87, 1998.

[67] A. Lopes and F. Almeida, "A force-impedance controlled industrial robot using an active robotic auxiliary device," *Journal Robotics and Computer Integrated Manufacturing*, Vol. 24, Issue 3, pp. 299-309, 2008.

[68] H. Nagata, Y. Inoue, and K. Yasuda, "Sensorless Flexible Control for Industrial Robot," *16th Conference of RSJ*, Vol. 3, pp. 1533-1534, 1998.

[69] R. Schiavi and A. Bicchi, "Integration of Active and Passive Compliance Control for Safe Human-Robot Coexistence," *IEEE InternationalConference on Robotics and Automation*, Kobe, Japan, pp. 259-264, 2009.

[70] H.G. Sage, M.F. de Mathelin and E. Ostertag, "Robust Control of Robot Manipulators: a Survey," *International Journal of Control*, vol. 72, pp. 1498-1522, 1999.

[71] S. Lee and H. Moradi, "A real Time Dual Arm Collision Avoidance Algorithm for Assembly," *Journal of Robotics System*, vol. 18, pp. 477-486, 2001.

[72] P. Sorenti, "Efficient robotic welding for shipyards - virtual reality simulation holds the key," *Industrial Robot: An International Journal*, Vol. 24 Iss: 4, pp.278 - 281, 1997.

[73] L. Zlajpah, "Simulation in robotics," *Science Direct, Mathematics and Computers in Simulation 79*, pp. 879-897, 2008.

[74] S. Goto, "Forcefree control for flexible motion of industrial articulated robot

arm," *Industrial Robotics: Theory, Modeling and Control, Advanced Robotic Systems International*, Pro literatur Verlag , Chapter 30, pp. 813-840, 2007.

[75] S. Singh and M. C. Leu, "Optimal Trajectory Generation for Robot Manipulators Using Dynamic Programming", *Trans. of the ASME Journal of Dynamic Systems, Measurement, and Control*, vol. 109, pp. 88-96, 1987.

[76] A. Pallegedara, Y. Matsuda, T.Matsumoto, K. Tsukamoto, N. Egashira and S. Goto, "Remote Control of Robot Arms via Network by Force-Free Control Followed Template Matching", *Proceedings of the SICE Annual Conference*, Tokyo, Japan, 2011.

[77] J. De Schutter, H. Bruyninckx, W. H. Zhu and M. W. Spong, "Force control: A bird's eye view", *In Siciliano and Valavanis (Eds.), Control problems in robotics and automation.*, Srpinger, London, 1998.

[78] S. Chiaverini, B. Siciliano and L. Villani, "A Survey of robot interation control schemes with experimental comparison", *IEEE/ASME Transactions on Mechatronics*, Vol. 4, pp. 273-285, 1999.

[79] D. Kushida, M. Nakamura, S.Goto and N. Kyura, "Forcefree control of articulated robot arm with assigned locus", *Japan-USA Symposium on flexible automation*, Hiroshima, Japan, 2002.

[80] L. Nocks, *The Robot: A Life Story of a Technology*, USA, Greenwood Press, pp. 68-74, 2007.

[81] A. Sanfeliu, N. Hagita and A. Saffiottid, "Network robot systems," *Robotics and Autonomous Systems*, Vol. 56, pp. 793-797, 2008.

[82] T. B. Sheridan, "Teleoperation, Telerobotics and Telepresence: A Progress Report," *Control Engineering Practice*, Vol. 3, No. 2, pp. 205-214, 1995.

[83] H. G. Stassen and G. J. F. Smets, "Telemanipulation and telepresence," *Control Engineering Practice*, vol. 5, no. 3, pp. 363-374, 1997.

[84] B. Challacombe and P. Dasgupta, "Telemedicine – the Future of Surgery," *The Journal of Surgery*, Vol. 1, No. 1, pp. 15-17, 2003.

[85] C. M. R. Marohn and C. E. J. Hanly, "Twenty-first century surgery using twenty-first century technology: Surgical robotics," *Current Surgery*, Vol. 61, No. 5, pp. 466-473, 2004.

[86] B. J. Park, R. M. Flores and V. W. Rusch, "Robotic assistance for video-assisted thoracic surgical lobectomy: Technique and initial results," *The Journal of Thoracic and Cardiovascular Surgery*, Vol. 131, No. 1, pp. 54-49, 2006.

[87] J. D. Geeter, M. Decrrton and E. Colon, "The challenges of Telerobotics in a Nuclear Environment," *Robotics and Autonomous Systems*, Vol. 28, pp. 5-17, 1999.

[88] K. Nickels, M. DiCicco, M. Bajracharya and P. Backes, "Vision Guided Manipulation for Planetary Robotics — Position control," *Robotics and Autonomous Systems*, Vol. 58, No. 1, pp. 121-129, 2010.

[89] S. Hutchinson, G. D. Hager and P. I. Corke, "A turorial on visual servo control,"

IEEE Transaction on Robotics and Automation, Vol. 12, No. 5, pp. 651-670, 1996.

[90] G. Bradski and A. Kaehler, *Learning OpenCV: Computer Vision with the OpenCV Library*, O'Reilly Media, CA, 2008.

[91] K. S. Fu, R. C. Gonsalsz and S. G. Lee, *Robotics: Control, Sensing, Vision and Intelligence*, New York, McGraw-Hill, pp. 82-102, 304-446, 1987.

[92] J. Funda, R. H. Taylor, B. Eldrdge, S. Gomory and K. G. Gruben, "Constrained Cartesian Motion Control for Teleoperated Surgical Robots," *IEEE Transactions on Robotics and Automation*, Vol. 12, No. 3, pp. 453-465, 1996.

[93] G. Song and S. Guo, "A Novel Force Feedback-based Teleoperation system for medical application," *International Journal of Innovative Computing, Information and Control*, Vol. 3, No. 3, pp. 737-750, 2007.

[94] A. Eusebi and C. Melchiorri, " Force Reflecting Telemanipulators with Time-Delay: Stability Analysis and Control Design," *IEEE Transactions on Robotics and Automation*, Vol. 14, No. 4, pp. 635-639, 1998.

[95] T. Itoh, K. Kosuge and T. Fukuda, "Human-Machine Cooperative Telemanipulation with Motion and Force Scaling Using Task-Oriented Virtual Tool Dynamics," *IEEE Transactions on Robotics and Automation*, Vol. 16, No. 5, pp. 505-516, 2000.

[96] D. Lee and M. W. Spong, "Passive Bilateral Teleoperaion with Constant Time-Delays," *Proceedings of IEEE Conference on Robotics and Automation*, pp. 2902-2907, Orlando FL, USA, 2006.

[97] S. Goto, *Robot Manipulators Trends and development* ("Teleoperation System of Industrial Articulated Robot Arms by Using Forcefree Control"), Advanced Robotic Systems International, IN-TECH, Chapter 15, pp. 321-334, 2010.

[98] D. E. Comer and D. L. Stevens, *Internetworking with TCP/IP Vol III: Client-Server Programming And Applications Linux/POSIX Sockets Version*, New Jersey, Prentice Hall, 2001.

[99] K. Fredriksson, V. Mkinen and G. Navarro, "Rotation and lighting invariant template matching," *In Proc. 6th Latin American Symposium on Theoretical Informatics*, pp. 39-48, 2004.

[100] L. D. Stefano, S. Mattoccia and F. Tombari, "ZNCC-based template matching using bounded partial correlation," *Pattern Recognition Letters*, Vol. 26, No. 2, pp. 2129-2134, 2005.

[101] S. K. Lam, C. Y. Yeong, C. T. Yew, W. S. Chai and S. A. Suandi, "A Study on Similarity Computations in Template Matching Technique for Identity Verification," *International Journal on Computer Science and Engineering*, Vol. 02, No. 08, pp. 2659-2665, 2010.

[102] E. Mills and N. Borg, "Trends in recommended lighting levels: an international comparison." *J. Illuminating Eng. Soc.*, Vol. 28, pp. 155163, 1999.

[103] Burt PJ, Yen C and Xu X (1982) Local correlation measures for motion analysis: a comparative study. In Proceedings of the IEEE Conference on Pattern Recognition and Image Processing,pp. 269274.

[104] Stevens WR (1998), Unix Network Programming, Networking APIs: Sockets and XTI, Upper Saddle River, NJ, Prentice Hall Inc.

[105] Goldberg K (2000), The Robot in the Garden: Telerobotics and Telepistemology in the Age of the Internet, MIT Press, Cambridge, Massachusetts, USA.

[106] Taylor K and Trevelyan J (1995), A Telerobot on The World Wide Web, National Conference of the Australian Robot Association, Melbourne: Australian Robotics Association.

[107] Taylor K and Dalton B (1997), Issues in Internet Telerobotics, International Conference on Field and Service Robotics (FSR 97), Canberra, Australia: The Australian National University, pp. 151-157.

[108] Teresa T and Zhang H (1999), Internet-Based Tele-Manipulation, Proceedings of the 1999 IEEE Canadian Conference on Electrical and Computer Engineering, Shaw Conference Center, Edmonton, Alberta, Canada, pp. 1425-1430.

[109] Conway L, Volz RA and Walker MW (1993), Teleautonomous systems: projecting and coordinating intelligent action at a distance, IEEE Transactions on Robotics and Automation, Vol. 6, No. 2, pp. 146-158.

[110] Sheridan TB (1992), Telerobotics, Automation and Human Supervisory Control, MIT Press, Cambridge, Massachusetts, USA.

[111] A. Pallegedara, Y. Matsuda, T. Matsumoto, K. Tsukamoto N. Egashira and S. Goto, "Teleoperation Of Robot Arms Using Force-Free Control And Template Matching," International Journal of Innovative Computing, Information and Control IJICIC 2012, ISSN 1349-4198, Volume 8, Number 10, pp. 6869-6884, October 2012.

[112] A. Pallegedara, Y. Matsuda, N. Egashira, T. Sugi and S. Goto, "Experimental Evaluation of Teleoperation System with Force-free Control and Visual Servo Control by Human Operator Perception," Artificial Life and Robotics, ISSN 1433-5298, Volume 17,Combined 3-4,pp. 388-394, ISAROB November 2012.

[113] Norman DA and Draper SW (1986), User Centered System Design: New Perspectives on Human-Computer Interaction, Lawrence Erlbaum Associates, Hillsdale, New Jersey London.

[114] Howie DE, Janzen ME and Vicente KJ (1996), Research on Factors Influencing Human Cognitive Behaviour (III). CEL Technical Reports Series, CEL No. 96-06.

[115] Hannaman GW, Spurgin AJ and Luckic YD (1985), A model for assessing human cognitive reliability in PRA studies, Proceedings of the IEEE Conference on Human Factors and Power Plants, pp. 343353.

[116] A. Pallegedara, Y. Matsuda, T. Matsumoto, K. Tsukamoto N. Egashira and S. Goto "Teleoperation Of Robot Arms Using Force-Free Control And Template Matching," *International Journal of Innovative Computing, Information and*

Control (IJICIC) ISSN 1349-4198 Volume 8, Number 10, October 2012 *(Online version)*.

[117] S. Goto, T. Usui, N. Kyura and M. Nakamura, "Forcefree control with independent compensation for industrial articulated robot arms," *Control Engineering Practice*, ELSEVIER, Vol. 15, pp. 627-638, 2007.

[118] A. Pallegedara, Y. Matsuda, N. Egashira, T. Sugi and S. Goto, "Comparison of Interaction Forces of Robot Arm on Force-free Control and Impedance Control by Model Based Simulations," *Proceedings of the SICE Annual Conference*, August 20-23, Akita, Japan, 2012.

[119] S. Goto, N. Kyura and M. Nakamura, "Forcefree Control with Independent Compensation for Inertia, Friction and Gravity of Industrial Articulated Robot Arms," *Proc. of IEEE International Conference on Robotics and Automation*, pp. 4386-4391, 2003.

[120] V. Kecman, *Learning and Soft Computing*, MIT Press, Cambridge Massachusetts, Chapters 4,5 and 8, 2001.

[121] D. B. Fogel, "An Introduction to Simulated Evalutionary Optimization," *IEEE Trans. on Neural Networks*, Vol. 5, no. 1, pp.3-14, 1994.

[122] J. H. Kim and H. Myung, "Evalutionary Programing Techniques for Constrained Optimization Problems," *IEEE Trans. on Evolutionary Computation*, Vol. 1, no. 2, pp. 129-140, 1997.

[123] T. Zhang and M. Nakamura, "High-Precision Contour Control by Gaussian Neural Network Controller for Industrial Articualted Robot Arm with Uncertainties," *ICASE: The Institute of Control, Automatic and Systems Engineers, KOREA*, Vol. 3, No. 4, Dec. 2001.

[124] K. Kiguchi and T. Fukuda, "Intelligent Position/Force Controller for Industrial Robot Manipulators by Application of Fuzzy Neural Networks," *IEEE Trans. on Industrial Electronics*, Vol. 44, no. 6 pp. 753-761, 1997.

[125] S. Goto, M. Nakamura and N. Kyura "Accurate Contour Control of Mechatronic Servo Systems Using Goussian Networks", *IEEE Transactions on Industrial Electronics*, Vol. 43, No. 4, 1996.

[126] Y. Karai *Present condition of servo technology*, Japan Mechanical Design Industries Association 1991, vol. 35, pp. 30-36.

[127] Yaskawa Electric Factory, *A guide of servo technical for mechatronics*, Nikkan Kogyo Shimbun, 1986.

[128] R. P. Paul, B. Shimano and G. E. Mayer, "Kinematic control equations for simple manipulators," *IEEE Trans. Syst., Man, Cybern.*, Vol. SMC-11, pp. 449-455, June 1981.

[129] C. S. G. Lee and M. Zeigler, "Geometric approach in solving inverse kinematics of PUMA robots," *IEEE Trans. Aerosp. Electron. Syst.*, vol. MECH-2, pp. 188-184, Sept. 1984.

[130] Yaskawa Electric Corp., *User's Manual of σ Series*, SGM/SGDA, 1997.

[131] A. Pallegedara, Y. Matsuda, N. Egashira, T. Sugi and S. Goto, "Simulation and

Analysis of Dynamics of the Force-free Control for Industrial Robot Arms", *12th International Conference on Control, Automation and Systems*, Jeju Island, Korea, 2012.

[132] A. Pallegedara, Y. Matsuda, N. Egashira, T. Sugi and S. Goto, "Development and Evaluation of Simulation Model for Force-free Control Strategies," *Proc. of IEEE International Conference on ICIAfS*, Beijing, China, 2012.

[133] L. Y. Kuo and J. Y. Yen "Servo parameter tuning for a 5-axis machine center based upon GA rules", *International Journal of Machine Tools and Manufacture*, vol. 41, pp.1535-1550, 2001.